NEW ON-LINE MASS SPECTROMETRIC TOOLS FOR STUDYING URBAN ORGANIC AEROSOL SOURCES

A thesis submitted to the University of Manchester for the degree of

Doctor of Philosophy

in the Faculty of Science and Engineering

2017

ERNESTO REYES VILLEGAS

SCHOOL OF EARTH AND ENVIRONMENTAL SCIENCES

Blank page

Contents

Word count: 58113

New on-line mass spectrometric tools for studying urban organic aerosol sources

A thesis submitted to the University of Manchester
for the degree of Doctor of Philosophy, 2017 Ernesto Reyes Villegas

Abstract

Atmospheric aerosols have been shown to have a significant impact on air quality and health in urban environments. Organic aerosols (OA) are one of the main constituents of submicron particulate matter. They are composed of thousands of different chemical species, which makes it challenging to identify and quantify their sources. OA sources have been previously studied; however quantitative knowledge of aerosol composition and their processes in urban environments is still limited.

The results presented here investigate OA, their chemical composition and sources as well as their interaction with gases. On-line measurements of species in the particle and the gas phase were performed both from field-based and laboratory studies. Aerosol Mass Spectrometers (AMS) were used together with the Chemical Ionisation Mass Spectrometer (CIMS) and the Filter Inlet for Gases and AEROsols (FIGAERO).

Two ambient datasets were analysed to develop methods for source apportionment, using the Multilinear Engine (ME-2), in order to gain new insights into aerosol sources in Manchester and London. Long-term measurements in London allowed the opportunity to perform seasonal analysis of OA sources and look into the relationship of hydrogen-like OA (HOA) and heavy- and light-duty diesel emissions. The seasonal analysis provided information about OA sources that was not possible to observe on the long-term analysis. During Bonfire Night in Manchester, with high aerosol concentrations, particularly biomass burning OA (BBOA), it was possible to identify particulate organic oxides of nitrogen (PON), with further identification of primary and secondary PON and their light absorbing properties. Through laboratory work, new insights into cooking organic aerosols (COA) were gained, a higher relative ion efficiency (RIE_{OA}) value of around 3.3 for OA-AMS compared with the typical RIE_{OA} of 1.4 was determined, which implies COA concentrations are overestimated when using the RIE_{OA} value of 1.4. Dilution showed to have a significant effect on food cooking experiments, increasing both the gas/particle ratios and the O:C ratios. The data generated in this work, OA-AMS mass spectra and markers from both gas and particle phase identified with FIGAERO-CIMS, provide significant information that will contribute to the improvement of source apportionment in future studies.

This work investigates OA, with a focus on primary organic aerosols originated from anthropogenic activities. These scientific findings increase our understanding of OA sources and can help to improve inventories and models as well as to develop plans and policies to mitigate the air pollution in urban environments.

Declaration

I declare that no portion of the work referred to in the thesis has been submitted in support of an application for another degree or qualification of this or any other university or other institute of learning;

Ernesto Reyes Villegas

Copyright statement

Acknowledgements

It has been a long and fruitful journey to get to this stage and many people have helped me along the course. I am really thankful for my Supervisors James Allan and Hugh Coe. James, your extensive knowledge and passion for atmospheric research has given me the support and inspiration I needed throughout my PhD. Hugh, I really appreciate the conversations we had and your comments about my work over the years; they opened my eyes to a broader perspective of aerosol science and helped me to orientate my research in the best way.

Thank you Mike Le Breton, Tom Bannan and Mike Priestley for your support on the CIMS analysis. I know I am responsible for some of the grey hair Tom is getting. However, the conversations we had and the recommendations all of you gave me when I was struggling with the analysis were invaluable.

I wish to thank the aerosol group. I really enjoyed the Monday meetings. The friendly environment and the opportunity to listen to the different research topics helped me to increase my knowledge and to think about different ways to approach my investigation.

Thank you Mike, Dany, Gillian and Nick. My office mates and witnesses of the process of this work. The word of the day is Gracias.

I am particularly grateful to the National Council of Science and Technology–Mexico (CONACYT) for the scholarship I received under registry number 217687.

My family has been an essential support to go all this way from the elementary school "Vicente Guerrero" to my postgraduate studies at the University of Manchester. I would not have gone that far in my studies without all of them.

I came to the UK to increase my knowledge about atmospheric science and try to do my part in helping to improve air quality. I did not know I was going to find my best half! Thank you Zara for being by my side all this time. Your love and support gave me the energy I needed every day. Te amo Zarita.

Thesis overview

This thesis is written following the journal format, which involves the results section to be composed of scientific papers. **Chapter 1** describes urban air pollution in cities and the effects of aerosols on air quality. An overview of frameworks and regulations is presented, focusing on Manchester and London; cities where the ambient measurements were performed. In **Chapter 2**, a review of atmospheric aerosols is conducted, with a focus on their effects on air quality, sources and chemical composition. This chapter highlights the importance studying aerosols, in the PM_1 fraction, and in specific organic aerosols (OA). **Chapter 3** describes the current techniques used to measure aerosols, with an overview of mass spectrometry and a description of the mass spectrometers used in this work. The different source apportionment techniques are presented, with detailed information of the factorisation tools used in this work, positive matrix factorisation (PMF) and multilinear engine (ME-2). **Chapter 4** presents an overview of the current OA measurements with mass spectrometers. The characteristic markers to identify OA sources are discussed with a description of OA sources identified in previous studies. **Chapter 5** gives an outline of the chapters that form this work and the objectives to be addressed.

Chapter 6 compiles the three scientific papers prepared as part of this thesis, where a range of different mass spectrometers was used to perform on-line measurements of particles and gases. **Paper 1** (Section 6.1) shows the results of performing source apportionment to OA concentrations measured in London, UK. Here a methodology to explore the solution space to identify the optimal solution is proposed and OA sources seasonality is studied. In **Paper 2,** OA sources are investigated during Bonfire Night with high biomass burning (Section 6.2). OA source apportionment was performed with further analysis of nitrogen chemistry. In **Paper 3**, a laboratory-based experiment was designed in order to study food cooking emissions, both in particle and gas phases (Section 6.3). Here different types of food and cooking methods were used and diluted experiments were performed to study the semi-volatile effect on food cooking aerosols. The final chapter of this thesis, **Chapter 7,** presents the conclusions, and future work.

Chapter 1

Urban air pollution

Ambient air pollution is a serious problem in urban areas. The World Health Organization (WHO) has recognised atmospheric pollution as a high public health priority, stating air pollution kills nearly three million people a year (WHO 2016) and with about 90% of people breathing air that does not comply with WHO air quality guidelines (WHO 2006).

Anthropogenic pollution has been deemed a serious health and an environmental problem. Poor air quality increases the risk of heart disease, respiratory infections, stroke and lung cancer. With vulnerable population groups including children, the elderly and people with compromised immune systems are the most susceptible, with the effects on individuals ranging from subclinical effects to premature death (Samet and Krewski 2007). There is also an economic impact due to poor air quality; the Department for Environment, Food and Rural Affairs (DEFRA) states that air pollution caused health costs of around £15 billion to UK citizens (DEFRA 2010), as a result of hospital admissions, missed work days, among other causes.

The decline in air quality was first observed many decades ago, with anthropogenic atmospheric pollution in urban environments being recognised as being directly related to combustion activities. For instance, in the early 19th century, the Manchester area grew rapidly from small towns to a major industrial urbanised city. Manchester became a pioneer in many industrial and commercial activities: the first passenger railway, the first industrial canal, built the first steam engine to manufacture cotton, the first inter-basin domestic water transfer in the UK (Douglas et al. 2002). However, all this industrial development came together with atmospheric pollutants mainly emitted from combustion sources.

One extremely poor air quality situation in London, UK, was the Great Smoke of 1952. During December 1952, a period of cold weather combined with anticyclone and low wind speeds produced favourable conditions for high concentrations of pollutants to accumulate, mainly particulate matter and sulphur dioxide, with a subsequent oxidation in the atmosphere producing sulphuric acid particulate matter. The pollution that was mostly from coal burning within the city, whose consumption increased due to the cold weather, is estimated to have caused 4000 deaths, over a two-week period, and 15,000 Londoners fell ill and were off work (Brunekreef and Holgate 2002).

The United States has also suffered from significant air quality problems in the past, which caused increments in mortality and morbidity (McCarroll 1967). In New York, during the smog crisis of 1953, a mixture of carbon monoxide, sulphur dioxide and smog killed between 170 and 260 people in six days (Greenburg et al. 1962). Two more critical situations with poor air quality were present in 1963 and 1966 in New York, which caused 405 and 168 deaths, respectively.

1.1 Frameworks and regulations

In response to the critical situation during the Great Smog in 1952, the UK government passed the Clean Air Act in 1956 (http://www.legislation.gov.uk/ukpga/Eliz2/4-5/52/enacted, accessed: 02/12/2017). This act implemented different resolutions including regulations on motor fuels and the creation of smoke control areas. Moreover, the consumption of cleaner energy, for instance, the use of liquid and gaseous fuels, as well as the use of electricity for daily activities improved the air quality in London during the 1960s and 1970s.

In 1970, great efforts were made by the United States to tackle the air pollution situation resulted in the creation of the Environmental Protection Agency (EPA), with the subsequent creation of the Clean Air Act, which sets the National Ambient Air Quality Standards (NAAQS). There are two types of NAAQS; primary standards, which aim to provide public health protection and secondary standards to provide welfare protection, for instance, decreased visibility and damage to vegetation, animals and edifications (EPA 2006). The NAAQS are defined for six pollutants named "criteria" pollutants, carbon monoxide (CO), lead (Pb), nitrogen dioxide (NO_2), ozone (O_3) and particle matter with an aerodynamic diameter less than 10 and 2.5 micrometres, denoted PM_{10} and $PM_{2.5}$ respectively.

In 1987, the World Health Organization (WHO) elaborated the Air Quality Guidelines (AQG), based on expert evaluations and scientific evidence, aiming to assist in reducing health impacts of air pollution. The AQG were updated in 2005 with information related to four common pollutants: sulphur dioxide (SO_2), O_3, NO_2 and PM (WHO 2006). $PM_{2.5}$ is one of the typical pollutants that can be used as a parameter to assess air quality because of their significant impacts on health; due to their small size, $PM_{2.5}$ may be inhaled and penetrate deep into the lungs.

The European Union (EU) has been working on air quality legislation since the early 1980s (http://ec.europa.eu/environment/air/quality/existing_leg.htm, accessed: 04/12/2017). With the aim of protecting human health, in 2008, the EU Ambient Air Quality Directive 2008/50/EC set target concentrations of various pollutants (Parliament 2008), with an annual target of 25 $\mu g \cdot m^{-3}$ for $PM_{2.5}$. Table 1 presents, in summary, a comparison of the $PM_{2.5}$ limits defined by the EPA, WHO and EU. The WHO recommends an annual $PM_{2.5}$ mean concentration of 10 $\mu g \cdot m^{-3}$ as the long-term exposure limit, which represents the lowest concentrations to which cardiopulmonary and lung cancer mortality has been proven (Pope et al. 2002). The EU limit is set to 25 $\mu g \cdot m^{-3}$ with the objective to decrease this limit in subsequent years.

Table 1: Comparison of average $PM_{2.5}$ limits between the EPA, WHO and EU.

Averaging time	Standard	EPA-NAAQS ($\mu g \cdot m^{-3}$)	WHO guidelines ($\mu g \cdot m^{-3}$)	EU Air Quality Directive ($\mu g \cdot m^{-3}$)
1 year	primary	[a]12	[a]10	25
	secondary	[a]15		
24 hours	primary and secondary	[b]35	[b]25	

[a] annual mean, averaged over 3 years
[b] 98th percentile, averaged over 3 years

The Air Quality Strategy for England, Scotland, Wales and Northern Ireland was presented in 2007, supported with scientific, economic and regulatory evidence to reduce health impacts of atmospheric pollutants and to improve air quality by protecting the environment (DEFRA 2007). The measures outlined in this strategy could help to reduce the impact on average life expectancy from eight to five months by 2020. However, this strategy recognises not being able to meet objectives for three of nine pollutants (particles, ozone and nitrogen dioxide). While the areas of exceedance are relatively small, there may be significant members of the population likely to be exposed, as the exceedances tend to be in urban areas.

1.2 Air quality in The UK

The UK has shown concern about atmospheric pollutants and has recognised their negative effect on human health for decades. The first measurements of particulate air pollution were performed in the 1920s, measuring black smoke (Quincey 2007). The black smoke network started performing extensive measurements in 1962. In the 1970s the number of monitoring sites was at its highest at 1,400, decreasing to 600 in early 1980s and less than 100 in 2004 (Loader 2006). In 2008, the black smoke samplers were replaced by Aethalometers (AE22, Mageesci) to start the black carbon (BC) network, comprising 14 sites and covering a wide range of monitoring sites (Butterfield et al. 2016).

The implementation of regulations and the development of new technologies decreased pollutant concentrations such as black smoke and sulphur dioxide. However, due to increasing road traffic, other pollutants such as CO and nitrogen oxides (NO_x) begun to have a significant impact on air quality (Harrison et al. 2012). Situations like these highlighted the need to install monitoring sites to study the air quality in London. These sites formed the basis for the creation of the Automatic Urban and Rural Network (AURN) in the early 90s with some monitoring sites operating since 1972 and currently operating with 108 sites (DEFRA 2017).

Since 1985, the National Atmospheric Emissions Inventory has been compiling data on greenhouse gases and air pollutant emissions from different UK sectors (DEFRA 2016). The sectors include agriculture/waste; combustion in industry/commercial residential; road transport; production processes; public electricity and heat production; and other transport. $PM_{2.5}$ emissions have decreased since early 1990, as a result of reducing coal combustion. However, the combustion in industry/commercial residential sector remains to be the main $PM_{2.5}$ emitter with 64 kilotons in 2015.

1.2.1 Manchester

All the advances in Manchester during the industrialisation of the 19th century, together with an increasing population had impacts on the environment and human health, and hence a series of regulations were developed: Manchester had the first urban smokeless zones in the UK and implemented the Sanitary, Vaccination and Public Health Acts. In 1912, the Manchester City Council established the Air Pollution Advisory Board (Douglas et al. 2002).

In 2016, Greater Manchester had an estimated population of 2,685,000 inhabitants, with a land area of 630 km^2 and a density of 4,100 inhabitants.km^{-2} (Demographia 2017), integrating 10 Boroughs including Bolton, Bury, Manchester, Oldham, Rochdale, Salford, Stockport, Tameside, Trafford, and Wigan. The website http://www.greatairmanchester.org.uk/ (accessed: 07/11/2017) stores information about the air quality in Greater Manchester. There are three automatic monitoring sites; an urban site (Piccadilly Gardens), a suburban site (close to Manchester airport - South Manchester) and a kerbside (close to the city centre), with different types of measurements such as NO, NO_2, NO_x, SO_2, O_3, PM_{10} and $PM_{2.5}$. Piccadilly Gardens and South Manchester are part of the AURN (https://uk-air.defra.gov.uk/networks/, accessed: 07/11/2017).

The Greater Manchester air quality action plan (2016-2021) recognised traffic emissions as a priority to reduce air pollution, which will be achieved by focusing on three tasks: to reduce traffic, increase efficiency to achieve smother emissions and improve fleet. Private cars represent more than 70% of vehicles transiting on roads, so efforts will be orientated to reduce the use of cars and motivate the use of public transport, cycling and walking (GMCA 2016).

1.2.2 London

London, which is recognised as a megacity taking into account the wider metropolitan area, has an estimated population of 10,470,000 inhabitants, with a land area of 1,738 km^2 and a density of 5,600 inhabitants per square kilometre (Demographia 2017). Due to the sheer number of inhabitants and the associated anthropogenic air pollutant emissions resulting from the inhabitants' daily activities (transportation, energy production and industrial activities), it is necessary to study the air pollution to devise mitigation strategies.

In 1993, the London Air Quality Network (LAQN) was created to collect data from the majority of London's 33 boroughs. This provides the opportunity to obtain data from a wide variety of monitoring stations: rural, suburban, urban-background, roadside, kerbside and industrial. 53 monitoring sites measure PM_{10} and 14 sites measure $PM_{2.5}$. Around 90% of the sites monitoring $PM_{2.5}$ achieved the EU target annual value of 25 $\mu g{\cdot}m^{-3}$ while only one site met the WHO guideline value of 10 $\mu g{\cdot}m^{-3}$ (Mittal and Fuller 2017).

Different sources of air pollutants have been identified in London, the majority of them related to combustion sources. The London atmospheric emissions inventory (GLA 2013) reports road transportation, river, rail, Non-Road Mobile Machinery, domestic and commercial, aviation, construction and demolition, industry and resuspension to be primary sources of $PM_{2.5}$. Road transport is the main source contributing to 54% of the total $PM_{2.5}$ annual emissions during 2013 and 8% of total $PM_{2.5}$ assigned to "other", suggesting there are still other sources to be identified.

The UK has shown a great improvement in tackling the air pollution, with Manchester and London presenting a considerable improvement compared to previous decades. However, there is still more work to do in the UK in order to reduce the $PM_{2.5}$ concentrations. The WHO limit of 10 $\mu g{\cdot}m^{-3}$ is a difficult but likely target to meet in the future if the scientific community and decision-makers work together to identify new approaches to tackle air pollution.

1.3 Current $PM_{2.5}$ situation in Europe

The implementation of frameworks and the deployment of air quality networks in cities mitigated the air quality issues, reducing deaths related to air pollutants and increasing the life expectancy. However, negative effects on health are still present in urban environments (Sexton and Linder 2015;McCarthy et al. 2009).

The European Environment Agency (EEA 2017) states that in 2015, from 28 member states of the European Union (Fig. 1), 7% - 8% of the population was exposed to $PM_{2.5}$ concentrations over the annual limit of the European Union (25 μg·m^{-3}) and 82% – 85% of the population was exposed to $PM_{2.5}$ concentrations over the annual limit of the WHO (10 μg·m^{-3}). Developed countries have made great improvements in air quality. However, more efforts to reduce particulate matter concentrations must be made in cities for the population to live in an environment with cleaner air.

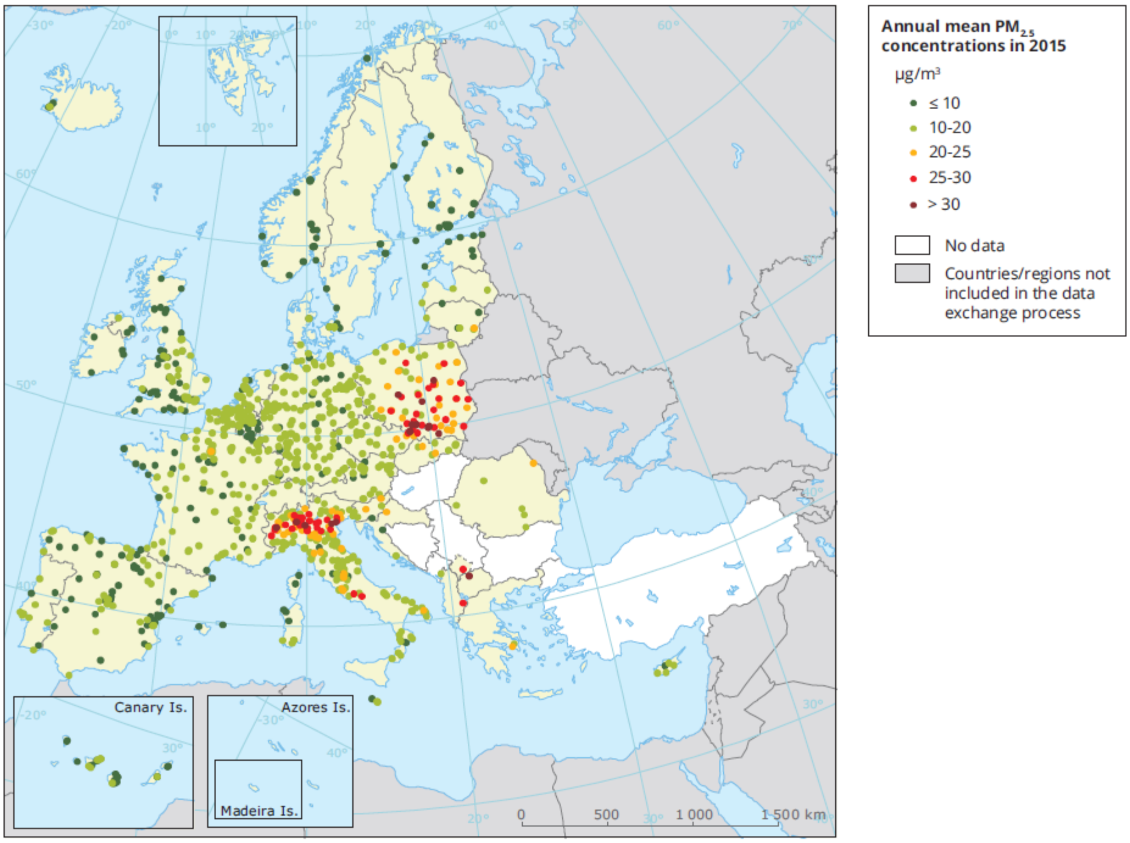

Figure 1: Mean $PM_{2.5}$ annual concentrations in 2014. Reproduced from (EEA 2017).

Chapter 2

Aerosols and air quality

Aerosols are a combination of liquid and/or solid particles in the air (Seinfeld and Pandis 2016), which are either directly emitted from anthropogenic and natural sources as well as produced in the atmosphere from physicochemical processes. The interest to investigate aerosols is due to the significant effects on climate (Satheesh and Krishna Moorthy 2005;Pöschl 2005) and air quality (Watson 2002;Peng et al. 2005;Pope III and Dockery 2006). Two main impacts of aerosol pollution are observed with regard to air quality: harm to human health and the environment. The impact of aerosols on human health has been previously studied (Brunekreef and Holgate 2002;Peng et al. 2005;Valavanidis et al. 2008;Ramgolam et al. 2009). While is true that air pollution has decreased in the recent decades as a result of improvements in combustion fuels and processes, there is still a high health risk due to the wide range of aerosol chemical composition and size.

As previously mentioned in Chapter 1, the size of aerosols is a key factor when determining the impact to human health. Depending on their size, aerosols can reach different areas of the respiratory system (Elmes and Gasparon 2017); particles equal to or larger than PM_{10} remain in the nasal cavity and/or the throat; $PM_{2.5}$-PM_{10} are known as thoracic particles, deposited in the trachea; the cut size <$PM_{2.5}$ is the respirable fraction which can reach the alveoli. Ultrafine particles (<0.1 μm), are potentially more harmful to health as they can penetrate deeper into the respiratory tract and can reach the alveoli (Valavanidis et al. 2008) and can be absorbed directly into the bloodstream (Oberdorster et al. 2005).

Pope III and Dockery (2006) collected evidence from different studies that indicate that exposure to aerosols has adverse effects on cardiovascular and cardiopulmonary health. Ramgolam et al. (2009) determined a stronger correlation between aerosol concentrations and respiratory diseases. This study was performed collecting ambient samples of aerosols with low-pressure cascade impactors; for biological studies, four size stages of particulate matter (PM) were gathered: $PM_{2.5-10}$, $PM_{1-2.5}$, $PM_{0.17-1}$, and $PM_{0.03-0.17}$. Samples were sonicated and human bronchial epithelial cells were exposed to different PM concentrations. It was possible to determine different pro-inflammatory responses according to the range of PM sizes, with $PM_{0.17-1}$, and $PM_{0.03-0.17}$ being the PM sizes that showed the most damaging effects on the epithelial cells. This study concluded that these pulmonary effects may lead to chronic (long-term problem) and acute (severe and sudden) respiratory problems, ultimately increasing hospital admissions and hence economic costs.

The effects aerosols have on air quality and human health depend on their physical and chemical properties, hence why these properties need to be studied and measured in order to determine strategies to reduce emissions and mitigate their adverse impact.

2.1 Aerosol sources and sinks

Atmospheric aerosol sources may be either natural or anthropogenic. Examples of natural sources are sea spray, windborne dust, thunderstorms, volcanic activities and unintentional forest fires, while anthropogenic sources may be generated by incomplete combustion of fossil fuels, industrial processes, and transportation (Pöschl 2005). Aerosols are also classified, according to their origin, as primary or secondary. Primary aerosols are directly emitted from a range of sources while secondary aerosols are produced from gaseous precursors, for instance, sulphur dioxide, oxides of nitrogen and volatile organic compounds, by chemical reactions in the atmosphere as well as from physical processes including condensation, coagulation, absorption, adsorption, solubility and agglomeration, among others (Kolb and Worsnop 2012).

The main sources and sinks of atmospheric aerosols are presented in Table 2. Nitrate is considered to have a secondary origin, as it is produced from the oxidation of NOx. Black carbon (BC), mineral dust and sea spray have primary sources while sulphate and OA have both primary and secondary related sources.

Table 2: Properties of main atmospheric aerosols. Reproduced from (IPCC 2013).

Aerosol Species	Size Distribution	Main Sources	Main Sinks	Tropospheric Lifetime
Sulphate	Primary: Aitken, accumulation and coarse modes Secondary: Nucleation, Aitken, and accumulation modes	Primary: marine and volcanic emissions. Secondary: oxidation of SO2 and other gases from natural and anthropogenic sources	Wet deposition Dry deposition	~ 1 week
Nitrate	Accumulation and coarse modes	Oxidation of NOx	Wet deposition Dry deposition	~ 1 week
Black carbon	Freshly emitted: <100 nm Aged: accumulation mode	Combustion of fossil fuels, biofuels and biomass	Wet deposition Dry deposition	1 week to 10 days
[a]**Organic aerosol**	POA: Aitken and accumulation modes. SOA: nucleation, Aitken and mostly accumulation modes. Aged OA: accumulation mode	Combustion of fossil fuel, biofuel and biomass. Continental and marine ecosystems. Some anthropogenic and biogenic non-combustion sources	Wet deposition Dry deposition	~ 1 week
Mineral dust	Coarse and super-coarse modes, with a small accumulation mode	Wind erosion, soil resuspension. Some agricultural practices and industrial activities (cement)	Sedimentation Dry deposition Wet deposition	1 day to 1 week depending on size
Sea spray	Coarse and accumulation modes	Breaking of air bubbles induced e.g., by wave breaking. Wind erosion.	Sedimentation Wet deposition Dry deposition	1 day to 1 week depending on size

[a]POA = primary organic aerosol, SOA = secondary organic aerosol.

Eventually, particles can be removed from the atmosphere by dry and wet deposition. Dry deposition involves the removal of particles by convective transport, diffusion and adhesion to the Earth's surface (soil, water bodies, vegetation and structures). With wet deposition, particles are incorporated into cloud droplets during the formation of precipitation (Seinfeld and Pandis 2016). Wet deposition is the main sink of atmospheric aerosols. However, dry deposition is highly relevant from an air quality and human health perspective due to the adhesion to buildings and monuments as well as inhalation and deposition in the respiratory tract due to aerosol submicron size (Pöschl 2005).

2.2 Aerosol size and lifetime

The lifetime of aerosols in the atmosphere depends on variables such as aerosol size, rain frequency, wind speed and physicochemical processes. According to their size, aerosols are classified into three different modes (Table 3): nucleation mode (particles with a diameter lower than 0.1 μm), accumulation mode (particles between 0.1 μm-1 μm in diameter) and coarse mode (particles with a diameter larger than 1 μm). Particles with the nucleation mode have a lifetime of minutes to hours, days to weeks in the case of accumulation mode and minutes to days in the coarse mode. This information is consistent with Lawrence et al. (2007), who stated that the lifetime of several aerosols including SO_4^{2-}, NO_3^-, organic carbon (OC) and elemental carbon (EC) is between 1 and 10 days.

The reason why the lifetime of the nucleation mode is that short is due to the main removal mechanisms such as diffusion onto solid surfaces, cloud particles and coagulation to form larger particles. Coarse mode particles also have a short lifetime with sedimentation as the main removal process. PM with diameters between 0.2 μm and 2 μm have weak sinks and strong sources including coagulation of nanoparticles and particles left behind from evaporation of cloud droplets as well as primary sources (Wallace and Hobbs 2006).

Table 3: Aerosol properties based on size distribution. Reproduced from (Lagzi et al. 2013).

	Nucleation mode	Accumulation mode	Coarse mode
Size:	d < 0.1 μm	0.1 μm < d < 1 μm	d > 1 μm
Sources	Combustion Gas to particle conversion Chemical reactions	Combustion Gas to particle conversion Chemical reactions	Dust Soil Biological sources Ocean spray
Formation	Chemical reactions Nucleation Condensation Coagulation	Nucleation Condensation Coagulation Evaporation of droplet	Mechanical disruption of surface Suspension of dust Evaporation of ocean spray Chemical reactions
Composition	Sulphate Elemental carbon Trace metals, Low-volatility organic compounds	Sulphate Nitrate Ammonium Elemental Carbon Organic Component Trace metals (Pb, Cd, V, Ni, Cu, Zn, Fe, etc.)	Dust Ash Crustal elements Sea salt Nitrate Biogenic organic particles
Solubility	Largely soluble, hygroscopic	Largely soluble, hygroscopic	Largely insoluble, non-hygroscopic
Travel distance	<a few 10 of km	a few 100 to 1000 of km	<a few 10 of km (sometimes larger)
Typical atmospheric lifetime	Minutes to hours	Days to weeks	Minutes to days
Sinks	Growth into accumulation mode, wet and dry deposition	Wet deposition, dry deposition (Brownian diffusion, turbulence)	Wet deposition, dry deposition (sedimentation, turbulence)

Different sizes present different chemical composition. For instance, nucleation and accumulation modes are conformed of sulphate, nitrate, elemental carbon and organic aerosols, while dust, ash, sea salt and crustal elements are components of the coarse mode (Lagzi et al. 2013). Table 3 states that, in general, accumulation mode is largely soluble and coarse mode is largely insoluble. However, there are significant variations in hygroscopicity within the same mode; for instance, in accumulation mode, sulphate, ammonium and nitrate are hygroscopic while elemental carbon is non-hygroscopic. Moreover, elemental carbon, when mixed with soluble substances, can increase its hygroscopicity. The fact aerosols have different sizes with different chemical composition and lifetime in the atmosphere explains why they have different effects on human health.

2.3 Aerosol chemical composition and spatial concentrations

Based on their chemical characteristics, aerosols can be classified as inorganic and organic aerosols (OA). The main inorganic aerosols include sulphate (SO_4^{2-}), nitrate (NO_3^-), ammonium (NH_4^+), chloride (Cl^-), black carbon (BC), sea salt and dust. OA composition is challenging to study due to the fact that OA are composed of thousands of different compounds (Hallquist et al. 2009). The importance of understanding OA composition, sources and processes is due to the fact that they comprise a high percentage of submicron particulate matter. Research carried out by Zhang et al. (2007) showed that OA comprises 20%-90% of the total non-refractory submicron particle mass (NR-PM_1) depending on the measurement location.

The composition of the non-refractory fraction of aerosol particles (particles that evaporate within seconds under high vacuum at 600 °C) from different studies in the Northern Hemisphere are shown in Figure 2. The aerosol concentrations range from 2 $\mu g \cdot m^{-3}$ in a remote site in Finland to 71 $\mu g \cdot m^{-3}$ at an urban site in China; the concentrations in Manchester are 5.2 and 14.0 $\mu g \cdot m^{-3}$ during winter and summer respectively. OA presented a high contribution to PM_1 in the majority of the monitoring sites. Moreover, there is a wide variability of aerosol composition, with high concentrations in urban environments.

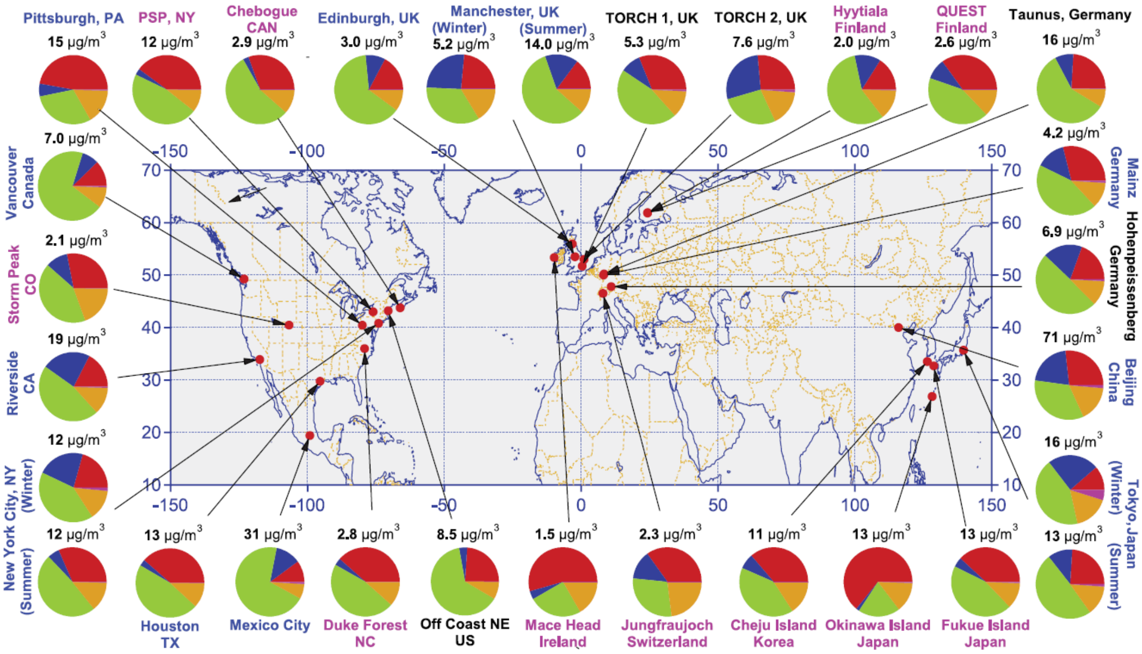

Figure 2: Average mass concentration of aerosols in the northern hemisphere. Reproduced from (Zhang et al. 2007). Colours for labels indicate the type of sampling site. Urban areas (blue), <100 miles downwind of major cities (black), and rural/remote areas >100 miles downwind (pink). Pie chart colours: organics (green), sulphate (red), nitrate (blue), ammonium (orange), and chloride (purple) of NR-PM1.

Chapter 3

Main techniques to study aerosols

Historically, there have been events of poor air quality causing hundreds of deaths and health problems in urban environments around the world. The implementation of frameworks and regulations have helped to reduce these impacts by controlling a series of atmospheric pollutants, with focus on $PM_{2.5}$ and PM_{10}. Particulate matter concentrations have been successfully reduced. However, further work needs to be done to further reduce submicron particulate matter concentrations, specifically PM_1, which has a complex chemical composition, and may pose a more detrimental effect on health compared to $PM_{2.5}$.

Modelling has been an important tool to determine the spatial-temporal behaviour of aerosols in the atmosphere. Hence, the physical-chemical characterisation of aerosols with on-line measurements in a high time resolution is fundamental information in order to improve models performance. From an environmental perspective, it will be possible to improve or to create frameworks and regulations based on knowledge of the aerosol composition and concentrations to lessen the environmental impact of aerosols.

There are different techniques and equipment available to measure aerosol properties. The two main approaches are off-line measurements, which involve collecting samples for further laboratory analysis and on-line measurements, where the equipment directly performs measurements in near-real time. Both approaches have advantages and disadvantages depending on the type of analysis required and the questions to be answered. Off-line measurements are time-consuming, with low time resolution and there is the possibility of an artifact due to sample handling. However, they may be less expensive, offer qualitative and quantitative analyses and it is possible to perform more than one analysis per sample, providing integral aerosol characterisation. On-line measurements may require expensive equipment and highly trained users. However, it is possible to obtain data immediately after being measured with a high time resolution, providing a more detailed temporal aerosol evolution.

Physical and chemical properties of aerosols are determined by using different techniques (Baron and Willeke 2001). As shown in section 2.2, aerosol size is an important physical property to be measured. There are different instruments to measure aerosol size distribution. One instrument that is widely utilised is the scanning mobility particle sizer (SMPS, TSI Inc.) (Wang and Flagan 1990), which comprises a differential mobility analyser (DMA) and a condensation particle counter (CPC). The DMA separates aerosols of a broad size of 2.5 - 1,000 nanometres, based on the electrical mobility and the CPC measures aerosol total number concentration.

The aerodynamic particle sizer (Baron 1986) provides high resolution, real-time measurements of particle aerodynamic diameter in the range of 0.5 to 20 μm. Particle velocity is measured by passing through two laser beams. The time delay between two pulses of scatter light is related the velocity and hence to the aerodynamic diameter of the particle. This instrument also determines the optical diameter of particles by measuring the scattered light intensity, providing an equivalent optical size range of 0.37 to 20 μm. Optical particle counters use the intensity of light scattering to determine the size of particles. Instruments using this method are the Ultra High Sensitivity Aerosol Spectrometer (Cai et al. 2008) and the Passive Cavity Aerosol Spectrometer Probe (Cai et al. 2013).

The light scattering and absorption coefficient are important optical properties, The Nephelometer measures the total amount of light scattered by aerosols (Heintzenberg and Charlson 1996) and the Aethalometer measures the absorption coefficient (Allen et al. 1999). Based on the light configuration, there are two versions of Aethalometers: a two-Wavelength (880 nm for Black Carbon - 370 nm for aromatic organic compounds) and a seven-Wavelength (from 370 nm to 950 nm). The Aethalometer (Magee Scientific) is capable of providing black carbon concentrations using an algorithm to convert the optical signal to a mass concentration.

Gravimetric analysis is performed to quantify the mass of particulate matter, another important physical parameter. In this method, the particulate matter is collected on a filter to determine the mass. The total mass concentration can be calculated using the sampling time and the airflow used during collection. The tapered element oscillating microbalance (TEOM) performs on-line measurements of mass concentrations (Allen et al. 1997). Gravimetric analysis can also be performed with off-line sampling. Here, the sample is collected on a filter of a known weight. The difference in the weight after and before collection gives the mass of particulate matter collected. This method is usually accompanied with other analytic techniques to perform chemical characterisation (O'Connor et al. 2014). The possible interferences are minimised by taking laboratory blanks and field blanks.

Depending on the chemical species of interest, the chemical aerosol composition can be measured using different techniques. This review will cover the on-line instrumentation available to characterise OA, which will vary based on the percentage of mass analysed and the level of OA characterisation. The OC/EC instrument measures organic carbon (OC) and elemental carbon (EC) via thermal desorption from filter measurements (Bauer et al. 2009). This instrument uses inert helium as a carrier gas and a ramping temperature up to ~500˚ C to allow OC to be separated from EC. Subsequently, EC is oxidised using a mixture of helium-oxygen with the temperature increasing to around 850˚ C. The instrument operates with a quartz oven design capable of measuring low carbon concentrations with no oxygen contamination. This instrument provides a quantification of OC and EC concentrations. However, it is not capable of providing molecular identification.

On the other hand, GC-MS and LC-MS, both offer molecular identification, combining gas chromatography (GC) and liquid chromatography (LC), respectively, using mass spectrometry (MS). Chromatography is a technique that separates the analytes of interest from the sample by passing a carrier fluid over a solid or liquid phase on which the analyte is selectively adsorbed and slowed relative to the carrier, named stationary phase. Further analysis using mass spectrometry provides a full molecular identification and quantification of the analytes of interest (Calvo et al. 2013). However, it measures only the analytes that chromatography previously separated, depending on the stationary phase and/or the carrier gas.

Another available chromatographic technique for aerosol characterisation is ion chromatography. This instrument, depending on the column used, can measure anions and cations. The on-line version of these instruments collect the sample at ambient pressure and use external impactors to determine the diameter cut size between PM_{10}, $PM_{2.5}$ and PM_1. Currently, there are three instruments available on the market; the URG ambient ion monitor (Wu and Wang 2007), the particle-into-liquid sampler ion chromatography (PILS-IC) (Takegawa et al. 2009) and the monitor for aerosol and gases in ambient air (MARGA) (Du et al. 2011). The MARGA has the additional capability of measuring gas phase ions.

While there is not a perfect instrument, mass spectrometers offer an extensive level of chemical characterisation with a high percentage of mass analysed. These characteristics, together with the high time resolution obtained from on-line measurements, offer the possibility to quantify particle and gas concentrations to better understand their sources and processes.

3.1 On-line mass spectrometry

On-line mass spectrometric instrumentation has been developed during the last two decades. The first instruments were designed using a quadrupole mass spectrometer (QMS) (Bertram et al. 2011). However, the main disadvantage of QMS is the reduction in the sampling duty cycle. This is due to the QMS being tuned to scan over different mass-to-charge (m/z) ratios and the greater number of values to be scanned the shorter the sampling duty cycle, which increases the detection limit. Further development of techniques such as time of flight (ToF) mass spectrometry allowed measurements in high resolution, with it being possible to identify different species with similar molecular masses.

The principle of mass spectrometry is to separate ions based on their m/z ratio and to detect them quantitatively. Mass spectrometers are composed of five different sections; sample inlet, ion source, mass analyser, detector and data logger. There are different methods to generate the ions before accessing the mass analyser. The main ionisation methods will be explained in the following paragraphs.

The Matrix Assisted Laser Desorption/Ionization (MALDI) uses a liquid solution as a matrix where the analyte of interest is mixed. This mixture is added to the mass spectrometer and left to dry leaving only a crystallised matrix. The sample is irradiated with a laser, typically with a laser near the UV region, to be desorbed and ionised before finally being analysed by the mass spectrometer (Herrera et al. 2016). This ionisation technique has been utilised to analyse biomolecules and large organic molecules such as polymers.

Electrospray ionisation is based on applying a determined voltage to a liquid solution and, with the use of a capillary tube, produces fine drops which then come into contact with the analyte of interest (Holmes et al. 2007). Recently, (Zhao et al. 2017b) employed the electrospray ionisation with a chemical ionisation mass spectrometer using a diluted salt solution in methanol. A voltage power supply is used to apply a voltage of 2-5 kV to force the solution to go through the spray needle to produce drops. The drops then are evaporated before accessing the ion-molecule reaction chamber in contact with the sampling flow.

Electron ionisation (EI) produces ions by interactions of electrons with the analyte that must have been previously transferred to the gas phase (De Hoffmann and Stroobant 2007). Ions are generated by a hot filament and accelerated by a difference in charge to form an ion beam with ionisation energy of 70 eV. At this ionisation energy, the electron-ionization cross section of the majority of the molecules is maximised, which offers a high ionisation efficiency (Jimenez et al. 2003). The charge of the ion can be either positive or negative, depending on the ionisation method (Gross 2004).

In chemical ionisation (CI), ions are produced through reactions of the analyte of interest with an ionised reagent gas. CI is softer compared with EI ionisation, as it produces ions with little excess energy (De Hoffmann and Stroobant 2007); hence, CI identifies molecular ions which then can be termed ions of the molecular species. The sensitivity of reagent ions to an analyte depends on its polarity and hydrogen bonding capability, hence selectivity will vary with different reagent ions. Ammonia (Reinhold 1987) identifies aliphatic and aromatic organochlorine compounds; methane (Barceló 1992) has good sensitivity for the majority of organic compounds; acetate (Veres et al. 2008) with high selectivity to trace acids; nitrate (Kurtén et al. 2011) is used to measure sulfuric acid and RO_2 compounds; and iodide (Lee et al. 2014) is used as a reagent ion to measure various inorganic species and oxigenated VOCs.

Photoionisation and secondary ionisation techniques have been used for many decades. However, it has been only during recent years that these techniques have been implemented in on-line instrumentation. Photoionisation is a physical process that offers a soft ionisation; ions are formed as a result of photons interacting with the analyte of interest (McCulloch et al. 2017). The secondary ionisation technique is used to analyse the chemical composition of solid surfaces. It focuses a primary ion beam onto the surface of the sample in order to ionise the analytes of interest, with further analysis of the secondary ions in the mass spectrometer (Li et al. 2017c).

Once the gas phase ions have been produced they need to be separated, according to the molecular mass, to finally be detected. Ions are separated in the mass analysers using different methods such as; quadrupole, time-of-flight, and magnetic sector (Gross 2004). There are different principles of molecular mass separation such as kinetic energy, momentum, trajectory stability, resonance frequency, and velocity (time-of-flight). Together with the ionisation method, the principle of separation will affect the resolution of the mass spectra. Table 4 presents a comparison of different mass analysers and their characteristics. Here it is possible to see a wide range of the main parameters, mass limit resolution and accuracy.

Table 4: Mass analysers comparison. Reproduced from (De Hoffmann and Stroobant 2007).

	Quadruple	Ion trap	ToF	ToF reflectron	Magnetic	FTICR	Orbitrap
Mass limit	4000 Th	6000 Th	>1000000 Th	10000 Th	20000 Th	30000 Th	50000 Th
resolution FWHM (m/z 1000)	2000	4000	5000	20000	100000	500000	100000
Accuracy	100 ppm	100 ppm	200 ppm	10 ppm	< 10 ppm	< 5 ppm	< 5 ppm
Ion sampling	Continuous	Pulsed	Pulsed	Pulsed	Continuous	Pulsed	Pulsed
Pressure	10-5 Torr	10-3 Torr	10-6 Torr	10-6 Torr	10-6 Torr	10-10 Torr	10-10 Torr
Tandem mass spectrometry	Triple quadrupoles	-	-	PSD or ToF/ToF	consecutive sectors	-	-
	MS/MS	MSn	-	MS/MS	MS/MS	MS	-
	fragments	fragments		fragments	fragments	fragments	
	precursors				precursors		
	neutral loss				neutral loss		
	low-energy collision	low-energy collision	-	low or high-energy collision	high-energy collision	low-energy collision	- collision

This section presented an overview of on-line mass spectrometry and the different principles and measurement techniques. The following sections provide information about the mass spectrometers used in this work with a description of their operational principles.

3.1.1 Aerosol Mass Spectrometer (AMS)

The AMS is an instrument, designed and developed by Aerodyne Research Inc. that has the ability to quantitatively measure the aerosol size-resolved chemical composition of non-refractory particulate matter with a fast time resolution from seconds to minutes. These measurements include OA and SO_4, NO_3, NH_4 and Cl ions. The instrument combines an aerodynamic particle focusing lens, high vacuum thermal particle vaporization, EI, and mass spectrometry (Jayne et al. 2000).

The AMS collects aerosols, which are introduced through a critical orifice, separated from gaseous species by aerodynamic lenses followed by a series of apertures; with a subsequent thermal vaporization (approximately 600° C) and EI at 70 eV (Jayne et al. 2000). Finally, the AMS measures the chemical composition in the mass analyser (Fig.

3). Depending on the type of mass spectrometer used to measure ions, there are different AMS models; Quadrupole AMS (Q-AMS) (Jayne et al. 2000), compact Time-of-Flight AMS (c-ToF-AMS) (Drewnick et al. 2005) and high resolution Time-of-Flight AMS (HR-ToF-AMS) (DeCarlo et al. 2006), all of them providing a wealth of aerosol chemical information.

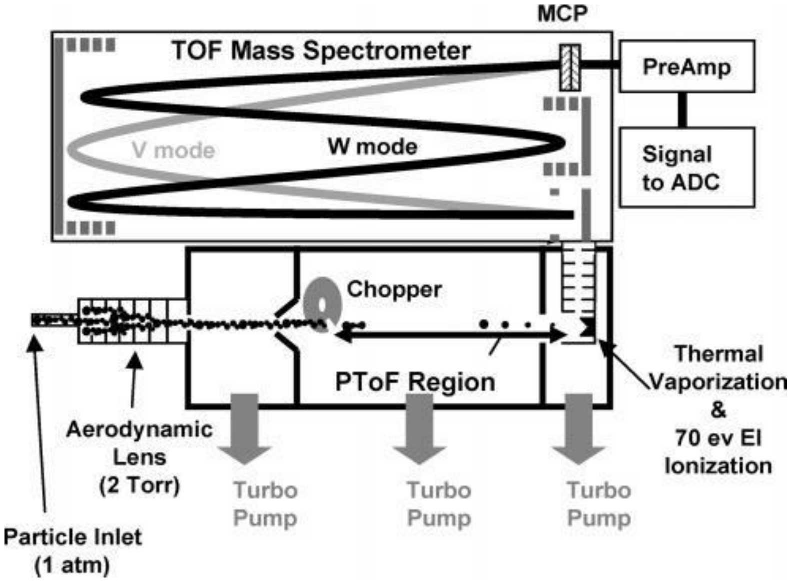

Figure 3: Schematic of the HR-ToF-AMS. Reproduced from (DeCarlo et al. 2006).

The AMS quantifies mass concentrations of ionised analytes at different m/z ratios. Ions are generally single charged, hence m/z ratio represents the molecular weight of ions measured. Aerosols measured using the AMS may be composed of different types of compounds, many of which may be identified at the same m/z ratio. Moreover, due to the strong electron ionisation, ions tend to present fragmentation, making the AMS analysis challenging. In this context, the data analysis of AMS measurements was significantly improved with the introduction of fragmentation tables developed by Allan et al. (2004).

The fragmentation tables may be user-defined through the AMS analysis toolkit (Allan et al. 2004), with the possibility of being updated or edited depending on the case study. With the fragmentation tables, it is possible to extract mass spectra of specific species depending on their contribution to a particular m/z ratio and their fragmentation patterns. Table 5 shows the key ion fragments used to identify aerosol species from AMS mass spectra.

Table 5: Main fragments to identify organic and inorganic compounds in AMS spectra. Bold text highlights the most useful fragments. Reproduced from (Canagaratna et al. 2007).

Group	Molecule/species	Ion fragments	Mass Fragments
Water	H_2O	**H_2O+**, HO+, O+	**18**, 17, 16
Ammonium	NH_3	NH_3^+, **NH_2^+**, NH^+	17, **16**, 15
Nitrate	NO_3	HNO_3^+, **NO_2^+**, **NO^+**	63, **46**, **30**
Sulphate	H_2SO_4	$H_2SO_4^+$, HSO_3^+, SO_3^+, **SO_2^+**, **SO^+**	98, 81, 80, **64**, **48**
Organic (oxygenated)	$C_nH_mO_y$	H_2O^+, CO^+, **CO_2^+**, **$H_3C_2O^+$**, HCO_2^+, $C_nH_m^+$	18, 28, **44**, **43**, 45, …
Organic (hydrocarbon)	C_nH_m	$C_nH_m^+$	27, 29, **41**, **43**, **55**, **57**, 69, 71, …

3.1.2 Aerosol Chemical Speciation Monitor (ACSM)

In principle, the ACSM (Aerodyne Research Inc.) is designed and built under the same sampling and detection technology as the state-of-the-art AMS instruments to measure non-refractory submicron particles (OA, NO_3, SO_4, NH_4 and Cl). Due to its lower size, weight, cost, and power requirements, it is also more affordable to operate and it is capable of measuring over long periods without supervision. This instrument offers a detection limit of 0.2 μg·m^{-3} for a typical average sampling time of 30 min (Ng et al. 2011). These characteristics make the ACSM to be suited for air quality monitoring applications. Figure 4 presents a schematic of the ACSM, with a similar arrangement as the AMS but with the use of only three pumps. There are two ACSM versions available which vary with regard to the mass spectrometer used: the quadrupole ACSM (Ng et al. 2011) and the ToF-ACSM (Frohlich et al. 2013).

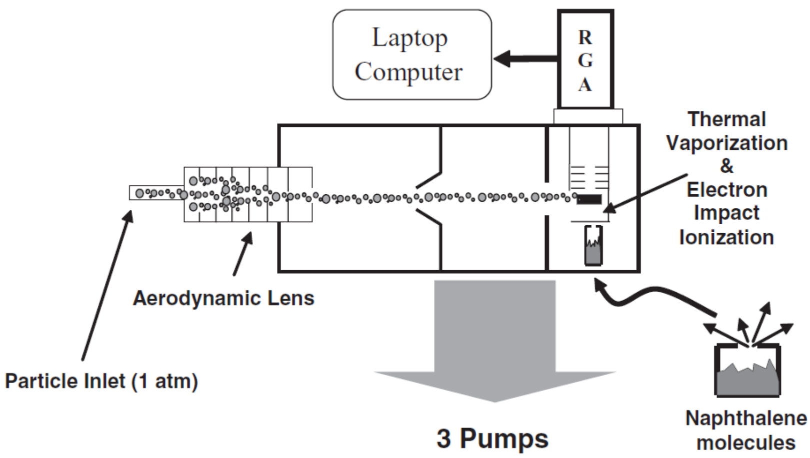

Figure 4: Schematic of the ACSM. Reproduced from (Ng et al. 2011).

The ACSM sensitivity and time resolution are reduced compared to the AMS due to the use of lower-costing components. However, the ACSM has sufficient sensitivity to provide chemically speciated mass concentrations and aerosol mass spectra for typical urban aerosol loading (Takahama et al. 2013).

3.1.3 Chemical Ionisation Mass Spectrometer (CIMS)

The HR-ToF-CIMS (hereafter CIMS) measures concentrations of gas-phase compounds in real time by chemically ionising the analyte. This instrument is capable of providing measurements every second, which gives the opportunity to measure oxygenated VOC compounds in a high time resolution. The CIMS using iodide as reagent ion was first presented by Lee et al. (2014). Here a mixture of gas methyl iodide and H_2O with N_2 as the carrier gas was used to finally generate ions using polonium-210 (Le Breton et al. 2014). Figure 5 shows a schematic of the CIMS, where ions are focused through four stages of differential pumping, by using five pumps. Sections S2 and S3 house quadrupole guides to provide energetic homogenization. Section S4 focuses ions, by using optical lenses, onto the ToF mass spectrometer, giving a high sensitivity of >300 ions·s^{-1}·$pptv^{-1}$. Due to the soft ionisation, the CIMS preserves the chemical composition of the parent molecule.

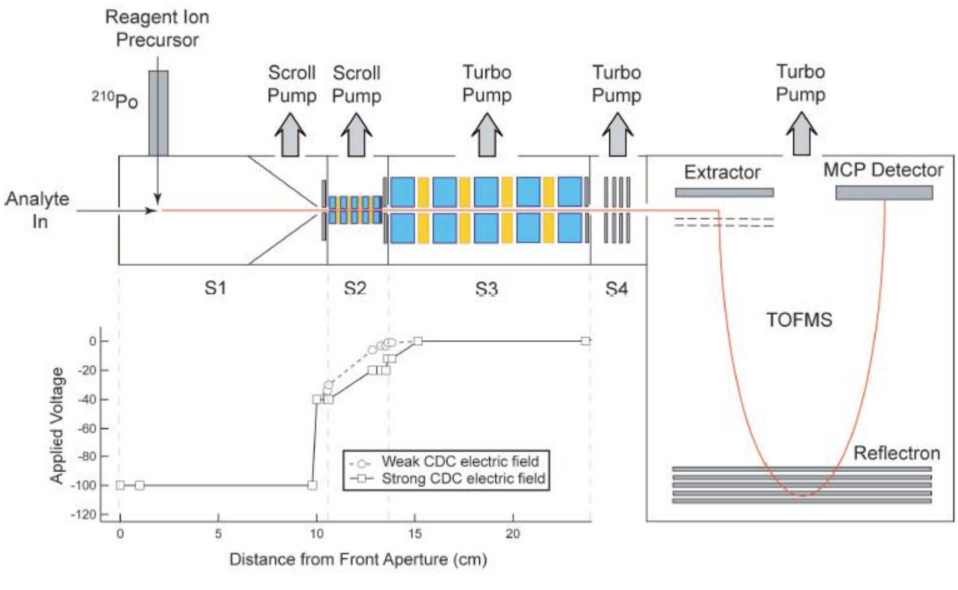

Figure 5: Schematic of the CIMS. Reproduced from (Bertram et al. 2011).

Iodide is used as a reagent ion due to the following characteristics: it has a large negative mass defect, allowing it to remain separate from other ions, it ionises a wide range of detectable compounds (mainly oxygenated volatile organic compounds and various inorganic species) and it is relatively easy to generate iodide ions (Brophy and Farmer 2015).

3.1.4 Filter Inlet for Gases and AEROsols (FIGAERO)

The FIGAERO, when coupled to the CIMS, collects particles on a Teflon filter while gases are being measured by CIMS with further thermal desorption of particles that are then analysed using separate ports. This arrangement allows measurements in near real-time both gases and aerosols (Lopez-Hilfiker et al. 2014). The inlet allows continuous measurements of gases while collecting particles on a Teflon filter.

Detail information of the components of FIGAERO inlet is shown in Figure 6. The movable tray (red), which holds a filter, is used to change between sampling gases while collecting particles (Fig. 6.B) and particle analysis mode (Fig. 6.C). In the particle analysis mode, once the particles are collected, the tray changes position to the heating tube where a thermal desorption takes place using N_2, which is heated ramping from ambient temperature up to 200° C, typically over 15 minutes. For quality assurance, it is recommended to take blank filters to determine background particle concentrations. Particle blank manifold is used to block particles from reaching the main manifold in order to determine background concentrations in the filter.

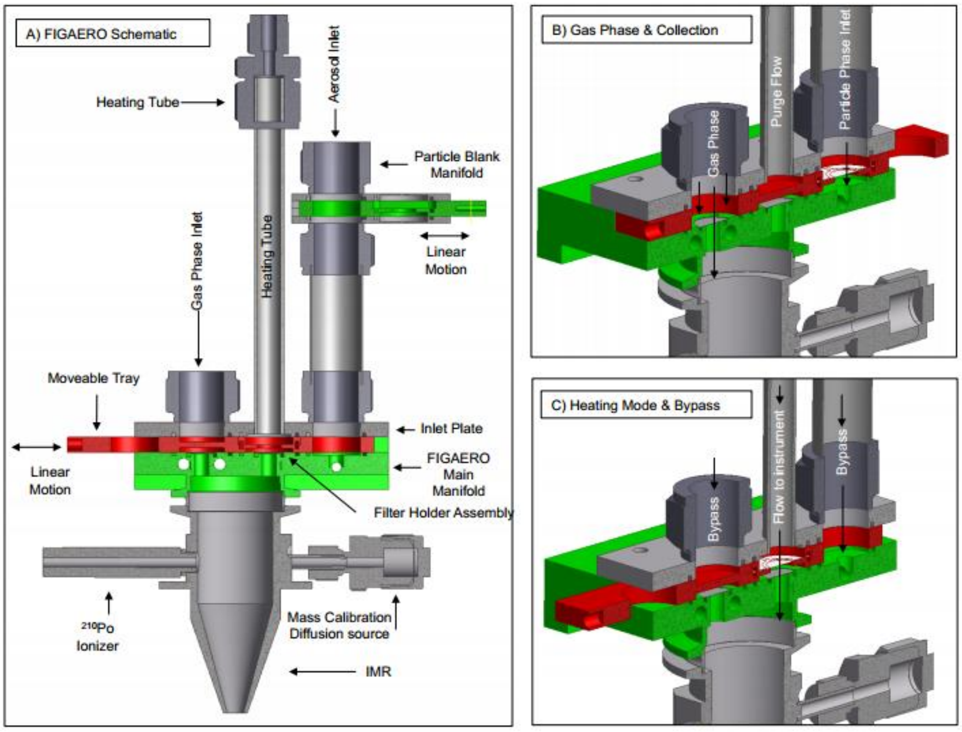

Figure 6: Schematic of the FIGAERO. Reproduced from (Lopez-Hilfiker et al. 2014).

3.2 Source apportionment techniques

The human being is the basic tool to identify the source of different pollutants. Whether by sight or smell, we can identify where pollutants are coming from and possibly, to determine specific pollutant sources; such as chlorine from swimming pools, gas leaks from stoves or smog from a fire.

Source apportionment is an invaluable tool for policy making. The information obtained is of fundamental importance to determine which anthropogenic activity should be aimed to be reduced, eliminated or not even started, depending on the environmental impact. Another application of source apportionment tools is to perform health studies. There are different steps to study the impact of air pollution on health, which involve identifying the source of pollutants; characterising pollutants and their concentrations; quantifying pollutant concentrations to which the public is exposed; determining the actual dose the public intakes; to determining the human health response (NRC 1998). Poor air quality is originated from the source of pollutants; hence, in order to more efficiently mitigate the impact of air pollution on health, it is necessary to understand the different sources related to atmospheric pollutants.

The first techniques for source identification include numerical and statistical analysis, for instance, correlation of wind direction and speed with pollutants to determine source locations (Henry et al. 2002;Rigby and Toumi 2008). Another way to evaluate monitoring data is to subtract the measured concentrations at regional background levels from urban background or roadside levels to identify contributions among the different sites (Yin et al. 2010). More sophisticated computational tools to identify sources and to quantitatively determine their concentrations include numerical modelling, which involves the use of mathematical equations to determine the number and type of atmospheric pollutant sources.

Based on the type of analysis, there are two types of models: source-orientated and receptor-orientated models. Source-orientated models use mathematical algorithms to simulate pollutants dispersion in the atmosphere; starting from the source emissions, simulating the transport, the chemical processes (when the model involves chemical reactions) and the deposition (Leelossy et al. 2014). Receptor-orientated models use the pollutant concentrations measured at the receptor site to determine the source contribution, using the mass conservation of the species principle (Henry 2002).

3.2.1 Source-orientated models

Source-orientated models are used to determine the transport of pollutants, emitted from specific sources, and their spatial concentrations. These emissions can be estimated from previous knowledge of a set of sources (i.e. industrial processes), using emission factors and from emission inventories. Source-orientated models use data from emission inventories to simulate the emissions dispersion (Kulmala et al. 2011;Beevers et al. 2013). This approach is not only useful when analysing the current pollutant concentration but it can also be used to study the different possible scenarios when applying mitigations or increasing concentrations. However, one downside of using inventories data is not available or is not elaborated in the detail required (Viana et al. 2008).

Apart from knowing pollutant concentrations and contributions from different sources, source-orientated models can be used to determine specific areas affected by high pollutant concentrations. When varying input data to the model, it is possible to simulate different scenarios and determine sites of impact. For example, if a new industry is going to be built, it is possible to determine the location with least impact to the inhabitants of a city. It is also possible to design monitoring networks according to different sources and characteristics of the city that will influence ambient concentrations, where the objective would be to determine the number of monitoring sites that should be representative of the area of interest.

There are different model classifications: based on the frame time there are short-term and long-term models, based on geographical context there are global, continental, regional and local models. Based on the chemistry processing, they can be categorised according to whether they involve pollutant chemical reactions, known as chemical transport models (CTM) or if they only involve transport into the atmosphere without chemical processes, known as dispersion models (De Visscher 2014).

Gaussian plume models are the basic source-orientated model. This class of models considers wind speed, wind direction and turbulent diffusivity to be constant over time and space, considerations that are not met in real conditions. The advantage of these models is their simplicity and reduced computational time, while compromising accuracy compared to more sophisticated models. They tend to offer a good accuracy below 10-20 km of the study area (De Visscher 2014). Examples of these models are the Industrial Source Complex (ISC3) models, (with the short and long-term versions available), the SCREEN3 and AERMOD (https://www.epa.gov/scram, accessed: 20/11/2017). The UK has developed a wide range of modelling software (http://www.cerc.co.uk/environmental-software.html, accessed: 05/12/2017), with different versions of the advanced dispersion model (ADMS). For instance, the ADMS5 simulates emissions from existing and planned industrial complexes. The ADMS-Urban model is used for air quality management in urban areas, with the possibility to analyse motorways, roads and industrial areas to a street resolution. The AMS-Roads simulates the dispersion of emissions from networks of roads and the ADMS-Airport simulates the air quality at airports.

Another way to categorise source-orientated models is the way they analyse the system: Eulerian or Lagrangian models, which study the fluid motion from different perspectives (Leelossy et al. 2014). Eulerian models use a gridded system monitoring atmospheric processes and properties over time. They show a good performance over long distances and show a better performance with area (as opposed to point) sources than Lagrangian. However, they are computationally time-consuming and the time increases when a high grid resolution is needed. This class of model is suitable for chemical reactions and can predict photochemical smog. An example of an Eulerian model is the Community Multiscale Air Quality Modeling System, CMAQ (Byun and Ching 1999).

On the other hand, Lagrangian models study the system by defining an "air parcel", where individual air parcels are followed from source to receptor. The different position over time is called trajectory and it is possible to follow trajectories either backward (backward trajectories) or forward (forward trajectories). An example of a Lagrangian model is Numerical Atmospheric Dispersion Modelling Environment (NAME), which is a model developed by the UK Meteorological Office (https://www.metoffice.gov.uk, accessed: 02/11/2017).

3.2.2 Receptor-orientated modelling

Receptor-orientated modelling, which has been a useful tool proven to be effective to identify pollutants' sources for many decades (Henry 2002), determines the source of pollutants measured at a specific site. Receptor-orientated models use on-site measurements to identify sources and apportion concentrations based in the principle of mass conservation, where it is assumed that pollutant concentrations measured at the receptor site are made of the sum of all sources (Hopke 1991). Receptor models differ based on the information needed to run it and the equations used to separate the sources. The two main modelling approaches are Chemical Mass Balance (CMB) and multiple factor analysis.

CMB is used to quantify sources of atmospheric pollutants. This model requires profiles of potentially contributing sources and data collected at a single receptor site (Schauer et al. 1996). In order to determine a composition profile, it is essential to identify the chemical species related to the source and their corresponding proportion to the source. CMB separates sources, sample by sample, giving the opportunity of getting daily information, which is useful to address air quality matters (Begum et al. 2007). As CMB can be applied even to a single sample, it offers valuable information when having a limited number of samples, where other receptor models cannot be used.

CMB considers the number of sources and their composition is known (Schauer et al. 1996). The disadvantages are that it cannot deconvolve sources that have a similar composition and it can deconvolve only the sources to which the user has the composition profiles. When analysing daily samples, CMB cannot give higher time resolution, which can be achieved with other receptor models that deconvolve sources from high time resolution measurements. Composition profiles from a large dataset can be used in a smaller dataset if it is expected to have similar sources on both sites (Begum et al. 2007).

Examples of multiple factor analysis include positive matrix factorisation (PMF) and the multilinear engine (ME-2). PMF and ME-2 are the solvers used in this work, hence they will be explained more in detail in the following sections.

3.2.3 Positive Matrix Factorisation (PMF)

PMF is a least-squares approach based on a receptor-only bilinear factor analysis model (Paatero and Tapper 1994). PMF is "a posteriori" technique, which means that it does not use previous knowledge of pollutants. The advantage of PMF is the fact that it constrains positive profiles and contributions, an important characteristic for real environmental parameters such as pollutant concentrations (Paatero et al. 2002).

$$X = GF + E \tag{1}$$

Equation 1 is the bilinear model, where X is the measured matrix. G represents the time series of a factor and F the profile of this factor (mass spectrum when analysing mass spectrometer measurements). E represents the model residual. PMF determines the solution using a weighted least square fit to calculate the proper e_{ij} by minimizing the sum of the normalized Q (Equation 2).

$$Q = \sum_{i=1}^{m}\sum_{j=1}^{n}\left(\frac{e_{ij}}{\sigma_{ij}}\right)^2 \tag{2}$$

Where e_{ij} are the residuals and σ_{ij} the estimated uncertainty for the points i and j.

However, analysing Q may not be the best way to monitor the solutions due to the fact that the expected value depends on the number of selected factors and the size of the data matrix. Thus, it is better to normalize Q by the degree of freedom of the model solution, named Qexp using equation 3 (Paatero et al. 2002).

$$Q_{exp} \cong n * m - p * (m + n) \tag{3}$$

Where p is the number of factors chosen, n is the number of samples and m the number of mass spectra.

Ideally, if the model accurately captured the variability of the measured data, it would be expected to have Q/Q_{exp} values close to 1. However, this value tends to change due to different variations in the data and overestimation of input data errors. Thus, it is advisable to explore the relative change of this ratio within different model runs; large decreases suggest an improvement in the different solutions. Solutions using least squares approach to solving a factor analysis problem may have linear transformations (also known as rotations). Rotational ambiguity represents all the "allowed" rotational transformations, T, that may be applied to G and F (Equation 4). There are two types of rotations: pure and approximate. For pure rotations, Q does not change after the rotations:

$$\bar{G} = GT \qquad \text{and} \qquad \bar{F} = FT^{-1} \tag{4}$$

T is the non-singular matrix of dimension p x p
T^{-1} is the inverse of T
$\bar{G}$ and $\bar{F}$ are the rotated matrices of G and F respectively.

Thus, the multiplication of $\bar{G}\bar{F}$ is equal to the multiplication of GF and Q does not change.

For approximate rotations, the multiplication GF changes and, therefore Q also changes. These rotations are considered acceptable if the Q value does not increase "significantly" (Paatero et al. 2002). It is advisable to explore the different solutions to study the changes in Q/Q_{exp}. PMF limits these rotations by constrained non-negative values. However, there are cases where rotations are possible even with this constraint, giving the possibility of having an infinite number of possible solutions. PMF controls rotations with the user-defined parameter Φ, called fpeak (Paatero et al. 2002).

3.2.4 Multilinear Engine 2 (ME-2)

ME-2 is a multivariate solver (Paatero 1999) that can determine solutions using the same data model as PMF. One advantage of ME2 over PMF is that the rotational ambiguity can be reduced by using the previous knowledge of profiles or time series. ME-2 can range from the completely constrained profiles in CMB to the unconstrained PMF as well as all the partially constrained solutions (Paatero and Hopke 2009). ME-2 partially constrains solutions using the *a* value approach (Canonaco et al. 2013). In the *a* value approach, the factor profiles (elements of F matrix) and/or the time series (elements of G matrix) may be constrained using target mass spectra/time series as a reference (Equations 5 and 6). The *a* value ranges from zero to one, the closer to zero the more constrained the solution is.

$$f_{j,solution} = f_j \pm a * r_j \tag{5}$$

$$g_{j,solution} = g_j \pm a * r_j \tag{6}$$

Where f and g represent a row and a column of the F and G matrices, respectively. The *a* value controls the range of the output F/G to vary from the input F/G, with values ranging between 0 and 1. If one factor is partially constrained with a-value=0.1 with a specific target mass spectrum, it means ME-2 will be looking for the lowest Q/Qexp among solutions that match this target mass spectrum and allowing it to vary ± 10%.

3.2.5 Summary of source apportionment techniques.

With different advantages and disadvantages, both source-orientated and receptor-orientated models provide important information to study aerosol spatial-temporal behaviour and identify their main sources. Source-orientated models range from computationally basic Gaussian plume models to more accurate, fundamental models which are highly computational demanding.

Direct comparisons have been performed between these two approaches. For instance Chen et al. (2016), investigated the VOC emissions of two petrochemical complexes, evaluating the performance of CMB and ISC and performing a health risk assessment. When comparing with monitoring data, ISC showed to be reliable, with small variances under different conditions such as day-night time and dry-wet seasons. Also, CMB results were more consistent with data from Taiwan Emission Data System. However, when looking at the adverse health risks estimation, ISC was overestimated (75%-134%) when compared with measured data and CMB underestimated (27%-54%). It is important to carefully select the model to be used based on the resources available and the questions to be answered, among other selected criteria, to obtain the performance required when doing source apportionment.

From the three main receptor models, CMB, PMF and ME-2, the latter has the advantage of offering flexibility in the analysis by partially constraining the solutions with the use of information from previous studies, in the way of mass spectra or time series. While PMF does not require previous information, CMB requires complete information of the sources to determine the different concentrations. This use of additional constraints on ME-2 source apportionment tool was seen as a great advantage and to be the future of source apportionment by Henry (2002). However, the ME-2 analysis needs to be performed with caution as the success depends on the target mass spectra/time series used and the methodology applied to objectively select the solution that best deconvolves OA sources.

It is worth remembering source apportionment models apply mathematical equations and do not identify pollutant sources automatically. It is the user who, after analysing results and preferably comparing with external data, interprets the different factors as potential pollutant sources. The highest accuracy will be achieved when the model has been chosen according to the needs and resources of the user.

Chapter 4

Recent Organic Aerosol studies

The use of factorization tools such as PMF and ME-2 deconvolvolves OA sources from aerosol mass spectrometry measurements. Characteristic peaks are used for the mass spectrum interpretation in order to to identify different sources. Biomass burning OA (BBOA) have characteristic peaks at m/z 60 ($C_2H_4O^+$) and 73 ($C_3H_5O^+$); m/z 60 is related to anhydrosugar fragments, such as levoglucosan, which are produced during cellulose pyrolysis (Alfarra et al. 2007). Correlations of BBOA with acetonitrile, levoglucosan, and potassium have been previously identified (Ng et al. 2010). In different environments, Cooking OA (COA) has been identified to have a significant contribution to OA (Allan et al. 2010;Mohr et al. 2012;Crippa et al. 2013). COA presents m/z peaks similar to the hydrocarbon-like OA (HOA) spectrum (m/z 55 and m/z 57, dominated by the $C_xH_y^+$ family) but with a lower peak at m/z 57. These two peaks have been used to identify this important source (Lanz et al. 2007;Mohr et al. 2009;Allan et al. 2010).

SOA are the main constituents of OA, ranging from 20% in urban areas to 90% in rural sites (Zhang et al. 2007). In general, there are two types of SOA, one highly aged oxygenated fraction with low volatility, namely Low Volatile Oxygenated OA (LVOOA) and one more volatile fraction known as Semi-volatile Oxygenated OA (SVOOA). In general, SVOOA represent fresh SOA, which, after photochemical processing, evolve into LVOOA (Jimenez et al. 2009). LVOOA can be distinguished by a dominant peak at m/z 44 (corresponding to the CO_2^+ ion) and SVOOA components typically showing a higher peak at m/z 43 (mostly $C_2OH_3^+$). SOA, more than a source, are considered as a continuum of oxygenated organic aerosol properties in atmospheric aerosols. This ageing of OA components can be explored in the f43-f44 space (f43 and f44 represent the ratio of m/z 43 and m/z 44 total signal, respectively to the total signal of the mass spectrum), where LVOOA has higher f44 and lower 43 than SVOOA. (Ng et al. 2010;Morgan et al. 2010). It is important to bear in mind that Ng et al. (2010) states that classification of LVOOA and SVOOA, as well as their composition, may change from site to site, thus the LVOOA composition at one site is not the same as in a different place.

Studies suggest that LVOOA follows the time trends of SO_4 with a build-up in the afternoon (Lanz et al. 2007) and SVOOA may have a temperature dependent correlation with NO_3 by condensing during the night and further reevaporation during the day (Ulbrich et al. 2009). However, not every site presents this behaviour; for instance, in a study carried out at North Kensington site, London by Young et al. (2015), a difference in the time series of SVOOA and NO_3 was found, suggesting they presented different properties and/or sources. NO_3 concentrations depend on the availability of precursor emissions but also on the season, ambient conditions, and air mass trajectory rather than any one factor (Young et al. 2015).

Organic-nitrogen containing species, their characteristics and effects on human health have been identified and investigated for decades (Fernandez et al. 1992;Muthuramu et al. 1993). However, an increasing interest to investigate them in more detail has recently become apparent due to new methodologies developed in the last few years (Farmer et al. 2010;Hao et al. 2014;Lee et al. 2016). In this work, the acronym particulate organic oxides of nitrogen (PON) has been used, which involves both nitrate and nitro organic compounds. PON is composed of a wide range of different species, making it challenging to directly quantify its concentrations in a high time resolution scale. Hence, AMS measurements have been performed, using m/z 30 as a characteristic signal to identify nitrogen-containing aerosols, to quantify PON concentrations using the Farmer method (Farmer et al. 2010;Kiendler-Scharr et al. 2016) or PMF analysis (Hao et al. 2014;Xu et al. 2015).

4.1 On-line mass spectrometry studies

The AMS has been widely used for measuring aerosol concentrations all around the world in a wide range of locations. These include laboratory experiments to study different types of combustion scenarios (Schneider et al. 2006), aircraft measurements to determine the OA aging from biomass burning (Cubison et al. 2011) and to explore the vertical OA profile (Heald et al. 2011). During 2008-2009, Crippa et al. (2014) carried out a comparison between datasets of 25 AMS across Europe. The average OA concentrations for different types of sites were: 0.66 $\mu g \cdot m^{-3}$ Jungfraujoch (high altitude), 0.85 $\mu g \cdot m^{-3}$ Mace Head (remote), 3.21 $\mu g \cdot m^{-3}$ Harwell (rural) and 8.20 $\mu g \cdot m^{-3}$ Barcelona (urban), highlighting the effect anthropogenic emissions have on OA concentrations in urban environments. The first long-term sampling to study the behaviour of non-refractory aerosol in London was carried out employing a cToF-AMS from January 2012 to January 2013, located at the urban background site of North Kensington (Young et al. 2015). OA, NO_3, SO_4, NH_4 and Cl were measured, obtaining the following average concentrations: 4.32, 2.74, 1.39, 1.30 and 0.15 $\mu g{\cdot}m^{-3}$, contributing 43, 28, 14, 13 and 2%, respectively, to the total submicron mass. One of the conclusions of this study was that further research should be performed to increase our understanding of solid fuel OA and COA.

Recent AMS studies (Table 6), involve off-line AMS analysis (Daellenbach et al. 2017). Off-line samples, on quartz filters, were taken in nine different sites in Switzerland using a hi-volume sampler, with further OA source apportionment using ME-2. In order to perform AMS off-line analysis, four punches of 16 mm of diameter were sonicated with 10 mL of ultrapure water, nebulised, dried and injected to the AMS. Another off-line study was performed by Chakraborty et al. (2017) who quantified water soluble OA (WSOA), identifying the presence of organic nitrates (ON) in WSOA and determining that 2/3 of ON was found to be in WSOA.

Further aerosol characterisation using AMS, along with a variety of instruments, involve aerosol volatility distribution of food cooking OA in a laboratory study (Louvaris et al. 2017); wood burning OA characterisation (Florou et al. 2017). A focus in urban studies in different countries has been observed, for instance in Switzerland (Daellenbach et al. 2017), Finland (Pirjola et al. 2017), performing physico-chemical characteristation of aerosols measured in a mobile laboratory van, The United States (Parworth et al. 2017) and Italy (Struckmeier et al. 2016). Another important aspect of urban environments that has been recently studied looks at coastal sites such as Korea (Lee et al. 2017) and Ireland (Dall'Osto et al. 2017). On this topic, Rivellini et al. (2017) presents results of the first AMS deployed in Africa, with data of a coastal site in Mbour, Senegal.

Table 6: Description of recent studies using AMS. Last time updated: December 2017

Reference	Site location	Site type	Sampling time
(Chakraborty et al. 2017)	Kanpur and Allahabad, India	Urban, off-line	Dec 2015– Feb 2016
(Dall'Osto et al. 2017)	Cork, Ireland	Coastal-Urban	01-22 Feb 2009
(Louvaris et al. 2017)	Patras, Greece	Laboratory - COA	
(Daellenbach et al. 2017)	* Nine sites, Switzerland	Ambient, off-line	Jan-Dec 2013
(Florou et al. 2017)	Athens and Patras, Greece	Urban	Winter 2012 and Winter 2013
(Lee et al. 2017)	Boseong and Gwangju, Korea	Coastal and urban	Autumn 2012 and Autumn 2013
(Rivellini et al. 2017)	Mbour, Senegal	Coastal	March to June 2015
(Struckmeier et al. 2016)	Rome Italy	suburban and urban	Oct-Nov 2013, May-Jun 2014
(Pirjola et al. 2017)	Helsinki, Finland	Urban - mobile	15-27 February 2012
(Parworth et al. 2017)	California, USA	Urban	Jan-Feb 2013

* Basel,Bern, Payerne, Zürich, Frauenfeld, St. Gallen, Vaduz, Magadino and San Vittore.

The ACSM was deployed, for the first time, at Queens NY, from July 13th to August 4th, 2010 (Ng et al. 2011), where a comparison with a HR-ToF-AMS was performed. Both instruments showed a similar trend. These results revealed that there is a very good correlation between the ACSM and the HR-ToF-AMS data with Pearson values ranging from 0.81 to 0.91.

Minguillón et al. (2015) performed OA source apportionment from ACSM measurements in Montseny, a regional background site in Spain. Here, they identified three organic sources in summer (HOA, SVOOA and LVOOA) and three in winter (HOA, BBOA and OOA). SOA resulted to be the highest contributor to OA concentrations, making up more than 80% of total OA in summer and about 60% in winter. A similar high SOA contribution to OA concentrations was observed at the continental background site, Montsec, France. In this site OA, contributions of 71% (OOA), 5% (HOA) and 24% (BBOA) were calculated (Ripoll et al. 2015).

Many studies have been performed using the ACSM during the year 2017. Claeys et al. (2017) studied primary marine aerosol properties in a coastal site in the western Mediterranean. Another study in the Mediterranean area involves ACSM measurements along with VOCs and black carbon, being able to perform source apportionment on VOCs and OA-ACSM measurements (Michoud et al. 2017b). Drinovec et al. (2017)

performed ambient measurements in Paris, France to investigate the filter loading effect in photometers. China, in particular, has been recently studying atmospheric aerosols using the ACSM (Li et al. 2017e;Zhao et al. 2017a). Li et al. (2017a) studied the contribution of coal and biomass combustion to aerosol concentrations. Li et al. (2017d) investigated the influences of new particle formation in a suburban site. Other studies in China involve analysing local and regional aerosol sources during the spring festival (Wang et al. 2017a). Studies have been performed in different cities in China, focusing on nitrogen species and their formation mechanisms (Yang et al. 2017;Ge et al. 2017).

The FIGAERO inlet, attached to a CIMS, has been used in different environments. A study performed on a remote site investigated the volatility of SOA formed from alpha pinene ozonolysis and OH oxidation (Lopez-Hilfiker et al. 2015). This study found FIGAERO measurements to correlate well with OA measured by AMS, being able to explain at least 25%-50% of OA. Schobesberger et al. (2016) determined formic acid fluxes from measurements performed at a boreal forest canopy and their dependency on temperature and relative humidity. Liu et al. (2016) used the FIGAERO, along with other instruments, to measure isoprene SOA formation from non-IEPOX pathway in a chamber experiment, which allowed understanding SOA formation in biogenic-reach regions with limited anthropogenic emissions. Gaston et al. (2016) determined the molecular composition of wintertime particulate matter, identifying a major contribution from residential wood smoke. Levoglucosan concentrations from 0.002 to 19 $\mu g \cdot m^{-3}$ were measured, with a median mass concentration of 0.9 $\mu g \cdot m^{-3}$.

Thompson et al. (2017) performed an intercomparison of ground-based measurements of gas/particle (G/P) partitioning. Measurements were taken in Summer 2013 in the United States; pinonic acid ($C_{10}H_{16}O_3$), pinic acid ($C_9H_{14}O_4$), and hydroxyl glutaric acid ($C_5H_8O_5$) were compared with four instruments; the Semi-Volatile Thermal desorption Aerosol Gas chromatograph (SV-TAG), the HR Thermal Desorption Proton-Transfer Reaction Mass Spectrometer (HR-TD-PTRMS) and two FIGAERO-CIMS: one using acetate and the other one using iodide as reagent ions. Gas to particle (G/P) partitioning calculated from these measurements was also compared with modelled G/P partitioning. All the instruments showed similar G/P trend as values obtained with the model, increasing G/P ratios when increasing vapour pressure.

4.2 PMF/ME-2 studies

The first time PMF was applied to OA data measured with an AMS was performed by Lanz et al. (2007), using measurements taken at an urban background site in Zurich in the summer of 2005. Six sources were identified: LVOOA, SVOOA, HOA, Charbroiling-like OA, BBOA, and a minor source, COA. Subsequently, PMF was successfully applied to other datasets, acquired from a wide range of sampling sites and with different techniques.

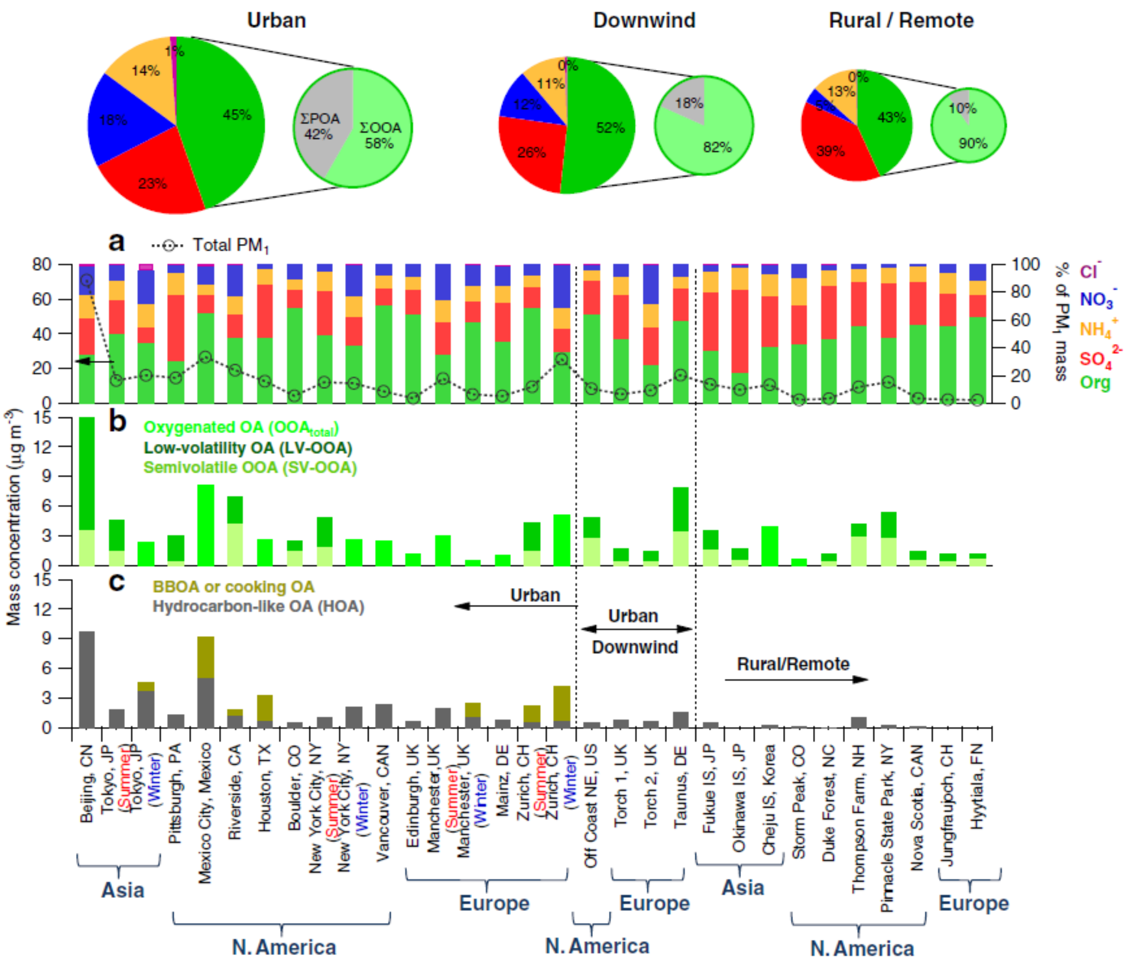

Figure 7: Results of PMF analysis to 43 studies around the world. Average total mass concentration (a); average mass concentration of SOA (b); average mass concentration of POA (c). Reproduced from (Ng et al. 2010).

Figure 7 presents the results of 43 studies carried out at different sites around the world (Ng et al. 2010). It is worth emphasizing the high proportion OA represented in the total aerosol concentrations at all the different sites (From urban to rural). This study provides a broad overview of aerosol composition and the importance of SOA. Despite showing only BBOA and HOA sources, in other studies it is possible to find other relevant sources such as COA (Allan et al. 2010;Huang et al. 2010;Liu et al. 2012;Mohr et al. 2012;Sun et al. 2013), these studies started showing interest in COA as an important contributor to POA concentrations.

Lanz et al. (2008) performed the first ME-2 analysis using data from an AMS deployed at an urban-background site in Zurich in 2008. In this study, ME-2 was successfully applied to deconvolve OA sources in a rural site during winter, an analysis not possible to realize with PMF. The analysis provided a three-factor solution (HOA, BBOA and OOA) determined by partially constraining HOA. The factor analysis results were compared with levoglucosan, SO_4, NO_3, CO, as well as with previously published AMS data, showing good correlations. However, after this study, ME-2 was not widely applied due to its highly time-consuming nature, since it requires a high level of data manipulation due to the possibility to explore the diverse factor solutions available with the different partial constraints. This situation has been improved with the use of the graphic user interface, Source Finder (SoFi, version 4.8) developed by Canonaco et al. (2013), which allows running the bilinear model, with or without constraints, being possible to run CMB, PMF or ME-2. SoFi allows to analyse and compare different solutions to determine the optimal solution.

ME-2 shows a better performance, compared to PMF, when a well-defined profile (chemical fingerprint, for instance, BBOA) has a high diurnal correlation with another factor. In this situation, their time series could not be separated with PMF (Lanz et al. 2010). Canonaco et al. (2013) also state that PMF does not have a good performance under meteorological conditions such as rainfall or boundary layer evolution, increasing the mixing factors. Under these conditions, ME-2 is a useful tool to determine different OA sources.

Crippa et al. (2014) applied the ME-2 tool to 25 AMS datasets across Europe within the framework of the European Integrated project on Aerosol, Cloud, Climate, and Air Quality Interactions (EUCAARI). The AMS collected data from three intensive campaigns part of the European Monitoring and Evaluation Programme (EMEP): 2008 (May–June and September–October) and 2009 (February–March). Figure 8 presents the sampling sites accounting for urban (UR), rural (RU), remote (RE) and high altitude (HA) sites, where is possible to observe higher OA concentrations at urban sites. COA was determined only in Barcelona (BCN) where a considerable contribution to the total OA was calculated. In this comparison with 25 AMS, it was found that constraining 3 factors (HOA-BBOA-COA) reduced the diurnal Q/Q_{exp} to a greater extent than when constraining only 2 factors (HOA-BBOA).

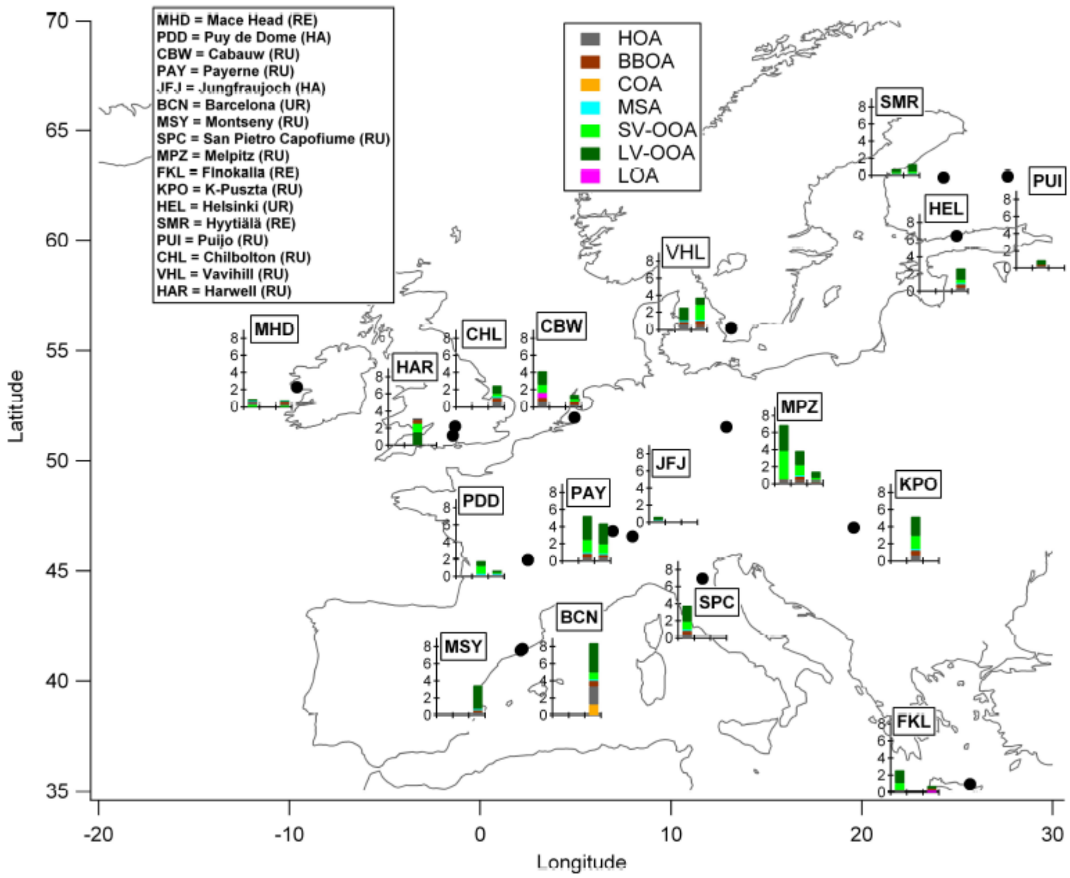

Figure 8: Sampling sites and average OA source contributions. Urban (UR); rural (RU); remote (RE) and high altitude (HA). Reproduced from (Crippa et al. 2014).

Kupiainen and Klimont (2007) determined that the main sources of POA in Europe were emissions from traffic and the residential combustion of solid fuels. Allan et al. (2010) found HOA, solid fuel OA and COA to be the main sources of OA in Manchester and London. Liu et al. (2011) also determined that the main OA sources in Manchester were HOA and BBOA, with emissions from BBOA to be higher during winter due to domestic heating.

Table 7: Studies of OA sources with ME-2 in 2017. Last time updated: December 2017.

Reference	OA sources identified	Site type	Sampling time	Site location
(Zhang et al. 2017b)	IEPOX-SOA, LVOOA, MOOA, HOA	Urban	Summer 2013	Nanjing, China
(Zhang et al. 2017a)	HOA, CCOA, COA, BBOA, OOA1, OO2	Urban	Oct-Dec 2014	Lanzhou, China
(Wolf et al. 2017)	Bacteria-like, COA, LVOOA, SVOOA, HOA	Urban – $PM_{2.5}$	07-19 April 2011	Zurich, Switzerland
(Wang et al. 2017b)	HOA, COA, BBOA, CCOA, LOOOA, MOOOA	Urban	Feb-Mar 2014	Baoji, China
(Schlag et al. 2017)	SVOOA, LVOOA, HULIS, MSAOA, BBOA, HOA	Rural	May-July 2012	Cabauw, Netherlands
(Rivellini et al. 2017)	LCOA, COA, HOA, OOA	coastal	March to June 2015	Mbour, Senegal
(Rattanavaraha et al. 2017)	HOA, BBOA, IEPOXOA, 91Frag, LVOOA, SVOOA	urban	March 2014 - Feb 2015	Atlanta, Georgia
(Qin et al. 2017)	HOA, COA, BBOA, SVOOA, LVOOA	urban	Nov-Dec 2014	Panyu, Guangzhou
(Michoud et al. 2017a)	HOA, SVOOA, LVOOA	Remote	July - August 2013	Ersa, France
(Li et al. 2017b)	HOA,CCOA, BBOA, OOA	Urban	Winter 2015	Handan, China
(Kaltsonoudis et al. 2017)	HOA, COA, BBOA, OOA	Mediterranean	February 2012	Patras, Greece
+(Bozzetti et al. 2017b)	BBOA, LOA, Summer OA and background OA	*three sites	Sep 2013-Sep 2014	*Lithuania
+(Bozzetti et al. 2017a)	HOA, COA, BBOA, OOA, INDOA	Mediterranean	Aug 2011- July 2012	Marseille, France

+ Off-line AMS measurements.

* Urban background (Vilnius), rural (Rūgšteliškis) and rural coastal (Preila).

Studies published during 2017 have identified a wide range of OA sources (Table 7). The most identified OA sources are BBOA, HOA, COA, and secondary OA. However, other types of sources involve; bacteria-like OA, methanesulfonic acid OA (MSAOA), industrial OA (INDOA) and coal combustion OA (CCOA). Bacteria-like OA were identified using a $PM_{2.5}$ inlet in the AMS and the m/z 70 as a tracer. This tracer is related to the contribution of decarboxylation products of amino acids to the $C4H8N^{+}$ ion (Wolf et al. 2015;Wolf et al. 2017). MSAOA factor was attributed to methanesulfonic acid and identified to be related to marine sources (Schlag et al. 2017). INDOA, which were quantified from aerosol off-line filter collection with further AMS-ME-2 analysis, were identified to have high correlations with selenium (Se) (Bozzetti et al. 2017a). CCOA is an important source in places like China, as a result of the high consumption of coal as an energy source. CCOA has been found to have characteristic signals at m/z 41, 43, 44, 55, 57, 69, 91 and 115 and good correlations with chloride (Cl^-) (Zhang et al. 2017a). However, these tracers, m/z ratios and Cl^-, may correlate also with other sources, for example, BBOA and HOA. Hence, it is recommended to analyse other parameters such as diurnal and daily concentrations.

ME-2 can be used to perform source apportionment with any other type of measurements. As a case in point, Visser et al. (2015) performed trace element source apportionment to $PM_{10–2.5}$, $PM_{2.5–1}$ and $PM_{1–0.3}$ measurements with two-hour time resolution. Nine trace element sources were identified varying with diameter size: $PM_{10–2.5}$, brake wear, traffic-related, re-suspended dust, sea/road salt, aged sea salt and industrial; in $PM_{2.5–1}$, brake wear, other traffic-related, re-suspended dust, sea/road salt, aged sea salt and S-rich; and in $PM_{1–0.3}$, traffic-related re-suspended dust, sea/road salt, aged sea salt, reacted Cl, S-rich and solid fuel. Zhang et al. (2015) identified fossil and non-fossil sources of carbonaceous aerosols in four cities in China. This analysis was performed using the following measurements; EC/OC, ions and polycyclic aromatic hydrocarbons (PAHs), oxygenated PAHs, resin acids, anhydrous sugars and AMS off-line measurements.

This section presented a description of the main OA sources including BBOA, HOA and COA, with other sources such as PON, CCOA, INDOA, MSAOA and Bacteria-like OA identified in different parts of the world in sites from rural, Mediterranean and urban. All these OA sources have been identified from aerosol mass spectrometer measurements, both off-line and on-line, and performing ME-2 analysis via the recently developed SoFi interphase. This software has facilitated the source apportionment analysis, with it being possible to identify OA sources around the world. POA have been shown to have an important contribution to total OA concentration. BBOA has a major contribution during winter as a result of biomass burning used for domestic heating. Different studies have been performed exploring COA chemical composition (Dall'Osto et al. 2015) and concentrations in urban environments. However further research has to be done in order to completely understand these sources, their composition and interactions with gases.

Chapter 5

Outline and objectives

Worldwide, air pollution is considered to have one of the greatest impacts on human health (Lim et al. 2012) as well as adverse effects on the environmental resources and damage to property. During the last few decades, air pollution has been a matter of concern in urban environments, especially in cities with more than 10 million inhabitants, known as megacities. It is important to state that the number of megacities has been increasing during the last few decades and this number is expected to continue to increase in the coming years (Molina and Molina 2004). Moreover, the United Nations estimates that by 2030, half of the world's population (4.9 billion inhabitants out of 8.3 billion) will be living in urban environments (United Nations 2012). Developed countries have made great improvements in air quality. Nevertheless, air pollution still represents a significant public health issue (Deguen et al. 2012).

It is important to study atmospheric aerosols due to their negative effects on air quality and climate (Fuzzi et al. 2015). Aerosols have a complex chemical composition, with a variety of sources and physicochemical processes between the particle and gas phases, which are yet to be completely understood. Organic aerosols (OA) represent around 20%-90% of total submicron particulate matter (Zhang et al. 2007). OA are composed of thousands of different species, which makes challenging to determine their sources. In urban environments, their main sources are related to traffic emissions, cooking food, burning biomass among other primary sources, as well as the contribution of secondary organic aerosols produced from physicochemical processes in the atmosphere.

Mass spectrometers have proven to be robust instruments to perform on-line measurements of chemical species. Along with the development of instruments to measure aerosol concentrations, the ability to determine the possible origin of these aerosols is needed; receptor models have been successfully used to identify pollutants sources. PMF is a factorisation tool that has been widely used to perform source apportionment. ME-2, which solves the same equations as PMF, was developed many years ago (Paatero 1999). However, due to its time consuming nature to explore the solution space, it was not until SoFi interphase was developed by Canonaco et al. (2013), which facilitates running and analysing solutions, that ME-2 started being widely applied to perform source apportionment. The increased use of ME-2 to identify pollutant sources showed the need for developing standardised methods to objectively explore the solution space.

The study of ambient measurements is essential to identify pollutant sources in urban environments and understand their processes. Moreover, it is important to study direct fresh emissions from anthropogenic sources in order to understand their chemical composition before they start reacting on the atmosphere and to provide target profiles to be used in future source apportionment studies.

The work presented in this thesis investigates organic aerosols, their sources and chemical characterisation, both from ambient and laboratory measurements. This will be performed by using on-line mass spectrometers such as ACSM, cToF-AMS, HR-ToF-AMS and FIGAERO-HR-ToF-CIMS. The study of ambient measurements will increase our knowledge about aerosol behaviour in urban environments, both during long-term measurements (10 months) and during a special event with high biomass burning concentrations, known as Bonfire Night. OA source apportionment, of ambient measurements, will be performed using PMF and ME-2 factorisation tools. Laboratory measurements will involve detailed analysis of cooking emissions (English breakfast, fish and chips and different types of meats and vegetables) in order to investigate their particle and gas physicochemical properties.

5.2 Objectives

The use of mass spectrometers, performing near real-time measurements of particles and gases, together with the use of tools to perform source apportionment, such as SoFi interphase, provide the opportunity to perform a detailed analysis of OA sources chemical characterisation in different scenarios. This will be investigated with the following objectives:

- To investigate the long-term and seasonal behaviour of OA sources in an urban environment.
- To test ME-2 performance both in long-term measurements and a special nocturnal event with high biomass burning emissions.
- To implement a new technique to objectively determine the optimal solution that separates the OA sources.
- To analyse night-time chemistry of OA, focusing on particulate organic oxides of nitrogen.
- To investigate cooking organic aerosols (COA), their chemical composition, both in the gas and particle phase and the effect of dilution on semi-volatility.
- To identify food cooking markers, both in gas and particle phases, to be used in future source apportionment models.
- To generate mass spectra of OA, both from ambient and laboratory measurements, to be used as input information for future source apportionment studies.

Chapter 6

Results

Paper 1

6.1 Organic aerosol source apportionment in London 2013 with ME-2: exploring the solution space with annual and seasonal analysis

Ernesto Reyes-Villegas, David C. Green, Max Priestman, Francesco Canonaco, Hugh Coe, André S. H. Prévôt, and James D. Allan

www.atmos-chem-phys.net/16/15545/2016/
doi:10.5194/acp-16-15545-2016

Research highlights:

- Here are shown the results of the first ACSM deployed in the UK, analysing long-term aerosol concentrations (10 months). OA sources were deconvolved using the PMF/ME-2 via the SoFi interfase.
- A strategy has been proposed, using predefined statistical tests, to explore the solution space and objectively determine the optimal solution that deconvolves OA sources.
- Five OA sources were identified: biomass burning OA (BBOA), hydrocarbon-like OA (HOA), cooking OA (COA), semivolatile oxygenated OA (SVOOA) and low-volatility oxygenated OA (LVOOA).
- A possible higher contribution of heavy-duty vehicles to air pollution compared to petrol vehicles was identified.

Author contributions:

For this work, Dr David Green and Max Priestman had previously collected the data. I conducted all the data analysis and personally wrote the manuscript and worked on the comments from co-authors as well as addressing the reviewer's comments. Always under the guidance of Dr James Allan as my supervisor.

Blank page

Atmos. Chem. Phys., 16, 15545–15559, 2016
www.atmos-chem-phys.net/16/15545/2016/
doi:10.5194/acp-16-15545-2016

Atmospheric Chemistry and Physics
Open Access
EGU

Organic aerosol source apportionment in London 2013 with ME-2: exploring the solution space with annual and seasonal analysis

Ernesto Reyes-Villegas[1], **David C. Green**[2], **Max Priestman**[2], **Francesco Canonaco**[3], **Hugh Coe**[1], **André S. H. Prévôt**[3], **and James D. Allan**[1,4]

[1]School of Earth, Atmospheric and Environmental Sciences, The University of Manchester, Manchester, M13 9PL, UK
[2]School of Biomedical and Health Sciences, King's College London, London, UK
[3]Laboratory of Atmospheric Chemistry, Paul Scherrer Institute, 5232 Villigen PSI, Switzerland
[4]National Centre for Atmospheric Science, The University of Manchester, Manchester, M13 9PL, UK

Correspondence to: James D. Allan (james.allan@manchester.ac.uk)

Received: 31 May 2016 – Published in Atmos. Chem. Phys. Discuss.: 2 June 2016
Revised: 28 September 2016 – Accepted: 12 November 2016 – Published: 16 December 2016

Abstract. The multilinear engine (ME-2) factorization tool is being widely used following the recent development of the Source Finder (SoFi) interface at the Paul Scherrer Institute. However, the success of this tool, when using the *a* value approach, largely depends on the inputs (i.e. target profiles) applied as well as the experience of the user. A strategy to explore the solution space is proposed, in which the solution that best describes the organic aerosol (OA) sources is determined according to the systematic application of predefined statistical tests. This includes trilinear regression, which proves to be a useful tool for comparing different ME-2 solutions. Aerosol Chemical Speciation Monitor (ACSM) measurements were carried out at the urban background site of North Kensington, London from March to December 2013, where for the first time the behaviour of OA sources and their possible environmental implications were studied using an ACSM. Five OA sources were identified: biomass burning OA (BBOA), hydrocarbon-like OA (HOA), cooking OA (COA), semivolatile oxygenated OA (SVOOA) and low-volatility oxygenated OA (LVOOA). ME-2 analysis of the seasonal data sets (spring, summer and autumn) showed a higher variability in the OA sources that was not detected in the combined March–December data set; this variability was explored with the triangle plots $f44:f43$ $f44:f60$, in which a high variation of SVOOA relative to LVOOA was observed in the $f44:f43$ analysis. Hence, it was possible to conclude that, when performing source apportionment to long-term measurements, important information may be lost and this analysis should be done to short periods of time, such as seasonally. Further analysis on the atmospheric implications of these OA sources was carried out, identifying evidence of the possible contribution of heavy-duty diesel vehicles to air pollution during weekdays compared to those fuelled by petrol.

1 Introduction

Developed countries have made great improvements in air quality. However, air pollution still represents a significant air quality issue, mainly in urban cities, due to the sheer number of inhabitants and the associated anthropogenic emissions resulting from the inhabitants' daily activities (transportation, energy production and industrial activities). Aerosols, in particular, have significant effects on air quality (Watson, 2002; Pope and Dockery, 2006; Keywood et al., 2015).

Organic aerosols (OA) are one of the main constituents of submicron particulate matter, composing 20–90 % of the total submicron particle mass (Zhang et al., 2007). OA are classified according to their origin, either as primary OA (POA) or secondary OA (SOA). POA are directly emitted from a range of sources while SOA are produced from gaseous precursors (volatile organic compounds, VOCs) by chemical reactions in the atmosphere. POA sources range from traffic emissions (hydrocarbon-like OA, HOA), biomass burning OA (BBOA) to OA emissions from cooking (COA), among others. Kupiainen and Klimont (2007) determined that the main sources of POA in Europe were emissions from traf-

Published by Copernicus Publications on behalf of the European Geosciences Union.

fic and the residential combustion of solid fuels. Allan et al. (2010) identified three POA sources in Manchester and London: transport, burning of solid fuels and cooking. SOA are the main constituents of OA, ranging from 64 in urban areas to 95 % in rural sites (Zhang et al., 2007). Previous source apportionment studies (Zhang et al., 2011) often identified a highly oxygenated fraction with low volatility (LVOOA) and a less oxygenated and more volatile species, semivolatile oxygenated OA (SVOOA). In general, SVOOA represent fresh SOA, which, after photochemical processing, evolve into LVOOA (Jimenez et al., 2009). POA and SOA concentrations vary over seasons and years, thus in order to study the OA sources and processes as well as their impacts on air quality, it is necessary to carry out long-term measurements and subsequent source apportionment data analysis.

Aerosol mass spectrometry has been widely used for measuring aerosol concentrations in a wide range of ground-based measurements (Hildebrandt et al., 2011; Mohr et al., 2012; Saarikoski et al., 2012; Young et al., 2015b). In particular, the Aerosol Chemical Speciation Monitor (ACSM), which has been recently developed (Ng et al., 2011), has been used to carry out long-term measurements of non-refractory submicron aerosols around the world, for instance in an industrial–residential area in Atlanta, Georgia (Budisulistiorini et al., 2014), on a high-elevation mountain in Canada (Takahama et al., 2011), at background locations in South Africa (Vakkari et al., 2014) and Spain (Minguillón et al., 2015a; Ripoll et al., 2015), on a semi-rural site in Paris (Petit et al., 2015) and at an urban background site in Switzerland (Canonaco et al., 2015).

Source apportionment techniques have been widely used to quantitatively determine aerosol sources. The main source apportionment models include chemical mass balance (CMB) and positive matrix factorization (PMF).

CMB uses prior knowledge of source profiles and assumes that the composition of all sources is well defined and known (Henry et al., 1984). This technique is ideal when changes between the source and the receptor are minimal, although this barely happens in real atmospheric conditions and the constraints may add a high level of uncertainty.

PMF is a least-squares approach based on a receptor-only multivariate factor analytic model (Paatero and Tapper, 1994). The main difference between PMF and CMB is that PMF does not require any information as input to the model and the profiles and contributions are uniquely modelled by the solver (Paatero et al., 2002). PMF was applied to OA data measured with an AMS for the first time by Lanz et al. (2007), using measurements taken at an urban background site in Zurich in the summer of 2005, where six OA sources were determined: LVOOA, SVOOA, HOA, charbroiling-like OA, BBOA and COA. Subsequently, PMF was successfully applied to other data sets, acquired from a wide range of sampling sites and with different techniques, Ng et al. (2010) compiled and analysed 43 studies carried out at different sites around the world. This study provided a broad overview of aerosol composition and the importance of SOA as well as BBOA and HOA sources. In other PMF studies, it was possible to find other relevant sources such as COA (Allan et al., 2010; Huang et al., 2010; Liu et al., 2012; Mohr et al., 2012; Sun et al., 2013; Crippa et al., 2013a).

ME-2 is a multivariate solver that determines solutions using the same equations as PMF (Paatero, 1999), with the possibility of using previous knowledge (factor time series and/or factor profiles) as inputs to the model to partially constrain the solution, thereby reducing the rotational ambiguity (Paatero et al., 2002). This leads to more interpretable PMF solution(s) as shown in Lanz et al. (2008), in which three sources of OA were successfully determined (traffic related, solid fuel and secondary OA) during winter in an urban background site in Zurich. Here, unconstrained PMF runs failed to identify the environmental solution. This was most probably due to a high degree of temporal covariation in the OA sources driven by low temperatures and periods of strong inversion.

The development of the Source Finder (SoFi) interface (Canonaco et al., 2013) written on the software package Igor Pro (WaveMetrics, Inc.), together with a further standardized approach developed by Crippa et al. (2014), allowed different OA source apportionment studies to be undertaken. These include a study at a suburban background site in Paris, France during January–March 2012 (Petit et al., 2014); laboratory studies analysing atmospheric ageing from the photo-oxidation of α-pinene and of wood combustion emissions in smog chambers and flow reactors (Bruns et al., 2015) and long-term measurements (February 2011–February 2012) carried out at an urban background site in Zurich, Switzerland on differences in oxygenated OA during summer and winter periods (Canonaco et al., 2015). As part of the ACTRIS project (Aerosols, Clouds, and Trace gases Research InfraStructure Network; Fröhlich et al., 2015), an intercomparison between 14 ACSMs and one high-resolution time-of-flight aerosol mass spectrometer (HR-ToF-AMS) was carried out at the SIRTA site in Gif-sur-Yvette near Paris, identifying four sources: hydrocarbon-like OA (HOA), OA related to cooking activities (COA), biomass burning related OA (BBOA) and oxygenated organic aerosol (OOA). These four sources were successfully identified from HR-ToF-AMS measurements with unconstrained PMF analysis. However, in the case of the ACSM data sets, it was necessary to partially constrain solutions via ME-2 analysis, probably due to the low signal to noise ratio of ACSM data compared to the AMS and the rural site type. Furthermore, new ME-2 source apportionment studies have been published this year (Bozzetti et al., 2016; Fountoukis et al., 2016; Milic et al., 2016; Elser et al., 2016), and even more are expected to come due to the successful application of SoFi. Thus, new strategies to systematically explore the solutions are needed.

This study includes data analysis of the first ACSM instrument deployed in the UK at the North Kensington site from March to December 2013, using the recently developed graphical interface SoFi to perform non-refractory OA source apportionment analysis with the ME-2 factorization tool, implementing a strategy to determine the solution that best identifies OA sources, according to the statistical tests applied and providing further discussion of the various identified OA sources.

2 Methodology

The data used in this analysis (5 March–30 December 2013) were obtained using an Aerosol Chemical Speciation Monitor (ACSM), deployed at the urban background site in North Kensington, London. This instrument is owned by The Department for Environment, Food and Rural Affairs (DEFRA) and is part of the Aerosols, Clouds, and Trace gases Research InfraStructure Network (ACTRIS).

Source apportionment of OA was carried out using the PMF model implemented through the multilinear engine tool (ME-2) and controlled via the Source Finder (SoFi) graphical user interface version 4.8, developed at the Paul Scherrer Institute (PSI), Switzerland (Canonaco et al., 2013).

2.1 Site and instrumentation

North Kensington (51.5215°, −0.2129°) is an urban background site located adjacent to a school, 7 km to the west of central London. There is a residential road 30 m to the east with an average traffic flow of 8000 vehicles per day (Bigi and Harrison, 2010). This monitoring site is part of the DEFRA Automatic Urban and Rural Network (http://uk-air.defra.gov.uk/networks/network-info?view=aurn).

As an urban background site, North Kensington is not significantly influenced by a single source or street, and concentrations may be analysed as an integrated contribution from all sources upwind of the site in London. This site is widely accepted as representative of background air quality in central London and has a large set of long-term measurements for various pollutants (Bigi and Harrison, 2010). Different studies have been carried out at this site such as the analysis of elemental and organic carbon concentrations in offline measurements of particulate matter with a diameter less than 10 micrometres (PM_{10}; Jones and Harrison, 2005), PM_{10} and NO_x association with wind speed (Jones et al., 2010), properties of nanoparticles (Dall'Osto et al., 2011), PM_{10} and $PM_{2.5}$ (Liu and Harrison, 2011) and aerosol chemical composition (Beccaceci et al., 2015) in the atmosphere. The first long-term study of the behaviour of non-refractory inorganic and organic aerosols (PM_1) at the North Kensington site analysed cToF-AMS data collected from January 2012 to January 2013 (Young et al., 2015a) A source apportionment analysis was carried out, applying unconstrained PMF runs, with five identified sources: HOA, COA, solid fuel OA (SFOA), SVOOA and LVOOA.

The Aerosol Chemical Speciation Monitor (ACSM) measures, in real time, the mass and chemical composition of particulate organics, nitrate (NO_3), sulphate (SO_4), ammonium (NH_4) and chloride (Cl) ions, with a detection limit of $0.2\,\mu g\,m^{-3}$ for an average sampling time of 30 min (Ng et al., 2011). These chemical species measured by the ACSM are determined according to the same methodology used in the AMS as defined by Allan et al. (2004). In principle, the ACSM is designed and built under the same sampling and detection technology as the state-of-the-art Aerosol Mass Spectrometer (AMS) instruments. However, the ACSM is better suited for air quality monitoring applications due to its lower size, weight, cost, and power requirements; it is also more affordable to operate and is capable of measuring over long periods of time without supervision (Ng et al., 2011).

Time series of pollutants such as BC, CO, NO_x, OC, EC were downloaded from the DEFRA website for the North Kensington monitoring site. Wind speed and direction data were obtained from the meteorological station at Heathrow airport (located 17 km from the sampling site). Wind data from this site were used due to their representativeness of regional winds without being affected by surrounding buildings.

2.2 Source apportionment (ME-2)

The multilinear engine algorithm (Paatero, 1999) is a multivariate solver that is typically used to solve the PMF model, which is based on a receptor-only factor analytic model (Paatero and Tapper, 1994). The bilinear representation of PMF solves Eq. (1), written in matrix notation, which represents the mass balance between the factor profiles and the concentrations.

$$X = \mathbf{G} \times \mathbf{F} + E \tag{1}$$

The elements g_{ik} of matrix $\mathbf{G}$ represent the time series and the elements f_{kj} of matrix $\mathbf{F}$ represent the j elements of the profile (for example, mass spectrum) and E is the model residual.

The parameters f and g are fitted using a least squares approach that iteratively minimizes the variable Q (Paatero et al., 2002).

$$Q(fg) = \sum_{i=1}^{m} \sum_{j=1}^{n} \left(\frac{e_{ij}}{\sigma_{ij}} \right)^2, \tag{2}$$

where e_{ij} represent the residuals and σ_{ij} the estimated uncertainty for the points i and j.

The variable Q depends on the number of selected factors and the size of the data matrix; hence it is necessary to normalize Q by the degree of freedom of the model solution (Q_{exp}; Paatero et al., 2002) to monitor solutions.

$$Q_{\mathrm{exp}} \cong n \times m - p \times (m + n), \tag{3}$$

Table 1. Sets of target profiles used in the study.

a	c	s	w
BBOA	SFOA	HOA	SFOA
HOA	HOA	COA	HOA
COA	COA	SVOOA	COA

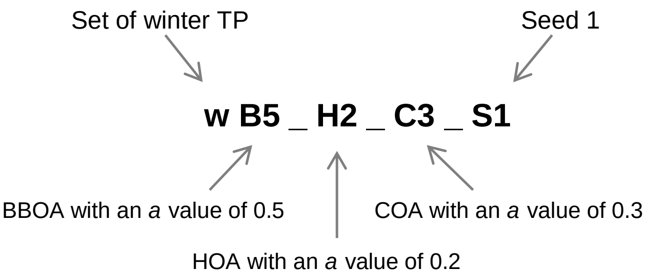

Figure 1. Coding used to identify the different runs.

where p is the number of factors chosen, n the number of samples and m the mass spectra. Ideally, if the model accurately captured the variability of the measured data, it would be expected to have a value of Q / $Q_{\text{exp}} = 1$, but this value depends on fluctuations in the source profiles, over- or underestimation of input data errors and the model error.

Solutions using a least squares approach to solve a factor analysis problem may have linear transformations, also known as rotations (Paatero and Hopke, 2009). One advantage of ME2 over PMF is that the rotational ambiguity can be reduced by using previous knowledge of profiles (for example mass spectra) or time series of different pollutants using the a value approach. Equation 4 was applied using different target profiles (TPs) (g_i) and a range of a values (a) to constrain OA sources in different runs ($g_{i,\text{run}}$).

$$g_{i,\text{run}} = g_i \pm a \times g_i \tag{4}$$

The a value is a parameter that represents the degree of variability of the target profile, which typically ranges from zero to one. The closer to zero, the more constrained the solution is (Lanz et al., 2008). The user should keep in mind that partially constrained solutions are carried out by compromising the Q / Q_{exp} value, which should be monitored to determine the feasibility of the solutions.

2.2.1 Target profiles and levels of constraint

In this study, solutions obtained with ME-2 were constrained using the a value approach, by using four different sets of mass spectra from previous studies of TPs (Table 1). Set a of the TPs represents BBOA and HOA average factor profiles obtained from an analysis carried out on different mass spectra from a variety of monitoring sites across Europe (Crippa et al., 2014) and COA obtained from a study in Paris (Crippa et al., 2013a). Sets c, s and w were provided by Young et al. (2015a) from a PMF analysis carried out on AMS measurements at the North Kensington site in London, 2012. The c TPs were obtained from an analysis performed on annual OA measured with a cToF-AMS (11 January 2012–23 January 2013). Sets s and w were obtained from summer and winter measurements and taken with an HR-AMS (January–February and July–August 2012, respectively). The ACSM was specifically designed to deliver mass spectra that were equivalent to the AMS. With the AMS having a higher signal to noise ratio, it is expected that the use of its mass spectra as TPs is appropriate. Moreover, we consider AMS-generated TPs to be convenient to use, especially considering there are more of these available, including the ones obtained from the same site. In this study, the suitability of different TPs will be systematically assessed in the determination of OA sources using a wide range of a values.

A wide range of combinations of TP and a values were used during this analysis, all of them being run with three random initial values (seeds) to determine the stability of the solutions. Constraints were applied using one, two and three TPs; in all the solutions, there were at least two unconstrained factors. Figure 1 shows the coding used to identify the different solutions, for example when constraining 3-factor profiles, e.g. wB5_H2_C3_S1.

2.3 Strategy to explore the solution space

The success of ME-2 relies on the additional use of a priori information in the form of constraints. However, without a well-defined strategy or a limited analysis of the solution space, it may lead to a subjectively and inaccurately selected solution. Moreover, when possible, TPs from different studies should be tested in order to determine which set of TPs are the most appropriate. Therefore, the following sections show the results of the analysis carried out on the data set of March–December 2013, to which the considerations provided by Crippa et al. (2014) were applied. Moreover, new analysis techniques were developed to explore the solution space.

PMF solutions are run to determine the number of factors (sources) in the solution. This is carried out by running PMF for a number of different factors. Once the number of possible sources has been chosen, different combinations of a values and constrained factors are tested to determine the solution that better identifies the OA sources. The residual of the solution provides important information; it is possible to determine whether the solution is overestimated (negative residual) or underestimated (positive residual). When a structure on the diurnal residual is observed, it allows the factor which is affecting the residual to be determined (Crippa et al., 2014), and a decision can be made as to whether the a value should be modified or even whether the TP is appropriate or not for this data set. Together with the residual, it is recommended to look at the total Q / Q_{exp}, which is a parameter used to monitor solutions. The best solution, according to the statistical tests applied, will be the one with values closest to one.

Trilinear regression is a new technique which is used to explore the solution space in ME-2 analysis. Multilinear regression has been previously applied to analyse the relationship between POA and combustion tracers (Allan et al., 2010; Liu et al., 2011; Young et al., 2015b) as well as polycyclic aromatic hydrocarbons (Elser et al., 2016). This is used instead of simple linear regression because many of the combustion related variables will have multiple sources, such as biomass burning and traffic. Equation (3) shows the trilinear regression equation used to analyse the relationship between POA and combustion tracers.

$$Y = A + B\,[\mathrm{BBOA}] + C\,[\mathrm{HOA}] + D[\mathrm{COA}]\,, \tag{5}$$

where Y is NO_x, BC, or CO.

B, C and D slopes represent the contribution of BBOA, HOA and COA to Y and the intercept A is representative of the Y background concentration. The following considerations should be taken into account: the slopes and intercepts should be positive as they represent air pollutant concentrations and the slope D is used as a validation parameter, which should be close to zero due to its low contribution to BC, NO_x and CO, owing to the fact that most cooking in the UK uses electricity or natural gas as a source of heat (DECC, 2016; DEFRA, 2016). A non-zero value would indicate correlation with combustion tracers and thus the possibility that it is receiving interference from HOA, which has a similar mass spectrum. Chi square is used as a "goodness of fit" for which the lower the value, the better the fit between the analysed pollutants.

3 Results

3.1 Exploring the solution space for March–December data set

This section shows the results from the analysis applied to determine the solution that best represents the OA sources for the complete data set March–December 2013, according to the statistical tests applied, when a total of eight unconstrained and 25 constrained solutions were analysed.

3.1.1 Solutions, *a* values and stability

Unconstrained runs with f peak $= 0$ and three different seeds were performed in order to determine the number of OA sources. Five was (BBOA, HOA, COA, SVOOA, LVOOA) the optimal number of sources (Fig. S1b in the Supplement), as it was possible to split the SOA into SVOOA and LVOOA. Further unconstrained analysis was performed by running 5-factor solutions with different f peaks, from -1 to 1 with steps of 0.1 (Fig. S4) in order to select the PMF solution to be compared with the ME-2 analysis. ME-2 is run using a range of a values, which were selected after trial and error and according to the literature (Lanz et al., 2008; Crippa et al., 2014; Petit et al., 2014), which suggests that a values depend on the similarity of the TP and the factor profile being analysed. HOA mass spectra do not show high variability when compared to different sites, thus it is possible to restrict the constraint with a values of 0.1–0.2. On the other hand, COA and BBOA mass spectra from different sites show high variability and a looser constraint should be applied (for example, a values 0.3–0.5 or higher).

Constraining only 1 or 2 factors of the 5-factor solutions gave the least favourable results with high residuals and mixing factor profiles. When analysing the different seeds, these solutions also showed high variability between seeds. Greater stability was found when 3 of the 5 factor solutions were constrained (Fig. S2), as also observed by Crippa et al. (2014). As a result, in this analysis, 5-factor solutions constraining 3 factors will be analysed for the first seed. One PMF solution and two solutions constraining 2 factors were also used during the exploration (Fig. 2) for three sets of TPs.

3.1.2 Q / Q_{exp}, diurnal residual and trilinear regression

As an ideal solution, a Q / Q_{exp} value of 1.0 would be expected. However, there is not a standard criterion to define a satisfactory Q / Q_{exp} value, as a certain amount of model error will cause it to be systematically higher than unity (Ulbrich et al., 2009). When comparing different solutions from the same data set (Fig. 2b), it is possible to observe that there is not a significant variation on the Q / Q_{exp} (ranging between 1.88–2.2) when using different a values, suggesting that all the solutions are mathematically acceptable. The unconstrained solution is the one with the lowest total Q / Q_{exp} with a value of 1.88, which is expected, as PMF calculates the solution by minimizing this value; however, the PMF solution has a high chi square and negative slope for COA (Fig. 2a), implying that this solution is not environmentally acceptable, thus it is necessary to analyse all the different parameters in Fig. 2 in order to select the solution that best identifies the OA sources.

Figure 2a shows the diurnal residual analysis in which solutions constrained with c TPs present a high positive residual around 14:00–19:00 h. Solutions constrained with w TPs have a negative residual during early morning with a positive residual at 21:00 h. Hence, the solution with a better diurnal residual is within the solutions constrained with a TPs.

Figure 2b shows the trilinear regression outputs between NO_x and POA for the different solutions (see Supplement Sect. S3 for BC and CO trilinear regressions). All the solutions properly identified the background NO_x concentrations (grey line). Solutions with c and w TPs showed similar undesirable results in the diurnal residual analysis, with c TPs presenting negative COA slopes and w presenting high COA slopes and chi-square values. This is consistent with the out-

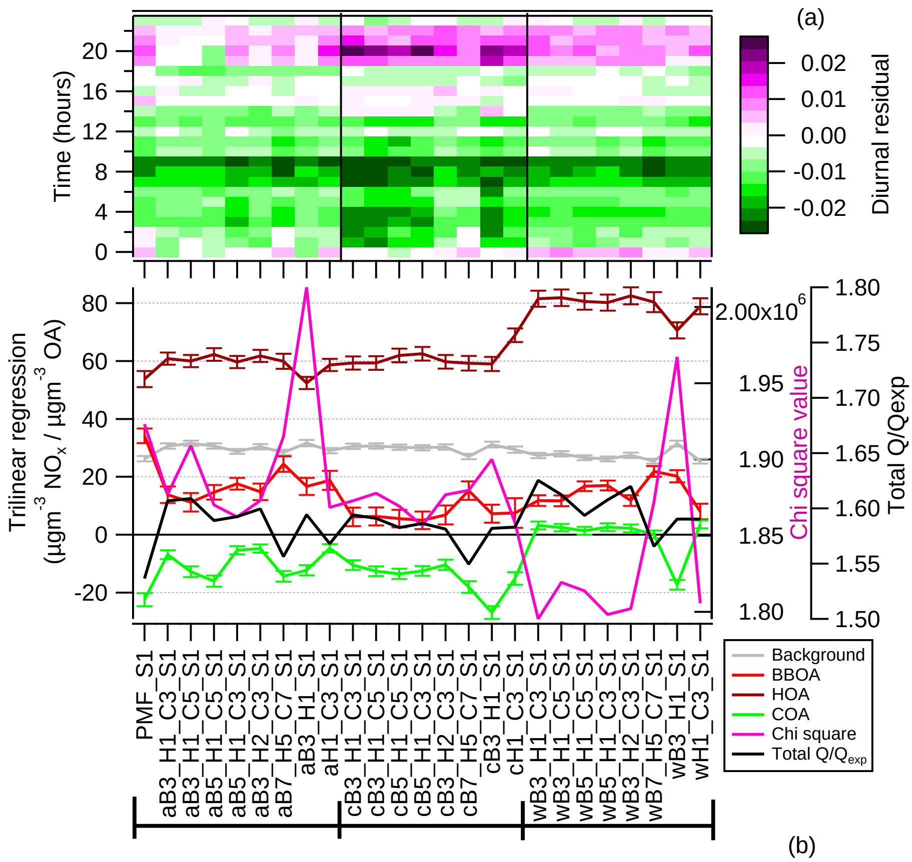

Figure 2. (a) Diurnal residual, y axis represents time up to 24 h and x axis represents the different solutions with a variety of target profiles and a values. **(b)** NO_x trilinear regression for solutions with different target profiles. BBOA represents the slope of $\mu g\,m^{-3}$ of NO_x per $\mu g\,m^{-3}$ of BBOA. The same applies for HOA and COA. Whiskers represent the 95 % confidence interval.

come of the diurnal residual analysis that the best solution, according to the statistical tests applied, is with the solutions constrained with a TPs. Additionally, trilinear regression outputs show variations between different solutions constrained with a TPs with changes mainly in the chi square and the BBOA.

3.1.3 Diurnal concentrations and mass spectra

OA sources have characteristic diurnal trends, and they may be used, together with their respective mass spectra, to analyse the solutions and determine whether all the factors in the solution are environmentally suitable. BBOA showed low concentrations during the day and high concentrations at night, mainly related to domestic heating (Alfarra et al., 2007). HOA presents two peaks during the day related to commuting, one in the morning and another in the evening (Zhang et al., 2005). COA has two peaks related to OA emissions from cooking activities, one peak at noon and one peak in the evening (Allan et al., 2010). SVOOA is temperature dependent with low concentrations during the day, which increase in the evening due to the condensation of gas phase pollutants. LVOOA, due to its regional origin, does not show high variations in its diurnal trend.

Diurnal concentrations for all the solutions (Supplement Sect. S3) were analysed to determine the main sources. Here, it was possible to observe that solutions with undesirable outputs in the residual, total $Q\,/\,Q_{\mathrm{exp}}$ and/or trilinear regression were likely to have mixed diurnal concentrations between two sources. For example, in the case of c TP solutions, CO and BC trilinear regressions (Fig. S5a and b) show better COA slopes with values close to zero; however, due to the high diurnal residual (Fig. 2a) and HOA, with high concentrations during the evening (Fig. S5c) suggesting mixing with BBOA, c TP solutions are not considered acceptable.

These previously observed undesirable outputs were also detected when analysing the mass spectra of the different solutions. Fig. S3 shows examples of diverse situations that were found: in the solution wB7_H5_C7_S1 it is possible to observe mixed factors where SVOOA has peaks of BBOA (m/z 60) and COA (m/z 55 and 57) as well as one source with only one strong peak in its mass spectrum (SVOOA in solution cB3_H1_S1). The PMF solution was not able to properly identify a BBOA factor with low peaks at m/z 60 and 73 and a peak at m/z 60 for COA, implying mixing with BBOA.

Finally, from this analysis, aB3_H2_C3_S1 was determined to be the solution that best represents the OA sources for the March–December analysis, according to the statistical tests applied.

3.2 Seasonal analysis

When applying source apportionment, ME-2 considers that both TPs and factor profiles remain constant over time, which may not be the case for long periods of time in which meteorological conditions and pollutant emissions related to human activities vary greatly (Canonaco et al., 2015; Ripoll et al., 2015). Thus, the same analysis that was carried out on the March–December data set was applied to data divided into seasons of the year: spring (March, April and May), summer (June, July and August) and autumn (September, October and November); see Supplement Sect. S.3 for detailed information of the seasonal analysis.

From analysing the spring data set (Fig. S7), solutions constrained with a and c TPs were found to present the least favourable results with high chi-square values and negative COA ratios in the trilinear analysis, as well as a higher negative diurnal residual. The solution wB3_H1_C3_S1 was deemed to be the best solution for the spring analysis. Solutions constrained with s and c TPs were the least favourable results for the summer analysis (Fig. S9), with low chi-square values in s target profiles, which show high negative residuals in the morning and at night. Since c TPs show a high positive residual around 15:00–18:00 h, the solution aB5_H1_C3_S1 was found to be the best solution for the summer analysis. In the autumn analysis (Fig. S11), solutions constrained with a and w TPs were found to be the least favourable results, with high positive residuals in the morning and a target profiles also showing high chi-square values. The solution cB3_H1_S1 was deemed the best solution for the autumn analysis according to the statistical tests applied. It is worth mentioning that all plausible solutions deconvolved a high percentage of the total OA mass (Fig. S12), with summer being the period with less OA mass estimated (90 %) and the other periods with more than 95 % of mass estimated from the total OA concentrations.

4 Discussion and atmospheric implications

4.1 Annual and seasonal solutions

In the following subsections, the outputs of annual and seasonal solutions are compared in order to further explore the variability of the different OA sources.

4.1.1 Total Q / Q_{exp} and diurnal residual

Having analysed the total Q / Q_{exp}, all the solutions obtained were mathematically acceptable and had small variations between their different values: 1.95 for March–December, 2.01 for spring, 1.95 for summer and 1.96 for autumn (Fig. 3a).

Q / Q_{exp} values obtained in this study are compared to values obtained in different ME-2 studies. For example, Petit et al. (2014), in a study using an ACSM, obtained a Q / Q_{exp} value of 6, while studies carried out in Spain during winter and summer obtained 1.15 and 0.38 respectively (Minguillón et al., 2015b). Q / Q_{exp} values obtained with PMF are also comparable with values obtained in this study, for example Young et al. (2015a) obtained a value of 1.35 from annual measurements carried out with a cToF-AMS at this site. Allan et al. (2010) obtained different Q / Q_{exp} values for the analysis carried out on three different data sets: a value of 3.9 from measurements obtained using a HR-ToF-AMS and values of 10.5 and 16.7 using a cToF-AMS. Crippa et al. (2013b) also identified a Q / Q_{exp} value of 4.59 from HR-ToF-AMS measurements during July 2009 at the urban background site in Paris. Due to all this variability of Q / Q_{exp} values found in the literature, this parameter alone cannot be used as a criterion to determine the solution that best identifies the OA sources.

It is in the diurnal residual where we can observe a high variation (Fig. 3b), with autumn proving to be the most overestimated with negative residuals of $-0.033\,\mu\mathrm{g\,m^{-3}}$, mainly in the morning and at night. On the other hand, summer appears to be the most underestimated solution with values of $0.018\,\mu\mathrm{g\,m^{-3}}$, particularly between midday and 17:00 UTC. The fact that summer is underestimated from 12:00 to 17:00 UTC is probably related to the increase on photochemical activity, a situation that ME-2 is not able to capture as the mass spectra remains constant over the period analysed. It is important to notice that these diurnal residuals of $0.03\,\mu\mathrm{g\,m^{-3}}$ or less are low compared with diurnal concentrations of the OA sources, which were in the range 0.1–$0.6\,\mu\mathrm{g\,m^{-3}}$.

4.1.2 Trilinear regression analysis

Looking at the trilinear outputs for the different periods analysed (Fig. 3a), HOA slopes present higher variability with values of 50.0 for March–December, 81.0 for spring, 41.0 for summer and 85.5 for autumn. The different BBOA and HOA slopes for spring, summer and autumn suggest that there are seasonal variations, perhaps affected by changes on the inhabitants' daily activities (i.e. domestic heating) and meteorological conditions, which the March–December solution does not completely capture on its own. With regard to COA slopes and background concentrations, they are well identified and relatively constant over the different periods analysed.

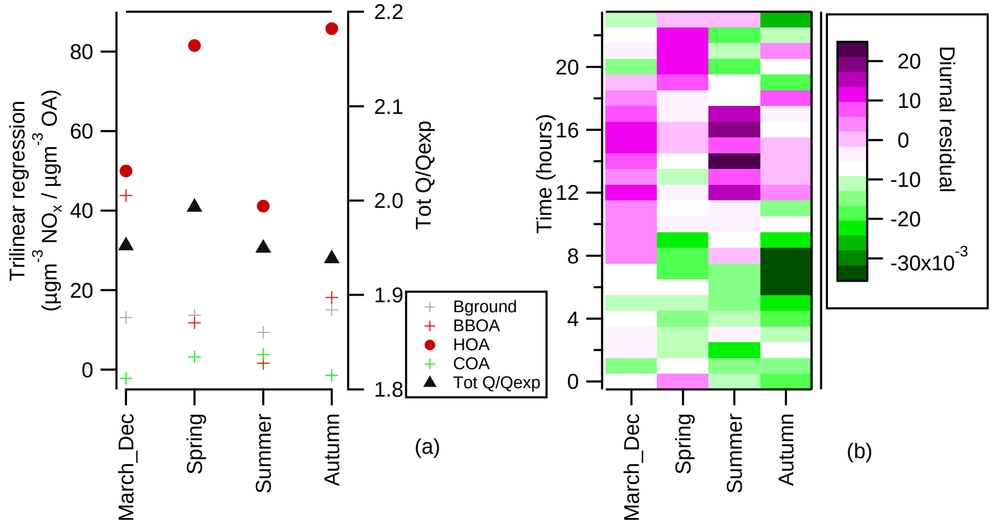

Figure 3. NO_x trilinear regression **(a)** and diurnal residual **(b)** for the different analyses.

The analysis presented in Sect. 4 shows that seasonal analysis more accurately deconvolves OA sources, being able to obtain more detailed information that will be lost when running ME-2 for long periods of time.

4.1.3 Target profiles (TPs) and their impact on the solutions

As previously mentioned, the chosen solutions were aB3_H2_C3_S1 for March–December, wB3_H1_C3_S1 for spring, aB5_H1_C3_S1 for summer and wB3_H1_S1 for autumn. The fact that the March–December and summer solutions were obtained with TP a is possibly due to the fact that these TPs represent an average from different mass spectra, becoming robust TPs which are able to deal with the variations of the two data sets. There was one large data set (March–December) and one data set with concentrations affected by the different photochemical processes due to the high temperatures (summer). On the other hand, spring and autumn do not show these variations and their OA sources may be apportioned using winter TPs which were obtained under similar temperatures.

Looking at the c and s TPs, these were the ones with the least favourable results of all analyses carried out. This may be attributed to c being the only TP obtained with a cToF-AMS while the rest were obtained using a HR-AMS. In the case of TP s, the unfavourable outputs are again related to the high variability present during this period of time. This analysis shows the importance of using the appropriate TP when doing source apportionment as well as exploring solutions with different types of TPs in order to determine the OA sources.

4.2 Variability of factor profiles

The variability of the different solutions previously obtained may be explored further with the triangle plots $f44$ vs. $f43$ (Ng et al., 2010; Morgan et al., 2010) and $f44$ vs. $f60$ (Cubison et al., 2011). The parameters $f43$, $f44$ and $f60$ represent the ratio of the integrated signal at m/z 43, 44 and 60, respectively, to the total signal in the organic component mass spectrum. Figure 4a shows that LVOOA, while having different values between solutions, is found in distinct areas of the plot (connecting lines are used to make the SVOOA variability clearer), whereas SVOOA shows values of $f44$ vs. $f43$ with high variability. This analysis shows that the factors derived for SOA do not always conform to the model of LVOOA and SVOOA proposed by Jimenez et al. (2009). Furthermore, the fact that the lines are going in different directions to the seasons of year means that the factorization is identifying different aspects of the chemical complexity, as LVOOA and SVOOA (rather than originating from primary emissions) are part of continuous physicochemical processes involving gases, aerosols and meteorological parameters among others. This serves to highlight that a 2-component model (LVOOA and SVOOA) is an oversimplification of a complex chemical system as concluded by Canonaco et al. (2015), who found significant $f44$ vs. $f43$ differences for summer and winter analyses.

By analysing Fig. 4b, it is possible to observe the variability in $f60$, with the lowest value obtained in summer (0.013) followed by spring, autumn and March–December (0.022, 0.024 and 0.034, respectively). Variability in biomass burning OA depends on the fuel type, burning conditions and level of processing (Weimer et al., 2008; Hennigan et al., 2011; Ortega et al., 2013; Young et al., 2015b). A study carried out by (Young et al., 2015b) in London in 2012 identified

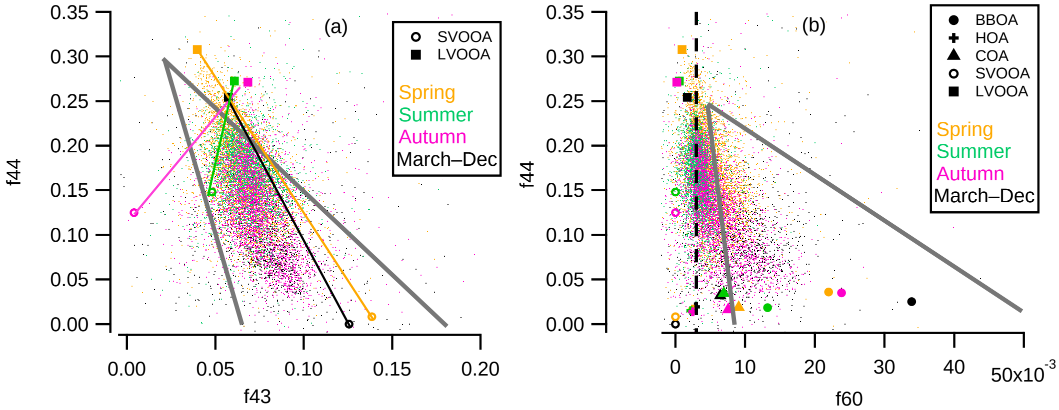

Figure 4. **(a)** $f44$ vs. $f43$ and **(b)** $f44$ vs. $f60$ plots for different periods of time.

two types of solid fuel OA factors, attributed to differences in burning efficiency. BBOA evolution has been frequently observed with high $f44$ and low $f60$ values due to ageing, oxidation and cloud processing (Huffman et al., 2009; Cubison et al., 2011). Thus, it was possible to obtain a variety of BBOA for the different seasons of the year, ranging from a fresh BBOA with a high $f60$ during autumn to a more oxidized BBOA with a low $f60$ during summer.

For all the solutions, COA presents an $f60$ value of approximately 0.01, which has been previously identified by Mohr et al. (2009), who obtained $f60$ values of 0.015–0.03 for different types of meat cooking. The fact that all the COA mass spectra present similar $f44 : f60$ ratios suggests that the COA footprint is relatively constant over the different seasons and, along with HOA, it is the more appropriate source to constrain when applying the a value approach.

4.3 Petrol and diesel contribution to traffic emissions

Traffic emissions contribute significantly to air pollution (Beevers et al., 2012; Carslaw et al., 2013; May et al., 2014). In order to better analyse traffic emissions and their impact on air quality, it is necessary to understand the fuel type and pollutant contribution from different vehicles. In particular, the United Kingdom has a considerable percentage of diesel-fuelled vehicles; according to the vehicle licensing statistics, the percentage of diesel-fuelled vehicles licensed has been increasing over the last few years from 22 in 2006 to 36.2 % in 2014 while petrol-fuelled vehicles decreased from 77.7 to 62.9 % (GOV.UK, 2015).

Diesel emits higher NO_x and HOA concentrations compared to petrol, while petrol emits higher concentrations of CO, according to the National Atmospheric Emissions inventory (DEFRA, 2016), during 2014 the emission factors (units in kilotonnes of pollutant per megatonne of fuel used) were 11–12 for diesel and 1.9–4.3 for petrol in the case of NO_x and 2.4–5.6 for diesel and 11–50 for petrol in the case of CO. Moreover, there are variations between light-duty diesel (LDD) and heavy-duty diesel (HDD) emissions (GLA, 2013), with LDD emitting higher NO_x concentrations and HDD emitting higher HOA concentrations.

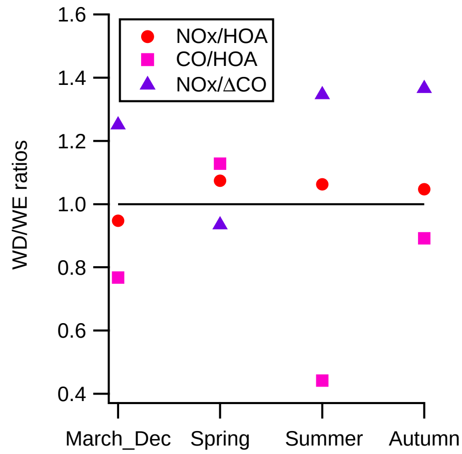

Figure 5. WD / WE ratios to analyse petrol and diesel contributions.

It is possible to qualitatively analyse the impact of different fuels on air pollution by looking at weekday/weekend ratios (WD / WE), as previously done in several studies (Bahreini et al., 2012; Tao and Harley, 2014; DeWitt et al., 2015) and stating the hypothesis that different fuels will have different pollutant contributions during the week. This analysis considers WD as Monday to Friday and WE as only Sunday to eliminate the mixed traffic on Saturday. Another consideration is that the heavy-duty/light-duty emissions fleet ratio is higher during the week (Lough et al., 2006; Bahreini et al., 2012; Heo et al., 2015). It is also important to state that heavy-duty vehicles are exclusively diesel fuelled whereas light-duty vehicles are fuelled with a mixture of diesel and petrol.

Trilinear regression, explained in Sect. 2.3, was used with data divided into WD (Monday to Friday) and WE (Sun-

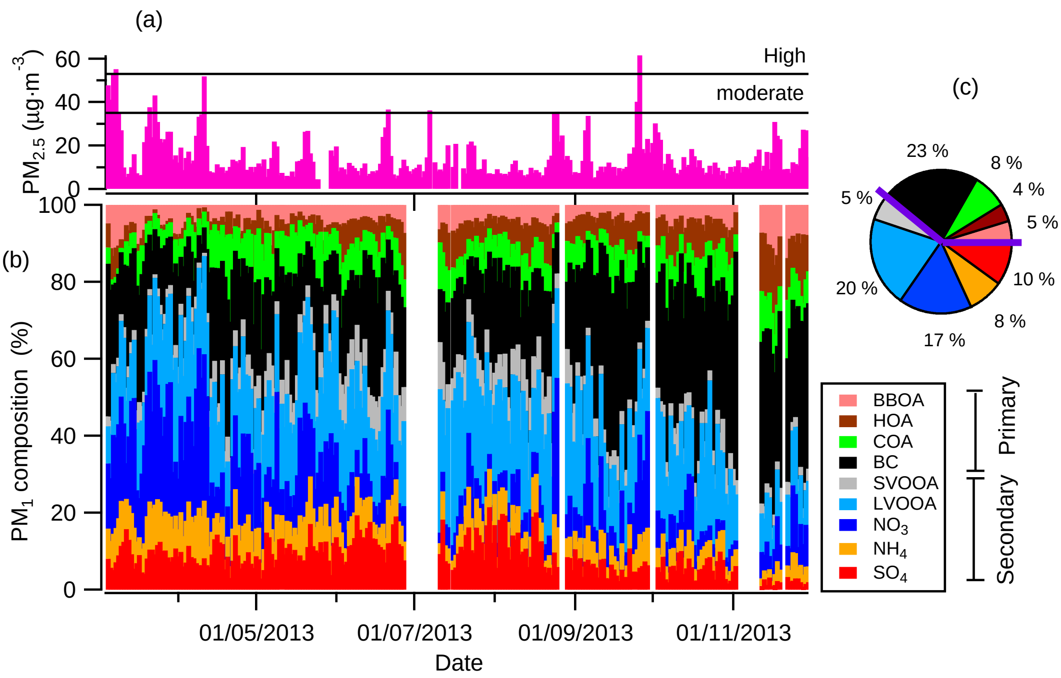

Figure 6. (a) Daily $PM_{2.5}$ concentrations, **(b)** daily and **(c)** total PM_1 composition, purple line in Fig. 6c separates secondary and primary aerosols.

day) to analyse the WD / WE contributions. Subsequently, it was possible to determine WD / WE ratios for the slopes NO_x / HOA and CO / HOA.

In order to compare these trilinear outputs with the WD / WE ratios between NO_x and CO, NO_x / ΔCO was calculated from average concentrations. There is a difference in lifetime between CO (lifetime of months) and NO_x (lifetime of hours), thus it is important to consider the background CO concentrations to be able to compare NO_x and CO concentrations. It is necessary to perform a linear regression between CO and NO_x and calculate ΔCO, which is the average CO concentration minus the intercept from the CO : NO_x linear regression.

Figure 5 shows the WD / WE ratios, from which it is possible to observe NO_x / ΔCO ratios of 1.25, 1.35 and 1.36 for March–December, summer and autumn, respectively, suggesting diesel has a higher contribution during WD compared to petrol. These findings are confirmed by the CO / HOA ratios, which, for the same periods of time, are lower than one (0.8, 0.45 and 0.9), suggesting a lower contribution of petrol during weekdays compared to diesel. In spring, there are no considerable changes to the WD / WE ratios, although a higher contribution of petrol is shown during WD with values of 1.28 for CO / HOA and low diesel contribution. Analysing the NO_x / HOA ratios, the seasonal ratios show values of 1.07, 1.06 and 1.05 suggesting a slightly higher contribution of LDD during WD than HDD.

4.4 $PM_{2.5}$ daily concentrations and PM_1 composition

$PM_{2.5}$ has been widely studied due to its potential to cause negative effects on health (Pope and Dockery, 2006; Harrison et al., 2012; Bohnenstengel et al., 2014). This adverse impact is directly connected to the size of the particles, making PM_1 more detrimental to health than $PM_{2.5}$ (Ramgolam et al., 2009). Moreover, analysing the aerosol contribution to PM_1 and its association with $PM_{2.5}$ concentrations allows the possible influence of PM_1 on $PM_{2.5}$ levels to be determined. According to the Daily Air Quality Index (DAQI), $PM_{2.5}$ concentrations are considered moderate when daily concentrations are between 35 and 52 $\mu g\,m^{-3}$ and high when levels are between 53 and 69 $\mu g\,m^{-3}$. Daily $PM_{2.5}$ concentrations during the sampling period show that the majority of daily concentrations were considered to be low episodes (Fig. 6a), with 10 episodes of moderate concentrations and only two episodes of high $PM_{2.5}$ concentrations (55.2 and 61.5 $\mu g\,m^{-3}$).

Considering that PM_1 is composed mainly of OA, SO_4, NO_3, NH_4 and BC, it is possible to analyse the PM_1 composition during $PM_{2.5}$ high concentrations (Fig. 6b). Episodes with moderate and high $PM_{2.5}$ concentrations were observed with low wind speeds (Fig. S13), NO_3 and LVOOA being the main PM_1 contributors. High NO_3 concentrations were observed during spring as found in a previous study by Young et al. (2015a), who determined that NO_3 concentrations in spring depend on air mass trajectory, precursors and meteorology. Different contributions from OA sources were identified. In the episode in March, high BBOA concentrations were observed, whereas during the episodes in April and September, higher concentrations of LVOOA were detected.

Defining BBOA, HOA COA and BC as primary and SVOOA, LVOOA, NO_3, NH_4 and SO_4 as secondary aerosols, the main PM_1 contributors to $PM_{2.5}$ concentrations are secondary aerosols with a total contribution of 61 % (Fig. 6c). These findings agree with a previous study at this same monitoring site carried out by Young et al. (2015a), who found secondary aerosols to be the predominant source of PM_1 over the year, with different secondary inorganic and organic aerosol contributions between winter and summer.

5 Conclusions

This study presents the source apportionment carried out using ME-2 within SoFi 4.8 of OA concentrations, measured with an ACSM from March to December 2013 at the urban background site in North Kensington, London; the first time it was deployed in the UK.

ME-2 proved to be a robust tool to deconvolve OA sources. This study highlighted the importance of using appropriate mass spectra as target profiles and a values when exploring the solution space. With the implementation of new techniques to compare different solutions, it was possible to systematically determine the solution with the best separation of OA sources, mathematically and environmentally speaking. The comparison carried out between the solution for the March–December data set and the seasonal solutions showed high variations mainly in the SVOOA and the BBOA sources, with wide range of $f44:f43$ values for SVOOA (Fig. 4a) and $f60$ values ranging from 13×10^{-3} for summer to 24×10^{-3} for autumn (Fig. 4b). These variations support the importance of running ME-2 when weather conditions and emissions from human activities are less variable, such as seasonal analyses.

SVOOA presented a high variability in the oxidation state during the different seasons. This is due to the nature of SVOOA being affected mainly by high temperatures and ME-2 not being able to completely determine SVOOA concentrations. These results support the indication that is not an accurate practice to use SVOOA as a target profile when analysing solutions. Trilinear regressions deliver quantitative information about the ratios between combustion tracers and POA. These ratios may be used as a proxy for other urban background sites to estimate POA concentrations.

From analysing heavy- and light-duty diesel emissions, the main contributor on weekdays was found to be from diesel emissions, particularly LDD emissions. Thus, in order to reduce traffic emissions on weekdays, LDD vehicles should be targeted. For the $PM_{2.5}$ analysis (March–December 2013), the main PM_1 contributors to these concentrations were secondary aerosols and BC, which means that PM_1 contributors to $PM_{2.5}$ concentrations are related to emissions from combustion activities and secondary pollutants produced in the atmosphere.

This study delivers mass spectra and time series of OA sources for a long-term period as well as seasons of the year, and may be used in future ME-2 studies as TPs. Furthermore, the scientific findings provide significant information to strengthen legislation as well as to support health studies that aim to improve air quality in the UK.

6 Data availability

ACSM data used in this paper have been archived at http://browse.ceda.ac.uk/browse/badc/clearflo/data/long-term. Other monitoring data are available at https://uk-air.defra.gov.uk/data/data_selector.

The Supplement related to this article is available online at doi:10.5194/acp-16-15545-2016-supplement.

Author contributions. David C. Green, Ernesto Reyes-Villegas and James D. Allan designed the project; David C. Green and Max Priestman operated, calibrated and performed QA of ACSM data; Ernesto Reyes-Villegas performed the data analysis; Ernesto Reyes-Villegas, Francesco Canonaco, David C. Green, Hugh Coe, André S. H. Prévôt, and James D. Allan wrote the paper.

Acknowledgements. Ernesto Reyes-Villegas is supported by a studentship by the National Council of Science and Technology–Mexico (CONACYT) under registry number 217687.

Edited by: L. M. Russell
Reviewed by: four anonymous referees

References

Alfarra, M. R., Prevot, A. S. H., Szidat, S., Sandradewi, J., Weimer, S., Lanz, V. A., Schreiber, D., Mohr, M., and Baltensperger, U.: Identification of the mass spectral signature of organic aerosols from wood burning emissions, Environ. Sci. Technol., 41, 5770–5777, doi:10.1021/Es062289b, 2007.

Allan, J. D., Delia, A. E., Coe, H., Bower, K. N., Alfarra, M. R., Jimenez, J. L., Middlebrook, A. M., Drewnick, F., Onasch, T. B., Canagaratna, M. R., Jayne, J. T., and Worsnop, D. R.: A generalised method for the extraction of chemically resolved mass spectra from aerodyne aerosol mass spectrometer data, J. Aerosol. Sci., 35, 909–922, doi:10.1016/j.jaerosci.2004.02.007, 2004.

Allan, J. D., Williams, P. I., Morgan, W. T., Martin, C. L., Flynn, M. J., Lee, J., Nemitz, E., Phillips, G. J., Gallagher, M. W., and Coe, H.: Contributions from transport, solid fuel burning and cooking to primary organic aerosols in two UK cities, Atmos. Chem. Phys., 10, 647–668, doi:10.5194/acp-10-647-2010, 2010.

Bahreini, R., Middlebrook, A. M., de Gouw, J. A., Warneke, C., Trainer, M., Brock, C. A., Stark, H., Brown, S. S., Dube, W. P., Gilman, J. B., Hall, K., Holloway, J. S., Kuster, W. C., Perring, A. E., Prevot, A. S. H., Schwarz, J. P., Spackman, J. R., Szidat, S., Wagner, N. L., Weber, R. J., Zotter, P., and Parrish, D. D.: Gasoline emissions dominate over diesel in formation of secondary organic aerosol mass, Geophys. Res. Lett., 39, L06805, doi:10.1029/2011gl050718, 2012.

Beccaceci, S., McGhee, E. A., Brown, R. J. C., and Green, D. C.: A comparison between a semi-continuous analyzer and filter-based method for measuring anion and cation concentrations in pm10 at an urban background site in london, Aerosol Sci. Technol., 49, 793–801, doi:10.1080/02786826.2015.1073848, 2015.

Beevers, S. D., Westmoreland, E., de Jong, M. C., Williams, M. L., and Carslaw, D. C.: Trends in NO_x and NO_2 emissions from road traffic in great britain, Atmos. Environ., 54, 107–116, doi:10.1016/j.atmosenv.2012.02.028, 2012.

Bigi, A. and Harrison, R. M.: Analysis of the air pollution climate at a central urban background site, Atmos. Environ., 44, 2004–2012, doi:10.1016/j.atmosenv.2010.02.028, 2010.

Bohnenstengel, S. I., Belcher, S. E., Aiken, A., Allan, J. D., Allen, G., Bacak, A., Bannan, T. J., Barlow, J. F., Beddows, D. C. S., Bloss, W. J., Booth, A. M., Chemel, C., Coceal, O., Di Marco, C. F., Dubey, M. K., Faloon, K. H., Fleming, Z. L., Furger, M., Gietl, J. K., Graves, R. R., Green, D. C., Grimmond, C. S. B., Halios, C. H., Hamilton, J. F., Harrison, R. M., Heal, M. R., Heard, D. E., Helfter, C., Herndon, S. C., Holmes, R. E., Hopkins, J. R., Jones, A. M., Kelly, F. J., Kotthaus, S., Langford, B., Lee, J. D., Leigh, R. J., Lewis, A. C., Lidster, R. T., Lopez-Hilfiker, F. D., McQuaid, J. B., Mohr, C., Monks, P. S., Nemitz, E., Ng, N. L., Percival, C. J., Prévôt, A. S. H., Ricketts, H. M. A., Sokhi, R., Stone, D., Thornton, J. A., Tremper, A. H., Valach, A. C., Visser, S., Whalley, L. K., Williams, L. R., Xu, L., Young, D. E., and Zotter, P.: Meteorology, air quality, and health in london: The clearflo project, B. Am. Meteorol. Soc., 96, 779–804, doi:10.1175/bams-d-12-00245.1, 2014.

Bozzetti, C., Daellenbach, K. R., Hueglin, C., Fermo, P., Sciare, J., Kasper-Giebl, A., Mazar, Y., Abbaszade, G., El Kazzi, M., Gonzalez, R., Shuster-Meiseles, T., Flasch, M., Wolf, R., Křepelová, A., Canonaco, F., Schnelle-Kreis, J., Slowik, J. G., Zimmermann, R., Rudich, Y., Baltensperger, U., El Haddad, I., and Prévôt, A. S. H.: Size-resolved identification, characterization, and quantification of primary biological organic aerosol at a european rural site, Environ. Sci. Technol., 50, 3425–3434, doi:10.1021/acs.est.5b05960, 2016.

Bruns, E. A., El Haddad, I., Keller, A., Klein, F., Kumar, N. K., Pieber, S. M., Corbin, J. C., Slowik, J. G., Brune, W. H., Baltensperger, U., and Prévôt, A. S. H.: Inter-comparison of laboratory smog chamber and flow reactor systems on organic aerosol yield and composition, Atmos. Meas. Tech., 8, 2315–2332, doi:10.5194/amt-8-2315-2015, 2015.

Budisulistiorini, S. H., Canagaratna, M. R., Croteau, P. L., Baumann, K., Edgerton, E. S., Kollman, M. S., Ng, N. L., Verma, V., Shaw, S. L., Knipping, E. M., Worsnop, D. R., Jayne, J. T., Weber, R. J., and Surratt, J. D.: Intercomparison of an Aerosol Chemical Speciation Monitor (ACSM) with ambient fine aerosol measurements in downtown Atlanta, Georgia, Atmos. Meas. Tech., 7, 1929–1941, doi:10.5194/amt-7-1929-2014, 2014.

Canonaco, F., Crippa, M., Slowik, J. G., Baltensperger, U., and Prévôt, A. S. H.: SoFi, an IGOR-based interface for the efficient use of the generalized multilinear engine (ME-2) for the source apportionment: ME-2 application to aerosol mass spectrometer data, Atmos. Meas. Tech., 6, 3649–3661, doi:10.5194/amt-6-3649-2013, 2013.

Canonaco, F., Slowik, J. G., Baltensperger, U., and Prévôt, A. S. H.: Seasonal differences in oxygenated organic aerosol composition: implications for emissions sources and factor analysis, Atmos. Chem. Phys., 15, 6993–7002, doi:10.5194/acp-15-6993-2015, 2015.

Carslaw, D. C., Williams, M. L., Tate, J. E., and Beevers, S. D.: The importance of high vehicle power for passenger car emissions, Atmos. Environ., 68, 8–16, doi:10.1016/j.atmosenv.2012.11.033, 2013.

Crippa, M., DeCarlo, P. F., Slowik, J. G., Mohr, C., Heringa, M. F., Chirico, R., Poulain, L., Freutel, F., Sciare, J., Cozic, J., Di Marco, C. F., Elsasser, M., Nicolas, J. B., Marchand, N., Abidi, E., Wiedensohler, A., Drewnick, F., Schneider, J., Borrmann, S., Nemitz, E., Zimmermann, R., Jaffrezo, J.-L., Prévôt, A. S. H., and Baltensperger, U.: Wintertime aerosol chemical composition and source apportionment of the organic fraction in the metropolitan area of Paris, Atmos. Chem. Phys., 13, 961–981, doi:10.5194/acp-13-961-2013, 2013a.

Crippa, M., El Haddad, I., Slowik, J. G., DeCarlo, P. F., Mohr, C., Heringa, M. F., Chirico, R., Marchand, N., Sciare, J., Baltensperger, U., and Prevot, A. S. H.: Identification of marine and continental aerosol sources in paris using high resolution aerosol mass spectrometry, J. Geophys. Res.-Atmos., 118, 1950–1963, doi:10.1002/Jgrd.50151, 2013b.

Crippa, M., Canonaco, F., Lanz, V. A., Äijälä, M., Allan, J. D., Carbone, S., Capes, G., Ceburnis, D., Dall'Osto, M., Day, D. A., DeCarlo, P. F., Ehn, M., Eriksson, A., Freney, E., Hildebrandt Ruiz, L., Hillamo, R., Jimenez, J. L., Junninen, H., Kiendler-Scharr, A., Kortelainen, A.-M., Kulmala, M., Laaksonen, A., Mensah, A. A., Mohr, C., Nemitz, E., O'Dowd, C., Ovadnevaite, J., Pandis, S. N., Petäjä, T., Poulain, L., Saarikoski, S., Sellegri, K., Swietlicki, E., Tiitta, P., Worsnop, D. R., Baltensperger, U., and Prévôt, A. S. H.: Organic aerosol components derived from 25 AMS data sets across Europe using a consistent ME-2 based source apportionment approach, Atmos. Chem. Phys., 14, 6159–6176, doi:10.5194/acp-14-6159-2014, 2014.

Cubison, M. J., Ortega, A. M., Hayes, P. L., Farmer, D. K., Day, D., Lechner, M. J., Brune, W. H., Apel, E., Diskin, G. S., Fisher, J. A., Fuelberg, H. E., Hecobian, A., Knapp, D. J., Mikoviny, T., Riemer, D., Sachse, G. W., Sessions, W., Weber, R. J., Weinheimer, A. J., Wisthaler, A., and Jimenez, J. L.: Effects of aging on organic aerosol from open biomass burning smoke in aircraft and laboratory studies, Atmos. Chem. Phys., 11, 12049–12064, doi:10.5194/acp-11-12049-2011, 2011.

Dall'Osto, M., Thorpe, A., Beddows, D. C. S., Harrison, R. M., Barlow, J. F., Dunbar, T., Williams, P. I., and Coe, H.: Remarkable dynamics of nanoparticles in the urban atmosphere, Atmos. Chem. Phys., 11, 6623–6637, doi:10.5194/acp-11-6623-2011, 2011.

DEFRA: National atmospheric emissions inventory, http://naei.defra.gov.uk/data/, last access: 15 August 2016.

DeWitt, H. L., Hellebust, S., Temime-Roussel, B., Ravier, S., Polo, L., Jacob, V., Buisson, C., Charron, A., André, M., Pasquier, A., Besombes, J. L., Jaffrezo, J. L., Wortham, H., and Marchand, N.: Near-highway aerosol and gas-phase measurements in a high-diesel environment, Atmos. Chem. Phys., 15, 4373–4387, doi:10.5194/acp-15-4373-2015, 2015.

Digest of United Kingdom energy statistics 2015: https://www.gov.uk/government/uploads/system/uploads/attachment_data/file/450302/DUKES_2015.pdf(last access: 12 August 2016), 2015.

Elser, M., Huang, R.-J., Wolf, R., Slowik, J. G., Wang, Q., Canonaco, F., Li, G., Bozzetti, C., Daellenbach, K. R., Huang, Y., Zhang, R., Li, Z., Cao, J., Baltensperger, U., El-Haddad, I., and Prévôt, A. S. H.: New insights into $PM_{2.5}$ chemical composition and sources in two major cities in China during extreme haze events using aerosol mass spectrometry, Atmos. Chem. Phys., 16, 3207–3225, doi:10.5194/acp-16-3207-2016, 2016.

Fountoukis, C., Megaritis, A. G., Skyllakou, K., Charalampidis, P. E., Denier van der Gon, H. A. C., Crippa, M., Prévôt, A. S. H., Fachinger, F., Wiedensohler, A., Pilinis, C., and Pandis, S. N.: Simulating the formation of carbonaceous aerosol in a European Megacity (Paris) during the MEGAPOLI summer and winter campaigns, Atmos. Chem. Phys., 16, 3727–3741, doi:10.5194/acp-16-3727-2016, 2016.

Fröhlich, R., Crenn, V., Setyan, A., Belis, C. A., Canonaco, F., Favez, O., Riffault, V., Slowik, J. G., Aas, W., Aijälä, M., Alastuey, A., Artiñano, B., Bonnaire, N., Bozzetti, C., Bressi, M., Carbone, C., Coz, E., Croteau, P. L., Cubison, M. J., Esser-Gietl, J. K., Green, D. C., Gros, V., Heikkinen, L., Herrmann, H., Jayne, J. T., Lunder, C. R., Minguillón, M. C., Mocnik, G., O'Dowd, C. D., Ovadnevaite, J., Petralia, E., Poulain, L., Priestman, M., Ripoll, A., Sarda-Estève, R., Wiedensohler, A., Baltensperger, U., Sciare, J., and Prévôt, A. S. H.: ACTRIS ACSM intercomparison – Part 2: Intercomparison of ME-2 organic source apportionment results from 15 individual, co-located aerosol mass spectrometers, Atmos. Meas. Tech., 8, 2555–2576, doi:10.5194/amt-8-2555-2015, 2015.

GOV UK: Vehicles statistics, https://www.gov.uk/government/collections/vehicles-statistics, last access: 4 August 2015.

Harrison, R. M., Laxen, D., Moorcroft, S., and Laxen, K.: Processes affecting concentrations of fine particulate matter (pm2.5) in the uk atmosphere, Atmos. Environ., 46, 115–124, doi:10.1016/j.atmosenv.2011.10.028, 2012.

Hennigan, C. J., Miracolo, M. A., Engelhart, G. J., May, A. A., Presto, A. A., Lee, T., Sullivan, A. P., McMeeking, G. R., Coe, H., Wold, C. E., Hao, W.-M., Gilman, J. B., Kuster, W. C., de Gouw, J., Schichtel, B. A., Collett Jr., J. L., Kreidenweis, S. M., and Robinson, A. L.: Chemical and physical transformations of organic aerosol from the photo-oxidation of open biomass burning emissions in an environmental chamber, Atmos. Chem. Phys., 11, 7669–7686, doi:10.5194/acp-11-7669-2011, 2011.

Henry, R. C., Lewis, C. W., Hopke, P. K., and Williamson, H. J.: Review of receptor model fundamentals, Atmos. Environ., 18, 1507–1515, doi:10.1016/0004-6981(84)90375-5, 1984.

Heo, J., de Foy, B., Olson, M. R., Pakbin, P., Sioutas, C., and Schauer, J. J.: Impact of regional transport on the anthropogenic and biogenic secondary organic aerosols in the los angeles basin, Atmos. Environ., 103, 171–179, doi:10.1016/j.atmosenv.2014.12.041, 2015.

Hildebrandt, L., Kostenidou, E., Lanz, V. A., Prevot, A. S. H., Baltensperger, U., Mihalopoulos, N., Laaksonen, A., Donahue, N. M., and Pandis, S. N.: Sources and atmospheric processing of organic aerosol in the Mediterranean: insights from aerosol mass spectrometer factor analysis, Atmos. Chem. Phys., 11, 12499–12515, doi:10.5194/acp-11-12499-2011, 2011.

Huang, X.-F., He, L.-Y., Hu, M., Canagaratna, M. R., Sun, Y., Zhang, Q., Zhu, T., Xue, L., Zeng, L.-W., Liu, X.-G., Zhang, Y.-H., Jayne, J. T., Ng, N. L., and Worsnop, D. R.: Highly time-resolved chemical characterization of atmospheric submicron particles during 2008 Beijing Olympic Games using an Aerodyne High-Resolution Aerosol Mass Spectrometer, Atmos. Chem. Phys., 10, 8933–8945, doi:10.5194/acp-10-8933-2010, 2010.

Huffman, J. A., Docherty, K. S., Mohr, C., Cubison, M. J., Ulbrich, I. M., Ziemann, P. J., Onasch, T. B., and Jimenez, J. L.: Chemically-resolved volatility measurements of organic aerosol from different sources, Environ. Sci. Technol., 43, 5351–5357, doi:10.1021/es803539d, 2009.

Jimenez, J., Canagaratna, M., Donahue, N., Prevot, A., Zhang, Q., Kroll, J., DeCarlo, P., Allan, J., Coe, H., and Ng, N.: Evolution of organic aerosols in the atmosphere, Science, 326, 1525–1529, 2009.

Jones, A. M. and Harrison, R. M.: Interpretation of particulate elemental and organic carbon concentrations at rural, urban and kerbside sites, Atmos. Environ., 39, 7114–7126, doi:10.1016/j.atmosenv.2005.08.017, 2005.

Jones, A. M., Harrison, R. M., and Baker, J.: The wind speed dependence of the concentrations of airborne particulate matter and nox, Atmos. Environ., 44, 1682–1690, doi:10.1016/j.atmosenv.2010.01.007, 2010.

Keywood, M., Cope, M., Meyer, C. P. M., Iinuma, Y., and Emmerson, K.: When smoke comes to town: The impact of biomass burning smoke on air quality, Atmos. Environ., 121, 13–21, doi:10.1016/j.atmosenv.2015.03.050, 2015.

Kupiainen, K. and Klimont, Z.: Primary emissions of fine carbonaceous particles in europe, Atmos. Environ., 41, 2156–2170, doi:10.1016/j.atmosenv.2006.10.066, 2007.

Lanz, V. A., Alfarra, M. R., Baltensperger, U., Buchmann, B., Hueglin, C., and Prévôt, A. S. H.: Source apportionment of submicron organic aerosols at an urban site by factor analytical modelling of aerosol mass spectra, Atmos. Chem. Phys., 7, 1503–1522, doi:10.5194/acp-7-1503-2007, 2007.

Lanz, V. A., Alfarra, M. R., Baltensperger, U., Buchmann, B., Hueglin, C., Szidat, S., Wehrli, M. N., Wacker, L., Weimer, S., Caseiro, A., Puxbaum, H., and Prevot, A. S. H.: Source attribution of submicron organic aerosols during wintertime inversions by advanced factor analysis of aerosol mass spectra, Environ. Sci. Technol., 42, 214–220, doi:10.1021/Es0707207, 2008.

Liu, D., Allan, J., Corris, B., Flynn, M., Andrews, E., Ogren, J., Beswick, K., Bower, K., Burgess, R., Choularton, T., Dorsey, J., Morgan, W., Williams, P. I., and Coe, H.: Carbonaceous aerosols contributed by traffic and solid fuel burning at a polluted rural site in Northwestern England, Atmos. Chem. Phys., 11, 1603–1619, doi:10.5194/acp-11-1603-2011, 2011.

Liu, Q., Sun, Y., Hu, B., Liu, Z. R., Akio, S., and Wang, Y. S.: In situ measurement of pm1 organic aerosol in beijing winter using a high-resolution aerosol mass spectrometer, Chinese Sci Bull., 57, 819–826, doi:10.1007/s11434-011-4886-0, 2012.

Liu, Y. J. and Harrison, R. M.: Properties of coarse particles in the atmosphere of the united kingdom, Atmos. Environ., 45, 3267–3276, doi:10.1016/j.atmosenv.2011.03.039, 2011.

GLA: London atmospheric emissions inventory 2013, http://data.london.gov.uk/dataset/london-atmospheric-emissions-inventory-2013 (last access: 18 August 2016), 2013.

Lough, G. C., Schauer, J. J., and Lawson, D. R.: Day-of-week trends in carbonaceous aerosol composition in the urban atmosphere, Atmos. Environ., 40, 4137–4149, doi:10.1016/j.atmosenv.2006.03.009, 2006.

May, A. A., Nguyen, N. T., Presto, A. A., Gordon, T. D., Lipsky, E. M., Karve, M., Gutierrez, A., Robertson, W. H., Zhang, M., Brandow, C., Chang, O., Chen, S., Cicero-Fernandez, P., Dinkins, L., Fuentes, M., Huang, S.-M., Ling, R., Long, J., Maddox, C., Massetti, J., McCauley, E., Miguel, A., Na, K., Ong, R., Pang, Y., Rieger, P., Sax, T., Truong, T., Vo, T., Chattopadhyay, S., Maldonado, H., Maricq, M. M., and Robinson, A. L.: Gas- and particle-phase primary emissions from in-use, on-road gasoline and diesel vehicles, Atmos. Environ., 88, 247–260, doi:10.1016/j.atmosenv.2014.01.046, 2014.

Milic, A., Miljevic, B., Alroe, J., Mallet, M., Canonaco, F., Prevot, A. S. H., and Ristovski, Z. D.: The ambient aerosol characterization during the prescribed bushfire season in brisbane 2013, Sci. Total Environ., 560–561, 225–232, doi:10.1016/j.scitotenv.2016.04.036, 2016.

Minguillón, M. C., Brines, M., Pérez, N., Reche, C., Pandolfi, M., Fonseca, A. S., Amato, F., Alastuey, A., Lyasota, A., Codina, B., Lee, H. K., Eun, H. R., Ahn, K. H., and Querol, X.: New particle formation at ground level and in the vertical column over the barcelona area, Atmos. Res., 164–165, 118–130, doi:10.1016/j.atmosres.2015.05.003, 2015a.

Minguillón, M. C., Ripoll, A., Pérez, N., Prévôt, A. S. H., Canonaco, F., Querol, X., and Alastuey, A.: Chemical characterization of submicron regional background aerosols in the western Mediterranean using an Aerosol Chemical Speciation Monitor, Atmos. Chem. Phys., 15, 6379–6391, doi:10.5194/acp-15-6379-2015, 2015b.

Mohr, C., Huffman, J. A., Cubison, M. J., Aiken, A. C., Docherty, K. S., Kimmel, J. R., Ulbrich, I. M., Hannigan, M., and Jimenez, J. L.: Characterization of primary organic aerosol emissions from meat cooking, trash burning, and motor vehicles with high-resolution aerosol mass spectrometry and comparison with ambient and chamber observations, Environ. Sci. Technol., 43, 2443–2449, doi:10.1021/Es8011518, 2009.

Mohr, C., DeCarlo, P. F., Heringa, M. F., Chirico, R., Slowik, J. G., Richter, R., Reche, C., Alastuey, A., Querol, X., Seco, R., Peñuelas, J., Jiménez, J. L., Crippa, M., Zimmermann, R., Baltensperger, U., and Prévôt, A. S. H.: Identification and quantification of organic aerosol from cooking and other sources in Barcelona using aerosol mass spectrometer data, Atmos. Chem. Phys., 12, 1649–1665, doi:10.5194/acp-12-1649-2012, 2012.

Morgan, W. T., Allan, J. D., Bower, K. N., Highwood, E. J., Liu, D., McMeeking, G. R., Northway, M. J., Williams, P. I., Krejci, R., and Coe, H.: Airborne measurements of the spatial distribution of aerosol chemical composition across Europe and evolution of the organic fraction, Atmos. Chem. Phys., 10, 4065–4083, doi:10.5194/acp-10-4065-2010, 2010.

Ng, N. L., Canagaratna, M. R., Zhang, Q., Jimenez, J. L., Tian, J., Ulbrich, I. M., Kroll, J. H., Docherty, K. S., Chhabra, P. S., Bahreini, R., Murphy, S. M., Seinfeld, J. H., Hildebrandt, L., Donahue, N. M., DeCarlo, P. F., Lanz, V. A., Prévôt, A. S. H., Dinar, E., Rudich, Y., and Worsnop, D. R.: Organic aerosol components observed in Northern Hemispheric datasets from Aerosol Mass Spectrometry, Atmos. Chem. Phys., 10, 4625–4641, doi:10.5194/acp-10-4625-2010, 2010.

Ng, N. L., Herndon, S. C., Trimborn, A., Canagaratna, M. R., Croteau, P., Onasch, T. B., Sueper, D., Worsnop, D. R., Zhang, Q., and Sun, Y.: An aerosol chemical speciation monitor (acsm) for routine monitoring of the composition and mass concentrations of ambient aerosol, Aerosol Sci. Technol., 45, 780–794, 2011.

Ortega, A. M., Day, D. A., Cubison, M. J., Brune, W. H., Bon, D., de Gouw, J. A., and Jimenez, J. L.: Secondary organic aerosol formation and primary organic aerosol oxidation from biomass-burning smoke in a flow reactor during FLAME-3, Atmos. Chem. Phys., 13, 11551–11571, doi:10.5194/acp-13-11551-2013, 2013.

Paatero, P. and Tapper, U.: Positive matrix factorization: A non-negative factor model with optimal utilization of error estimates of data values, Environmetrics, 5, 111–126, 1994.

Paatero, P.: The multilinear engine: A table-driven, least squares program for solving multilinear problems, including the n-way parallel factor analysis model, J. Comput. Graph. Stat., 8, 854–888, doi:10.2307/1390831, 1999.

Paatero, P. and Hopke, P. K.: Rotational tools for factor analytic models, J. Chemom., 23, 91–100, 2009.

Paatero, P., Hopke, P. K., Song, X. H., and Ramadan, Z.: Understanding and controlling rotations in factor analytic models, Chemometr. Intell. Lab., 60, 253–264, doi:10.1016/S0169-7439(01)00200-3, 2002.

Petit, J.-E., Favez, O., Sciare, J., Canonaco, F., Croteau, P., Mocnik, G., Jayne, J., Worsnop, D., and Leoz-Garziandia, E.: Submicron aerosol source apportionment of wintertime pollution in Paris, France by double positive matrix factorization (PMF2) using an aerosol chemical speciation monitor (ACSM) and a multi-wavelength Aethalometer, Atmos. Chem. Phys., 14, 13773–13787, doi:10.5194/acp-14-13773-2014, 2014.

Petit, J.-E., Favez, O., Sciare, J., Crenn, V., Sarda-Estève, R., Bonnaire, N., Mocnik, G., Dupont, J.-C., Haeffelin, M., and Leoz-Garziandia, E.: Two years of near real-time chemical composition of submicron aerosols in the region of Paris using an Aerosol Chemical Speciation Monitor (ACSM) and a multi-wavelength Aethalometer, Atmos. Chem. Phys., 15, 2985–3005, doi:10.5194/acp-15-2985-2015, 2015.

Pope III, C. A. and Dockery, D. W.: Health effects of fine particulate air pollution: Lines that connect, J. Air Waste. Manage., 56, 709–742, 2006.

Ramgolam, K., Favez, O., Cachier, H., Gaudichet, A., Marano, F., Martinon, L., and Baeza-Squiban, A.: Size-partitioning of an urban aerosol to identify particle determinants involved in the proinflammatory response induced in airway epithelial cells, Part Fibre Toxicol., 6, 2009.

Ripoll, A., Minguillón, M. C., Pey, J., Jimenez, J. L., Day, D. A., Sosedova, Y., Canonaco, F., Prévôt, A. S. H., Querol, X., and Alastuey, A.: Long-term real-time chemical characterization of submicron aerosols at Montsec (southern Pyrenees, 1570 m a.s.l.), Atmos. Chem. Phys., 15, 2935–2951, doi:10.5194/acp-15-2935-2015, 2015.

Saarikoski, S., Carbone, S., Decesari, S., Giulianelli, L., Angelini, F., Canagaratna, M., Ng, N. L., Trimborn, A., Facchini, M. C., Fuzzi, S., Hillamo, R., and Worsnop, D.: Chemical characterization of springtime submicrometer aerosol in Po Valley, Italy, Atmos. Chem. Phys., 12, 8401–8421, doi:10.5194/acp-12-8401-2012, 2012.

Sun, Y. L., Wang, Z. F., Fu, P. Q., Yang, T., Jiang, Q., Dong, H. B., Li, J., and Jia, J. J.: Aerosol composition, sources and processes during wintertime in Beijing, China, Atmos. Chem. Phys., 13, 4577–4592, doi:10.5194/acp-13-4577-2013, 2013.

Takahama, S., Schwartz, R. E., Russell, L. M., Macdonald, A. M., Sharma, S., and Leaitch, W. R.: Organic functional groups in aerosol particles from burning and non-burning forest emissions at a high-elevation mountain site, Atmos. Chem. Phys., 11, 6367–6386, doi:10.5194/acp-11-6367-2011, 2011.

Tao, L. and Harley, R. A.: Changes in fine particulate matter measurement methods and ambient concentrations in california, Atmos. Environ., 98, 676–684, doi:10.1016/j.atmosenv.2014.09.044, 2014.

Ulbrich, I. M., Canagaratna, M. R., Zhang, Q., Worsnop, D. R., and Jimenez, J. L.: Interpretation of organic components from Positive Matrix Factorization of aerosol mass spectrometric data, Atmos. Chem. Phys., 9, 2891–2918, doi:10.5194/acp-9-2891-2009, 2009.

Vakkari, V., Kerminen, V. M., Beukes, J. P., Tiitta, P., Van Zyl, P. G., Josipovic, M., Venter, A. D., Jaars, K., Worsnop, D. R., Kulmala, M., and Laakso, L.: Rapid changes in biomass burning aerosols by atmospheric oxidation, Geophys. Res. Lett., 41, 2644–2651, doi:10.1002/2014gl059396, 2014.

Watson, J. G.: Visibility: Science and regulation, J. Air Waste Manage., 52, 628–713, doi:10.1080/10473289.2002.10470813, 2002.

Weimer, S., Alfarra, M. R., Schreiber, D., Mohr, M., Prévôt, A. S. H., and Baltensperger, U.: Organic aerosol mass spectral signatures from wood-burning emissions: Influence of burning conditions and wood type, J. Geophys. Res.-Atmos., 113, D10304, doi:10.1029/2007jd009309, 2008.

Young, D. E., Allan, J. D., Williams, P. I., Green, D. C., Flynn, M. J., Harrison, R. M., Yin, J., Gallagher, M. W., and Coe, H.: Investigating the annual behaviour of submicron secondary inorganic and organic aerosols in London, Atmos. Chem. Phys., 15, 6351–6366, doi:10.5194/acp-15-6351-2015, 2015a.

Young, D. E., Allan, J. D., Williams, P. I., Green, D. C., Harrison, R. M., Yin, J., Flynn, M. J., Gallagher, M. W., and Coe, H.: Investigating a two-component model of solid fuel organic aerosol in London: processes, PM1 contributions, and seasonality, Atmos. Chem. Phys., 15, 2429–2443, doi:10.5194/acp-15-2429-2015, 2015b.

Zhang, Q., Worsnop, D. R., Canagaratna, M. R., and Jimenez, J. L.: Hydrocarbon-like and oxygenated organic aerosols in Pittsburgh: insights into sources and processes of organic aerosols, Atmos. Chem. Phys., 5, 3289–3311, doi:10.5194/acp-5-3289-2005, 2005.

Zhang, Q., Jimenez, J. L., Canagaratna, M. R., Allan, J. D., Coe, H., Ulbrich, I., Alfarra, M. R., Takami, A., Middlebrook, A. M., Sun, Y. L., Dzepina, K., Dunlea, E., Docherty, K., DeCarlo, P. F., Salcedo, D., Onasch, T., Jayne, J. T., Miyoshi, T., Shimono, A., Hatakeyama, S., Takegawa, N., Kondo, Y., Schneider, J., Drewnick, F., Borrmann, S., Weimer, S., Demerjian, K., Williams, P., Bower, K., Bahreini, R., Cottrell, L., Griffin, R. J., Rautiainen, J., Sun, J. Y., Zhang, Y. M., and Worsnop, D. R.: Ubiquity and dominance of oxygenated species in organic aerosols in anthropogenically-influenced northern hemisphere midlatitudes, Geophys. Res. Lett., 34, L13801, doi:10.1029/2007gl029979, 2007.

Zhang, Q., Jimenez, J. L., Canagaratna, M. R., Ulbrich, I. M., Ng, N. L., Worsnop, D. R., and Sun, Y.: Understanding atmospheric organic aerosols via factor analysis of aerosol mass spectrometry: A review, Anal. Bioanal. Chem., 401, 3045–3067, 2011.

Supplement of Atmos. Chem. Phys., 16, 15545–15559, 2016 http://www.atmos-chem-phys.net/16/15545/2016/
doi:10.5194/acp-16-15545-2016-supplement

Atmospheric Chemistry and Physics

Supplement of

Organic aerosol source apportionment in London 2013 with ME-2: exploring the solution space with annual and seasonal analysis

Ernesto Reyes-Villegas et al.

Correspondence to: James D. Allan (james.allan@manchester.ac.uk)

S1. PMF solutions to determine the number of sources.

PMF runs (Fig S1) with different number of factors (sources) were performed to determine the number of OA sources. The six-factor solution (figure S1.c) shows two split factors (dark blue and green) which correspond to the same source, LVOOA. The five-factor solution (Figure S1.b) was able to separate two secondary organic aerosol sources in SVOOA and LVOOA showing to be the more acceptable number of sources.

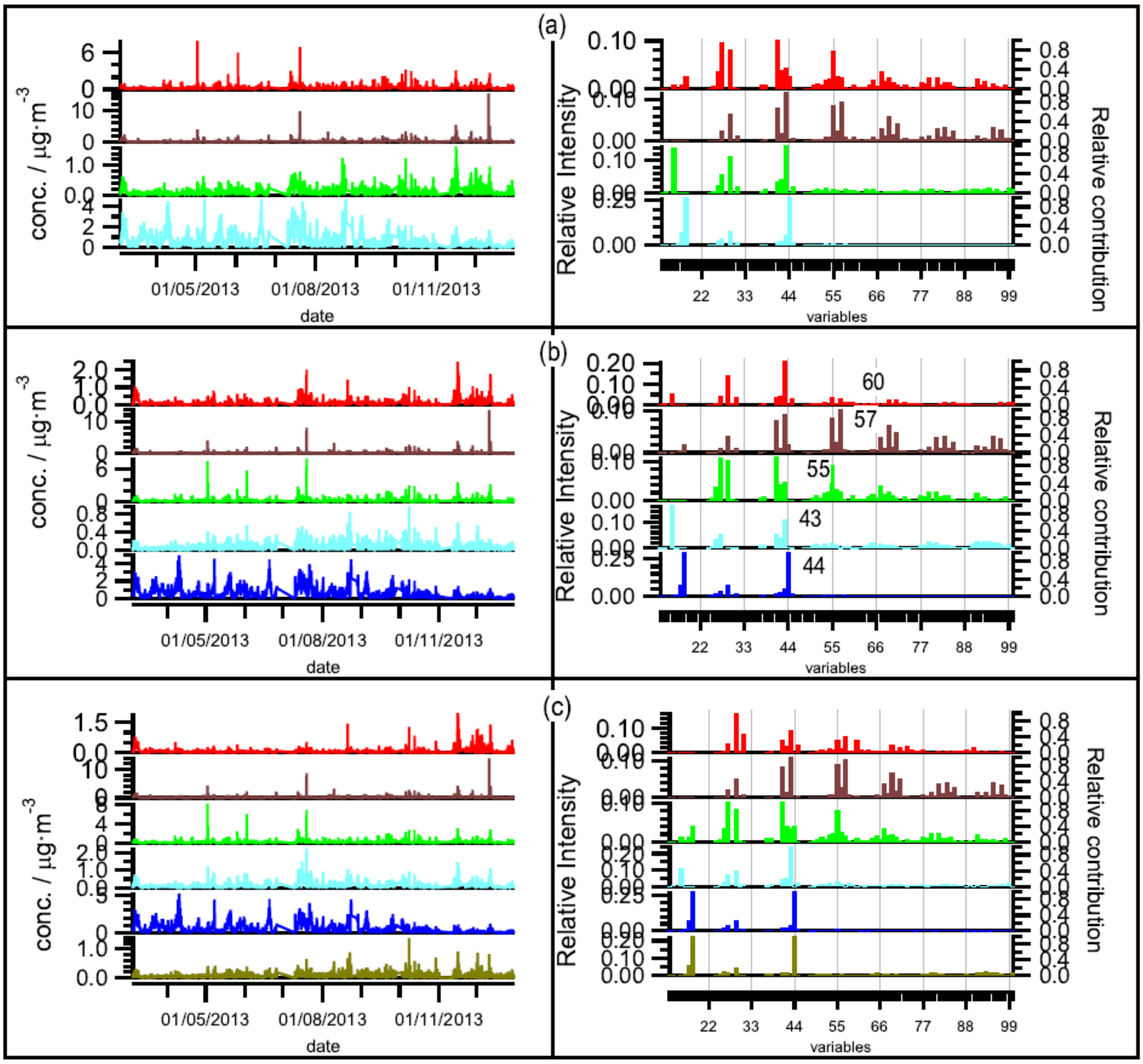

Figure S1: PMF solutions: four-factor solution (a), five-factor solution (b) and six-factor solution (c) to determine the number of OA sources.

S2. Seed and mass spectral analysis.

In order to deal with rotational ambiguity, ME-2 runs may be initialised from different random values, also called seeds. Figure S2 shows the analysis performed to the three different seeds from the best solution chosen for March-December (aB3_H2_C3) to determine stability on the solutions. This stability proves that solutions may be repeatable with the three solutions presenting the same five factors with similar Q/Qexp (S2.a), mass spectrum (S2.b) and time series (S2.c).

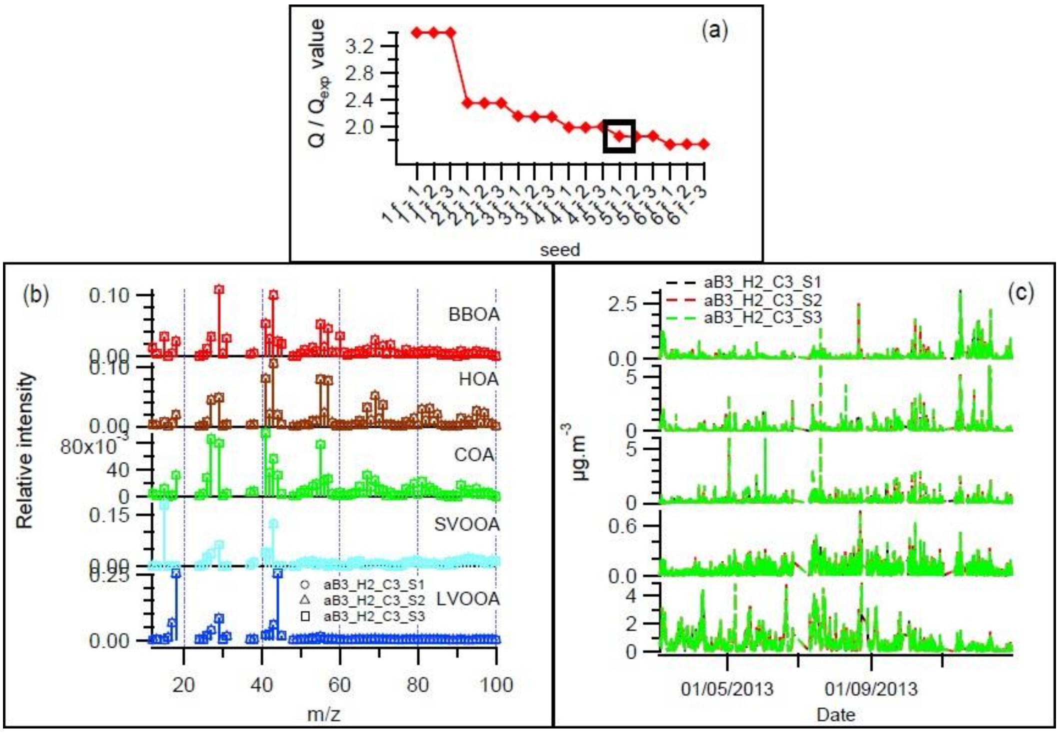

Figure S2: Seed analysis (a). Mass spectra (b) and time series (c).

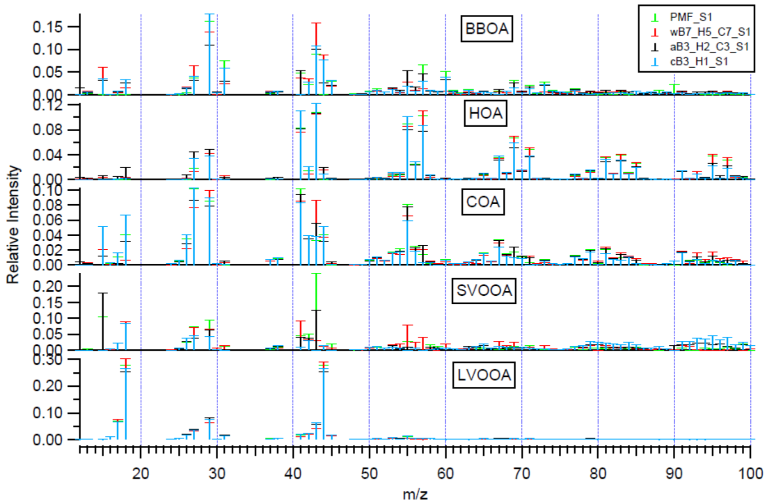

Figure S3: Mass spectra comparison for undesirable solutions for March-December analysis. Example of mass spectra of solutions with mixed factors for unconstrained and constrained solutions.

S3. Analysis to determine the best solution for the different periods of time.

PMF runs were performed, for the March-December period, from fpeak -1 to 1 with steps of 0.1. Figure 4 shows the comparison of the runs that converged (some of the fpeaks did not converge) in order to determine the PMF solution that better identified the OA sources to be compared to the ME-2 solutions. Run number 4 is chosen to be the best solution, according to the statistical tests applied, with low diurnal residual and positive COA for CO and BC trilinear regressions.

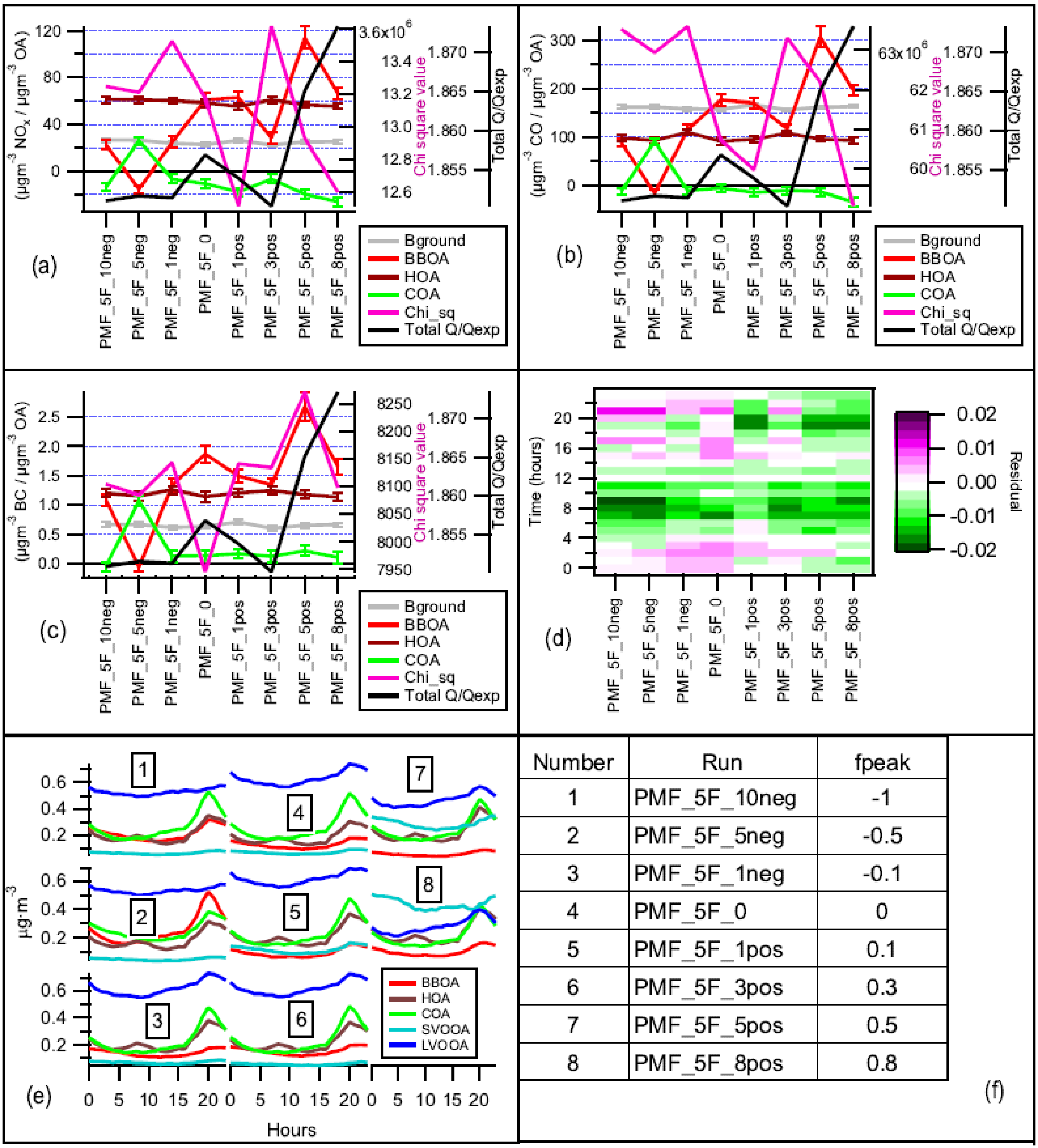

Number	Run	fpeak
1	PMF_5F_10neg	-1
2	PMF_5F_5neg	-0.5
3	PMF_5F_1neg	-0.1
4	PMF_5F_0	0
5	PMF_5F_1pos	0.1
6	PMF_5F_3pos	0.3
7	PMF_5F_5pos	0.5
8	PMF_5F_8pos	0.8

Figure S4 : NOx, CO and BC trilinear regression (a, b, c), diurnal residual (d), diurnal concentrations (e) and solution list for March-Dec PMF analysis (f).

Figure S5 shows the analysis carried out to determine the best solution for the March-December period. As mentioned in the main text of this paper, “c” and “w” target profiles (TP) show the less desirable results, “c” TP show a high positive residual (Figure 2.a) and “w” TP show a high chi-square and COA slope. (Figures C1.a and S4.b). From the “a” TP, aB3_H2_C3_S1 solution is chosen to present the best results from this analysis due to COA slope close to zero for NOx (Figure 2.b) and CO (Figure S5.a) trilinear regression and low diurnal residual (Figure 2.a).

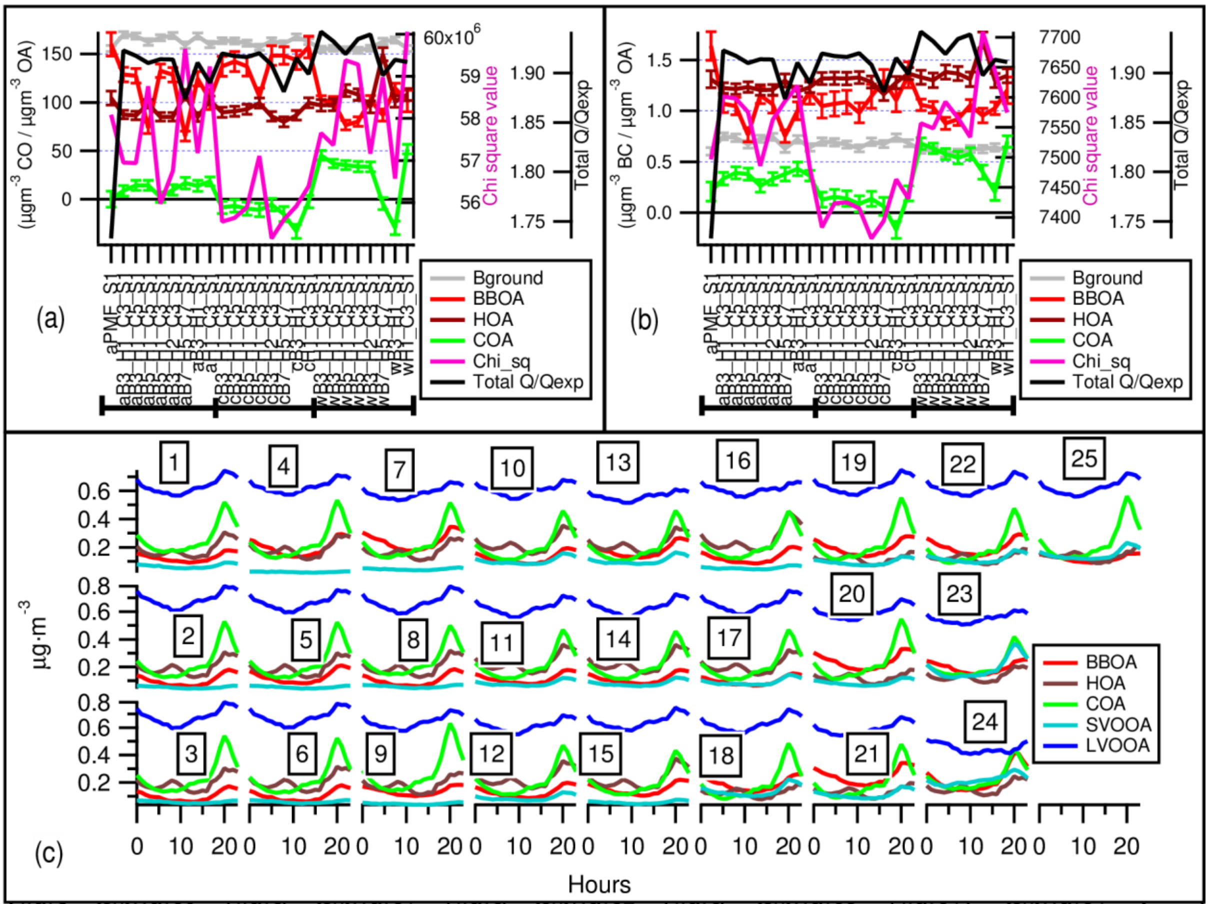

1	aPMF_S1	6	aB3_H2_C3_S1	11	cB3_H1_C5_S1	16	cB3_H1_S1	21	wB5_H1_C3_S1
2	aB3_H1_C3_S1	7	aB7_H5_C7_S1	12	cB5_H1_C5_S1	17	cH1_C3_S1	22	wB3_H2_C3_S1
3	aB3_H1_C5_S1	8	aB3_H1_S1	13	cB5_H1_C3_S1	18	wB3_H1_C3_S1	23	wB7_H5_C7_S1
4	aB5_H1_C5_S1	9	aH1_C3_S1	14	cB3_H2_C3_S1	19	wB3_H1_C5_S1	24	wB3_H1_S1
5	aB5_H1_C3_S1	10	cB3_H1_C3_S1	15	cB7_H5_C7_S1	20	wB5_H1_C5_S1	25	wH1_C3_S1

(d)

Figure S5: CO and BC trilinear regression (a, b), diurnal concentrations (c) and solution list for March-Dec analysis (d).

Figure S6 shows the PMF analysis for the spring period. All solutions show similar diurnal concentrations with negative COA slope fo the three trilinear regressions. Solutions 2 and 3 have the lower Q/Qexp, Solution 3 was chosen to be compared with ME-2 solutions.

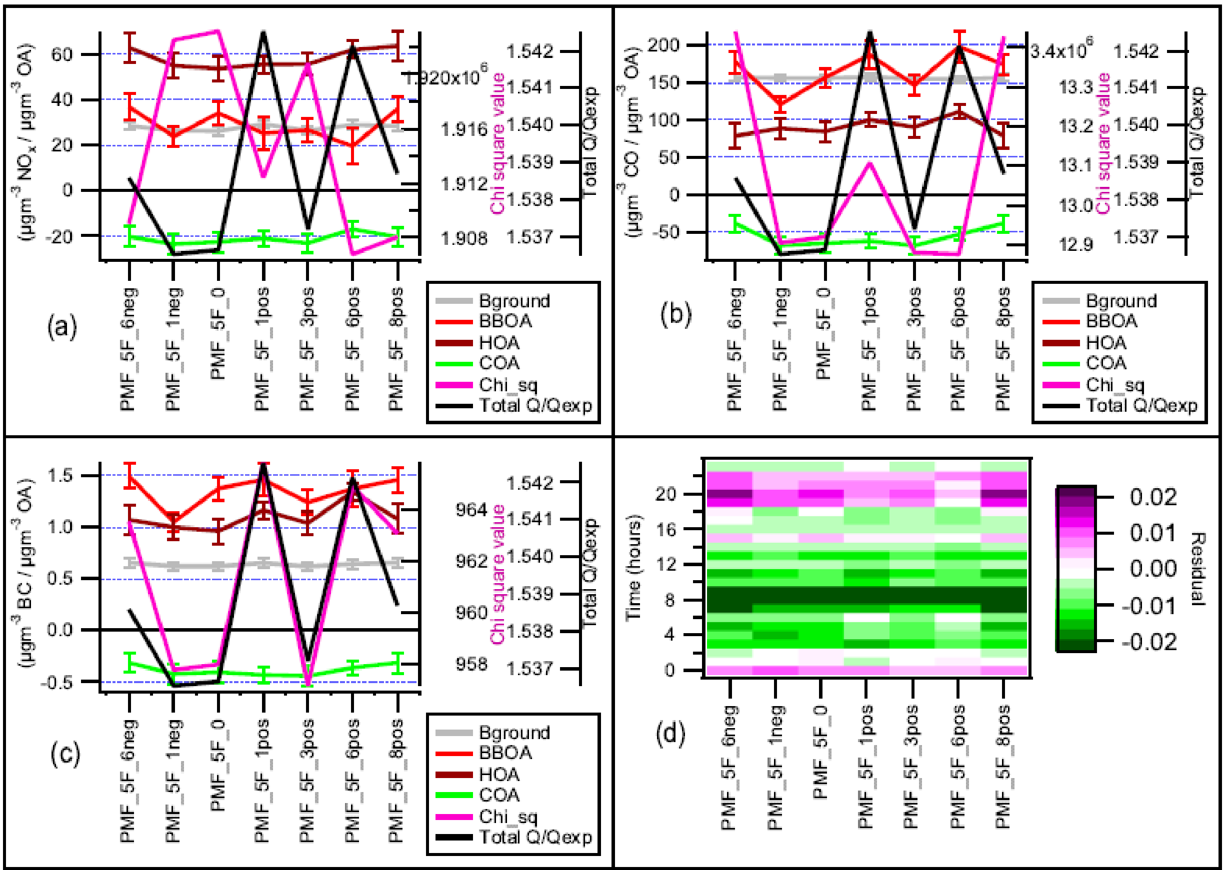

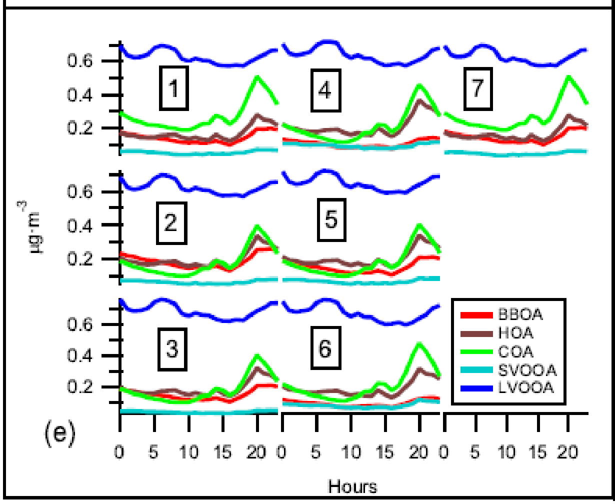

Number	Run	fpeak
1	PMF_5F_6neg	-0.6
2	PMF_5F_1neg	-0.1
3	PMF_5F_0	0
4	PMF_5F_1pos	0.1
5	PMF_5F_3pos	0.3
6	PMF_5F_6pos	0.6
7	PMF_5F_8pos	0.8

(f)

Figure S6: NOx, CO and BC trilinear regression (a, b, c), diurnal residual (d), diurnal concentrations (e) and solution list for spring PMF analysis (f).

Figure S7 shows the analysis performed to determine the best solution for spring period. Solutions with "a" and "c" TP show the less desirable results with negative slopes for COA and high chi-square in the trilinear regression (Figures S5.a, S5.b and S5.c), "c" TP also show high diurnal residuals. The solution wB3_H1_C3_S1 is chosen to present the best results from this analysis with low chi-square and diurnal residuals.

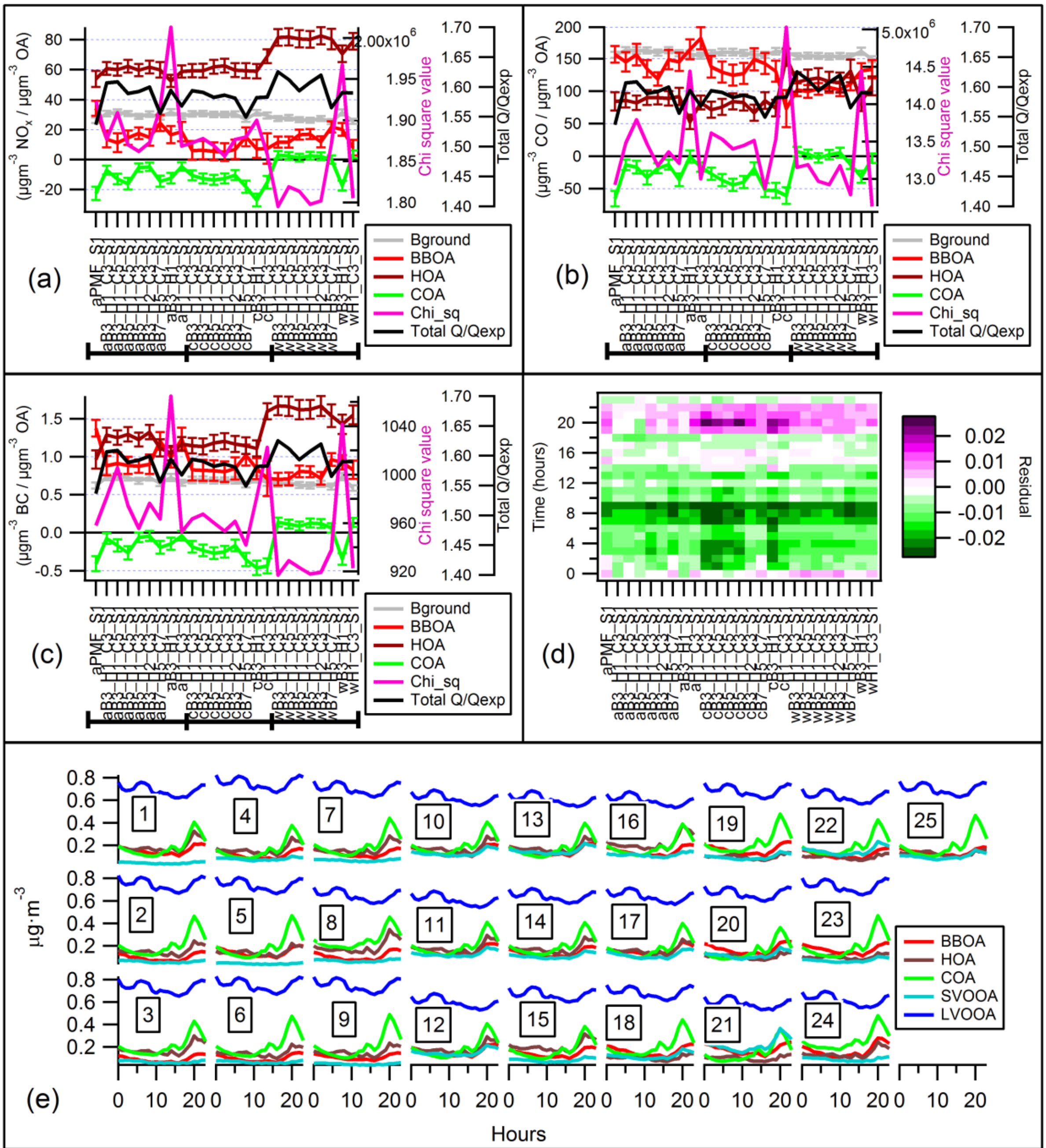

1	aPMF S1	6	aB3 H2 C3 S1	11	cB3 H1 C5 S1	16	cB3 H1 S1	21	wB5 H1 C3 S1
2	aB3 H1 C3 S1	7	aB7 H5 C7 S1	12	cB5 H1 C5 S1	17	cH1 C3 S1	22	wB3 H2 C3 S1
3	aB3 H1 C5 S1	8	aB3 H1 S1	13	cB5 H1 C3 S1	18	wB3 H1 C3 S1	23	wB7 H5 C7 S1
4	aB5 H1 C5 S1	9	aH1 C3 S1	14	cB3 H2 C3 S1	19	wB3 H1 C5 S1	24	wB3 H1 S1
5	aB5 H1 C3 S1	10	cB3 H1 C3 S1	15	cB7 H5 C7 S1	20	wB5 H1 C5 S1	25	wH1 C3 S1

(f)

Figure S7: NOx, CO and BC trilinear regression (a,b,c), diurnal residual (d),diurnal concentrations (e) all the solutions for spring analysis (f).

Figure S8 shows the PMF analysis for the summer period. Solution 4 has a high Q/Qexp but as it shows a COA slope close to zero in the three trilinear analyses and a low diurnal residual compared to the other PMF solutions, it has been chosen to be compared with ME-2 solutions.

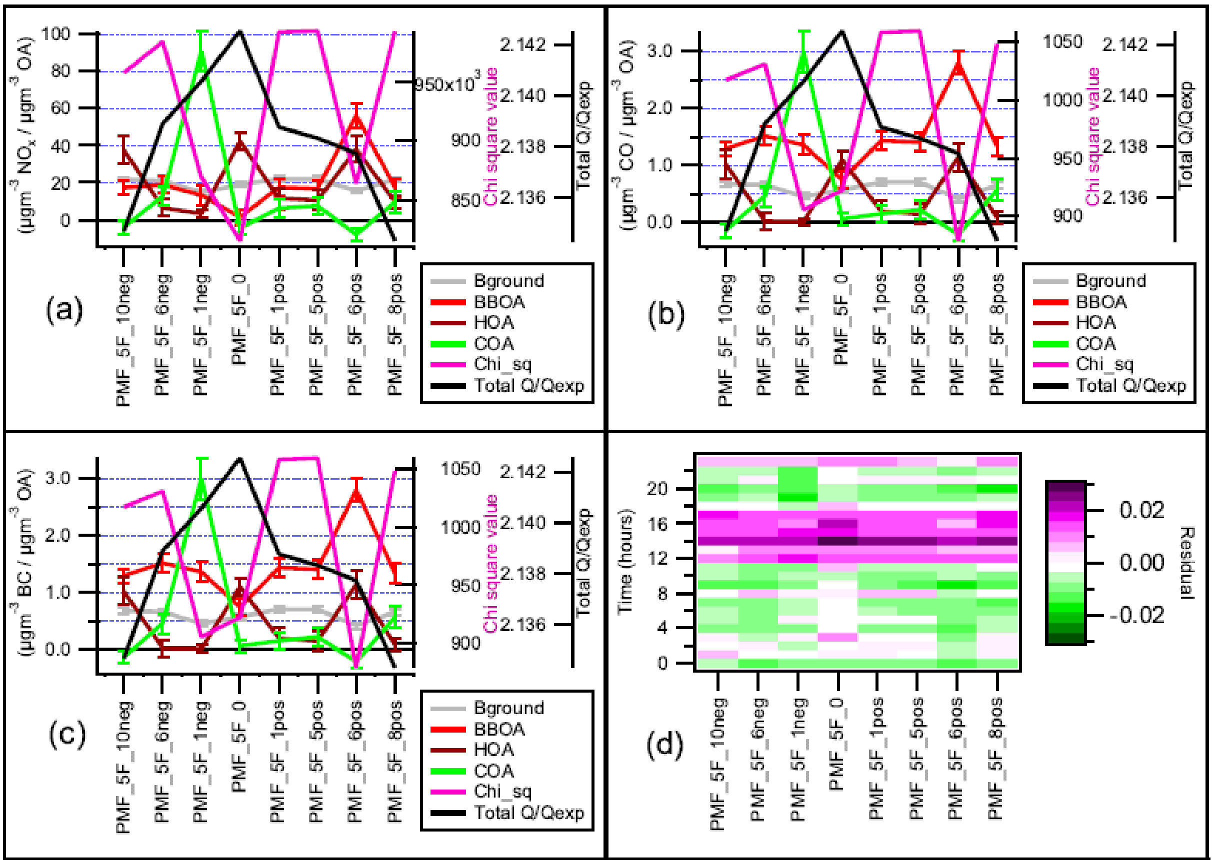

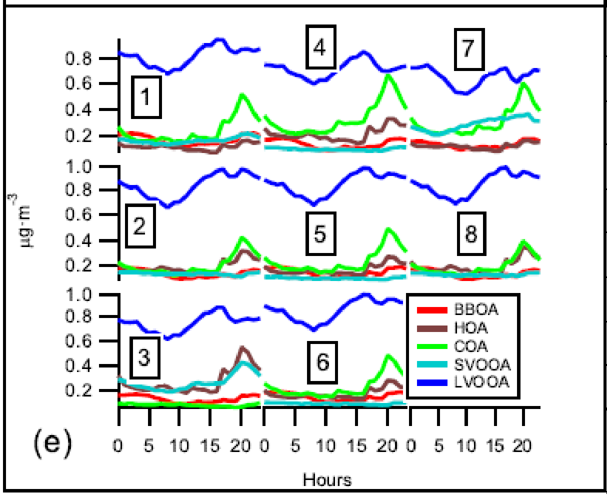

Number	Run	fpeak
1	PMF_5F_10neg	-1
2	PMF_5F_5neg	-0.6
3	PMF_5F_1neg	-0.1
4	PMF_5F_0	0
5	PMF_5F_1pos	0.1
6	PMF_5F_5pos	0.5
7	PMF_5F_5pos	0.6
8	PMF_5F_8pos	0.8

(f)

Figure S8: NOx, CO and BC trilinear regression (a, b, c), diurnal residual (d), diurnal concentrations (e) and solution list for summer PMF analysis (f).

Figure S9 shows the analysis performed to determine the best solution for summer period. Solutions with “c” and “s” TP show the less desirable results. “s” TP show low chi-square values, however, they present high negative residuals in the morning and at night. “c” TP show a high positive residual around 15:00-18:00 hrs. The solution aB5_H1_C3_S1 is chosen to present the best results from this analysis due to the low diurnal residual, COA slope close to zero and the low BBOA slope in the NOx, BC and COA trilinear regressions (Figures S9.a, S9.b and S9.c).

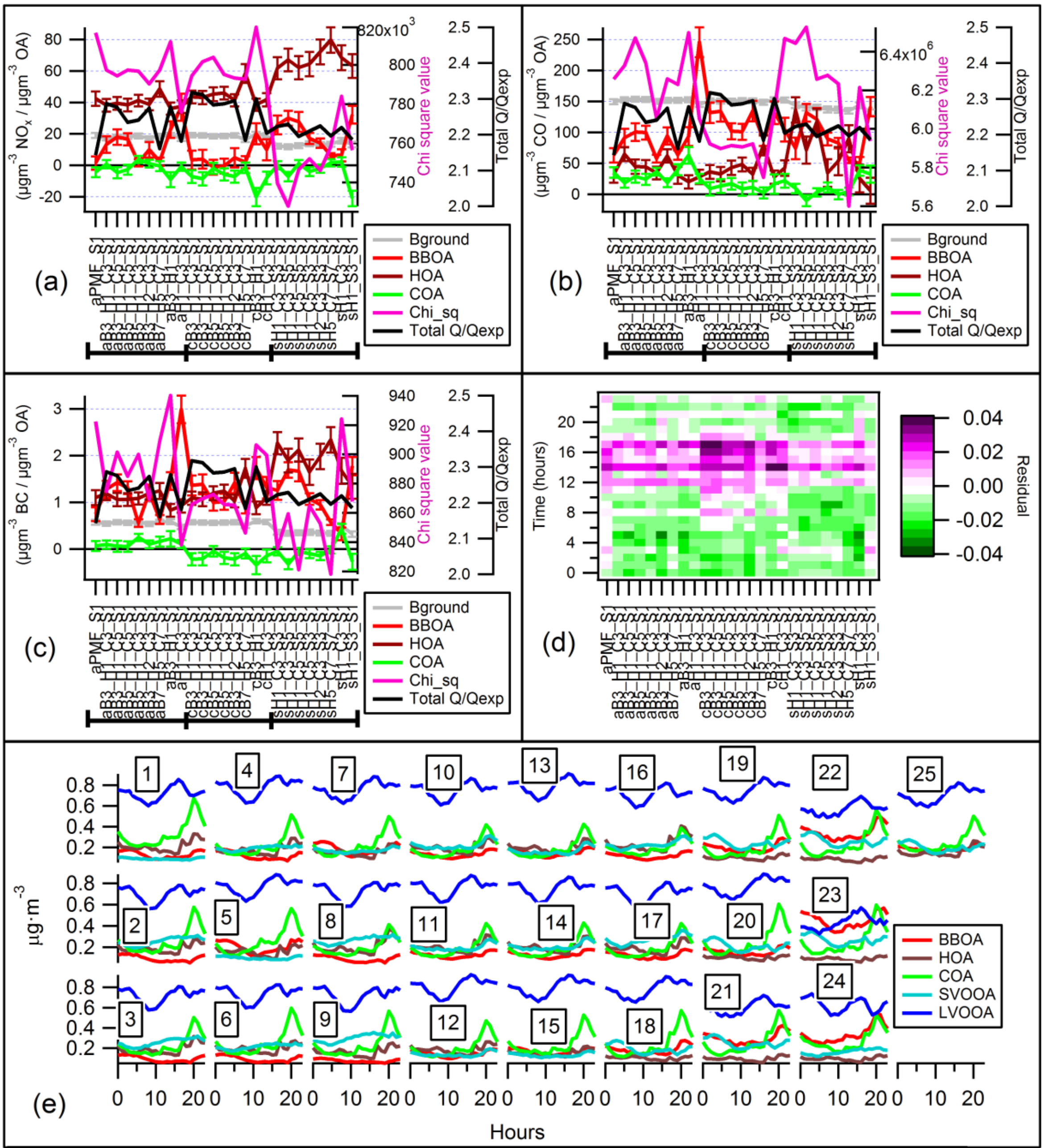

1	aPMF S1	6	aB3 H2 C3 S1	11	cB3 H1 C5 S1	16	cB3 H1 S1	21	sH1 C5 S3 S1
2	aB3 H1 C3 S1	7	aB7 H5 C7 S1	12	cB5 H1 C5 S1	17	cH1 C3 S1	22	sH2 C3 S3 S1
3	aB3 H1 C5 S1	8	aB3 H1 S1	13	cB5 H1 C3 S1	18	sH1 C3 S3 S1	23	sH5 C7 S7 S1
4	aB5 H1 C5 S1	9	aH1 C3 S1	14	cB3 H2 C3 S1	19	sH1 C3 S5 S1	24	sH1 C3 S1
5	aB5 H1 C3 S1	10	cB3 H1 C3 S1	15	cB7 H5 C7 S1	20	sH1 C5 S5 S1	25	sH1 S3 S1

(f)

Figure S9: NOx, CO and BC trilinear regression (a,b,c), diurnal residual (d),diurnal concentrations (e) all the solutions for summer analysis (f).

Figure S10 shows the PMF analysis for the autumn period. Solution 4 has been the chosen solution to be compared with ME-2 solutions because of its low Q/Qexp and a COA slope close to zero for the NOx trilinear regression and a lower diurnal residual compared to the other PMF solutions.

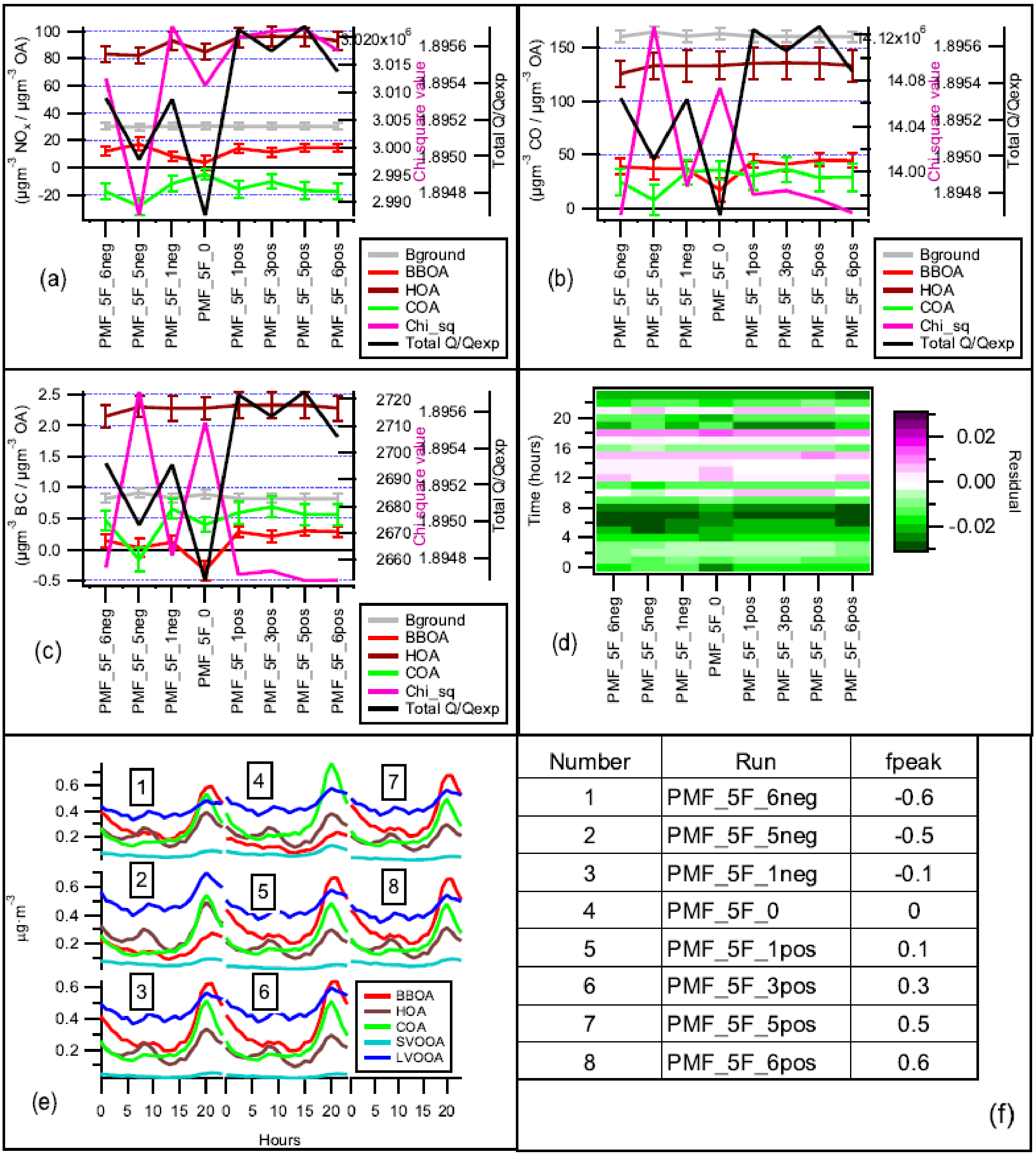

Number	Run	fpeak
1	PMF_5F_6neg	-0.6
2	PMF_5F_5neg	-0.5
3	PMF_5F_1neg	-0.1
4	PMF_5F_0	0
5	PMF_5F_1pos	0.1
6	PMF_5F_3pos	0.3
7	PMF_5F_5pos	0.5
8	PMF_5F_6pos	0.6

Figure S10: NOx, CO and BC trilinear regression (a, b, c), diurnal residual (d), diurnal concentrations (e) and solution list for autumn PMF analysis (f).

Figure S11 shows the analysis performed to determine the best solution for autumn period. Solutions with “a” TP show the less favourable Chi square results in the three trilinear regression figures (Figures S11.a, S11.b and S11.c). wB3_H1_S1 solution is chosen to present the best results from this analysis with low chi-squares and COA slope close to zero in the trilinear regression with NOx (Figures S11.a).

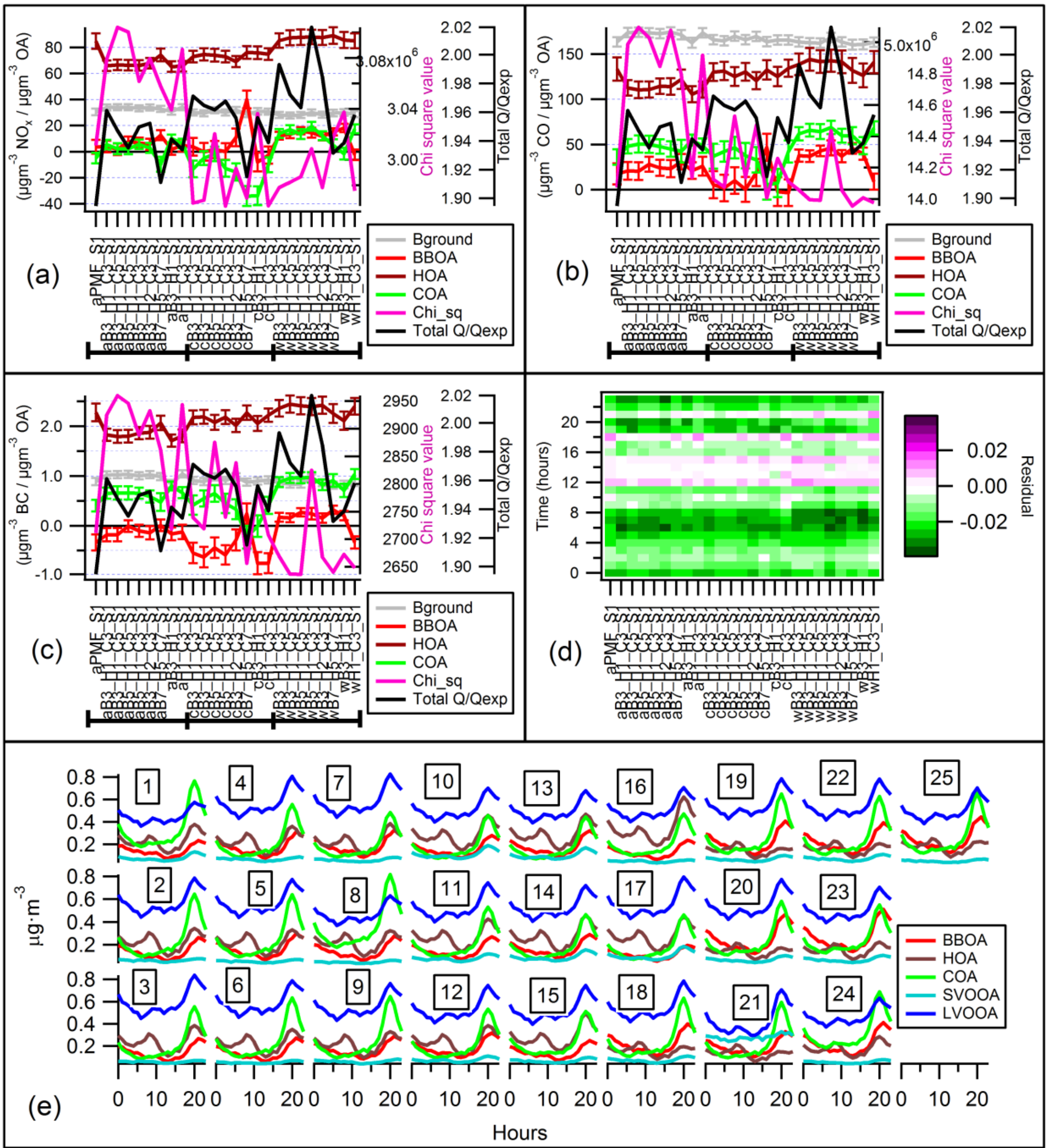

1	aPMF S1	6	aB3 H2 C3 S1	11	cB3 H1 C5 S1	16	cB3 H1 S1	21	wB5 H1 C3 S1
2	aB3 H1 C3 S1	7	aB7 H5 C7 S1	12	cB5 H1 C5 S1	17	cH1 C3 S1	22	wB3 H2 C3 S1
3	aB3 H1 C5 S1	8	aB3 H1 S1	13	cB5 H1 C3 S1	18	wB3 H1 C3 S1	23	wB7 H5 C7 S1
4	aB5 H1 C5 S1	9	aH1 C3 S1	14	cB3 H2 C3 S1	19	wB3 H1 C5 S1	24	wB3 H1 S1
5	aB5 H1 C3 S1	10	cB3 H1 C3 S1	15	cB7 H5 C7 S1	20	wB5 H1 C5 S1	25	wH1 C3 S1

(f)

Figure S11: NOx, CO and BC trilinear regression (a,b,c), diurnal residual (d),diurnal concentrations (e) all the solutions for autumn analysis (f).

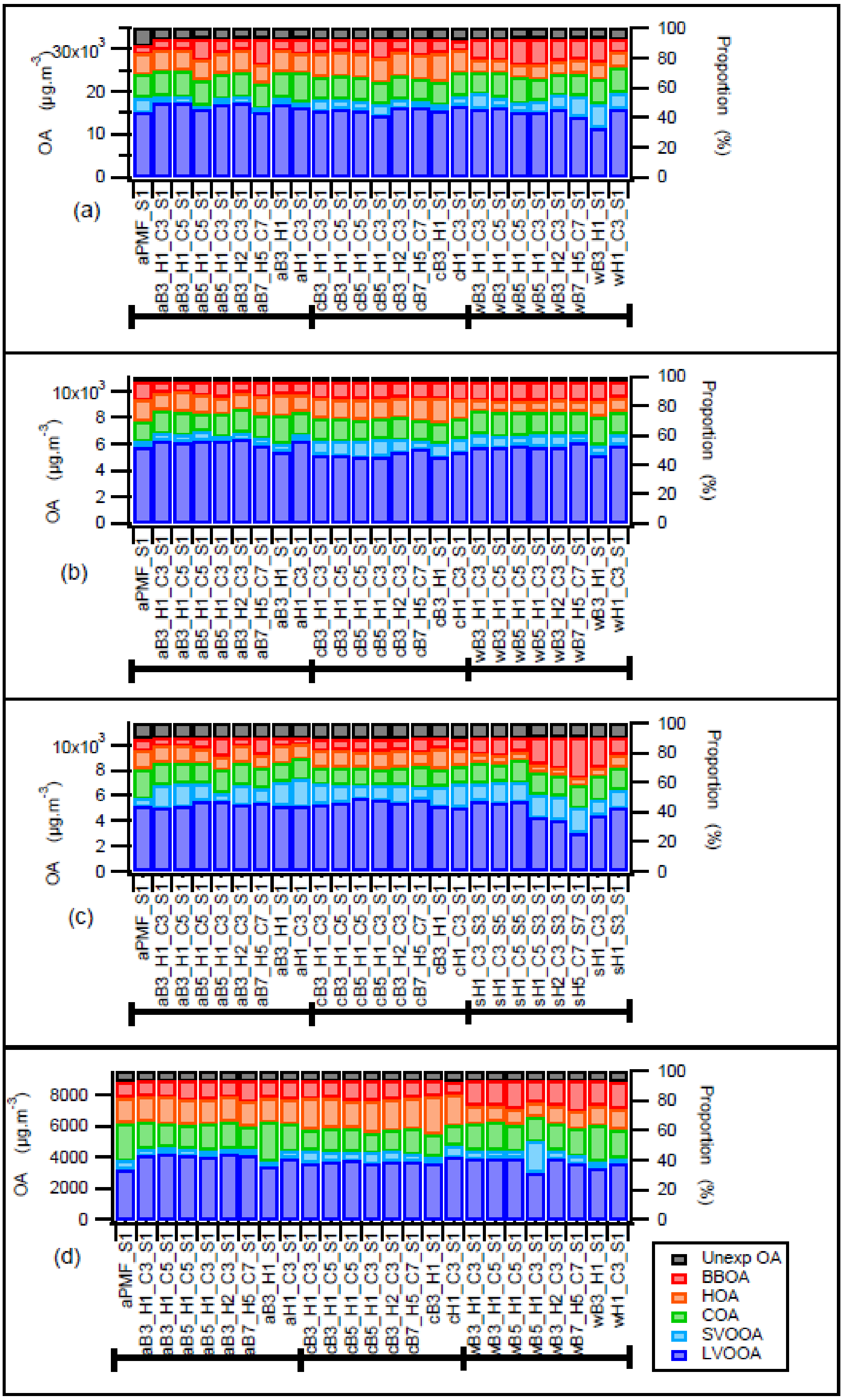

Figure S12: OA concentrations and proportions of the different OA sources to the total OA. March-Dec (a), spring (b), Summer (c) and autumn (d).

S13. OA and meteorology time series to analyse $PM_{2.5}$ concentrations.

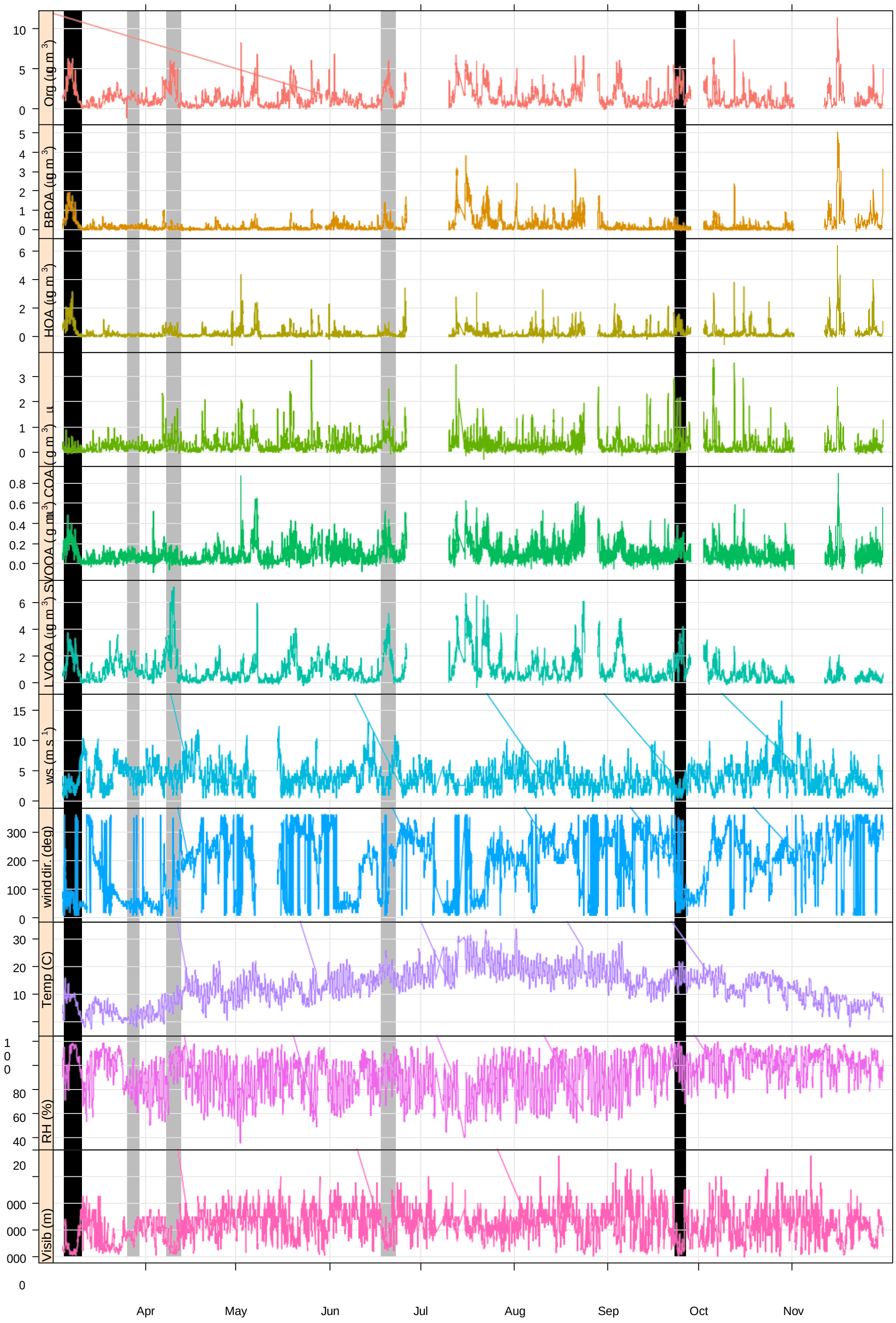

Figure S13: OA and meteorology showing moderate (grey) and high (black) $PM_{2.5}$ concentrations.

Paper 2

6.2 Simultaneous Aerosol Mass Spectrometry and Chemical Ionisation Mass Spectrometry measurements during a biomass burning event in the UK: Insights into nitrate chemistry

Ernesto Reyes-Villegas, Michael Priestley, Yu-Chieh Ting, Sophie Haslett, Thomas Bannan, Michael Le Breton, Paul I. Williams, Asan Bacak, Michael J. Flynn, Hugh Coe, Carl Percival, James D. Allan.

The DOI of the paper on ACPD is: doi.org/10.5194/acp-2017-605

The manuscript version presented in this thesis is the final version that will be published once I process the invoice.

Research highlights:

- OA sources were deconvolved, using PMF/ME-2, during a special event in 2014 with high biomass burning concentrations, named Bonfire Night.
- While PMF/ME-2 were performed under different tests aiming to identify the best way to deconvolve OA, it was not possible to completely deconvolve OA during the event with high biomass burning aerosol concentrations.
- Particulate organic oxides of nitrogen (PON) concentrations were quantified. The results suggest that secondary PON does not absorb light at 470 nm while primary PON and LVOOA absorb light at 470 nm.

Author contributions:

This study was an in-house project carried out by researchers from the University of Manchester. I participated in the aerosol instrumentation deployment, the AMS calibration and supervision of the instruments during the measurement campaign. Yu-Chieh Ting, Sophie Haslett, Dr Paul I. Williams, Dr Michael J. Flynn and Dr James D. Allan collaborated with the aerosol measurements. Dr Thomas Bannan, Dr Michael Le Breton and Dr Asan Bacak performed the CIMS measurements. I personally performed the data analysis with support of Michael Priestley in the CIMS analysis. I wrote the manuscript and worked on the comments from co-authors as well as addressing the reviewer's comments, under the guidance of Dr James Allan and Dr Hugh Coe.

Blank page

Atmos. Chem. Phys., 18, 1–19, 2018
https://doi.org/10.5194/acp-18-1-2018

Atmospheric Chemistry and Physics
Open Access

Simultaneous aerosol mass spectrometry and chemical ionisation mass spectrometry measurements during a biomass burning event in the UK: insights into nitrate chemistry

Ernesto Reyes-Villegas[1], **Michael Priestley**[1], **Yu-Chieh Ting**[1], **Sophie Haslett**[1], **Thomas Bannan**[1], **Michael Le Breton**[1,a], **Paul I. Williams**[1,2], **Asan Bacak**[1], **Michael J. Flynn**[1], **Hugh Coe**[1], **Carl Percival**[1,b], and **James D. Allan**[1,2]

[1]School of Earth, Atmospheric and Environmental Sciences, The University of Manchester, Manchester, M13 9PL, UK
[2]National Centre for Atmospheric Science, The University of Manchester, Manchester, M13 9PL, UK
[a]now at: Department of Chemistry & Molecular Biology, University of Gothenburg, 40530 Gothenburg, Sweden
[b]now at: Jet Propulsion Laboratory, 4800 Oak Grove Drive, Pasadena, CA 91109, USA

Correspondence: Ernesto Reyes-Villegas (ernesto.reyesvillegas@manchester.ac.uk)

Received: 29 June 2017 – Discussion started: 11 July 2017
Revised: 10 January 2018 – Accepted: 29 January 2018 – Published:

Abstract. Over the past decade, there has been an increasing interest in short-term events that negatively affect air quality such as bonfires and fireworks. High aerosol and gas concentrations generated from public bonfires or fireworks were measured in order to understand the night-time chemical processes and their atmospheric implications. Nitrogen chemistry was observed during Bonfire Night with nitrogen containing compounds in both gas and aerosol phases and further N_2O_5 and $ClNO_2$ concentrations, which depleted early next morning due to photolysis of NO_3 radicals and ceasing production. Particulate organic oxides of nitrogen (PONs) concentrations of 2.8 $\mu g\, m^{-3}$ were estimated using the m/z 46 : 30 ratios from aerosol mass spectrometer (AMS) measurements, according to previously published methods. Multilinear engine 2 (ME-2) source apportionment was performed to determine organic aerosol (OA) concentrations from different sources after modifying the fragmentation table and it was possible to identify two PON factors representing primary (pPON_ME2) and secondary (sPON_ME2) contributions. A slight improvement in the agreement between the source apportionment of the AMS and a collocated AE-31 Aethalometer was observed after modifying the prescribed fragmentation in the AMS organic spectrum (the fragmentation table) to determine PON sources, which resulted in an $r^2 = 0.894$ between biomass burning organic aerosol (BBOA) and b_{abs_470wb} compared to an $r^2 = 0.861$ obtained without the modification. Correlations between OA sources and measurements made using time-of-flight chemical ionisation mass spectrometry with an iodide adduct ion were performed in order to determine possible gas tracers to be used in future ME-2 analyses to constrain solutions. During Bonfire Night, strong correlations (r^2) were observed between BBOA and methacrylic acid (0.92), acrylic acid (0.90), nitrous acid (0.86), propionic acid, (0.85) and hydrogen cyanide (0.76). A series of oxygenated species and chlorine compounds showed good correlations with sPON_ME2 and the low volatility oxygenated organic aerosol (LVOOA) factor during Bonfire Night and an event with low pollutant concentrations. Further analysis of pPON_ME2 and sPON_ME2 was performed in order to determine whether these PON sources absorb light near the UV region using an Aethalometer. This hypothesis was tested by doing multilinear regressions between b_{abs_470wb} and BBOA, sPON_ME2 and pPON_ME2. Our results suggest that sPON_ME2 does not absorb light at 470 nm, while pPON_ME2 and LVOOA do absorb light at 470 nm. This may inform black carbon (BC) source apportionment studies from Aethalometer measurements, through investigation of the brown carbon contribution to b_{abs_470wb}.

Published by Copernicus Publications on behalf of the European Geosciences Union.

1 Introduction

Exposure to combustion aerosols has been associated with a range of negative health effects. In particular, wood smoke aerosols have been shown to present respiratory and cardiovascular health effects (Naeher et al., 2007). Bonfires and fireworks are one of the main sporadic events with high emissions of atmospheric pollutants (Vassura et al., 2014; Joshi et al., 2016); even when these high emissions only last a couple of hours, high pollutant concentrations may instigate adverse effects on human health (Moreno et al., 2007; Godri et al., 2010) and severely reduce visibility (Vecchi et al., 2008). Ravindra et al. (2003) found that the short-term exposure to air pollutants increases the likelihood of acute health effects.

Due to these adverse effects, different studies have been performed to analyse air pollution during important festivities around the world, for instance New Year's Eve celebrations (Drewnick et al., 2006; Zhang et al., 2010), the Lantern Festival in China (Wang et al., 2007) and Diwali festival in India (Pervez et al., 2016) as well as football matches such as during the Bundesliga in Mainz, Germany in 2012 (Faber et al., 2013). In the UK, the Bonfire Night festivity takes place on 5 November to commemorate Guy Fawkes' unsuccessful attempt to destroy the Houses of Parliament in 1605 (Ainsworth, 1850). During this celebration, bonfires, usually followed by fireworks, are lit domestically and on a larger scale communally in public parks. Different studies have been carried out to assess the air pollution during Bonfire Night in the UK; for instance targeting the particle size distribution (Colbeck and Chung, 1996), investigating PM_{10} concentrations in different cities around the UK during Bonfire Night celebrations (Clark, 1997) and measuring dioxins in ambient air in Oxford (Dyke et al., 1997); polycyclic aromatic hydrocarbons were measured in Lancaster in 2000 (Farrar et al., 2004), potentially toxic elements were measured and their association with health risks was assessed in London (Hamad et al., 2015).

Receptor modelling has been widely used to determine organic aerosol (OA) sources in urban environments. However, it has been used in just a small number of studies with sporadic events of high pollutant concentrations. For instance, Vecchi et al. (2008) were the first to analyse measurements taken during firework displays using positive matrix factorisation (PMF). Tian et al. (2014) did a PMF analysis of $PM_{2.5}$ components, identifying five different sources: crustal dust, coal combustion, secondary particles, vehicular exhausts and fireworks. In Riccione, Italy, Vassura et al. (2014) determined that levoglucosan, organic carbon (OC), polycyclic aromatic hydrocarbons (PAHs), Al and Pb, emitted from bonfires during St. Joseph's Eve, can be used as markers for bonfire emissions.

Particulate organic oxides of nitrogen (PONs), a term we use here to encompass nitro-organics and organic nitrates, have been found to absorb light near the ultraviolet (UV) region (Mohr et al., 2013) and to present potential toxicity to human health (Fernandez et al., 1992; Qingguo et al., 1995). PONs also act as a NO_x reservoir at night, releasing NO_x concentrations when the sun rises with the possibility of increasing O_3 production (Perring et al., 2013; Mao et al., 2013). PONs are important components of OAs; for instance Day et al. (2010), in measurements taken during winter at an urban location, found that PON concentrations accounted for up to 10 % of organic matter. Kiendler-Scharr et al. (2016) concluded that, on a continental scale, PONs represent 34 to 44 % of aerosol nitrate. Organic oxides of nitrogen can be categorised, according to their origin, into two types: primary and secondary. Primary organic nitrates are related to combustion sources (Zhang et al., 2016) such as fossil fuels (Day et al., 2010) and biomass burning emissions (Kitanovski et al., 2012; Mohr et al., 2013). Secondary organic oxides of nitrogen are produced in the atmosphere, for example when NO_3 reacts with unsaturated hydrocarbons (Ng et al., 2017). Nitrophenols are produced from reactions of phenols, both during the day reacting with $OH + NO_2$ and at night reacting with $NO_3 + NO_2$ (Harrison et al., 2005; Yuan et al., 2016).

The Aethalometer (Magee Scientific, USA) has been widely used to measure light absorbing carbon, proving to be a robust instrument that can operate in a variety of environments and is currently being used at many different locations around the world. The European Environment Agency, in a technical report published in 2013 (EEA, 2013), states that there are at least 11 European countries using Aethalometers. The UK has a black carbon (BC) network comprising of 14 sites covering a wide range of monitoring sites (https://uk-air.defra.gov.uk/networks/network-info?view=_ukbsn) and, in 2016, India started a BC network with 16 Aethalometers (Laskar et al., 2016). Commonly, Aethalometers have been used to separate sources of light-absorbing aerosols following Sandradewi et al. (2008). The approach separates absorption from traffic, predominately resulting from BC, which absorbs light in the infrared region and from wood burning, which includes BC and absorbing organic matter that also absorbs near the UV region. The Aethalometer model is based on the differences in aerosol absorption, using the absorption Ångström exponent, at a specific wavelength of light chosen to run the model. Absorption Ångström exponent values range from 0.8 to 1.1 for traffic and 0.9–3.5 for wood burning (Zotter et al., 2017). It is known that brown carbon (BrC) is organic matter capable of absorbing light near the UV region (Bones et al., 2010; Saleh et al., 2014) and that PONs are a potential contributor to BrC (Mohr et al., 2013). However, the mechanistic principle that links this behaviour to wood burning has not been completely resolved and there may be other sources such as secondary organic aerosols (SOAs) that can absorb near the UV region.

Here we present an analysis performed on data collected during Bonfire Night celebrations in Manchester, UK (29 October to 10 November 2014) using a compact time-of-flight aerosol mass spectrometer (cToF-AMS) and a high-resolution time-of-flight chemical ionisation mass spectrometer (HR-ToF-CIMS) along with other instruments to measure both aerosols and gaseous pollutants with the aim of understanding the night-time chemical processes and their atmospheric implications. Very high concentrations of pollutants occurred as a result of the meteorological conditions, which presented a good opportunity to investigate the detailed phenomenon as a case study, particularly the possibility to determine PON concentrations, their nature and interaction with Aethalometer measurements.

2 Methods

2.1 Site and instrumentation

Online measurements of aerosols and gases were taken from ambient air, between 29 October and 10 November 2014, at a rooftop location at the University of Manchester (53.467° N, 2.232° W), in order to quantify atmospheric pollution during Bonfire Night celebrations on and around 5 November. Figure S1 in the Supplement shows a map with the location of the monitoring site and nine public parks where bonfire and/or fireworks were displayed around greater Manchester. This is the same dataset presented by Liu et al. (2017).

A cToF-AMS (hereafter AMS) was used to perform 5 min measurements of OA, sulfate (SO_4^{2-}), nitrate (NO_3^-), ammonium (NH_4^+) and chloride (Cl^-) (Drewnick et al., 2005). This version of AMS provides unit mass resolution mass spectra information. A HR-ToF-CIMS (hereafter CIMS) was used to measure gas phase concentrations, using iodide as a reagent (Lee et al., 2014). The methodology to calculate gas phase concentrations from CIMS measurements have been described by Priestley et al. (2018). An Aethalometer (model AE31, Magee Scientific) measured light absorption at seven wavelengths (370, 450, 571, 615, 660, 880 and 950 nm) and a multi-angle absorption photometer (MAAP; Thermo model 5012) measured BC concentrations (Petzold et al., 2002). NO_x, CO, O_3 and meteorology data were downloaded from Whitworth observatory (http://www.cas.manchester.ac.uk/restools/whitworth/data/), which were measured at the same location. From 31 October to 10 November, a catalytic stripper was attached to the AMS, switching every 30 min between direct measurements and through the catalytic stripper. These measurements were performed as part of a different experiment (Liu et al., 2017). In the present study we used the AMS data from the direct measurements only, aerosol and gas data from other instruments were averaged to AMS sampling times.

2.2 Source apportionment

2.2.1 Aethalometer model

The aerosol light absorption depends on the wavelength and may be used to apportion BC from traffic and wood burning from Aethalometer measurements as proposed by Sandradewi et al., 2008. The absorption coefficients (b_{abs}) are related to the wavelengths at which the absorptions are measured (λ) and the Ångström absorption exponents (α) with the relationship $b_{\mathrm{abs}} \propto \lambda^{\alpha i}$, thus the following equations can be solved:

$$\frac{b_{\mathrm{abs\_470tr}}}{b_{\mathrm{abs\_950tr}}} = \left(\frac{470}{950}\right)^{-\alpha_{\mathrm{tr}}}, \tag{1}$$

$$\frac{b_{\mathrm{abs\_470wb}}}{b_{\mathrm{abs\_950wb}}} = \left(\frac{470}{950}\right)^{-\alpha_{\mathrm{wb}}}, \tag{2}$$

$$b_{\mathrm{abs}}\,(470_{\mathrm{nm}}) = b_{\mathrm{abs\_470tr}} + b_{\mathrm{abs\_470wb}}, \tag{3}$$

$$b_{\mathrm{abs}}\,(950_{\mathrm{nm}}) = b_{\mathrm{abs\_950tr}} + b_{\mathrm{abs\_950wb}}. \tag{4}$$

Here, it is possible to calculate the wood burning (wb) and traffic (tr) contributions to BC at 470 and 950 nm as used in previous studies (Crilley et al., 2015; Harrison et al., 2012). Wavelengths of 470 and 950 nm were chosen as Zotter et al. (2017) determined that using this pair of wavelengths resulted in fewer residuals compared with using the wavelengths 470–880 and 370–880 nm. Before the Aethalometer model was applied, the absorption coefficients (b_{abs}) needed to be corrected following Weingartner et al. (2003) as attenuation is affected by scattering and loading variations. The following parameters were calculated: multiple scattering constant $C = 3.16$ and filter loading factors (f) of 1.49 and 1.28 for the wavelengths 470 and 950 nm, respectively. Refer to Sect. S3 in the Supplement for detailed information.

2.2.2 Particulate organic oxides of nitrogen (PONs)

Concentrations of PONs were calculated following the method proposed by Farmer et al. (2010) and the considerations used by Kiendler-Scharr et al. (2016). This method has been previously used in studies looking at aerosols from biomass burning (Tiitta et al., 2016; Zhu et al., 2016; Florou et al., 2017). Equation (5) calculates the PON fraction (X_{PON}), using the signals at m/z 30 and m/z 46 to calculate m/z ratios 46 : 30 from AMS measurements (R_{meas}), from ammonium nitrate calibrations (R_{cal}), and from organic nitrogen (R_{ON}) to quantify PON concentrations.

$$X_{\mathrm{PON}} = \frac{(R_{\mathrm{meas}} - R_{\mathrm{Cal}})\,(1 + R_{\mathrm{ON}})}{(R_{\mathrm{ON}} - R_{\mathrm{cal}})\,(1 + R_{\mathrm{meas}})}, \tag{5}$$

where ratios from ammonium nitrate calibrations $R_{\mathrm{cal}} = 0.5$; $R_{\mathrm{meas}} = m/z$ 46 : 30 ratio from measurements; m/z 46 : 30 ratio from ON $R_{\mathrm{ON}} = 0.1$, Following Kostenidou et al. (2015) consideration, $R_{\mathrm{ON}} = 0.1$ was calculated as the minimum m/z 46 : 30 ratio observed. A R_{ON} value of 0.1 has been used in previous studies (Kiendler-Scharr et al., 2016; Tiitta et al., 2016).

$$\mathrm{PON} = X_{\mathrm{PON}} \cdot NO_3^- \tag{6}$$

Finally, Eq. (6) calculates PON concentrations ($\mu g\,m^{-3}$) where NO_3^- is the total nitrate measured by the cToF-AMS.

The method proposed by Farmer et al. (2010) is based on HR-ToF-AMS measurements where m/z 30 represents the NO^+ ion and m/z 46 the NO_2^+ ion, while the cToF-AMS gives unit mass resolution mass spectra information, hence there is the possibility to have interference of the CH_2O^+ ion at m/z 30. However, when analysing mass spectra from previous laboratory and ambient studies using HR-ToF-AMS to investigate biomass burning emissions, we can confirm that the signal of CH_2O^+ at m/z 30 is low compared to signals at m/z's 29 and 31, while in this study m/z 30 is the main signal (Fig. 5c). Hence, in this study an interference of CH_2O^+ at m/z 30 is unlikely and if there were any interference of CH_2O^+ it would be negligible. Table S1 in the Supplement shows m/z 30/29 and 30/31 from previous laboratory and ambient studies investigating biomass burning emissions.

Another possible interference would be the presence of mineral nitrates at m/z 30 (e.g. KNO_3 and $NaNO_3$). However, mineral nitrate salts tend to be large particles (Allan et al., 2006; Chakraborty et al., 2016) and also have a low vaporisation efficiency (Drewnick et al., 2015), which makes it unlikely to be measured by the AMS in large quantities.

2.2.3 Multilinear engine 2 (ME-2)

Multilinear engine 2 (ME-2; Paatero, 1999) is a multivariate solver used to determine factors governing the behaviour of a two-dimensional data matrix, which can then be interpreted as pollutant sources. ME-2 uses the same data model as PMF, which is also a receptor model that performs factorisation by using a weighted least squares approach (Paatero and Tapper, 1994).

In order to explore the solution space, ME-2 is capable of using information from previous studies, for example pollutant time series or mass spectra, as inputs to the model (named target time series and target profiles) to constrain the runs. These constraints are performed using the a-value approach, to determine the extent to which the output is allowed to vary. For example, by using an a-value of 0.1 to a specific source, the user is allowing the output to vary 10 % from the input. For more details refer to Canonaco et al. (2013).

In this study, ME-2 and PMF were used through the source finder interface, (SoFi version 4.8; Canonaco et al., 2013) to identify OA sources using the suggestions made by Crippa et al. (2014) and the strategy proposed by Reyes-Villegas et al. (2016). ME-2 was performed using mass spectra (BBOA, HOA and COA) from two different studies as target profiles (TP) to constrain the runs: London (Young et al., 2015) and Paris (Crippa et al., 2013), Fig. S5 explains the labelling used to identify the different runs.

Solutions were explored with PMF using different FPEAK values (ranging from -1.0 to 1.0 with steps of 0.1) and ME-2 using different a-values (nine runs with the London TP and nine runs with the Paris TP) looking at 4, 5 and 6-factor solutions. Section S7.1 shows the strategy used to determine the optimal solution. Factorisation struggles to separate two or more sources if they are highly correlated, for example during stagnant conditions due to low temperatures and wind speed, which was the case during Bonfire Night 2014. The pollutants were well-mixed, making it difficult to separate the sources. Hence, four tests were performed using different time sets in order to identify the best way to perform source apportionment:

- Test 1 performs factorisation on all of the dataset.
- Test 2 (hereafter Test2) involves factorising the event before and after Bonfire Night and using mass spectra from this analysis as TP to factorise the Bonfire Night event.
- Test 3 involves factorising the Bonfire Night event and using mass spectra from this analysis as TP as applied to the complete dataset.
- Test 4 involves factorising the event before and after Bonfire Night and using mass spectra from this analysis as TP to factorise the full dataset.

PONs may exhibit covariance with other types of OA, thus their inclusion in the source apportionment analysis may improve the factorisation and highlight their co-emission with other OA types. Previous studies have quantified PON concentrations from AMS-PMF analysis to both rural and urban measurements (Sun et al., 2012; Hao et al., 2014; Xu et al., 2015; Zhang et al., 2016). In this study, an experiment was designed by modifying the fragmentation table, through the AMS analysis toolkit 1.56, in order to identify a PON source. The fragmentation table contains the different chemical species measured by the AMS, with each row representing m/z for specific species and the user can define peaks that exist in each species' partial mass spectrum with their dependency on other peaks (Allan et al., 2004). The following steps were performed to modify the fragmentation table:

- Time series of a new ratio named R_{ON_30} is calculated by $R_{ON\_30} = PON / m/z$ 30, where PON is the time series calculated in Sect. 2.2.2 and m/z 30 is the time series of the signal at $m/z = 30$ measured by the AMS.
- Using the AMS analysis toolkit, the fragmentation table is modified (in the column "frag_Organic" at m/z 30) by multiplying $R_{ON\_30} \cdot 30$. See Fig. S4 for a screenshot of the fragmentation table.
- PMF inputs are generated to be used in the SoFi software.

3 Results

3.1 Meteorology and pollutant overview

During Bonfire Night festivities on 5 November, a temperature of 4 °C and wind speed of 1.5 m s^{-1} were observed

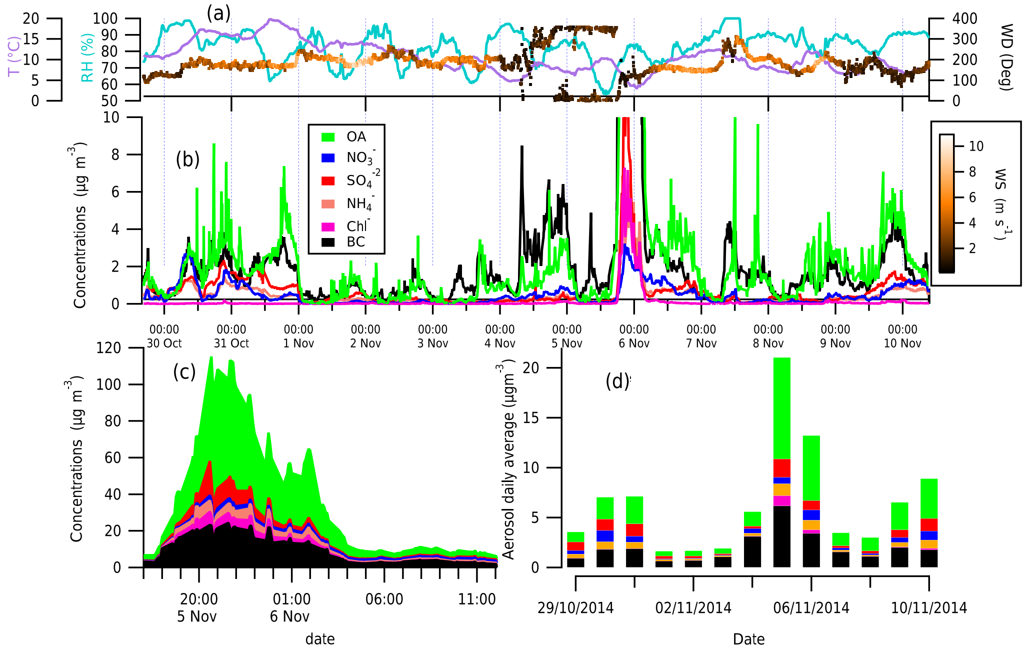

Figure 1. Meteorology **(a)**, aerosol concentrations during all measurement periods **(b)**. Chemical component mass concentrations during Bonfire Night plotted cumulatively **(c)**. Daily aerosol concentrations **(d)**.

(Fig. 1a), causing stagnant conditions which facilitated pollutant accumulation. Looking at the time series for the whole sampling time (Fig. 1b), it was possible to observe four separate events with different pollutant behaviour (marked with coloured lines over the x axis in Fig. 1), driven by different meteorological conditions: one event had high secondary concentrations (HSC, yellow line) from 30 October to 1 November, which experienced a relatively high temperature of 17–20 °C; another event of low pollutant concentrations (LC, grey line) from 1 to 3 November was observed when continental air masses were present; Bonfire Night (bfo, blue line), with a temperature of 4 °C; and a winter-like episode (WL, purple line) from 8 to 10 November, with temperatures of 5–6 °C and high primary pollutant concentrations. Figure S3 shows back trajectories of the different events.

Aerosol concentrations during Bonfire Night were particularly high (Fig. 1c), with the highest peak concentrations of 65.0, 19.0, 6.8, 6.0, 5.9 and 3.2 $\mu g\,m^{-3}$ for OA, BC, SO_4, Cl, NH_4 and NO_3 respectively measured around 20:30 LT (local time) on 5 November. It is worth noting how high these concentrations are compared to concentrations before and after Bonfire Night (Fig. 1b), where aerosol concentrations ranged from 0.5 to 7.0 $\mu g\,m^{-3}$. Measured PM_1 concentrations (sum of BC, organic and inorganic aerosols) of 115 $\mu g\,m^{-3}$ (Fig. 1c) were observed during Bonfire Night.

Looking at the daily concentrations (Fig. 1d), it is possible to observe PM_1 daily concentrations of 25 $\mu g\,m^{-3}$ on Bonfire Night compared to the low concentrations observed between 1 and 2 November with concentrations ranging between 3 and 4 $\mu g\,m^{-3}$. The impact of the emissions during Bonfire Night is present even during the next day with PM_1 concentrations of 14 $\mu g\,m^{-3}$.

Gas phase pollutants were measured at the Whitworth observatory. Figure 2 shows high SO_2, CO and NO_x concentrations during Bonfire Night; these primary pollutants are well-known combustion-related pollutants. The high SO_2 concentrations during Bonfire Night are expected as solid fuels such as wood emit SO_2 when burned. This can also explain the SO_2 peak on the night of 10–11 November when SO_2 concentrations may be related to solid fuels used for domestic heating as a result of the low temperatures (6 °C). CO and NO were present at higher concentrations during Bonfire Night compared to previous days with concentrations reaching 1600 ppb (CO) and 99 ppb (NO) during Bonfire Night compared to 1 November with concentrations of 230 ppb of CO and 16 ppb of NO. Some O_3 concentrations were measured during Bonfire Night but given the very high NO concentrations, these are considered to be an interference with the measurement.

3.2 Bonfire Night analysis

3.2.1 Traffic and wood burning contributions to BC

OA concentrations started increasing at 19:30 LT, while BC concentrations started increasing 2 h earlier around 17:00 LT (Fig. 1c). This rise in BC concentrations may be due to bonfire emissions, although they may also be related to traffic

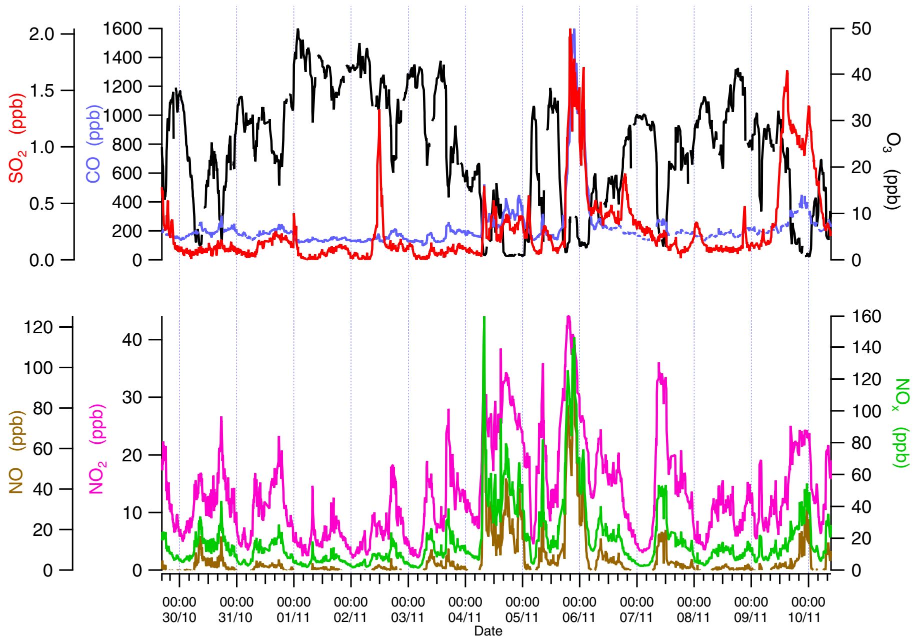

Figure 2. Time series of gases measured at Whitworth observatory.

emissions; thus the Aethalometer model was used to identify both traffic and wood burning contributions to BC.

Once b_{abs} values are corrected, equations shown in Sect. 2.2.1 are used to apply the Aethalometer model, with Ångström absorption exponents (α) of 1.0 for traffic (α_{tr}), using the wavelength 470 nm, and 2.0 for wood burning (α_{wb}) using the wavelength 950 nm, to determine traffic and wood burning contributions. Figure 3 shows the absorption coefficients for wood burning b_{abs_470wb} (blue) and traffic b_{abs_950tr} (red), both increasing around 17:00–18:00 LT to values lower than 100 Mm^{-1}, while b_{abs} indicates contributions from wood burning and traffic during this event. When the majority of bonfire events are taking place, around 20:00, when b_{abs_470wb} shows the greatest increase, with values reaching 480 Mm^{-1} compared to 150 Mm^{-1} for b_{abs_950tr}.

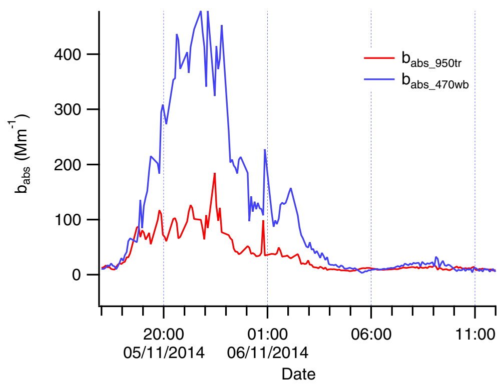

Figure 3. Absorption coefficients for Wood burning (wb) and traffic (tr).

3.2.2 PON identification and quantification

Currently, there is no direct technique to quantify online integrated PON concentrations. However, it is possible to estimate PON concentrations from AMS measurements using the m/z 46 : 30 ratios (Farmer et al., 2010) as explained in Sect. 2.2.2. This event during Bonfire Night 2014, with high pollutant concentrations provided the opportunity to identify the presence of PON. Inorganic nitrate from NH_4NO_3 has been detected at m/z 46 : 30 ratios between 0.33 and 0.5 (Alfarra et al., 2006) and of 0.37 (Fry et al., 2009), although each instrument-specific ratio is determined during routine calibrations. PON has been identified with m/z 46 : 30 ratios of 0.07–0.10 (Hao et al., 2014) and 0.17–0.26 (Sato et al., 2010). In this study, m/z 46 : 30 ratios of 0.11–0.18 were observed during Bonfire Night (Fig. 4), confirming the presence of PON during this event. Figure 4 shows PON concentrations of up to 2.8 $\mu g\,m^{-3}$ during Bonfire Night, which are over the detection limit of 0.1 $\mu g\,m^{-3}$ reported by Bruns et al. (2010). PON concentrations are considered high compared to previous studies with concentrations between 0.03 and 1.2 $\mu g\,m^{-3}$ from a wide variety of sites across Europe (Kiendler-Scharr et al., 2016), while high PON concentrations of 4.2 $\mu g\,m^{-3}$ were observed during a biomass burning event in Beijing, China (Zhang et al., 2016).

3.3 OA source apportionment

This event with high pollutant concentrations during Bonfire Night gave the opportunity to test the ME-2 factorisation tool

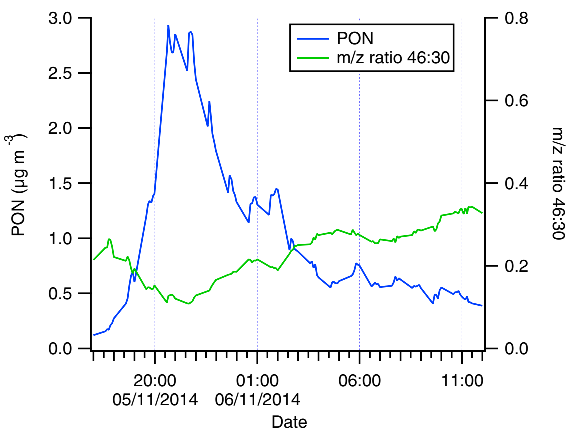

Figure 4. PON concentrations during Bonfire Night.

under these conditions and determine the best way to perform OA source apportionment on a case study event such as this. A number of different approaches for determining the optimal apportionment were tried and the one that yielded the most statistically optimal version was treated as a "best estimate", although it is acknowledged that even this may not be perfect. Indeed, it may not be possible to describe these data completely using the PMF data model. Six different tests were compared: four tests before modifying the fragmentation table and two tests when modifying the fragmentation table to determine a PON source. Test2_ON was the optimal "best estimate" solution, a brief description is given here after being compared to the other tests (Sect. S7.2). From this analysis, Test2 resulted in being the best way to deconvolve OA sources, with the lowest parameters analysed: residuals, Q/Qexp values and Chi square. After modifying the fragmentation table, Test2_ON still shows a good performance with low parameters (Fig. S6–S8). Refer to Sect. S7 for detailed information about the source apportionment strategy and analysis performed to determine the optimal solution.

Two steps were involved in Test2_ON: in step (a), PMF/ME-2 were run for the event before and after the Bonfire Night (named as not bonfire event, nbf). In step (b), mass spectra from the solution identified in step (a) were used as TP to analyse the bonfire-only (bfo) event. Finally, both solutions (nbf and bfo) were merged for further analysis. Different OA sources were identified in Test2_ON (Fig. 5), five sources were identified during the nbf event: biomass burning OA (BBOA), hydrocarbon-like OA (HOA), cooking OA (COA), secondary particulate organic oxides of nitrogen (sPON_ME2) and low volatility OA (LVOOA). These sources are identified by characteristic peaks in their respective mass spectra: BBOA, which is generated during the combustion of biomass, has a peak at m/z 60, related to levoglucosan (Alfarra et al., 2007); HOA, related to traffic emissions, presents high signals at m/z 55 and m/z 57 typical of aliphatic hydrocarbons (Canagaratna et al., 2004); COA, emitted from food cooking activities, is similar to HOA with a higher m/z 55 and lower m/z 57 (Allan et al., 2010; Slowik et al., 2010; Mohr et al., 2012); LVOOA, identified as a SOA, has a high signal at m/z 44 dominated by the CO_2^+ ion (Ng et al., 2010); sPON_ME2 has a strong signal at m/z 30 and it has been identified as secondary as it follows the same trend as LVOOA (Fig. 5a). In the case of the bfo event, six different sources were identified: BBOA, HOA, COA, LVOOA and two factors with peaks at m/z 30, which is related to PON (Sun et al., 2012). These two PON factors may have different sources: one may be secondary (sPON_ME2) and the other primary (pPON_ME2), which has a similar trend as BBOA (Fig. 5b). Further details about the nature of pPON_ME2 and sPON_ME2 will be explored in Sect. 4.2.

4 Discussion

4.1 OA source apportionment during the bfo event

It is worth noting that while all sources have their characteristic peaks and no apparent mass spectral "mixing" between sources (for example COA with a signal at m/z 60), COA, HOA and LVOOA present high concentrations during Bonfire Night (Fig. 5b). High concentrations of these sources could be expected as these (traffic and cooking activities) increase before and after the main bonfire events and the night represented a very strong inversion (which will trap all pollutants), but given the high concentrations experienced during the event and known variability for biomass burning emissions, the "model error" and thus rotational freedom is likely to be substantial. The result is that these two factors could contain indeterminate contributions from minor variabilities within the biomass burning profile and therefore must be interpreted with caution.

b_{abs_470wb} has the same source as BBOA, thus the correlation between these two can be used to evaluate the effectiveness of BBOA deconvolution from OA concentrations (Fröhlich et al., 2015; Visser et al., 2015), r^2 values are calculated and analysed using the following considerations: strong correlation ($r^2 \geq 0.75$), moderate correlation ($0.5 < r^2 < 0.75$) and low correlation ($r^2 \leq 0.5$). Here r^2 values are calculated for the bfo event between b_{abs_470wb} and the two BBOA obtained; BBOA, obtained without modifying the fragmentation table and BBOA_2 obtained after modifying the fragmentation table to identify a PON factor. A slightly higher correlation between b_{abs_470wb} and BBOA_2 was observed with $r^2 = 0.880$ compared to $r^2 = 0.839$ for b_{abs_470wb} and BBOA. While both have strong correlations from a quantitative point of view, qualitatively there is an improvement in BBOA_2. This improvement in BBOA_2 is explained by the fact that the PON factor may be mixed with BBOA and when both sources are separated, a higher correlation between BBOA_2 and b_{abs_470wb} is present. There is the possibility that the lower r^2 between b_{abs_470wb} and BBOA is due to

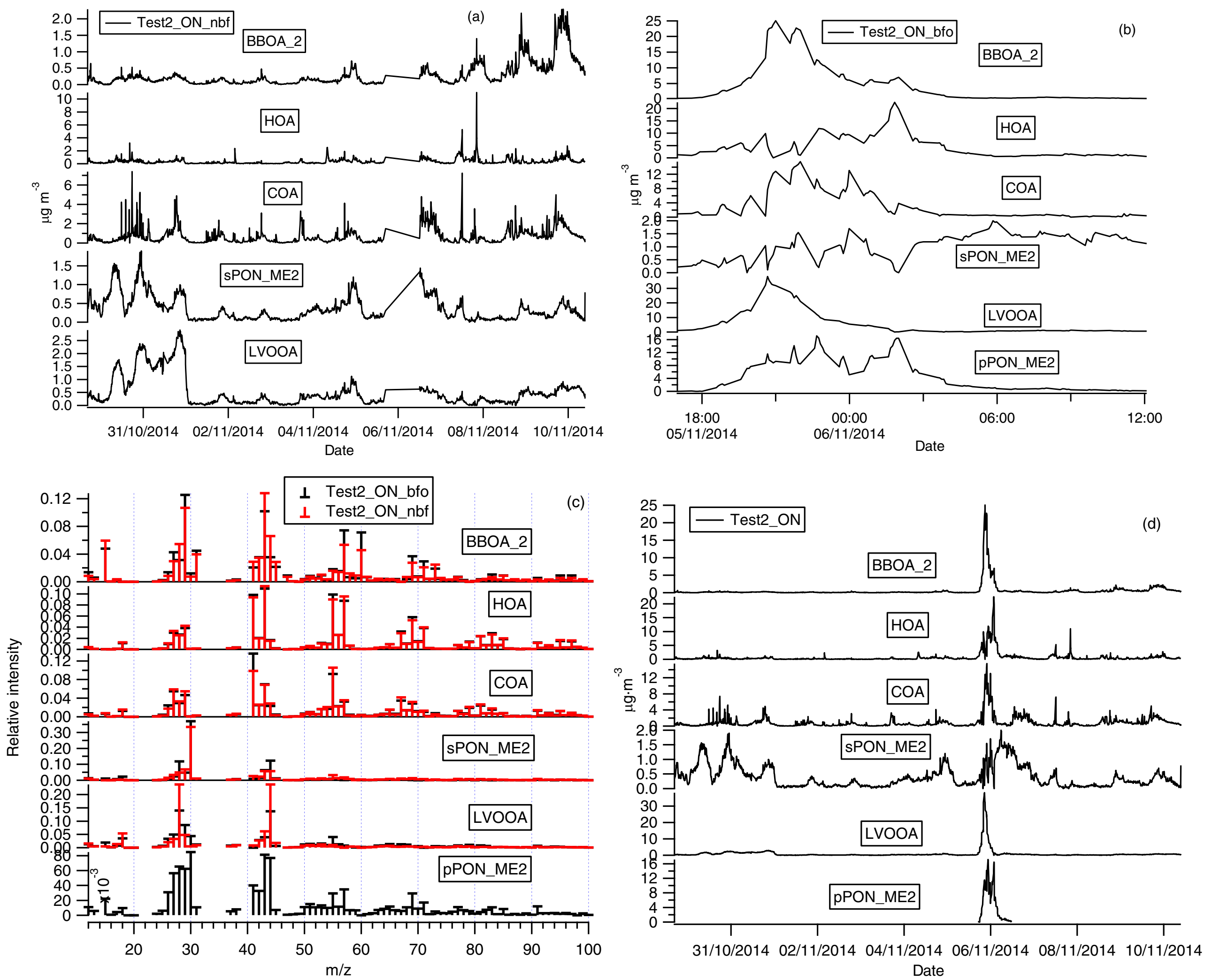

Figure 5. OA sources mass spectra and time series for Test2_ON for bonfire only (bfo) and not bonfire events (nbf). Figure 6d shows time series of both events.

having two BBOA factors in Test2. However, an $r^2 = 0.813$ between b_{abs_470wb} and the sum of BBOA + BBOA_1 is still lower than 0.880.

This shows the importance of performing OA source apportionment using different approaches in order to identify the best way to deconvolve OA sources. PMF and ME-2 source apportionment tools could not completely deconvolve OA sources during the bfo event. However, due to the strong correlation between b_{abs_470wb} and BBOA_ 2 ($r^2 = 0.880$), we consider that while BBOA_2 might not represent the total OA concentrations from the Bonfire Night event, it does represent the trend of OA emitted from the biomass burning.

4.2 Primary and secondary PONs

PON concentrations obtained from the m/z ratios 46 : 30 (blue line in Fig. 6) have a similar trend as BBOA, both increasing at the same time, suggesting a primary origin, but after 22:00 LT, when BBOA concentrations drop, PON concentrations remain present with a slow decrease and maintaining low concentrations when BBOA concentrations were not present anymore. This suggests the hypothesis that there might not be only one type of PON, and it could be divided into primary and secondary organic nitrate as reported in previous studies performed in western Europe (Mohr et al., 2013; Kiendler-Scharr et al., 2016).

Using this working hypothesis, primary and secondary PON concentrations were estimated using the slope between PON and BBOA, calculated from 18:00 to 12:00 LT, a time when the main Bonfire Night event took place (Fig. S10). PON concentrations were multiplied by this slope in order to calculate the primary PON (pPON) and secondary PON (sPON) and were calculated as sPON = PON − pPON. Figure 6 shows the time series of this estimation where

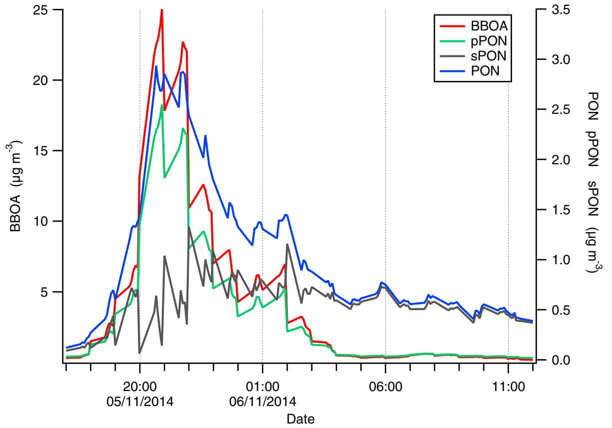

Figure 6. Secondary (sPON) and primary (pPON) organic nitrate time series estimated from PON and BBOA.

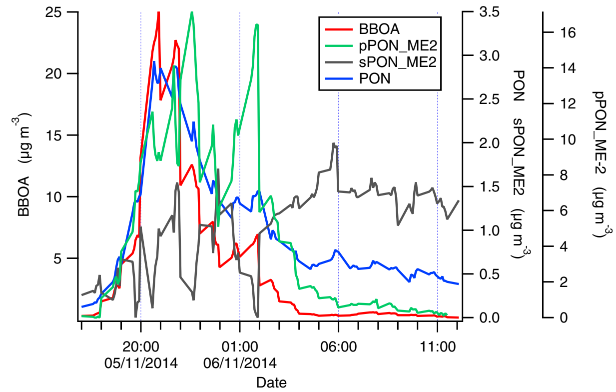

Figure 7. Secondary and primary organic nitrate time series obtained from ME-2 analysis.

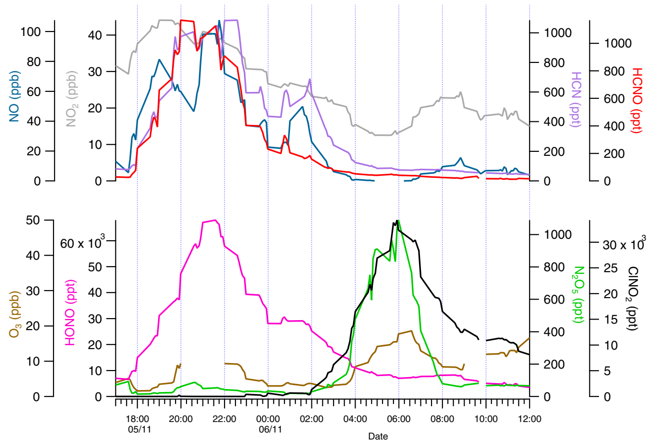

Figure 8. Time series of gases pollutants during Bonfire Night.

pPON reaches 2.5 µg m^{-3} and sPON with concentrations of 0.5 µg m^{-3}.

A similar behaviour with two different PON sources was observed in the source apportionment analysis performed in Sect. 3.3, where it was possible to separate two factors with a peak at m/z 30, characteristic of PON. Figure 7 shows that around 02:00 LT concentrations of the pPON_ME2 started to decrease (green line) while sPON_ME2 concentrations (grey line) increased. This analysis shows the presence of two different types of PON; pPON_ME2 are primarily emitted along with BBOA concentrations with the further presence of a different PON, considered to be secondary, which increase when primary pollutants start to decrease. Primary and secondary sources of PON have been previously identified from AMS-PMF analyses; Hao et al. (2014) identified PON to be secondary in nature, produced from the interaction between forest and urban emissions, while Zhang et al. (2016) determined PON to be related to primary combustion sources. In this study, it is worth noticing that the increase in sPON_ME2 takes place around 02:00 LT, a period when NO concentrations started decreasing and CIMS-measured N_2O_5 and $ClNO_2$ started to increase, suggesting that nitrate radical chemistry was occurring (Fig. 8), which is possibly the source of the sPON, although the exact mechanism can only be speculated.

Nitrate chemistry at night is important as nitrate radicals can be the main oxidants in polluted nocturnal environments away from enhanced NO and can create reservoirs and sinks of NO_x. The main NO_x removal at night is via the uptake of dinitrogen pentoxide (N_2O_5) into aerosols, as at night N_2O_5 is formed from NO_3 and NO_2. In the presence of chloride in the particle phase (e.g. in sea salt particles), N_2O_5 reacts to produce nitryl chloride ($ClNO_2$). In the morning, following overnight accumulation of $ClNO_2$, photochemical reactions take place to produce Cl and NO_2. N_2O_5 and $ClNO_2$ processing and interactions with nitrate chemistry have been previously studied in the UK (Le Breton et al., 2014a; Bannan et al., 2015). Figure 8 shows N_2O_5, $ClNO_2$ and O_3 concentrations increasing when NO and NO_2 concentrations decrease. All these processes may facilitate the sPON production at night. N_2O_5 concentrations reduce quickly after the sun rises, around 08:00 LT, while $ClNO_2$ concentrations decrease at a slower rate, with the lowest concentrations observed around 13:00 LT. Along with NO_3 chemistry, it was possible to observe other nitrogen-containing gases during Bonfire Night using the CIMS such as hydrogen cyanide (HCN) and nitrous acid (HONO), which have been found to be emitted from fires (Le Breton et al., 2013; Wang et al., 2015). High HONO concentrations at night are high the next morning when HONO reacts to produce OH and NO, which impacts both the OH budget and NO_x concentrations early the next morning (Lee et al., 2016).

4.3 OA factors and CIMS correlations

Analysing the CIMS measurements and comparing them with the OA factors, it may be possible to identify gas markers that can be used as inputs (target time series) to constrain solutions in future ME-2 analyses or as proxies when AMS data are not available. A linear regression was performed between the OA sources determined in Sect. 3.4.1 and CIMS peaks that have been considered positively identified (Priestley et al., in preparation), performing a coefficient of determination (r^2) analysis for the complete dataset (ALL), and the events HSC, LC, bfo and WL. During the event HSC, none of the OA sources showed an r^2 higher than 0.6. HOA did not have an r^2 higher than 0.6 with any of the different events analysed. There were no specific markers identified for COA, while COA showed r^2 values higher than 0.6 for the bfo event, these r^2 values were also observed with BBOA with even higher values. Table S4 shows the r^2 values, higher or equal to 0.4, obtained in this analysis. It is worth noting that r^2 values in the ALL event seem to be influenced by the bfo event; this is the case for BBOA, COA and LVOOA, which show similar r^2 values in both events. Thus, the analysis will only be explained for the individual events (bfo, LC and WL).

As expected, during bfo, BBOA is the OA source that shows the highest number of correlations during Bonfire Night. During the bfo episode, strong correlations were observed with BBOA and methacrylic acid ($r^2 = 0.92$), acrylic acid (0.90), nitrous acid (0.86), propionic acid, (0.85) and hydrogen cyanide (0.76), which have been previously determined as biomass burning tracers (Veres et al., 2010; Le Breton et al., 2013). Formic acid presented a strong correlation ($r^2 = 0.86$) with BBOA during Bonfire Night; however, this value drops to 0.52 for the complete dataset, which suggests formic acid during Bonfire Night is mainly primary, while formic acid concentrations measured for the whole dataset may be related to primary and secondary sources. This agrees with Le Breton et al. (2014b) who explored both primary and secondary origins of formic acid.

During the bfo event, LVOOA did not show a characteristic gas marker, as all the r^2 values were also observed with BBOA. This suggests two hypotheses: that the LVOOA was mixed with BBOA, in the form of humic-like material (Paglione et al., 2014), which cannot be differentiated from secondary OA in the mass spectra (Fig. 5c); or it could also be that secondary LVOOA may actually be present at the same time as BBOA concentrations, as during high relative humidity and low temperatures, enhanced partitioning of semi-volatile material to the particle phase occurs, where subsequent oxidation and oligomerisation may occur. Moreover, due to the high aerosol concentration present during Bonfire Night, there is a greater surface available for gases to be condensed and more particulate bulk to absorb into, thus it could be speculated that there would be high secondary aerosol concentrations. However, this is deemed unlikely as there may be little gas phase oxidation occurring in the presence of such high NO concentrations, which will remove ozone and nitrate radicals, the main source of oxidants at night.

During the bfo event, pPON_ME2 showed high r^2 values with carbon monoxide (0.78) and hydrogen cyanide (0.77) and moderate correlations with methylformamide (0.65) and dimethylformamide (0.63), all of which are typical primary pollutants related to combustion processes (Borduas et al., 2015, and references therein). sPON_ME2 showed moderate correlations with $ClNO_2$ (0.52) and $ClNO_3$ (0.53). Moderate r^2 values were also observed during the LC episode between $ClNO_2$–$ClNO_3$ and LVOOA (0.67–0.66) and sPON (0.74–0.69) proving their secondary origin. Cl_2, which has previously been identified to be related to both primary and secondary sources (Faxon et al., 2015), shows low correlations with pPON_ME2 (0.44) during the bfo event and sPON_ME2 (0.55) during the LC event.

4.4 PON and its relationship with $b_{\mathrm{abs\_470wb}}$ and BBOA

Organic oxides of nitrogen, originating from biomass burning, have been previously found to absorb light near the UV region (Jacobson, 1999; Flowers et al., 2010; Mohr et al., 2013). However, there is still a question of whether this absorption is due to primary or secondary PON. Here, the relationship between $b_{\mathrm{abs\_470wb}}$, PON and BBOA will be analysed to determine if PONs absorb at 470 nm, which would interfere with Aethalometer measurements.

In order to quantitatively determine any contribution from PON to the Aethalometer data products, a multilinear regression (MLR) analysis was performed on the complete dataset (ALL), and the events HSC, LC, bfo and WL (Table 1). This analysis was done in three ways: a multilinear regression (MLR1) with BBOA from OA source apportionment without modifying the fragmentation table and PON from m/z 46 : 30 analysis; a multilinear regression (MLR2) with BBOA_2 from OA source apportionment after modifying the fragmentation table and PON from 46 : 30 analysis; and a multilinear regression (MLR3) with BBOA_2 and PON sources from OA source apportionment after modifying the fragmentation table. The following bilinear regression was used:

$$b_{\mathrm{abs\_470wb}} = A + B \cdot x1 + C \cdot x2, \quad (7)$$

with $x1 = \mathrm{BBOA}$ and $x2 = \mathrm{PON}$ for MLR1; $x1 = \mathrm{BBOA\_2}$ and $x2 = \mathrm{PON}$ for MLR2; $x1 = \mathrm{BBOA\_2}$ and $x2 = \mathrm{sPON\_ME2}$ for MLR3. Additionally, a trilinear regression was performed to *HSC and *bfo with $x3 = \mathrm{LVOOA}$ in *HSC and $x3 = \mathrm{pPON}$ in *bfo. A is the origin and the partial slopes B, C and D represent the contribution of $x1$, $x2$ and $x3$ to $b_{\mathrm{abs\_470wb}}$, respectively.

As used in previous studies (Elser et al., 2016; Reyes-Villegas et al., 2016), multilinear regression analysis allows for the relationship of one parameter between two or more variables to be determined. Here we are analysing the partial slopes and origin to determine the correlation of $b_{\mathrm{abs\_470wb}}$ with the other variables. Table 1 shows the MLR outputs where; A represents the background, B, C and D represent

Table 1. Multilinear (MLR) and linear regression analysis between $b_{\mathrm{abs\_470wb}}$ and OAs.

			ALL	HSC	LC	bfo	WL
MLR 1	A	background	0.000	4.555	1.004	0.000	1.293
	B	b_{abs}:BBOA	14.340	3.547	18.284	11.926	10.318
	C	b_{abs}:PON	54.495	9.212	12.046	73.115	21.724
		B/C	0.263	0.385	1.518	0.163	0.475
		r^2_MLR1	0.912	0.064	0.364	0.898	0.760
Linear 1	r^2	b_{abs}:BBOA	0.861	0.043	0.358	0.839	0.739
		b_{abs}:PON	0.819	0.060	0.275	0.897	0.311
MLR 2	A	background	0.000	2.527	0.753	0.000	0.079
	B	b_{abs}:BBOA_2	15.653	27.288	26.481	14.319	10.018
	C	b_{abs}:PON	42.840	0.000	1.200	54.353	18.982
		B/C	0.365	***	22.060	0.263	0.528
		r^2_MLR2	0.922	0.392	0.480	0.902	0.804
Linear 2	r^2	b_{abs}:BBOA_2	0.894	0.392	0.480	0.880	0.788
		b_{abs}:PON	0.819	0.060	0.275	0.897	0.311

			ALL	HSC	*HSC	LC	*bfo	WL
MLR 3	A	background	0.000	2.527	1.649	0.763	6.093	0
	B	b_{abs}:BBOA_2	21.545	27.288	22.764	26.668	16.657	8.577
	C	b_{abs}:sPON_ME2	3.926	0.000	0.000	0.191	0.000	9.017
	D	D			1.138		7.357	
		B/C	5.488	***	***	***	***	0.951
		B/D			20.005		2.264	
		r^2_MLR3	0.896	0.392	0.418	0.480	0.910	0.803
Linear 3	r^2	b_{abs}:BBOA_2	0.894	0.392	0.392	0.480	0.880	0.788
		b_{abs}:sPON_ME2	0.024	0.000	0.000	0.273	0.188	0.647
		b_{abs}:D			0.225		0.633	

ALL = complete dataset; HSC = episode with high secondary concentrations (30 October to 1 November); LC = episode with low concentrations (1–3 November); bfo = episode with bonfire-only concentrations (5 November 17:00 LT to 6 November 12:00 LT); WL = Episode with winter-like characteristics (8–10 November). PON is the particulate organic nitrate estimate from 46 : 30 ratios. *Trilinear regression was performed as in *bfo analysis there were two PON factors from ME-2 analysis; pPON_ME2 and sPON_ME2, with the slope $D = b_{\mathrm{abs}}$:pPON and r^2_D is the r^2 between b_{abs}:pPON. In *HSC analysis; BBOA, sPON and LVOOA were used, with the slope $D = b_{\mathrm{abs}}$:LVOOA and r^2_D is the r^2 between b_{abs}:LVOOA.

the partial slope between $b_{\mathrm{abs\_470wb}}$ and the respective OA. B/C represents the ratio between B and C partial slopes, with the following considerations: if $B/C < 1$, then there is a higher contribution of PON to b_{abs_470wb}; if $B/C > 1$, then there is a higher contribution of BBOA to $b_{\mathrm{abs\_470wb}}$. Looking at the coefficient of determination of the multilinear regression (r^2_MLR) for the three MLR analyses, it is possible to observe that, on the one hand, HSC and LC events present low r^2_MLR values ranging from 0.064 and 0.480; On the other hand, bfo and WL events have strong correlations with values between 0.760 and 0.910, which shows that when high primary OA emissions are present a strong correlation between $b_{\mathrm{abs\_470wb}}$ and BBOA and PON is observed.

These high r^2 values, particularly during the bfo event which presented the highest r^2 (0.910), are consistent with previous studies that found organic nitrates to absorb at short wavelengths; Mohr et al. (2013) identified correlation values of 0.65 between nitrophenols and $b_{\mathrm{abs\_370wb}}$. Teich et al. (2017), in a recent study from offline filters, determined nitrated aerosol concentrations with further analysis of the light absorption of aqueous filter extracts ($b_{\mathrm{abs\_370}}$) and identified r^2 values between $b_{\mathrm{abs\_370}}$ and nitrated aerosol concentrations of 0.67 to 0.74 depending on acidic or alkaline conditions, respectively.

In MLR3, it is possible to observe that, during the bfo event, the main contribution to $b_{\mathrm{abs\_470wb}}$ is attributed to both BBOA_2 (16.657) and pPON_ME2 (7.357), while b_{abs}:sPON_ME-2 values were zero, with an optimum r^2 of 0.910. This lack of correlation between b_{abs} and sPON is observed in the linear regression b_{abs}:sPON_ME2 with an r^2 of 0.188. These results show that while there is evidence of pPON_ME2 absorbing at 470 nm, with a partial slope of 16.657, sPON_ME2 did not show to be absorbing at 470 nm. The implication of the background not going to zero (6.093) is that there is still an unexplained contribution to the absorption at 470 nm, unrelated to sPON_ME2.

In order to further explore the possibility of sPON_ME-2 absorbing at 470 nm, the HSC event was analysed, where sPON_ME2 was shown to be non-absorbing at 470 nm with a partial slope of zero. BBOA_2 had a partial slope of 27.288 and background a value of 2.527. This background value suggests there is another component related to b_{abs_470wb} that is not sPON. Thus, a trilinear regression was performed to *HSC between b_{abs_470wb} and BBOA_2, sPON and LVOOA. Here, the background value drops to 1.649, sPON partial slope is zero and LVOOA presents a partial slope of 1.138. These results confirm that sPON do not absorb light at 470 nm while LVOOA, or at least part of the components of LVOOA, do absorb at 470 nm during the HSC event and pPON_ME2 during the bfo event.

These results agree with previous studies that found biomass burning BBOA to contain important concentrations of light absorbing BrC and that certain types of SOA are effective absorbers near UV light (Bones et al., 2010; Saleh et al., 2014; Washenfelder et al., 2015). The fact that pPON_ME2 and LVOOA were shown to be absorbing light at a short wavelength (470 nm) will have a direct impact on Aethalometer model studies; while pPON_ME2 could be considered a component of the wood burning aerosol apportioned using the Aethalometer, it may be that there is an interference from other forms of BrC in SOA. However, this work would suggest that sPON specifically does not contribute to the latter, so a different component of LVOOA would have to be responsible. As well as this Aethalometer interpretation, it is also worth mentioning that these findings may have implications for studies on the radiative properties of the atmosphere, as BrC is also thought to affect climate (Jacobson, 2014).

5 Conclusions

In order to better understand the aerosol chemical composition and variation in source contribution during periods of nocturnal pollution, online measurements of gases and aerosols were made in ambient air between 29 October and 10 November 2014 at the University of Manchester, with detailed analysis of the special high pollutant concentrations during Bonfire Night celebrations on 5 November. High aerosol concentrations were observed during the Bonfire Night event with 115 $\mu g\, m^{-3}$ of PM_1. Important nitrogen chemistry was present with high HCN, HCNO and HONO concentrations primarily emitted with the further presence of N_2O_5 and $ClNO_2$ concentrations from nocturnal nitrate chemistry taking place after NO_x concentrations decreased.

OA source apportionment was performed using the ME-2 factorisation tool. The particular high pollutant concentrations together with the complex mix of emissions did not allow the running of ME-2 for the complete dataset, thus the dataset was divided into different events. The best way to perform source apportionment was found to be to (a) analyse the event before and after Bonfire Night using BBOA, HOA and COA from a previous study in Paris as TP, and (b) conduct a further ME-2 analysis of the Bonfire Night event using BBOA, HOA and COA mass spectra from (a) as TP. Moreover, a slight improvement in the source apportionment was observed after modifying the fragmentation table in order to identify PON sources, increasing the r^2 value from linear regressions between b_{abs_470wb} (absorption coefficient of wood burning at 470 nm) and BBOA from 0.839 to 0.880. PMF and ME-2 source apportionment tools could not completely deconvolve OA sources during the bfo event as LVOOA, COA and HOA may be mixed with BBOA concentrations. However, due to the strong correlation between b_{abs_470wb} and BBOA ($r^2 = 0.880$) we consider that while BBOA might not represent the total OA concentrations from the Bonfire Night event, it does represent the trend of OA emitted from the biomass burning.

The combination of CIMS measurements and OA sources determined from AMS measurements provided important information about gas tracers to be used as inputs (target time series) to improve future ME-2 analyses, particularly gases correlating with BBOA, LVOOA and sPON. However, the use of these species as target time series should be used with care as their time variation is greatly affected by meteorological conditions.

The presence of two classes of PON, secondary (sPON_ME2) and primary (pPON_ME2), was identified both from looking at the BBOA:PON relationship and from the ME-2 analysis after modifying the fragmentation table. It is clear that, during Bonfire Night, pPON_ME2 concentrations increased when BBOA concentrations are present and sPON_ME2 concentrations started evolving when the primary concentrations decreased.

It was determined that pPON_ME2 absorbed light at a wavelength of 470 nm during Bonfire Night, where the multilinear regression performed between b_{abs_470wb}, BBOA and pPON_ME2 showed a strong r^2 of 0.910, while sPON_ME2 did not contribute to light absorption at 470 nm. During the HSC episode, LVOOA showed a partial slope of 1.138 in the multilinear regression and an r^2 from linear regression with b_{abs_470wb} of 0.225, implying secondary LVOOA (associated with SOA) may be absorbing at 470 nm and sPON_ME2 was not absorbing at this wavelength. These results will help us to understand the mechanistic contributions to UV absorption in the Aethalometer and will have direct implications for source apportionment studies, which may need to be corrected for SOA interferences near the UV region.

Data availability. The data are available upon request from the corresponding author and from James Allan (james.allan@manchester.ac.uk).

Appendix A: Source apportionment solution without modifying the fragmentation table

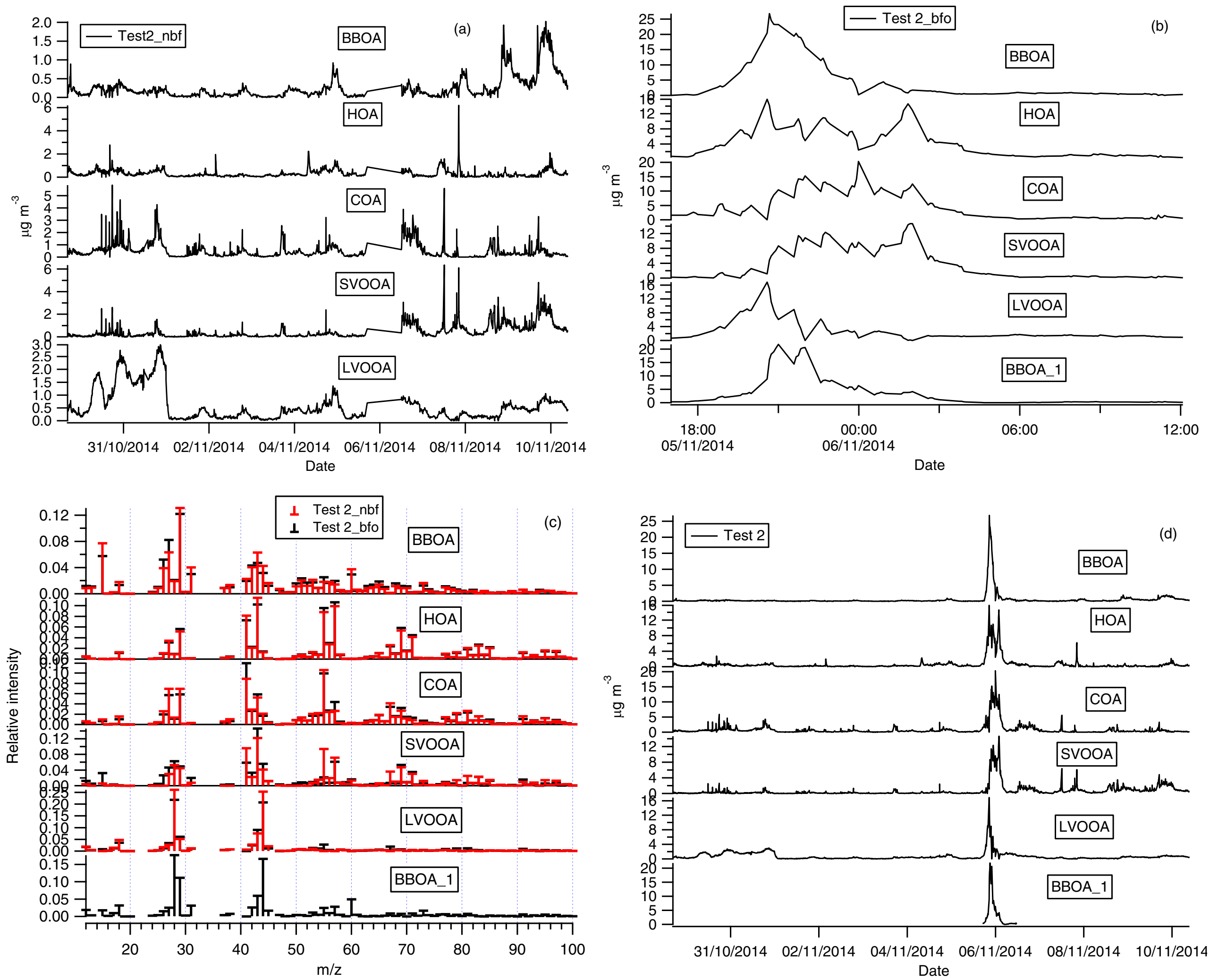

Figure A1. OA sources mass spectra and time series for Test2.

Figure A1 presents results obtained with Test2. Figure A1c shows mass spectra of the two chosen solutions: five sources were identified during the nbf period: BBOA, HOA, COA, SVOOA and LVOOA. In the case of the bfo period, six different sources were identified: BBOA; HOA; COA; factor4, which seems to be a mixed factor with a peak at m/z 43 (characteristic of SVOOA) and peaks at m/z 55 and m/z 57 (characteristic of HOA); LVOOA and BBOA_1. BBOA_1 source appears to be mixed between LVOOA (peaks at m/z 28 and m/z 44) and BBOA (peak at m/z 60). We can see here, that while Test2 resulted to be the best way to deconvolve OA sources compared to tests 1, 3 and 4, it still shows mixing with SVOOA, LVOOA and BBOA_1. A situation that improved when doing OA source apportionment after modifying the fragmentation table in Test2_ON.

Appendix B: Symbols and description of main parameters used

Symbol	Description
	Events
bfo	bonfire-only event (5 November 05:00–17:00 LT to 6 November 12:00 LT)
nbf	not bonfire (before and after bonfire night)
HSC	high secondary concentrations (30 October to 1 November)
LC	low concentrations (1–3 November)
WL	winter-like (8–10 November)
	Aethalometer correction and model
α	Ångström absorption exponent
α_{tr}	Ångström absorption exponent for traffic
α_{wb}	Ångström absorption exponent for wood burning
ATN	attenuation
BC	black carbon ($\mu g\, m^{-3}$)
b_{abs}	absorption coefficient (Mm^{-1})
b_{abs_470}	absorption coefficient at 470 nm (Mm^{-1})
b_{abs_950}	absorption coefficient at 950 nm (Mm^{-1})
σ_{ATN}	attenuation cross section ($m^2\, g^{-1}$)
λ	wavelength (nm)
b_{ATN}	uncorrected absorption coefficient (Mm^{-1})
b_{abs}	corrected absorption coefficient (Mm^{-1})
C	multiple scattering correction constant
R	filter loading correction
f	shadowing factor
	Organic aerosol factors
BBOA	biomass burning organic OA obtained without modifying the fragmentation table
BBOA_1	second biomass burning organic OA obtained without modifying the fragmentation table
BBOA_2	biomass burning organic OA obtained after modifying the fragmentation table
HOA	hydrocarbon-like OA
COA	cooking OA
SVOOA	semi-volatile OA
LVOOA	low volatility OA
PON	particulate organic oxides of nitrogen, calculated with 46 : 30 ratios.
pPON	primary particulate organic oxides of nitrogen, estimated using the slope between PON and BBOA
sPON	secondary particulate organic oxides of nitrogen, sPON = PON − pPON
pPON_ME2	primary particulate organic oxides of nitrogen, calculated from ME-2 analysis
sPON_ME2	secondary particulate organic oxides of nitrogen, calculated from ME-2 analysis

The Supplement related to this article is available online at https://doi.org/10.5194/acp-18-1-2018-supplement.

Author contributions. ERV, MF, HC, CP, JA designed the project; ERV, YCT, SH, TB, MLB, PW, AB, operated, calibrated and performed QA of instrument measurements; ERV and MP performed the data analysis; ERV, HC and JA wrote the paper.

Competing interests. The authors declare that they have no conflict of interest.

Acknowledgements. This work was supported through the UK Natural Environment Research Council (NERC) through the Com-Part (grant ref: NE/K014838/1). Ernesto Reyes-Villegas is supported by a studentship by the National Council of Science and Technology-Mexico (CONACYT) under registry number 217687.

Edited by: Astrid Kiendler-Scharr
Reviewed by: two anonymous referees

References

Ainsworth, W. H.: Guy fawkes; or, the gunpowder treason, Nottingham Society, London, UK, 1850.

Alfarra, M. R., Paulsen, D., Gysel, M., Garforth, A. A., Dommen, J., Prévôt, A. S. H., Worsnop, D. R., Baltensperger, U., and Coe, H.: A mass spectrometric study of secondary organic aerosols formed from the photooxidation of anthropogenic and biogenic precursors in a reaction chamber, Atmos. Chem. Phys., 6, 5279–5293, https://doi.org/10.5194/acp-6-5279-2006, 2006.

Alfarra, M. R., Prévôt, A. S. H., Szidat, S., Sandradewi, J., Weimer, S., Lanz, V. A., Schreiber, D., Mohr, M., and Baltensperger, U.: Identification of the mass spectral signature of organic aerosols from wood burning emissions, Environ. Sci. Technol., 41, 5770–5777, https://doi.org/10.1021/Es062289b, 2007.

Allan, J. D., Delia, A. E., Coe, H., Bower, K. N., Alfarra, M. R., Jimenez, J. L., Middlebrook, A. M., Drewnick, F., Onasch, T. B., Canagaratna, M. R., Jayne, J. T., and Worsnop, D. R.: A generalised method for the extraction of chemically resolved mass spectra from aerodyne aerosol mass spectrometer data, J. Aerosol Sci., 35, 909–922, https://doi.org/10.1016/j.jaerosci.2004.02.007, 2004.

Allan, J. D., Alfarra, M. R., Bower, K. N., Coe, H., Jayne, J. T., Worsnop, D. R., Aalto, P. P., Kulmala, M., Hyötyläinen, T., Cavalli, F., and Laaksonen, A.: Size and composition measurements of background aerosol and new particle growth in a Finnish forest during QUEST 2 using an Aerodyne Aerosol Mass Spectrometer, Atmos. Chem. Phys., 6, 315–327, https://doi.org/10.5194/acp-6-315-2006, 2006.

Allan, J. D., Williams, P. I., Morgan, W. T., Martin, C. L., Flynn, M. J., Lee, J., Nemitz, E., Phillips, G. J., Gallagher, M. W., and Coe, H.: Contributions from transport, solid fuel burning and cooking to primary organic aerosols in two UK cities, Atmos. Chem. Phys., 10, 647–668, https://doi.org/10.5194/acp-10-647-2010, 2010.

Bannan, T. J., Booth, A. M., Bacak, A., Muller, J. B. A., Leather, K. E., Le Breton, M., Jones, B., Young, D., Coe, H., Allan, J., Visser, S., Slowik, J. G., Furger, M., Prevot, A. S. H., Lee, J., Dunmore, R. E., Hopkins, J. R., Hamilton, J. F., Lewis, A. C., Whalley, L. K., Sharp, T., Stone, D., Heard, D. E., Fleming, Z. L., Leigh, R., Shallcross, D. E., and Percival, C. J.: The first uk measurements of nitryl chloride using a chemical ionization mass spectrometer in central london in the summer of 2012, and an investigation of the role of cl atom oxidation, J. Geophys. Res.-Atmos., 120, 5638–5657, https://doi.org/10.1002/2014JD022629, 2015.

Bones, D. L., Henricksen, D. K., Mang, S. A., Gonsior, M., Bateman, A. P., Nguyen, T. B., Cooper, W. J., and Nizkorodov, S. A.: Appearance of strong absorbers and fluorophores in limonene-o3 secondary organic aerosol due to nh4+-mediated chemical aging over long time scales, J. Geophys. Res.-Atmos., 115, D05203, https://doi.org/10.1029/2009jd012864, 2010.

Borduas, N., da Silva, G., Murphy, J. G., and Abbatt, J. P. D.: Experimental and theoretical understanding of the gas phase oxidation of atmospheric amides with oh radicals: Kinetics, products, and mechanisms, J. Phys. Chem. A, 119, 4298–4308, https://doi.org/10.1021/jp503759f, 2015.

Bruns, E. A., Perraud, V., Zelenyuk, A., Ezell, M. J., Johnson, S. N., Yu, Y., Imre, D., Finlayson-Pitts, B. J., and Alexander, M. L.: Comparison of ftir and particle mass spectrometry for the measurement of particulate organic nitrates, Environ. Sci. Technol., 44, 1056–1061, https://doi.org/10.1021/es9029864, 2010.

Canagaratna, M. R., Jayne, J. T., Ghertner, D. A., Herndon, S., Shi, Q., Jimenez, J. L., Silva, P. J., Williams, P., Lanni, T., Drewnick, F., Demerjian, K. L., Kolb, C. E., and Worsnop, D. R.: Chase studies of particulate emissions from in-use new york city vehicles, Aerosol Sci. Tech., 38, 555–573, https://doi.org/10.1080/02786820490465504, 2004.

Canonaco, F., Crippa, M., Slowik, J. G., Baltensperger, U., and Prévôt, A. S. H.: SoFi, an IGOR-based interface for the efficient use of the generalized multilinear engine (ME-2) for the source apportionment: ME-2 application to aerosol mass spectrometer data, Atmos. Meas. Tech., 6, 3649–3661, https://doi.org/10.5194/amt-6-3649-2013, 2013.

Chakraborty, A., Gupta, T., and Tripathi, S. N.: Chemical composition and characteristics of ambient aerosols and rainwater residues during indian summer monsoon: Insight from aerosol mass spectrometry, Atmos. Environ., 136, 144–155, https://doi.org/10.1016/j.atmosenv.2016.04.024, 2016.

Clark, H.: New directions. Light blue touch paper and retire, Atmos. Environ., 31, 2893–2894, https://doi.org/10.1016/s1352-2310(97)88278-7, 1997.

Colbeck, I. and Chung, M.-C.: Ambient aerosol concentrations at a site in se england during bonfire night 1995, J. Aerosol Sci., 27, Supplement 1, S449–S450, https://doi.org/10.1016/0021-8502(96)00297-2, 1996.

Crilley, L. R., Bloss, W. J., Yin, J., Beddows, D. C. S., Harrison, R. M., Allan, J. D., Young, D. E., Flynn, M., Williams, P., Zotter, P., Prevot, A. S. H., Heal, M. R., Barlow, J. F., Halios, C. H., Lee, J. D., Szidat, S., and Mohr, C.: Sources and contributions of wood smoke during winter in London: assessing local and regional influences, Atmos. Chem. Phys., 15, 3149–3171, https://doi.org/10.5194/acp-15-3149-2015, 2015.

Crippa, M., DeCarlo, P. F., Slowik, J. G., Mohr, C., Heringa, M. F., Chirico, R., Poulain, L., Freutel, F., Sciare, J., Cozic, J., Di Marco, C. F., Elsasser, M., Nicolas, J. B., Marchand, N., Abidi, E., Wiedensohler, A., Drewnick, F., Schneider, J., Borrmann, S., Nemitz, E., Zimmermann, R., Jaffrezo, J.-L., Prévôt, A. S. H., and Baltensperger, U.: Wintertime aerosol chemical composition and source apportionment of the organic fraction in the metropolitan area of Paris, Atmos. Chem. Phys., 13, 961–981, https://doi.org/10.5194/acp-13-961-2013, 2013.

Crippa, M., Canonaco, F., Lanz, V. A., Äijälä, M., Allan, J. D., Carbone, S., Capes, G., Ceburnis, D., Dall'Osto, M., Day, D. A., DeCarlo, P. F., Ehn, M., Eriksson, A., Freney, E., Hildebrandt Ruiz, L., Hillamo, R., Jimenez, J. L., Junninen, H., Kiendler-Scharr, A., Kortelainen, A.-M., Kulmala, M., Laaksonen, A., Mensah, A. A., Mohr, C., Nemitz, E., O'Dowd, C., Ovadnevaite, J., Pandis, S. N., Petäjä, T., Poulain, L., Saarikoski, S., Sellegri, K., Swietlicki, E., Tiitta, P., Worsnop, D. R., Baltensperger, U., and Prévôt, A. S. H.: Organic aerosol components derived from 25 AMS data sets across Europe using a consistent ME-2 based source apportionment approach, Atmos. Chem. Phys., 14, 6159–6176, https://doi.org/10.5194/acp-14-6159-2014, 2014.

Day, D. A., Liu, S., Russell, L. M., and Ziemann, P. J.: Organonitrate group concentrations in submicron particles with high nitrate and organic fractions in coastal southern california, Atmos. Environ., 44, 1970–1979, https://doi.org/10.1016/j.atmosenv.2010.02.045, 2010.

Drewnick, F., Hings, S. S., DeCarlo, P., Jayne, J. T., Gonin, M., Fuhrer, K., Weimer, S., Jimenez, J. L., Demerjian, K. L., Borrmann, S., and Worsnop, D. R.: A new time-of-flight aerosol mass spectrometer (tof-ams) – instrument description and first field deployment, Aerosol Sci. Tech., 39, 637–658, https://doi.org/10.1080/02786820500182040, 2005.

Drewnick, F., Hings, S. S., Curtius, J., Eerdekens, G., and Williams, J.: Measurement of fine particulate and gas-phase species during the new year's fireworks 2005 in mainz, germany, Atmos. Environ., 40, 4316–4327, https://doi.org/10.1016/j.atmosenv.2006.03.040, 2006.

Drewnick, F., Diesch, J.-M., Faber, P., and Borrmann, S.: Aerosol mass spectrometry: particle–vaporizer interactions and their consequences for the measurements, Atmos. Meas. Tech., 8, 3811–3830, https://doi.org/10.5194/amt-8-3811-2015, 2015.

Dyke, P., Coleman, P., and James, R.: Dioxins in ambient air, bonfire night 1994, Chemosphere, 34, 1191–1201, https://doi.org/10.1016/S0045-6535(97)00418-9, 1997.

EEA: Status of black carbon monitoring in ambient air in europe, Luxembourg, available at: http://www.eea.europa.eu/publications/status-of-black-carbon-monitoring (last access: 7 November 2017), 48TS1, 2013.

Elser, M., Huang, R.-J., Wolf, R., Slowik, J. G., Wang, Q., Canonaco, F., Li, G., Bozzetti, C., Daellenbach, K. R., Huang, Y., Zhang, R., Li, Z., Cao, J., Baltensperger, U., El-Haddad, I., and Prévôt, A. S. H.: New insights into $PM_{2.5}$ chemical composition and sources in two major cities in China during extreme haze events using aerosol mass spectrometry, Atmos. Chem. Phys., 16, 3207–3225, https://doi.org/10.5194/acp-16-3207-2016, 2016.

Faber, P., Drewnick, F., Veres, P. R., Williams, J., and Borrmann, S.: Anthropogenic sources of aerosol particles in a football stadium: Real-time characterization of emissions from cigarette smoking, cooking, hand flares, and color smoke bombs by high-resolution aerosol mass spectrometry, Atmos. Environ., 77, 1043–1051, https://doi.org/10.1016/j.atmosenv.2013.05.072, 2013.

Farmer, D. K., Matsunaga, A., Docherty, K. S., Surratt, J. D., Seinfeld, J. H., Ziemann, P. J., and Jimenez, J. L.: Response of an aerosol mass spectrometer to organonitrates and organosulfates and implications for atmospheric chemistry, P. Natl. Acad. Sci. USA, 107, 6670–6675, https://doi.org/10.1073/pnas.0912340107, 2010.

Farrar, N. J., Smith, K. E. C., Lee, R. G. M., Thomas, G. O., Sweetman, A. J., and Jones, K. C.: Atmospheric emissions of polybrominated diphenyl ethers and other persistent organic pollutants during a major anthropogenic combustion event, Environ. Sci. Technol., 38, 1681–1685, https://doi.org/10.1021/es035127d, 2004.

Faxon, C., Bean, J., and Ruiz, L.: Inland concentrations of cl2 and clno2 in southeast texas suggest chlorine chemistry significantly contributes to atmospheric reactivity, Atmosphere, 6, 1487, https://doi.org/10.3390/atmos6101487, 2015.

Fernandez, P., Grifoll, M., Solanas, A. M., Bayona, J. M., and Albaiges, J.: Bioassay-directed chemical analysis of genotoxic components in coastal sediments, Environ. Sci. Technol., 26, 817–829, https://doi.org/10.1021/es00028a024, 1992.

Florou, K., Papanastasiou, D. K., Pikridas, M., Kaltsonoudis, C., Louvaris, E., Gkatzelis, G. I., Patoulias, D., Mihalopoulos, N., and Pandis, S. N.: The contribution of wood burning and other pollution sources to wintertime organic aerosol levels in two Greek cities, Atmos. Chem. Phys., 17, 3145–3163, https://doi.org/10.5194/acp-17-3145-2017, 2017.

Flowers, B. A., Dubey, M. K., Mazzoleni, C., Stone, E. A., Schauer, J. J., Kim, S.-W., and Yoon, S. C.: Optical-chemical-microphysical relationships and closure studies for mixed carbonaceous aerosols observed at Jeju Island; 3-laser photoacoustic spectrometer, particle sizing, and filter analysis, Atmos. Chem. Phys., 10, 10387–10398, https://doi.org/10.5194/acp-10-10387-2010, 2010.

Fröhlich, R., Crenn, V., Setyan, A., Belis, C. A., Canonaco, F., Favez, O., Riffault, V., Slowik, J. G., Aas, W., Aijälä, M., Alastuey, A., Artiñano, B., Bonnaire, N., Bozzetti, C., Bressi, M., Carbone, C., Coz, E., Croteau, P. L., Cubison, M. J., Esser-Gietl, J. K., Green, D. C., Gros, V., Heikkinen, L., Herrmann, H., Jayne, J. T., Lunder, C. R., Minguillón, M. C., Mocnik, G., O'Dowd, C. D., Ovadnevaite, J., Petralia, E., Poulain, L., Priestman, M., Ripoll, A., Sarda-Estève, R., Wiedensohler, A., Baltensperger, U., Sciare, J., and Prévôt, A. S. H.: ACTRIS ACSM intercomparison – Part 2: Intercomparison of ME-2 organic source apportionment results from 15 individual, co-located aerosol mass spectrometers, Atmos. Meas. Tech., 8, 2555–2576, https://doi.org/10.5194/amt-8-2555-2015, 2015.

Fry, J. L., Kiendler-Scharr, A., Rollins, A. W., Wooldridge, P. J., Brown, S. S., Fuchs, H., Dubé, W., Mensah, A., dal Maso, M., Tillmann, R., Dorn, H.-P., Brauers, T., and Cohen, R. C.: Organic nitrate and secondary organic aerosol yield from NO_3 oxidation of β-pinene evaluated using a gas-phase kinetics/aerosol partitioning model, Atmos. Chem. Phys., 9, 1431–1449, https://doi.org/10.5194/acp-9-1431-2009, 2009.

Godri, K. J., Green, D. C., Fuller, G. W., Dall'Osto, M., Beddows, D. C., Kelly, F. J., Harrison, R. M., and Mudway, I. S.: Particulate oxidative burden associated with firework activity, Environ. Sci.

Please note the remarks at the end of the manuscript.

Technol., 44, 8295–8301, https://doi.org/10.1021/es1016284, 2010.

Hamad, S., Green, D., and Heo, J.: Evaluation of health risk associated with fireworks activity at central london, Air Qual. Atmos. Hlth., 9, 1–7, https://doi.org/10.1007/s11869-015-0384-x, 2015.

Hao, L. Q., Kortelainen, A., Romakkaniemi, S., Portin, H., Jaatinen, A., Leskinen, A., Komppula, M., Miettinen, P., Sueper, D., Pajunoja, A., Smith, J. N., Lehtinen, K. E. J., Worsnop, D. R., Laaksonen, A., and Virtanen, A.: Atmospheric submicron aerosol composition and particulate organic nitrate formation in a boreal forestland–urban mixed region, Atmos. Chem. Phys., 14, 13483–13495, https://doi.org/10.5194/acp-14-13483-2014, 2014.

Harrison, M. A. J., Barra, S., Borghesi, D., Vione, D., Arsene, C., and Iulian Olariu, R.: Nitrated phenols in the atmosphere: A review, Atmos. Environ., 39, 231–248, https://doi.org/10.1016/j.atmosenv.2004.09.044, 2005.

Harrison, R. M., Beddows, D. C. S., Hu, L., and Yin, J.: Comparison of methods for evaluation of wood smoke and estimation of UK ambient concentrations, Atmos. Chem. Phys., 12, 8271–8283, https://doi.org/10.5194/acp-12-8271-2012, 2012.

Jacobson, M. Z.: Isolating nitrated and aromatic aerosols and nitrated aromatic gases as sources of ultraviolet light absorption, J. Geophys. Res.-Atmos., 104, 3527–3542, https://doi.org/10.1029/1998jd100054, 1999.

Jacobson, M. Z.: Effects of biomass burning on climate, accounting for heat and moisture fluxes, black and brown carbon, and cloud absorption effects, J. Geophys. Res.-Atmos., 119, 8980–9002, https://doi.org/10.1002/2014jd021861, 2014.

Joshi, M., Khan, A., Anand, S., and Sapra, B. K.: Size evolution of ultrafine particles: Differential signatures of normal and episodic events, Environ. Pollut. B, 208, 354–360, https://doi.org/10.1016/j.envpol.2015.10.001, 2016.

Kiendler-Scharr, A., Mensah, A. A., Friese, E., Topping, D., Nemitz, E., Prevot, A. S. H., Äijälä, M., Allan, J., Canonaco, F., Canagaratna, M., Carbone, S., Crippa, M., Dall Osto, M., Day, D. A., De Carlo, P., Di Marco, C. F., Elbern, H., Eriksson, A., Freney, E., Hao, L., Herrmann, H., Hildebrandt, L., Hillamo, R., Jimenez, J. L., Laaksonen, A., McFiggans, G., Mohr, C., O'Dowd, C., Otjes, R., Ovadnevaite, J., Pandis, S. N., Poulain, L., Schlag, P., Sellegri, K., Swietlicki, E., Tiitta, P., Vermeulen, A., Wahner, A., Worsnop, D., and Wu, H. C.: Ubiquity of organic nitrates from nighttime chemistry in the european submicron aerosol, Geophys. Res. Lett., 43, 7735–7744, https://doi.org/10.1002/2016gl069239, 2016.

Kitanovski, Z., Grgic, I., Vermeylen, R., Claeys, M., and Maenhaut, W.: Liquid chromatography tandem mass spectrometry method for characterization of monoaromatic nitro-compounds in atmospheric particulate matter, J. Chromatogr. A, 1268, 35–43, https://doi.org/10.1016/j.chroma.2012.10.021, 2012.

Kostenidou, E., Florou, K., Kaltsonoudis, C., Tsiflikiotou, M., Vratolis, S., Eleftheriadis, K., and Pandis, S. N.: Sources and chemical characterization of organic aerosol during the summer in the eastern Mediterranean, Atmos. Chem. Phys., 15, 11355–11371, https://doi.org/10.5194/acp-15-11355-2015, 2015.

Laskar, S. I., Jaswal, K., Bhatnagar, M. K., and Rathore, L. S.: India meteorological department, India, Proceedings of Indian National Science Academy, 1021–1037, 2016.

Le Breton, M., Bacak, A., Muller, J. B. A., O'Shea, S. J., Xiao, P., Ashfold, M. N. R., Cooke, M. C., Batt, R., Shallcross, D. E., Oram, D. E., Forster, G., Bauguitte, S. J.-B., Palmer, P. I., Parrington, M., Lewis, A. C., Lee, J. D., and Percival, C. J.: Airborne hydrogen cyanide measurements using a chemical ionisation mass spectrometer for the plume identification of biomass burning forest fires, Atmos. Chem. Phys., 13, 9217–9232, https://doi.org/10.5194/acp-13-9217-2013, 2013.

Le Breton, M., Bacak, A., Muller, J. B. A., Bannan, T. J., Kennedy, O., Ouyang, B., Xiao, P., Bauguitte, S. J. B., Shallcross, D. E., Jones, R. L., Daniels, M. J. S., Ball, S. M., and Percival, C. J.: The first airborne comparison of N_2O_5 measurements over the uk using a cims and bbceas during the ronoco campaign, Anal. Methods-UK, 6, 9731–9743, https://doi.org/10.1039/c4ay02273d, 2014a.

Le Breton, M., Bacak, A., Muller, J. B. A., Xiao, P., Shallcross, B. M. A., Batt, R., Cooke, M. C., Shallcross, D. E., Bauguitte, S. J. B., and Percival, C. J.: Simultaneous airborne nitric acid and formic acid measurements using a chemical ionization mass spectrometer around the uk: Analysis of primary and secondary production pathways, Atmos. Environ., 83, 166–175, https://doi.org/10.1016/j.atmosenv.2013.10.008, 2014b.

Lee, B. H., Lopez-Hilfiker, F. D., Mohr, C., Kurtén, T., Worsnop, D. R., and Thornton, J. A.: An iodide-adduct high-resolution time-of-flight chemical-ionization mass spectrometer: Application to atmospheric inorganic and organic compounds, Environ. Sci. Technol., 48, 6309–6317, https://doi.org/10.1021/es500362a, 2014.

Lee, J. D., Whalley, L. K., Heard, D. E., Stone, D., Dunmore, R. E., Hamilton, J. F., Young, D. E., Allan, J. D., Laufs, S., and Kleffmann, J.: Detailed budget analysis of HONO in central London reveals a missing daytime source, Atmos. Chem. Phys., 16, 2747–2764, https://doi.org/10.5194/acp-16-2747-2016, 2016.

Liu, D., Whitehead, J., Alfarra, M. R., Reyes-Villegas, E., Spracklen, D. V., Reddington, C. L., Kong, S., Williams, P. I., Ting, Y.-C., Haslett, S., Taylor, J. W., Flynn, M. J., Morgan, W. T., McFiggans, G., Coe, H., and Allan, J. D.: Black-carbon absorption enhancement in the atmosphere determined by particle mixing state, Nat. Geosci., 10, 184–188, https://doi.org/10.1038/ngeo2901, 2017.

Mao, J., Paulot, F., Jacob, D. J., Cohen, R. C., Crounse, J. D., Wennberg, P. O., Keller, C. A., Hudman, R. C., Barkley, M. P., and Horowitz, L. W.: Ozone and organic nitrates over the eastern united states: Sensitivity to isoprene chemistry, J. Geophys. Res.-Atmos., 118, 11256–11268, https://doi.org/10.1002/jgrd.50817, 2013.

Mohr, C., DeCarlo, P. F., Heringa, M. F., Chirico, R., Slowik, J. G., Richter, R., Reche, C., Alastuey, A., Querol, X., Seco, R., Peñuelas, J., Jiménez, J. L., Crippa, M., Zimmermann, R., Baltensperger, U., and Prévôt, A. S. H.: Identification and quantification of organic aerosol from cooking and other sources in Barcelona using aerosol mass spectrometer data, Atmos. Chem. Phys., 12, 1649–1665, https://doi.org/10.5194/acp-12-1649-2012, 2012.

Mohr, C., Lopez-Hilfiker, F. D., Zotter, P., Prevot, A. S. H., Xu, L., Ng, N. L., Herndon, S. C., Williams, L. R., Franklin, J. P., Zahniser, M. S., Worsnop, D. R., Knighton, W. B., Aiken, A. C., Gorkowski, K. J., Dubey, M. K., Allan, J. D., and Thornton, J. A.: Contribution of nitrated phenols to wood burning brown carbon light absorption in detling, united kingdom during winter time, Environ. Sci. Technol., 47, 6316–6324, https://doi.org/10.1021/Es400683v, 2013.

Moreno, T., Querol, X., Alastuey, A., Cruz Minguillón, M., Pey, J., Rodriguez, S., Vicente Miró, J., Felis, C., and Gibbons, W.: Recreational atmospheric pollution episodes: Inhalable metalliferous particles from firework displays, Atmos. Environ., 41, 913–922, https://doi.org/10.1016/j.atmosenv.2006.09.019, 2007.

Naeher, L. P., Brauer, M., Lipsett, M., Zelikoff, J. T., Simpson, C. D., Koenig, J. Q., and Smith, K. R.: Woodsmoke health effects: A review, Inhal. Toxicol., 19, 67–106, https://doi.org/10.1080/08958370600985875, 2007.

Ng, N. L., Canagaratna, M. R., Zhang, Q., Jimenez, J. L., Tian, J., Ulbrich, I. M., Kroll, J. H., Docherty, K. S., Chhabra, P. S., Bahreini, R., Murphy, S. M., Seinfeld, J. H., Hildebrandt, L., Donahue, N. M., DeCarlo, P. F., Lanz, V. A., Prévôt, A. S. H., Dinar, E., Rudich, Y., and Worsnop, D. R.: Organic aerosol components observed in Northern Hemispheric datasets from Aerosol Mass Spectrometry, Atmos. Chem. Phys., 10, 4625–4641, https://doi.org/10.5194/acp-10-4625-2010, 2010.

Ng, N. L., Brown, S. S., Archibald, A. T., Atlas, E., Cohen, R. C., Crowley, J. N., Day, D. A., Donahue, N. M., Fry, J. L., Fuchs, H., Griffin, R. J., Guzman, M. I., Herrmann, H., Hodzic, A., Iinuma, Y., Jimenez, J. L., Kiendler-Scharr, A., Lee, B. H., Luecken, D. J., Mao, J., McLaren, R., Mutzel, A., Osthoff, H. D., Ouyang, B., Picquet-Varrault, B., Platt, U., Pye, H. O. T., Rudich, Y., Schwantes, R. H., Shiraiwa, M., Stutz, J., Thornton, J. A., Tilgner, A., Williams, B. J., and Zaveri, R. A.: Nitrate radicals and biogenic volatile organic compounds: oxidation, mechanisms, and organic aerosol, Atmos. Chem. Phys., 17, 2103–2162, https://doi.org/10.5194/acp-17-2103-2017, 2017.

Paatero, P.: The multilinear engine: A table-driven, least squares program for solving multilinear problems, including the n-way parallel factor analysis model, J. Comput. Graph. Stat., 8, 854–888, https://doi.org/10.2307/1390831, 1999.

Paatero, P. and Tapper, U.: Positive matrix factorization: A non-negative factor model with optimal utilization of error estimates of data values, Environmetrics, 5, 111–126, 1994.

Paglione, M., Kiendler-Scharr, A., Mensah, A. A., Finessi, E., Giulianelli, L., Sandrini, S., Facchini, M. C., Fuzzi, S., Schlag, P., Piazzalunga, A., Tagliavini, E., Henzing, J. S., and Decesari, S.: Identification of humic-like substances (HULIS) in oxygenated organic aerosols using NMR and AMS factor analyses and liquid chromatographic techniques, Atmos. Chem. Phys., 14, 25–45, https://doi.org/10.5194/acp-14-25-2014, 2014.

Perring, A. E., Pusede, S. E., and Cohen, R. C.: An observational perspective on the atmospheric impacts of alkyl and multifunctional nitrates on ozone and secondary organic aerosol, Chem. Rev., 113, 5848–5870, https://doi.org/10.1021/cr300520x, 2013.

Pervez, S., Chakrabarty, R. K., Dewangan, S., Watson, J. G., Chow, J. C., and Matawle, J. L.: Chemical speciation of aerosols and air quality degradation during the festival of lights (diwali), Atmos. Pollut. Res., 7, 92–99, https://doi.org/10.1016/j.apr.2015.09.002, 2016.

Petzold, A., Kramer, H., and Schonlinner, M.: Continuous measurement of atmospheric black carbon using a multi-angle absorption photometer, Environ. Sci. Pollut. R., 9, 78–82, 2002.

Priestley, M., Le Breton, M., Bannan, T. J., Leather, K. E., Bacak, A., Allan, J. D., Brazier, T., Reyes-Villegas, E., Shallcross, B. M. A., Khan, M. A., De Vocht, F., Shallcross, B. M., Brazier, T., Khan, M. A., Allan, J., Shallcross, D. E., Coe, H., and Percival, C. J.: Manchester, uk bonfire night 2014: Air quality and emission ratios during an anthropogenic biomass burning event using a time of flight chemical ionisation mass spectrometer, in preparation, 2018.

Qingguo, H., Liansheng, W., and Shuokui, H.: The genotoxicity of substituted nitrobenzenes and the quantitative structure-activity relationship studies, Chemosphere, 30, 915–923, https://doi.org/10.1016/0045-6535(94)00450-9, 1995.

Ravindra, K., Mor, S., and Kaushik, C. P.: Short-term variation in air quality associated with firework events: A case study, J. Environ. Monitor., 5, 260–264, https://doi.org/10.1039/b211943a, 2003.

Reyes-Villegas, E., Green, D. C., Priestman, M., Canonaco, F., Coe, H., Prévôt, A. S. H., and Allan, J. D.: Organic aerosol source apportionment in London 2013 with ME-2: exploring the solution space with annual and seasonal analysis, Atmos. Chem. Phys., 16, 15545–15559, https://doi.org/10.5194/acp-16-15545-2016, 2016.

Saleh, R., Robinson, E. S., Tkacik, D. S., Ahern, A. T., Liu, S., Aiken, A. C., Sullivan, R. C., Presto, A. A., Dubey, M. K., Yokelson, R. J., Donahue, N. M., and Robinson, A. L.: Brownness of organics in aerosols from biomass burning linked to their black carbon content, Nat. Geosci., 7, 647–650, https://doi.org/10.1038/NGEO2220, 2014.

Sandradewi, J., Prévôt, A. S. H., Szidat, S., Perron, N., Alfarra, M. R., Lanz, V. A., Weingartner, E., and Baltensperger, U. R. S.: Using aerosol light abosrption measurements for the quantitative determination of wood burning and traffic emission contribution to particulate matter, Environ. Sci. Technol., 42, 3316–3323, https://doi.org/10.1021/es702253m, 2008.

Sato, K., Takami, A., Isozaki, T., Hikida, T., Shimono, A., and Imamura, T.: Mass spectrometric study of secondary organic aerosol formed from the photo-oxidation of aromatic hydrocarbons, Atmos. Environ., 44, 1080–1087, https://doi.org/10.1016/j.atmosenv.2009.12.013, 2010.

Slowik, J. G., Vlasenko, A., McGuire, M., Evans, G. J., and Abbatt, J. P. D.: Simultaneous factor analysis of organic particle and gas mass spectra: AMS and PTR-MS measurements at an urban site, Atmos. Chem. Phys., 10, 1969–1988, https://doi.org/10.5194/acp-10-1969-2010, 2010.

Sun, Y. L., Zhang, Q., Schwab, J. J., Yang, T., Ng, N. L., and Demerjian, K. L.: Factor analysis of combined organic and inorganic aerosol mass spectra from high resolution aerosol mass spectrometer measurements, Atmos. Chem. Phys., 12, 8537–8551, https://doi.org/10.5194/acp-12-8537-2012, 2012.

Teich, M., van Pinxteren, D., Wang, M., Kecorius, S., Wang, Z., Müller, T., Mocnik, G., and Herrmann, H.: Contributions of nitrated aromatic compounds to the light absorption of water-soluble and particulate brown carbon in different atmospheric environments in Germany and China, Atmos. Chem. Phys., 17, 1653–1672, https://doi.org/10.5194/acp-17-1653-2017, 2017.

Tian, Y. Z., Wang, J., Peng, X., Shi, G. L., and Feng, Y. C.: Estimation of the direct and indirect impacts of fireworks on the physicochemical characteristics of atmospheric PM_{10} and $PM_{2.5}$, Atmos. Chem. Phys., 14, 9469–9479, https://doi.org/10.5194/acp-14-9469-2014, 2014.

Tiitta, P., Leskinen, A., Hao, L., Yli-Pirilä, P., Kortelainen, M., Grigonyte, J., Tissari, J., Lamberg, H., Hartikainen, A., Kuuspalo, K., Kortelainen, A.-M., Virtanen, A., Lehtinen, K. E.

J., Komppula, M., Pieber, S., Prévôt, A. S. H., Onasch, T. B., Worsnop, D. R., Czech, H., Zimmermann, R., Jokiniemi, J., and Sippula, O.: Transformation of logwood combustion emissions in a smog chamber: formation of secondary organic aerosol and changes in the primary organic aerosol upon daytime and nighttime aging, Atmos. Chem. Phys., 16, 13251–13269, https://doi.org/10.5194/acp-16-13251-2016, 2016.

Vassura, I., Venturini, E., Marchetti, S., Piazzalunga, A., Bernardi, E., Fermo, P., and Passarini, F.: Markers and influence of open biomass burning on atmospheric particulate size and composition during a major bonfire event, Atmos. Environ., 82, 218–225, https://doi.org/10.1016/j.atmosenv.2013.10.037, 2014.

Vecchi, R., Bernardoni, V., Cricchio, D., D'Alessandro, A., Fermo, P., Lucarelli, F., Nava, S., Piazzalunga, A., and Valli, G.: The impact of fireworks on airborne particles, Atmos. Environ., 42, 1121–1132, https://doi.org/10.1016/j.atmosenv.2007.10.047, 2008.

Veres, P., Roberts, J. M., Burling, I. R., Warneke, C., de Gouw, J., and Yokelson, R. J.: Measurements of gas-phase inorganic and organic acids from biomass fires by negative-ion proton-transfer chemical-ionization mass spectrometry, J. Geophys. Res.-Atmos., 115, D23302, https://doi.org/10.1029/2010jd014033, 2010.

Visser, S., Slowik, J. G., Furger, M., Zotter, P., Bukowiecki, N., Canonaco, F., Flechsig, U., Appel, K., Green, D. C., Tremper, A. H., Young, D. E., Williams, P. I., Allan, J. D., Coe, H., Williams, L. R., Mohr, C., Xu, L., Ng, N. L., Nemitz, E., Barlow, J. F., Halios, C. H., Fleming, Z. L., Baltensperger, U., and Prévôt, A. S. H.: Advanced source apportionment of size-resolved trace elements at multiple sites in London during winter, Atmos. Chem. Phys., 15, 11291–11309, https://doi.org/10.5194/acp-15-11291-2015, 2015.

Wang, L. W., Wen, L., Xu, C. H., Chen, J. M., Wang, X. F., Yang, L. X., Wang, W. X., Yang, X., Sui, X., Yao, L., and Zhang, Q. Z.: Hono and its potential source particulate nitrite at an urban site in north china during the cold season, Sci. Total Environ., 538, 93–101, https://doi.org/10.1016/j.scitotenv.2015.08.032, 2015.

Wang, Y., Zhuang, G., Xu, C., and An, Z.: The air pollution caused by the burning of fireworks during the lantern festival in beijing, Atmos. Environ., 41, 417–431, https://doi.org/10.1016/j.atmosenv.2006.07.043, 2007.

Washenfelder, R. A., Attwood, A. R., Brock, C. A., Guo, H., Xu, L., Weber, R. J., Ng, N. L., Allen, H. M., Ayres, B. R., Baumann, K., Cohen, R. C., Draper, D. C., Duffey, K. C., Edgerton, E., Fry, J. L., Hu, W. W., Jimenez, J. L., Palm, B. B., Romer, P., Stone, E. A., Wooldridge, P. J., and Brown, S. S.: Biomass burning dominates brown carbon absorption in the rural southeastern united states, Geophys. Res. Lett., 42, 653–664, https://doi.org/10.1002/2014gl062444, 2015.

Weingartner, E., Saathoff, H., Schnaiter, M., Streit, N., Bitnar, B., and Baltensperger, U.: Absorption of light by soot particles: Determination of the absorption coefficient by means of aethalometers, J. Aerosol Sci., 34, 1445–1463, https://doi.org/10.1016/S0021-8502(03)00359-8, 2003.

Xu, L., Suresh, S., Guo, H., Weber, R. J., and Ng, N. L.: Aerosol characterization over the southeastern United States using high-resolution aerosol mass spectrometry: spatial and seasonal variation of aerosol composition and sources with a focus on organic nitrates, Atmos. Chem. Phys., 15, 7307–7336, https://doi.org/10.5194/acp-15-7307-2015, 2015.

Young, D. E., Allan, J. D., Williams, P. I., Green, D. C., Harrison, R. M., Yin, J., Flynn, M. J., Gallagher, M. W., and Coe, H.: Investigating a two-component model of solid fuel organic aerosol in London: processes, PM_1 contributions, and seasonality, Atmos. Chem. Phys., 15, 2429–2443, https://doi.org/10.5194/acp-15-2429-2015, 2015.

Yuan, B., Liggio, J., Wentzell, J., Li, S.-M., Stark, H., Roberts, J. M., Gilman, J., Lerner, B., Warneke, C., Li, R., Leithead, A., Osthoff, H. D., Wild, R., Brown, S. S., and de Gouw, J. A.: Secondary formation of nitrated phenols: insights from observations during the Uintah Basin Winter Ozone Study (UBWOS) 2014, Atmos. Chem. Phys., 16, 2139–2153, https://doi.org/10.5194/acp-16-2139-2016, 2016.

Zhang, J. K., Cheng, M. T., Ji, D. S., Liu, Z. R., Hu, B., Sun, Y., and Wang, Y. S.: Characterization of submicron particles during biomass burning and coal combustion periods in beijing, china, Sci. Total Environ., 562, 812–821, https://doi.org/10.1016/j.scitotenv.2016.04.015, 2016.

Zhang, M., Wang, X., Chen, J., Cheng, T., Wang, T., Yang, X., Gong, Y., Geng, F., and Chen, C.: Physical characterization of aerosol particles during the chinese new year's firework events, Atmos. Environ., 44, 5191–5198, https://doi.org/10.1016/j.atmosenv.2010.08.048, 2010.

Zhu, Q., He, L.-Y., Huang, X.-F., Cao, L.-M., Gong, Z.-H., Wang, C., Zhuang, X., and Hu, M.: Atmospheric aerosol compositions and sources at two national background sites in northern and southern China, Atmos. Chem. Phys., 16, 10283–10297, https://doi.org/10.5194/acp-16-10283-2016, 2016.

Zotter, P., Herich, H., Gysel, M., El-Haddad, I., Zhang, Y., Mocnik, G., Hüglin, C., Baltensperger, U., Szidat, S., and Prévôt, A. S. H.: Evaluation of the absorption Ångström exponents for traffic and wood burning in the Aethalometer-based source apportionment using radiocarbon measurements of ambient aerosol, Atmos. Chem. Phys., 17, 4229–4249, https://doi.org/10.5194/acp-17-4229-2017, 2017.

Remarks from the typesetter

TS1 Does this number stand for total pages?

Supplement of

Simultaneous Aerosol Mass Spectrometry and Chemical Ionisation Mass Spectrometry measurements during a biomass burning event in the UK: Insights into nitrate chemistry

Ernesto Reyes-Villegas, Michael Priestley, Yu-Chieh Ting, Sophie Haslett, Thomas Bannan, Michael Le breton, Paul I. Williams, Asan Bacak, Michael J. Flynn, Hugh Coe, Carl Percival, James D. Allan

Correspondence to: Ernesto Reyes-Villegas (ernesto.reyesvillegas@manchester.ac.uk)

S1. Bonfire/firework locations during bonfire night 2014.

Locations of nine parks with main bonfire/fireworks during November 5th 2014.

Figure S1: Manchester map with locations of parks with bonfires/fireworks displays (red flames) and monitoring site (blue dot) at the University of Manchester. Map produced with Google Maps and location of bonfires was taken from [http://www.pocketmanchester.com/bonfire-night-2014-in-manchester/, accessed 03/05/2017].

S2. Literature review on lack of interference of CH_2O^+ fragment to m/z30.

Table S1. CH_2O^+ signals at m/z 29, 30 and 31 from HR-ToF-AMS data of previous studies. Comparison of m/z ratios 30/29 and 30/31 with values found in this study.

	Reference	30/29	30/31	m/z 29	m/z 30	m/z 31	Notes
ambient	**This study**	4.38	35.00	0.08	0.35	0.01	sPON_ME2
		1.42	8.50	0.06	0.09	0.01	pPON_ME2
	(Aiken et al., 2010)	0.16	0.32	0.05	0.008	0.025	pine burn
		0.20	0.45	0.045	0.009	0.02	BBOA Mex
	(Collier et al., 2016)	0.25	0.56	4	1	1.8	Ground plume
		0.20	0.60	3	0.6	1	Ground plume
		0.23	0.67	3.5	0.8	1.2	aircraft plume
		0.25	1.25	4	1	0.8	aircraft plume
	(Zhou et al., 2017)	0.18	0.88	8	1.4	1.6	no bb
		0.32	0.95	6	1.9	2	bb inf
		0.30	0.90	6	1.8	2	bb plm
Laboratory-based	(He et al., 2010)	0.25	0.75	0.06	0.015	0.02	Fir (diluted/cooled)
		0.21	0.68	0.07	0.015	0.022	pine burn
		0.20	0.56	0.05	0.01	0.018	Willow
		0.30	0.90	0.06	0.018	0.02	Wattle
		0.30	0.90	0.06	0.018	0.02	SugaCaneLeave
		0.30	0.08	0.05	0.015	0.2	Rice Straw
	(Heringa et al., 2011)	0.25	0.67	4	1	1.5	poa
		0.25	0.50	4	1	2	5h aging
	(Ortega et al., 2013)	0.15	0.50	13	2	4	start (oak)
		0.20	0.50	50	10	20	aged (oak)
		0.04	0.05	250	10	220	start (pine)
		0.07	0.10	270	20	200	aged (pine)
	(Corbin et al., 2015b)	0.20	0.80	4	0.8	1	start
			0.83		0.05	0.06	flaming
	(Corbin et al., 2015a)		0.50		0.01	0.02	Filtered and Oxid
			0.50		0.01	0.02	Oxidized
		0.25	0.50	0.04	0.01	0.02	Primary
	(Bruns et al., 2015)	0.43	6.00	0.07	0.03	0.005	OH and UV exp.
		0.34	1.00	0.065	0.022	0.022	OH and UV exp.
		0.40	1.00	0.045	0.018	0.018	OH and UV exp.
		0.34	1.00	0.065	0.022	0.022	OH and UV exp.
		0.40	1.00	0.045	0.018	0.018	OH and UV exp.
		0.23	1.00	0.048	0.011	0.011	OH and UV exp.
		0.20	1.00	0.04	0.008	0.008	OH and UV exp.
		0.25	1.00	0.048	0.012	0.012	OH and UV exp.

CH_2O^+ identification at m/z 30 is accompanied with signals at m/z 29 and m/z 31

Table S1 shows CH_2O^+ signals at m/z's 29, 30, and 31 from HR-ToF-AMS studies. It is possible to observe the low CH_2O^+ contribution to m/z 30 with 30/29 ratios between 0.01-0.40. The high values of 0.4 – 6 were observed when exposing aerosols to OH and UV. We can also see that 30/31 and 30/29 ratios do not show variations during and after biomass burning events or during fresh and aged emissions (Ortega et al., 2013;Corbin et al., 2015a;Corbin et al., 2015b), suggesting there is not substantial CH_2O^+ variability over the biomass burning process. In this study, a large contribution of m/z 30 signal to the mass spectra was observed with both sPON and pPON with 30/29 ratios (4.38 and 1.42 respectively) and 30/31 ratios (35.0 and 8.5 respectively) higher than unity. Showing that a CH_2O^+ interference at m/z30 would be unlikely.

S3. Aethalometer correction.

Aethalometer measurements (absorption coefficients, b_{ATN}) need to be corrected from two main effects: filter loading (R) and scattering correction (C) that compensates for the multiple-scattering effects from the matrix. There are different methods to correct aethalometer data (Weingartner et al., 2003;Arnott et al., 2005;Schmid et al., 2006). Coen et al. (2010) proposed a new method through a critical analysis of the effectiveness of the other methods, which involves corrections based on absorption and scattering measurements. In this study, wavelength-dependent scattering measurements were not available (A Photo Acoustic Soot Spectrometer was used to measure aerosol optical absorption coefficients. However, the scattering channels failed to report data during the bonfire event), thus the Weingartner method (Weingartner et al., 2003) was used to do these corrections.

The light attenuation (ATN) is defined by equation S1, where I_o is the intensity of the incoming light and I is the remaining light after passing through the filter.

$$\mathrm{ATN} = -100 * \ln\left(\frac{I_o}{I}\right) \tag{S1}$$

The attenuation cross section (σ_{ATN} in $m^2.g^{-1}$) is calculated using the equation S2, where 14625 [$m^2.g^{-1}$] is the mass specific attenuation cross-section proposed by the manufacturer and λ is the wavelength in nm.

$$\sigma_{\mathrm{ATN}\_\lambda} = \frac{14625}{\lambda} \tag{S2}$$

The absorption coefficient (b_{ATN}, Mm^{-1}) was calculated using equation S3, where BC is black carbon [$\mu g.m^{-3}$] measured by the aethalometer.

$$b_{ATN\_\lambda} = BC_\lambda * \sigma_{\mathrm{ATN}\_\lambda} \tag{S3}$$

$b_{\_ATN\_\lambda}$ values need to be corrected by calculating b_{abs} (corrected absorption coefficient).

$$b_{abs\_\lambda} = \frac{b_{ATN\_\lambda}}{C*R} \tag{S4}$$

Where C is a parameter for scattering correction and R, a wavelength dependent parameter, is related to the filter loading effect.

C is calculated as the slope of b_{ATN_630} from aethalometer and b_{abs_630} from MAAP, using the values with ATN<10% (Calculating C with this approach the effects from filter loading are minimized). The Aethalometer does not measure at 630 wavelength thus b_{ATN_630}, is calculated using equation S6, where the absorption Ångström exponent (α) is calculated using equation S5.

$$\alpha = \frac{\ln\left(\frac{b_{ATN_{470}}}{b_{ATN_{950}}}\right)}{\ln\left(\frac{950}{470}\right)} \tag{S5}$$

$$b_{ATN\_630} = b_{ATN\_660} * \left(\frac{630}{660}\right)^{-\alpha} \tag{S6}$$

C represents the slope of b_{ATN_630} from aethalometer vs b_{abs_630} from MAAP. Following this method, a value of C = 3.16 was calculated.

The shadowing parameter (f) is determined, similar to other studies (Sandradewi et al., 2008;Sciare et al., 2011;Ji et al., 2017) as the average of b_{ATN} ratios after and before filter changes for the complete dataset in order to minimise the difference before and after filter changes. The f values obtained were f_{470} = 1.49 and f_{950} = 1.28.

R is calculated with the following equation:

$$R = \left(\frac{1}{f} - 1\right)\frac{ln(\mathrm{ATN}) - ln(10\%)}{ln(50\%) - ln(10\%)} + 1 \qquad (S7)$$

Finally, with C and R being determined, the corrected absorption coefficients (b_{abs_λ}) are calculated with equation S4.

S4. Aethalometer model.

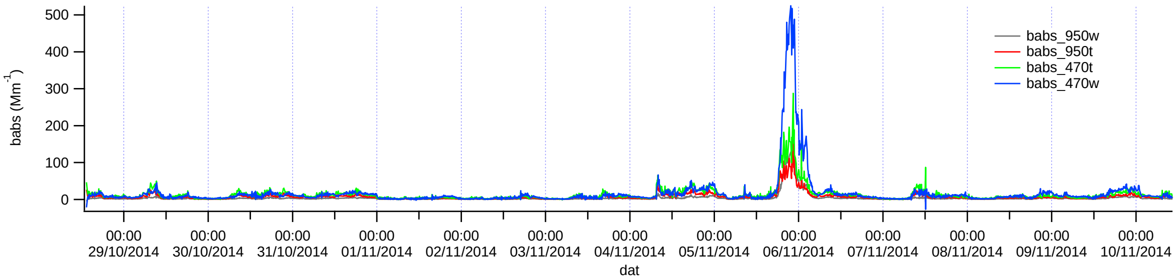

Figure S2: Absorption coefficients (b_{abs}) for wood burning and traffic.

S5. Back trajectories for the different pollutant episodes.

Hysplit model was used to run back trajectories, with 48 hrs of duration and three different hights (0, 205 and 500 m about ground level), for the episodes with different pollutant concentrations: an event with high secondary pollutants is observed from October 30th – November 1st; an event with low concentrations from November 1st – 3rd. Bonfire night from November 5th – 7th; an event with high primary emissions from November 8th -10th.

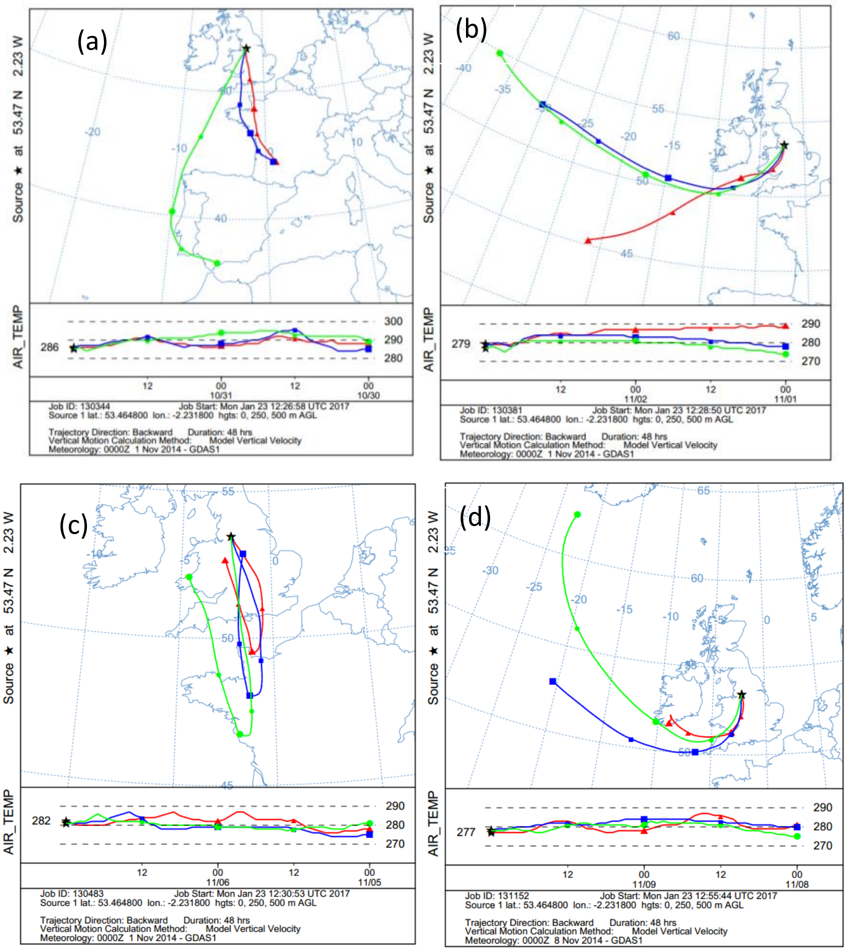

Figure S3: Back trajectories run for events with high secondary pollutant concentrations (a), low pollutant concentrations (b), bonfire night (c) and winter-like event (d).

S6. Fragmentation table to add PON to PMF analysis.

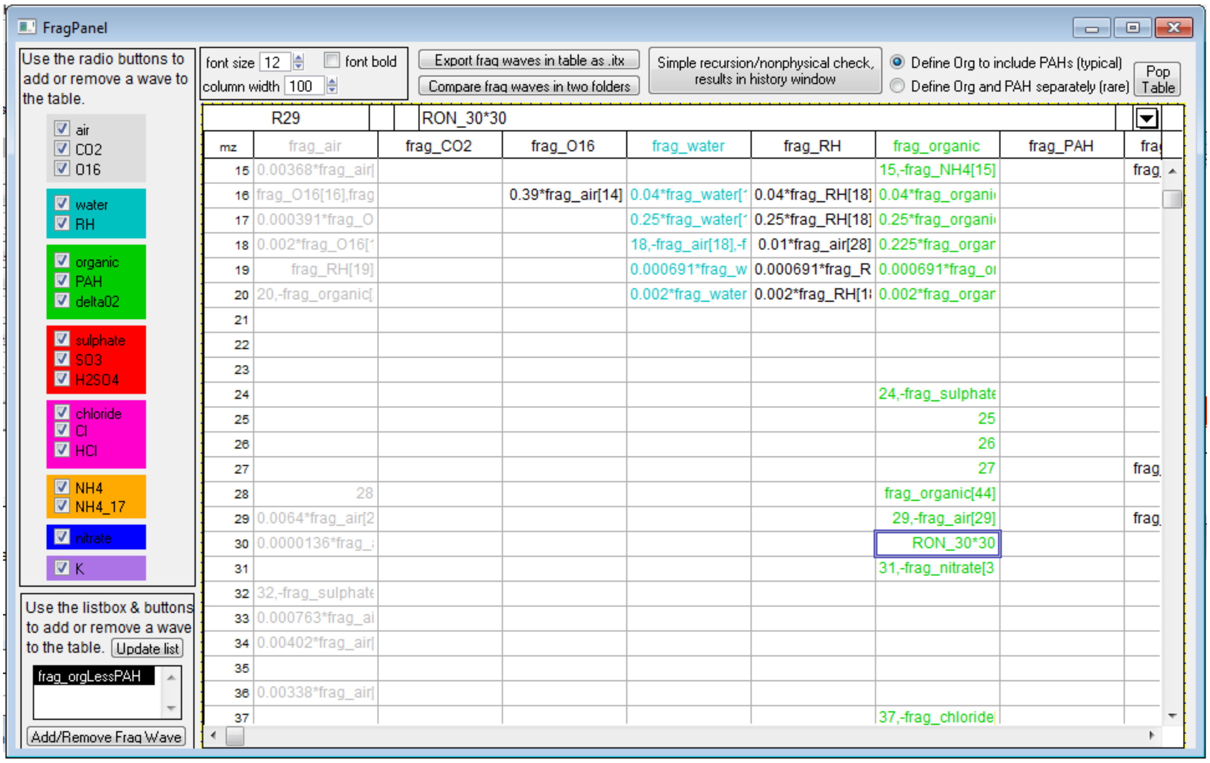

Figure S4: Modifying fragmentation table to add PON to PMF analysis.

S7. OA source apportionment.

PMF and ME-2 source apportionment analysis was performed following the strategy proposed by (Reyes-Villegas et al., 2016). A series of solutions were run under different conditions in order to determine the best way to deconvolve OA factors. PMF was run with f-peaks from -1.0 to 1.0 and steps of 0.1. ME-2 was run using different a-values to partially constrain the solutions (table S1), using mass spectra (BBOA, HOA and COA) from Young et al. (2015a) and Crippa et al. (2013) as target profiles (TP). Figure S5 shows the labelling used to identify the different runs performed with ME-2 and table S2 shows the different a-value combinations used to explore different solutions.

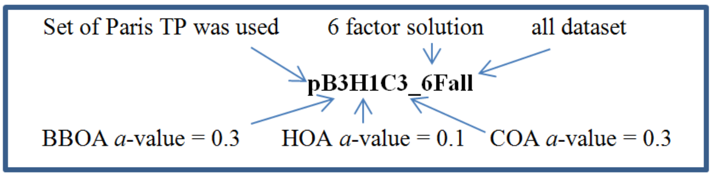

Figure S5: Labelling used to identify runs.

Table S2: List of ME-2 runs

Run	Run
B5H2C5	H1C3
B3H1C3	H2C5
B3H1C5	B3H1
B5H1C5	B5H2
B5H1C3	

S7.1 Strategy to select the solution that best apportions OA sources.

The OA source apportionment was performed using different f-peaks when running PMF and different a-values when running ME-2 (table S2) looking at solutions with 4, 5 and 6 factors,. These solutions were explored comparing their residuals and Q/Qexp for m/z's and time series; Total Q/Qexp and total residuals; diurnal profiles and trilinear regression (Reyes-Villegas et al., 2016). Looking for solutions with low residuals and Q/Qexp values. Trilinear regression is performed between BBOA, HOA and COA and NOx, since these three OA sources and NOx are related to combustion sources. With trilinear regression analysis, partial slopes should be positive as we are working with aerosol concentrations. Moreover, COA partial slope should be close to zero due to its low contribution to NOx. The chi square value from multilinear regression is used as goodness of fit, thus the lowest the value the best correlation between the different sources.

Here the analysis carried out to all the dataset is explained in detail.

Step 1. PMF runs looking at 4-factor solutions with f-peaks from -1.0 to 1.0 and steps of 0.1. One solution is chosen to be compared with ME-2 solutions.

Step 2. ME-2 runs looking at 4-factor solutions with different a-values using TP from Paris and London.

Step 3. Two solutions from step 2 are chosen together with the PMF solution, form step 1, to be the three 4-factor solutions to use in the further comparison.

Step 4. Repeat steps 1 to 3 to look at 5-factor and six-factor solutions to finally compare the 9 solutions.

Step 5. Choose one solution that better separates, according to this analysis, OA sources. Perform this analysis for the four tests mentioned in table S2 in order to have one solution for each test.

These steps were used to explore solutions for the different tests performed, generating more than 60 different plots that were analysed. Here, in order to avoid making an overly massive supplement material, only the final comparison between solutions from the different tests performed is shown (Section S7.2). Table S3 shows the chosen solution for each one of the tests performed.

S7.2 Chosen solutions for the different tests.

Table S3: Tests done to determine the solution that better deconvolves OA factors.

Analysis			Solution		Strategy
ID	a	b	a	b	From solution a to b
Test 1	° all		pH1C3_5all		
Test 2	* nbf	bfo	pB3H1C3_5nbf	× nB3H1C5_6bfo	nbf mass spectra were used as TP to analyse bfo dataset.
Test 3	+ bfo	all	PMF_6_0.7	Δ bB5H2C5_5all	bfo mass spectra were used as TP to analyse all dataset.
Test 4	nbf	all	pB3H1C3_5nbf	× nH2C5_5all	nbf mass spectra were used as TP to analyse all dataset.
Test 1_ON	° all		wB3H1_ON_5all		
Test 2_ON	* nbf	bfo	pH1C3_ON_5nbf	nB5H1C3_ON_6bfo	nbf mass spectra were used as TP to analyse bfo dataset.

° all = the whole dataset was analysed: 29/Oct/2014-10/Nov/2014
* nbf = not bonfire event: from 29/Oct to 05/Nov 15:00 and from 06/Nov 06:35 to 10/Nov/2014
+ bfo = bonfire only event: 05/Nov 15:00 - 06/Nov 06:35
× n = mass spectra from analysis a (nbf) were used as TP in the analysis b.
Δ b = means mass spectra from analysis a (bfo) were used as TP in the analysis b for test 3.
ON means the tests were performed after modifying the fragmentation table to determine a PON source.

When doing two analyses with ME-2 (in the case of tests 2, 3 and 4), in analysis “a” mass spectra from London (Young et al., 2015b), labelled as “w” and Paris (Crippa et al., 2013) labelled as “p” , were used as target profiles (TP). PMF runs were explored with different fpeak values ranging from -1.0 to 1.0 with steps of 0.1.

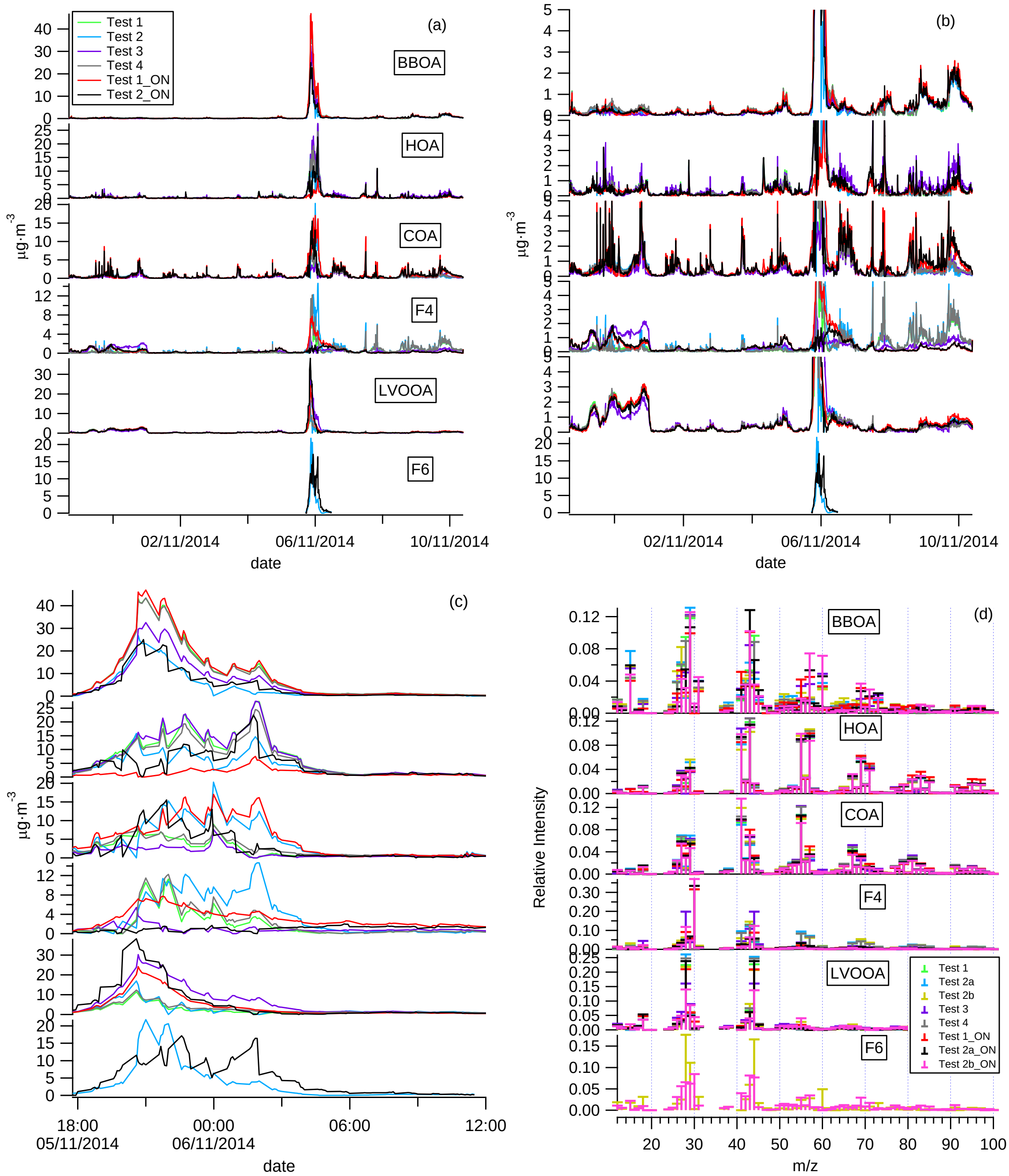

Figure S5: Comparison of the chosen solution for the four tests performed. Time series for the complete dataset (a), time series with a close up to y-axis to show low concentrations (b), time series during bonfire night event (c) and mass spectra.

S7.3 Comparison of different solution tests.

Here, the different tests performed without modifying the fragmentation table (test 1, test 2, test 3, and test4) and modifying it (test1_ON and test2_ON) are compared in order to determine the test that better separates OA factors.

The analysis was carried out by comparing the residuals and Q/Qexp for m/z's and time series for all the dataset (figure S6) and more into detail for the bonfire night (figure S7); trilinear regression between BBOA, HOA and COA with NOx (figure S8) and diurnal profiles (figure S9).

Analysis without modifying the fragmentation table is the first comparison performed, where test 2 resulted to be the test that better deconvolved OA factors with; low residuals (figures S6 and S7) and low chi square, used as a goodness of fit (figure S8). Then test1_ON and test2_ON were performed in order to determine the best way to deconvolve OA sources including organic nitrate factors, where test 2 showed to be a better way to deconvolve OA sources compared to test1_ON.

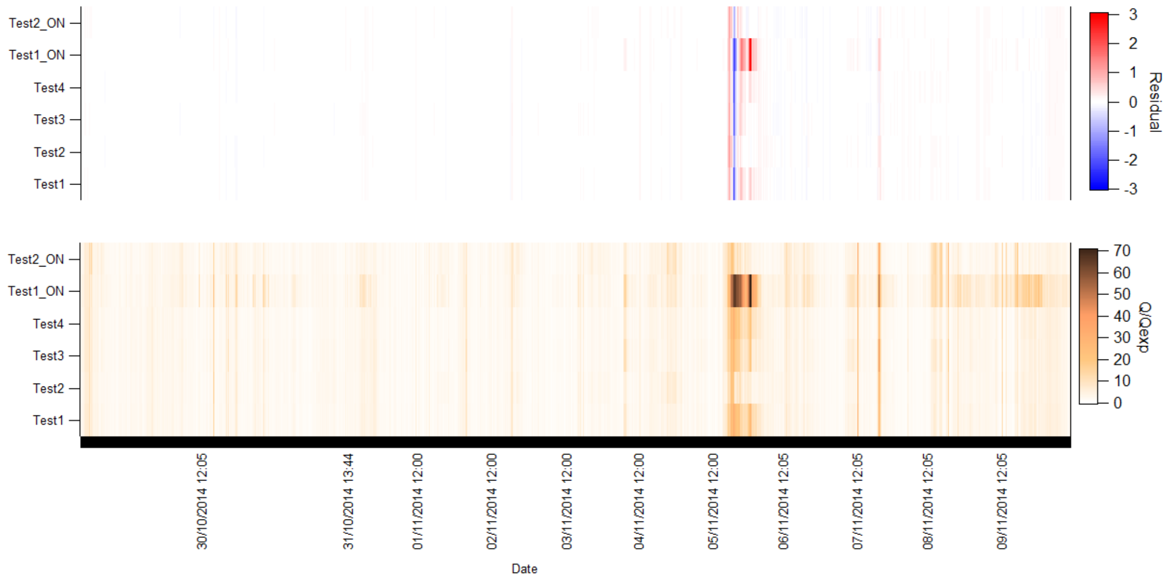

Figure S6: Comparison of the different solutions for all sampling period.

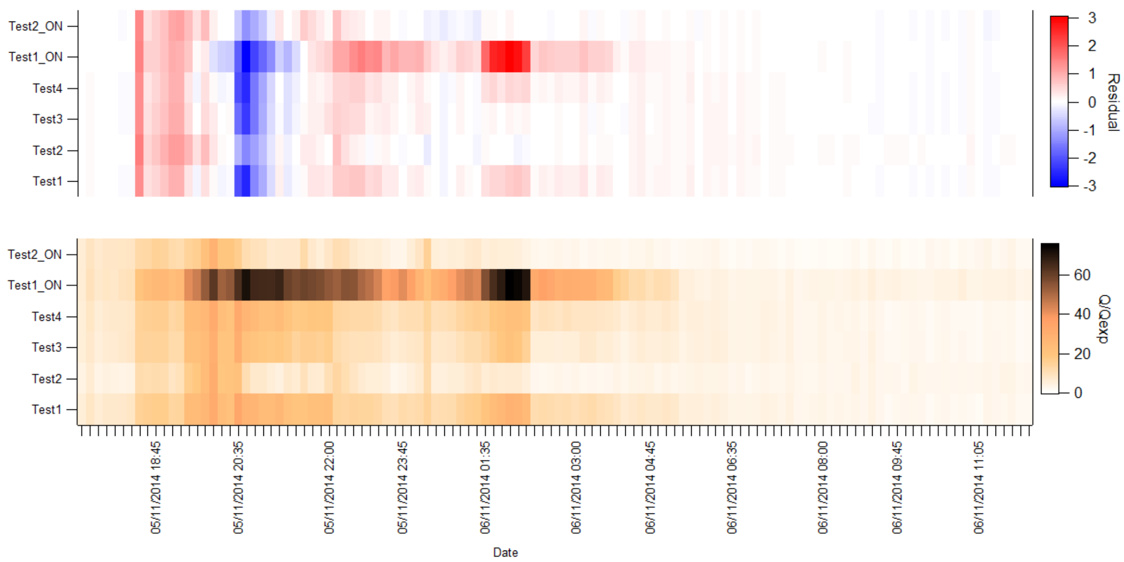

Figure S7: Comparison of the different solutions for the bfo event.

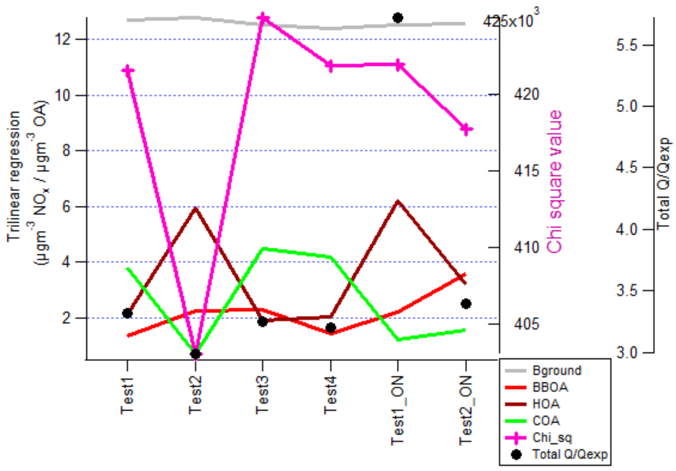

Figure S8: Trilinear regression between OA sources and NOx.

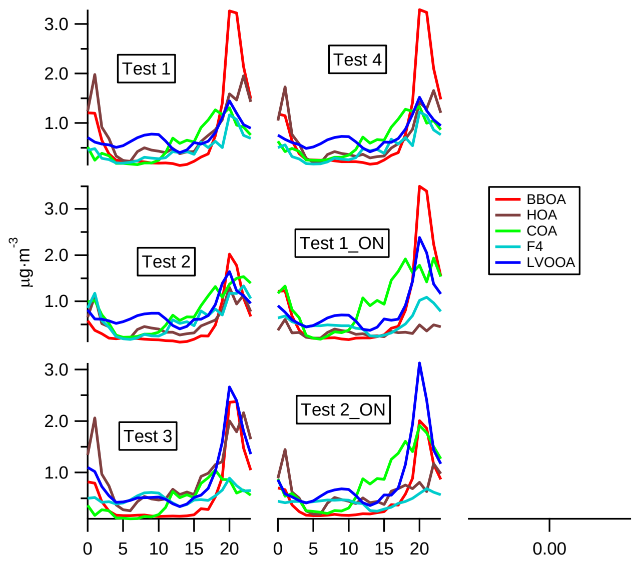

Figure S9: Diurnal profiles.

S8. Primary (pPON) and secondary (sPON) organic nitrate estimation.

The slope from a linear regression between PON, obtained from 46:30 ratios analysis in Section 2.2.2 in manuscript, and BBOA was used to calculate primary and secondary organic nitrate. Blue circles show the period where the slope between PON and BBOA was calculated (Section 4.2 in manuscript).

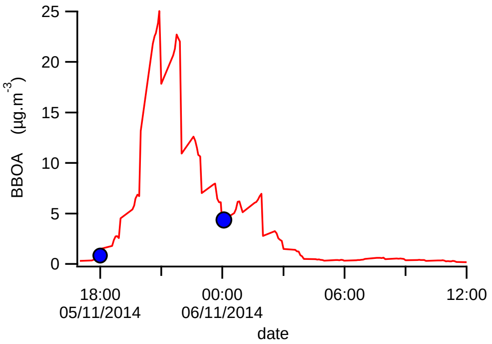

Figure S10: Time series used to calculate the slope between PON and BBOA

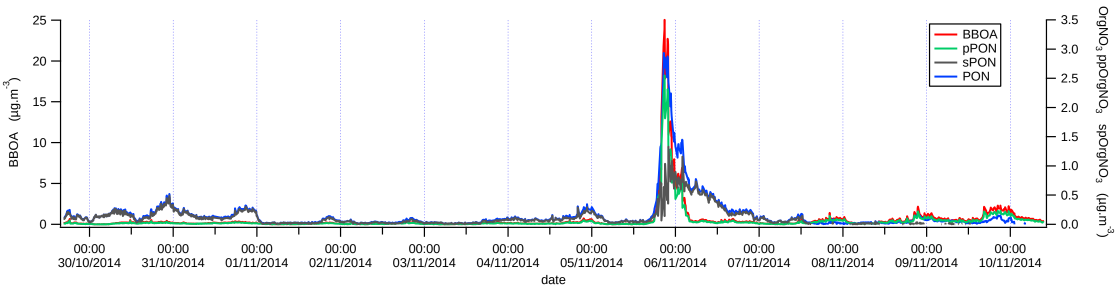

Figure S11: Time series of pPON and sPON for the whole period.

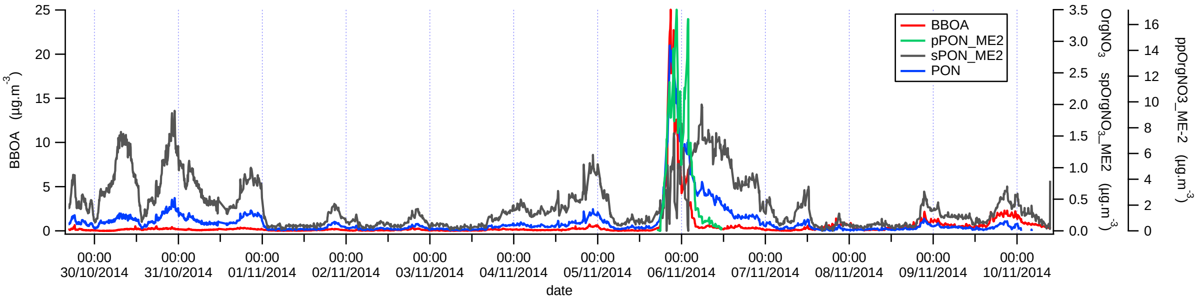

Figure S12: pPON_ME2 and sPON_ME2 obtained from ME-2 analysis.

Two methods have been used to determine primary and secondary PON. In the following plots we can see primary PON comparison has a good correlation with a pearson value of 0.7 while secondary PON comparison shows a different behaviour between them.

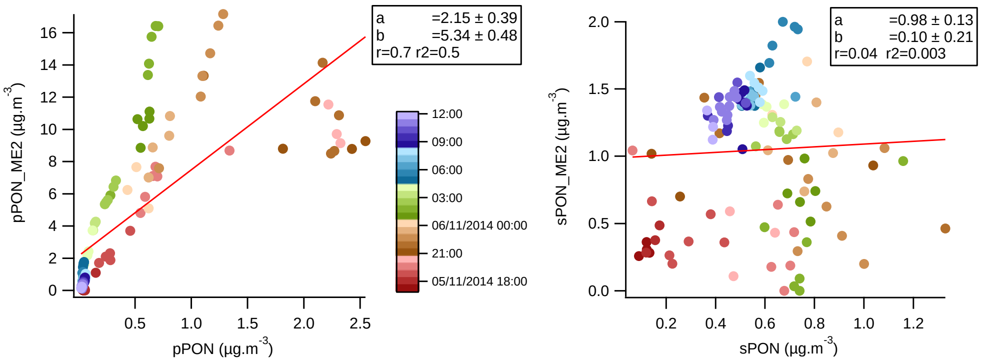

Figure S13: PON comparison for the two methods used.

S9. r^2 values between OA sources and CIMS measurements.

Table S4 show the r^2 values between the OA factors and CIMS measurements, for the different analyses; ALL, LC, bfo and WL. Only r^2 higher or equal to 0.4 are displayed.

Table S4: R^2 values between OA factors and CIMS measurements.

		BBOA					COA				sPON				LVOOA				pPON
Formula	Name	ALL	HSC	LC	bfo	WL	ALL	LC	bfo	WL	ALL	LC	bfo	WL	ALL	LC	bfo	WL	bfo
C4H6O2	methacrylic acid	0.89			0.92	0.53	0.64		0.77	0.48					0.78		0.82		0.52
C3H4O2	Acid_Acrylic	0.85			0.90	0.65	0.62		0.70	0.43				0.48	0.79		0.88		
H2COH2O	methylhydroperoxide	0.78			0.90		0.54		0.69						0.66		0.85		
C6H6O	Phenol	0.89			0.89		0.59		0.73						0.75		0.73		0.57
C7H6O2	Benzoic acid	0.89		0.57	0.89	0.86	0.65		0.83	0.45		0.71		0.73	0.67	0.72	0.64	0.58	0.57
C2H5NO	Methylformamide	0.88			0.89	0.47	0.61		0.79						0.65		0.67	0.56	0.65
C2H3NO	Methyl isocyanate	0.89	0.49	0.44	0.89	0.71	0.55		0.66					0.50	0.85		0.88		
C5H10O2	Pentanoic acid	0.77			0.87		0.60		0.76						0.54		0.66		
HNO2	nitrous acid	0.81			0.86	0.66	0.59		0.84					0.57	0.61		0.66		0.70
CH2O2	formic acid	0.52			0.86				0.62						0.58		0.88		
C3H7NO	Dimethylformamide	0.80			0.85		0.59		0.76						0.56		0.63	0.60	0.63
C3H6O2	propionic acid	0.87		0.67	0.85	0.72	0.53	0.45	0.62			0.41		0.67	0.78		0.78	0.63	
C2H5N3O2	C2H5N3O2				0.83				0.77								0.59		
CHNO	Isocyanic acid	0.86		0.64	0.83		0.56		0.68			0.81			0.84	0.80	0.86		0.47
C4H6O4	succinic acid				0.83				0.71								0.60		
C6H6O3	trihydroxybenzene	0.83	0.48	0.72	0.82	0.85	0.62		0.79	0.42		0.75		0.71	0.59	0.82	0.54	0.59	0.49
C4H8O2	butyric acid				0.80				0.58								0.76		
C2H2NO3	C2H2NO3	0.61			0.79		0.48		0.56			0.49			0.63		0.90		
HO2H2O	HO2H2O	0.53			0.77				0.63								0.70		
CHN	Hydrogen cyanide	0.80		0.66	0.76	0.84	0.57	0.36	0.70			0.60		0.74	0.62	0.69	0.61	0.54	0.77
C6H6O2	Catechol	0.73			0.73		0.44		0.56						0.63		0.62		
C7H8O	Cresol	0.79			0.72		0.50		0.59						0.59		0.51		0.65
C3H4O4	Malonic acid				0.69				0.50								0.52	0.54	
C7H8O2	guaiacol	0.63			0.62	0.78			0.45	0.43				0.62	0.58		0.57		
C2H4O3	Glycolic Acid				0.62		0.42		0.63										
CNO	anion isocyanate	0.66		0.61	0.61		0.48		0.50			0.81			0.74	0.76	0.74		
C3H7NO2	L-Alanine				0.54				0.64										0.65
*NO		0.40			0.63				0.59								0.58		0.46
*NO2					0.45	0.51			0.41				0.50				0.54		
*Nox					0.60	0.47			0.57								0.59		
*CO		0.79	0.55		0.81	0.67	0.64		0.80	0.42				0.48	0.58		0.56		0.78
*SO2					0.63				0.57								0.52		0.72
ClNO3	Chlorine nitrate			0.45							0.45	0.69	0.53			0.66			
ClNO2	nitryl chloride			0.47								0.74	0.52			0.67			
Cl2	Chlorine												0.51						0.44
C6H5NO3	nitrophenol		0.41															0.55	

ALL = all dataset, LC = low concentrations, bfo = bonfire night, WL = winter-like.

References

Aiken, A. C., De Foy, B., Wiedinmyer, C., Decarlo, P. F., Ulbrich, I. M., Wehrli, M. N., Szidat, S., Prevot, A. S. H., Noda, J., Wacker, L., Volkamer, R., Fortner, E., Wang, J., Laskin, A., Shutthanandan, V., Zheng, J., Zhang, R., Paredes-Miranda, G., Arnott, W. P., Molina, L. T., Sosa, G., Querol, X., and Jimenez, J. L.: Mexico city aerosol analysis during milagro using high resolution aerosol mass spectrometry at the urban supersite (t0)-part 2: Analysis of the biomass burning contribution and the non-fossil carbon fraction, Atmos Chem Phys, 10, 5315-5341, 10.5194/acp-10-5315-2010, 2010.
Arnott, W. P., Hamasha, K., Moosmuller, H., Sheridan, P. J., and Ogren, J. A.: Towards aerosol light-absorption measurements with a 7-wavelength aethalometer: Evaluation with a photoacoustic instrument and 3-wavelength nephelometer, Aerosol Science and Technology, 39, 17-29, 10.1080/027868290901972, 2005.
Bruns, E. A., Krapf, M., Orasche, J., Huang, Y., Zimmermann, R., Drinovec, L., Močnik, G., El-Haddad, I., Slowik, J. G., Dommen, J., Baltensperger, U., and Prévôt, A. S. H.: Characterization of primary and secondary wood combustion products generated under different burner loads, Atmos. Chem. Phys., 15, 2825-2841, 10.5194/acp-15-2825-2015, 2015.
Coen, M. C., Weingartner, E., Apituley, A., Ceburnis, D., Fierz-Schmidhauser, R., Flentje, H., Henzing, J. S., Jennings, S. G., Moerman, M., Petzold, A., Schmid, O., and Baltensperger, U.: Minimizing light absorption measurement artifacts of the aethalometer: Evaluation of five correction algorithms, Atmos Meas Tech, 3, 457-474, 2010.
Collier, S., Zhou, S., Onasch, T. B., Jaffe, D. A., Kleinman, L., Sedlacek, A. J., Briggs, N. L., Hee, J., Fortner, E., Shilling, J. E., Worsnop, D., Yokelson, R. J., Parworth, C., Ge, X., Xu, J., Butterfield, Z., Chand, D., Dubey, M. K., Pekour, M. S., Springston, S., and Zhang, Q.: Regional influence of aerosol emissions from wildfires driven by combustion efficiency: Insights from the bbop campaign, Environmental Science & Technology, 50, 8613-8622, 10.1021/acs.est.6b01617, 2016.
Corbin, J. C., Keller, A., Lohmann, U., Burtscher, H., Sierau, B., and Mensah, A. A.: Organic emissions from a wood stove and a pellet stove before and after simulated atmospheric aging, Aerosol Science and Technology, 49, 1037-1050, 10.1080/02786826.2015.1079586, 2015a.
Corbin, J. C., Lohmann, U., Sierau, B., Keller, A., Burtscher, H., and Mensah, A. A.: Black carbon surface oxidation and organic composition of beech-wood soot aerosols, Atmos. Chem. Phys., 15, 11885-11907, 10.5194/acp-15-11885-2015, 2015b.
Crippa, M., DeCarlo, P. F., Slowik, J. G., Mohr, C., Heringa, M. F., Chirico, R., Poulain, L., Freutel, F., Sciare, J., Cozic, J., Di Marco, C. F., Elsasser, M., Nicolas, J. B., Marchand, N., Abidi, E., Wiedensohler, A., Drewnick, F., Schneider, J., Borrmann, S., Nemitz, E., Zimmermann, R., Jaffrezo, J. L., Prevot, A. S. H., and Baltensperger, U.: Wintertime aerosol chemical composition and source apportionment of the organic fraction in the metropolitan area of paris, Atmos Chem Phys, 13, 961-981, DOI 10.5194/acp-13-961-2013, 2013.
He, L. Y., Lin, Y., Huang, X. F., Guo, S., Xue, L., Su, Q., Hu, M., Luan, S. J., and Zhang, Y. H.: Characterization of high-resolution aerosol mass spectra of primary organic aerosol emissions from chinese cooking and biomass burning, Atmos. Chem. Phys., 10, 11535-11543, 10.5194/acp-10-11535-2010, 2010.
Heringa, M. F., DeCarlo, P. F., Chirico, R., Tritscher, T., Dommen, J., Weingartner, E., Richter, R., Wehrle, G., Prévôt, A. S. H., and Baltensperger, U.: Investigations of primary and secondary particulate matter of different wood combustion appliances with a high-resolution time-of-flight aerosol mass spectrometer, Atmos. Chem. Phys., 11, 5945-5957, 10.5194/acp-11-5945-2011, 2011.
Ji, D., Li, L., Pang, B., Xue, P., Wang, L., Wu, Y., Zhang, H., and Wang, Y.: Characterization of black carbon in an urban-rural fringe area of beijing, Environmental Pollution, 223, 524-534, https://doi.org/10.1016/j.envpol.2017.01.055, 2017.
Ortega, A. M., Day, D. A., Cubison, M. J., Brune, W. H., Bon, D., de Gouw, J. A., and Jimenez, J. L.: Secondary organic aerosol formation and primary organic aerosol oxidation from biomass-burning

smoke in a flow reactor during flame-3, Atmos. Chem. Phys., 13, 11551-11571, 10.5194/acp-13-11551-2013, 2013.
Reyes-Villegas, E., Green, D. C., Priestman, M., Canonaco, F., Coe, H., Prévôt, A. S. H., and Allan, J. D.: Organic aerosol source apportionment in london 2013 with me-2: Exploring the solution space with annual and seasonal analysis, Atmos. Chem. Phys., 16, 15545-15559, 10.5194/acp-16-15545-2016, 2016.
Sandradewi, J., Prevot, A. S. H., Weingartner, E., Schmidhauser, R., Gysel, M., and Baltensperger, U.: A study of wood burning and traffic aerosols in an alpine valley using a multi-wavelength aethalometer, Atmos Environ, 42, 101-112, 10.1016/j.atmosenv.2007.09.034, 2008.
Schmid, O., Artaxo, P., Arnott, W. P., Chand, D., Gatti, L. V., Frank, G. P., Hoffer, A., Schnaiter, M., and Andreae, M. O.: Spectral light absorption by ambient aerosols influenced by biomass burning in the amazon basin. I: Comparison and field calibration of absorption measurement techniques, Atmos. Chem. Phys., 6, 3443-3462, 10.5194/acp-6-3443-2006, 2006.
Sciare, J., d'Argouges, O., Sarda-Estève, R., Gaimoz, C., Dolgorouky, C., Bonnaire, N., Favez, O., Bonsang, B., and Gros, V.: Large contribution of water-insoluble secondary organic aerosols in the region of paris (france) during wintertime, Journal of Geophysical Research: Atmospheres, 116, n/a-n/a, 10.1029/2011jd015756, 2011.
Weingartner, E., Saathoff, H., Schnaiter, M., Streit, N., Bitnar, B., and Baltensperger, U.: Absorption of light by soot particles: Determination of the absorption coefficient by means of aethalometers, J Aerosol Sci, 34, 1445-1463, 10.1016/S0021-8502(03)00359-8, 2003.
Young, D. E., Allan, J. D., Williams, P. I., Green, D. C., Flynn, M. J., Harrison, R. M., Yin, J., Gallagher, M. W., and Coe, H.: Investigating the annual behaviour of submicron secondary inorganic and organic aerosols in london, Atmos. Chem. Phys., 15, 6351-6366, 10.5194/acp-15-6351-2015, 2015a.
Young, D. E., Allan, J. D., Williams, P. I., Green, D. C., Harrison, R. M., Yin, J., Flynn, M. J., Gallagher, M. W., and Coe, H.: Investigating a two-component model of solid fuel organic aerosol in london: Processes, pm1 contributions, and seasonality, Atmos Chem Phys, 15, 2429-2443, 10.5194/acp-15-2429-2015, 2015b.
Zhou, S., Collier, S., Jaffe, D. A., Briggs, N. L., Hee, J., Sedlacek Iii, A. J., Kleinman, L., Onasch, T. B., and Zhang, Q.: Regional influence of wildfires on aerosol chemistry in the western us and insights into atmospheric aging of biomass burning organic aerosol, Atmos. Chem. Phys., 17, 2477-2493, 10.5194/acp-17-2477-2017, 2017.

Blank page

Paper 3

6.3 On-line aerosol and gas measurements from cooking emissions: implications for source apportionment

Ernesto Reyes-Villegas, Thomas Bannan, Michael Le Breton, Archit Mehra, Michael Priestley, Carl Percival, Hugh Coe, James D. Allan

The manuscript has been submitted to the Environmental Science and Technology journal. This version is the one sent to the journal after addressing the reviewer's comments.

Research highlights:

- On-line measurements of cooking a series of food (English breakfast, Fish&Chips, different types of meat and vegetables) were performed in a laboratory-based study.
- Mass spectra from different types of food were generated from AMS measurements and food cooking markers were identified, both in gas and particle, from FIGAERO-CIMS measurements, to be used in future source apportionment studies.
- An effect on semi volatility was observed from diluted experiments, with a higher gas/particle ratio in diluted experiments as a result of the light molecular mass species to prefer to remain in gas the phase rather than in the particle phase.

Author contributions:

I designed the measuring campaign selecting the different types of food cooked, cooking methods and cooking procedure. I participated in the AMS calibration and instrument deployment. I operated the aerosol instrumentation and cooked the food during the measuring campaign. Dr Michael Le Breton and Dr Thomas Bannan collaborated with the FIGAERO-CIMS measurements. Michael Priestley and Archit Mehra helped with formic and levoglucosan calibrations. I personally performed the data analysis with Dr Thomas Bannan guidance in the FIGAERO-CIMS data analysis. I wrote the manuscript and worked on the comments from co-authors. Dr James Allan supervised me during the design of the campaign, measurements and the preparation of the manuscript.

Blank page

Online chemical characterization of food cooking organic aerosols: implications for source apportionment

*Ernesto Reyes-Villegas[1, *], Thomas Bannan[1], Michael Le Breton[1, ϕ], Archit Mehra[1], Michael Priestley[1], Carl Percival[1, Δ], Hugh Coe[1], James D. Allan[1,2, ∇]*

[1]School of Earth, Atmospheric and Environmental Sciences, The University of Manchester, Manchester, M13 9PL, UK

[2]National Centre for Atmospheric Science, The University of Manchester, Manchester, M13 9PL, UK

[ϕ]Now at University of Gothenburg, 40530 Gothenburg, Sweden

[Δ]Now at Jet Propulsion Laboratory, 4800 Oak Grove Drive, Pasadena, CA 91109, USA

*Corresponding author: ernesto.reyesvillegas@manchester.ac.uk

Abstract. Food cooking organic aerosols (COA) are one of the main primary sources of submicron particulate matter in urban environments. However, there are still many questions surrounding source apportionment related to instrumentation as well as semi-volatile partitioning as COA evolve rapidly in the ambient air, making source apportionment more complex. Online measurements of emissions from cooking different types of food were performed in a laboratory in order to characterize particles and gases. Aerosol mass spectrometer (AMS) measurements showed that the relative ionization efficiency for OA was higher (1.56 - 3.06) relative to a typical value of 1.4, concluding AMS is overestimating COA and suggesting previous studies likely overestimated COA concentrations. Food cooking mass spectra were generated using AMS and gas and particle food markers were identified with FIGAERO-CIMS measurements to be used in future food cooking source apportionment studies. However, there is a considerable variability both on gas and particle markers and dilution plays an important role in the particle mass budget, showing the importance of using these markers with caution when receptor modeling. These findings can be used to better understand the chemical composition of COA and it provides useful information to be used in future source apportionment studies.

Keywords: AMS, FIGAERO-CIMS, Organic aerosols, Source apportionment, mass spectra.

1. Introduction

Atmospheric aerosols have been found to cause severe air quality problems.[1-3] Food cooking emissions are one of the main indoor and outdoor sources of particles around the world.[4] Cooking Organic Aerosols (COA) represent a high contribution to OA, particularly in urban environments. For instance, Huang, et al. [5], in a study performed during the Olympic Games Beijing 2008, identified that COA contribute 24% while Sun, et al. [6], in a study performed during summer 2009 at Queens College in New York, identified COA to contribute 16%. Moreover, COA contribution to OA (24%) was found to be higher than traffic-related hydrocarbon-like OA (HOA, 16%) in a study performed in 2012 in Lanzhou China. [7]

In 2005, the first study to identify COA from aerosol mass spectrometer (AMS) measurements was performed by Lanz, et al. [8] in Zurich, Switzerland identifying a 'minor' COA source. Allan, et al. [9] identified, for the first time in the UK, COA, which were found to contribute 34% to OA concentrations. Further ambient OA studies have investigated the COA seasonal trend in the UK[10, 11] and other parts of the world.[12-15] However, follow up studies in Barcelona, Spain did find specific markers for food activities. [16, 17] China, in particular, has performed several studies, over the last decade, towards online chemical aerosol characterization,[18] recognizing cooking emissions to be one of the main primary sources of OA, with studies in urban environments such as Lanzhou,[19, 20] Beijing[21] and Baoji.[22]

While COA have been investigated in different ambient studies, their complexity still makes it challenging to fully characterize their chemical properties. Dall'Osto, et al. [23] performed an in-depth characterization of COA at a rural site, where it was stressed that the COA factor, deconvolved from AMS measurements, included other emissions than food cooking. Another important aspect that makes challenging to quantify COA is the aging occurring in ambient air, making the mass spectra of COA experience a seasonal variation, hence there being a difference in summer and winter.[24]

The use of other techniques to study aerosols allows a better understanding of food cooking aerosols.[4, 18] Receptor modeling is a technique that has been successfully used to perform aerosol source apportionment.[25-27] Multilinear engine (ME-2) is a source apportionment tool that uses information from previous studies (i.e. mass spectra) as inputs to partially constrain solutions when identifying sources.[28] Chemical mass balance (CMB) uses source profiles or fingerprints to identify and quantify source contributions.[29] However, this technique has ambiguities of its own; there are uncertainties related to the representativeness of the profiles used and uncertainties surrounding the effect phenomena such as semi-volatile repartitioning and chemical aging have on the mass budget and markers. This situation increases the complexity to perform COA source apportionment as they evolve rapidly in the ambient air.[23]

Over more than 15 years, the Aerodyne aerosol mass spectrometers have proven to be a powerful tool to quantify and characterize the composition of non-refractory submicron aerosol concentrations.[30, 31] However, certain studies have identified an overestimation of OA concentrations measured with AMS when compared to collocated measurements. Yin, et al. [32] found food cooking aerosols, identified with positive matrix factorization (PMF), to overestimate CMB results by a factor of two, in spite of a good correlation. Minguillón, et al. [33] determined organic aerosols-to-organic carbon ratios to be higher than unity, stating this is explained by an underestimation of the relative ion efficiency of OA (RIE_{OA}), a parameter the instrument uses to calculate OA concentrations. Murphy [34] presented a model approach to estimate RIE based on molecular mass. While Jimenez, et al. [35] disagreed that the effect was as strong as suggested, however, both agree that RIE values have the potential to be higher than the typical RIE_{OA}=1.4.[36]

There has been a wide range of controlled experiments to investigate different aspects of food cooking aerosols. [37-39] However, until now there has been no laboratory study analyzing both particle and gas phase emissions using online measurements. Here, we present combined on-line measurements of the high-resolution time-of-flight aerosol mass spectrometer (HR-ToF-AMS) and the filter inlet for gases and aerosols (FIGAERO) attached to the high-resolution time-of-flight chemical ionization mass spectrometer (HR-ToF-CIMS). The HR-ToF-AMS quantifies high time resolution concentrations of OA. However, there is no molecular information due to the ion fragmentation produced by the strong electron ionization. Hence, the characterization of particles collected with FIGAERO and together with the soft chemical ionization from HR-ToF-CIMS provides additional information such as molecular weight and chemical formula of species within both the gas and particle phases, which will help in bridging the gap between PMF-AMS and CMB analyses and also to assist in interpreting ambient FIGAERO-CIMS data.

This study aims to provide a better understanding of food cooking aerosol chemical characterization, focusing on three main scientific objectives: 1. To investigate potential AMS quantification issues regarding COA; 2. To provide profiles in both the AMS and CIMS to assist in the interpretation of field data; 3. To establish whether emissions from cooking are semi-volatile, and to what extent this may impact upon source apportionment techniques.

2. Methodology

2.1 Measurements. Online measurements of gases and particles, emitted from cooking different types of food, were carried out in a laboratory. A variety of food (fish and chips, English breakfast, vegetables and different types of meat) was cooked using rapeseed (canola) oil. Two types of electric cooking equipment were used; a deep fryer, using three liters of cooking oil; and an induction hob to shallow fry in a pan with a diameter of 22 cm. When shallow frying meat on a flat frying pan, two cooking styles were used; stir-fried, which involves chopping meat into small pieces and stirring meat while cooking; and chop frying. The different cooking methods were used to determine whether they would have an effect on the aerosol chemical composition. The cooking time of each food was between 4-8 minutes depending on the time needed for the food to be completely cooked. A total of 36 experiments were performed. Emissions were directed to a movable extraction cowling where the common sample inlet was located (Figure S1). The sample inlet was optionally attached to a diluter (Dekati, DI-100), using compressed air to obtain a dilution factor of approximately 1:10. Diluted/non-diluted experiments were performed to investigate gas semi-volatile behavior and its effect on the aerosol budget.

2.2 HR-ToF-AMS and SMPS measurements. Submicron non-refractory aerosol concentrations (OA, SO_4^{2-}, NH_4^+, NO_3^-, and Cl^-) were measured with a HR-ToF-AMS [31], hereafter AMS. The procedure to quantify AMS mass concentrations has been previously described [40, 41]. The two main parameters AMS uses to quantify aerosol concentrations are collection efficiency (CE) and relative ionization efficiency (RIE). The CE measures how well particles are transmitted and detected, depending on three terms: the transmission efficiency of the aerodynamic lenses, the transmission loss due to nonsphericity of particles and bouncing of particles when impacting the vaporizer [42, 43]. Aerosols that tend to be liquid and with diameters between 60 and 600 nanometers (nm) present high CE [44, 45], thus in this study, a CE = 1.0 was used. RIE is the ratio of IE of a given analyte (defined as ions detected per available vapor molecule) relative to the IE of nitrate obtained from ammonium nitrate calibrations. The default value of RIE for OA (RIE_{OA}=1.4) used. [35, 36] However, after comparing the AMS aerosol concentrations with Scanning Mobility Particle Sizer (SMPS) measurements, it was found AMS to overestimate aerosol concentrations. This overestimation is attributed to RIE_{OA} to be higher than 1.4. Further details are provided in the Supplement S1. Elemental analysis was performed as described by Aiken, et al. [46] with the “improved ambient” method proposed by Canagaratna, et al. [47].

Particle number concentration and size distribution, with mobility diameter ranging from 18 to 514 nm, were measured using an SMPS (model 3936, TSI). In order to compare SMPS with AMS measurements, a density of 0.85 $g \cdot cm^{-3}$, average density of rapeseed oil and oleic acid [48], was used to convert SMPS volume concentration to mass concentration.

2.3 FIGAERO-HR-ToF-CIMS measurements. The HR-ToF-CIMS, hereafter CIMS, with iodide (I^-) as reagent ion [49], was used to measure oxidized organic compounds in the gas phase. [50] FIGAERO, coupled to the CIMS measured particle composition. CIMS measured gases over the time food was being cooked while particles were collected on a filter in the FIGAERO inlet. The gas phase measurements were followed by desorption of the collected particles into the CIMS, using a programmed desorption step, where 2 slpm flow of N_2 was ramped from ambient temperature up to 200° C over 15 minutes and passed through the filter into the inlet to be detected by the CIMS. Both gases and particles were collected using a flow of 2 slpm. Aerosols emitted when cooking English breakfast (composed of tomato, mushroom, eggs, bacon, black pudding and sausages) were collected on one filter, other experiments were also collected in one filter when cooking the same type of food, for example, stir-fried chicken and chop fried chicken. Table 1 shows the desorbed filters using this procedure. Details about FIGAERO-CIMS calibration is provided in Supplement S2.

3 Results

3.1 Aerosol concentrations overview. A wide range of aerosol concentrations was measured with AMS and SMPS. Table 1 shows the information for the performed experiments; non-diluted and diluted, using deep fried and shallow fried as cooking methods. Looking at SMPS concentrations of non-diluted experiments, higher aerosol concentrations were present on shallow fried compared to deep frying. For shallow fried experiments, aerosol average concentrations range from 9.6 $\mu g \cdot m^{-3}$ for black pudding to 395 $\mu g \cdot m^{-3}$ for sausages, while deep frying concentrations ranged between 4.3 – 223.5 $\mu g \cdot m^{-3}$. Other high concentrations include tomato (226.5 $\mu g \cdot m^{-3}$) and bacon (247.6 $\mu g \cdot m^{-3}$). The fact that tomato shows high concentrations may be explained by the fact that tomato was chopped in half and there was more surface area in contact with the oil/pan. Moreover, the chopped tomato would have a high moisture content, causing more sizzling and therefore mechanical ejection.

3.2 AMS oxidation state. Elemental analysis (oxygen and hydrogen to carbon ratios, O:C and H:C) is an approach to explore the oxidation state of OA. In this study O:C and H:C mean and standard deviation ellipse (SDE) were calculated for the experiments matching with the filters collected with FIGAERO (F0-F17), to study the OA oxidation state which may have implications on source apportionment. The standard deviation ellipse (SDE) used in the graphs to denote spread was calculated following the equations detailed in Gong [51]. Figure 1 shows the Van Krevelen diagram with O:C and H:C ratios. When analyzing the SDE in Figure 1.b, shallow frying (continuous lines) shows the greater variability both in O:C and H:C ratios compared to deep frying and (dotted lines). The variation in ratios when shallow frying is expected as this type of cooking involves flipping over the meat and/or stirring food while deep frying cooks food with continuous heating of three litters of oil and relatively little disturbance of the food itself. These findings suggest the effect cooking styles may have on aerosol composition.

Diluted experiments showed higher mean O:C ratios compared to non-diluted experiments (Fig. 1.d): English breakfast, deep fried sausages and Deep fried burgers with 0.28 (F11), 0.28 (F9) and 0.25 (F3) for diluted compared to 0.23 (F10), 0.17 (F8) and 0.19 (F8) for not diluted, respectively. This increment on O:C may result from the evaporation of more volatile molecules, leaving a relatively larger fraction of less volatile molecules with a possible higher O:C in the particle phase.

Circles and dotted lines represent deep frying samples in 1.a and 1.b and non-diluted samples in 1.c and 1.d. Triangles and continuous lines represent shallow frying samples in 1.a and 1.b and diluted samples in 1.c and 1.d. OS represents the oxidation state which increases with oxidative aging.[52] Blue and red dotted lines in 1.a represent f44 and f43 as used on the triangle plot proposed by Ng, et al. [53]. Figures 1.b and 1.d are a zoomed version of figures 1.a and 1.c respectively. Description of filters (f0-f17) is provided in Table 1.

Mean O:C (0.15-0.32) and H:C (1.69-1.86) values observed in this study are compared to the ones seen in the literature. Kaltsonoudis, et al. [24] in a laboratory study from charbroiling meat, exposing emissions to UV illumination and oxidants, found O:C values of 0.09-0.3, with O:C ratios increasing with chemical aging. Ambient O:C ratios from COA have been found with values of (0.10- 0.22). [7, 47, 54, 55] These values are similar to other POA such as HOA with values of 0.14-0.38 [47, 54, 56, 57], though HOA presents a higher H:C ratio. While high O:C ratios have been seen on secondary OA (SOA) 0.52-1.02. [47, 54, 56] This increment in O:C ratios from POA to SOA is due to the chemical aging aerosols present in the atmosphere.

While O:C and H:C ratios of this study are similar compared to the ratios from food cooking aerosols found in the literature, O:C and H:C ratios from food cooking aerosols are different from the ones of other primary OA such as HOA, which has a higher H:C or secondary OA with a higher O:C (Refer to Table S4 for more O:C ratios from literature). Diluted experiments presented an increment on O:C, showing what would be expected to happen when aerosols are emitted to the atmosphere with further dilution and aging, as we qualitatively expect the more polar compounds to have a lower vapor pressure.[58] Laboratory studies aiming to determine food cooking markers should consider performing diluted experiments to better represent ambient conditions.

3.3 FIGAERO - AMS comparison. The soft chemical ionization of the CIMS provides molecular information of chemical species and, with the use of the FIGAERO inlet, it is possible to identify food cooking markers both in particle and gas phase. In this study, 128 compounds were identified in the gas phase, from which 69 were also identified in the particle phase (Table S3). The sum of the average concentration of the 69 compounds in particle phase, identified in each desorbed filter, was compared to the average OA measurements from AMS. This comparison was performed as a way to validate particle measurements obtained from the FIGAERO. Table 1 indicates the filters taken with

FIGAERO to which AMS averages were calculated. Due to a technical issue, no filter data is available for the first six filters (F0 to F5), thus the following FIGAERO-CIMS analysis will be performed from filters F6 to F17. Additionally, a comparison was performed using levoglucosan, which is a compound identified both with FIGAERO-CIMS and AMS instruments. In the AMS it is typically identified at m/z 60 [59] while in the FIGAERO-CIMS it is identified with molecular mass 288.96 $g.mol^{-1}$ (molecular mass of $C_6H_{10}O_5$ + I). Figure 2 shows non-diluted deep fried sausages (F9) and English breakfast (F10) are the experiments with the highest aerosol concentrations. Both levoglucosan (Figure 2.a) and total aerosol concentrations (Figure2.b) present similar trend. A strong correlation is observed with $r = 0.88$ for the levoglucosan comparison and $r = 0.83$ for the total particles comparison. FIGAERO measured 22 times higher levoglucosan concentrations, which is expected as AMS concentrations are the m/z 60 related, a fragment related to levoglucosan. While in the total aerosol comparison, FIGAERO quantified 80% of OA measured by the AMS, results consistent with previous studies, which have identified FIGAERO to quantify 25-50% of OA concentrations. [60-62]

3.4 FIGAERO-CIMS food cooking markers

Deep frying emitted more gases than shallow frying (Table 2), which is expected due to the larger amount of oil used during deep frying. Eight organic acids were identified as cooking markers in the gas phase: isocyanic (HNCO), formic (CH_2O_2), acrylic ($C_3H_4O_2$), propionic ($C_3H_6O_2$), hydroxypropionic ($C_3H_6O_3$), malonic ($C_3H_4O_4$), hexanoic ($C_6H_{12}O_2$) and adipic ($C_6H_{10}O_4$). These organic acids were chosen as markers as they were present in all cooking samples with high concentrations. Hydroxypropionic acid was the compound with a higher presence in gas phase both on deep frying and shallow frying. In general, HNCO concentrations were identified in the majority of the samples. HNCO has been related to biomass burning [63] and traffic emissions.[64] However, to our knowledge, no studies in the literature have reported HNCO concentrations emitted from food cooking. Roberts, et al. [65] reported HNCO concentrations to be related to coal used as a fuel to cook but not to the food itself.

Nitrogen-containing compounds have been previously found to have negative effects to human health [66] and have been identified on cooking emissions. [4] They may be emitted either from the food itself or also from additives. In this study, 14 different nitrogen-containing compounds were identified both in the gas and particle phase (Table S5). $C_4H_2NO_2$ and parabanic acid ($C_3H_2N_2O_3$), during deep-frying experiments, were identified only in the gas phase. The rest of the nitrogen-containing compounds were identified mainly in the particle phase: Creatinine ($C_4H_7N_3O$), nitrobenzene ($C_6H_5NO_2$), $C_6H_7NO_2$, $C_5H_7N_2O_2$, $C_5H_8NO_3$, $C_6H_{13}NO_2$, $C_5H_9N_3O_2$ and $C_{13}H_{15}NO_2$ were present only in shallow frying experiments. Nicotinamide ($C_6H_6N_2O$), nitrobenzene, $C_6H_7NO_2$ and $C_5H_8NO_3$ were mainly emitted from non-diluted deep fried sausages (filter9), diluted shallow fried pork (filter15) and diluted shallow fried lamb (filter16). While it was not possible to determine or speculate at the structure of many of the identified nitrogen-containing compounds, given the potential impacts of this compound class, it is worth reporting their presence and contribution to food cooking emissions, which were mainly found in the particle phase. Further studies should be aimed to further characterize and quantify these nitrogen-containing compounds.

4 Discussion

4.1 Relative Ion Efficiency of OA. The AMS has been widely used to measure the chemical composition of non-refractory aerosols. However, it has been found to report food cooking OA concentrations to be greater than other measurement techniques.[32] Table S1 shows OA has higher concentrations compared to SMPS, resulting in OA/SMPS ratios to be higher than unity. OA concentrations were originally calculated with RIE_{OA}= 1.4. as suggested by Alfarra, et al. [36]. However, it has been previously shown that RIE_{OA} values may vary within functional groups.[40] An increment on RIE_{OA} will decrease the reported OA concentration. Hence, the hypothesis here is that the overestimation of OA measurements compared to SMPS is due to RIE_{OA} to be higher than 1.4.

This shows that RIE_{OA_corr} values are higher than 1.4, with values between 1.56 and 3.06 (Table S2). The highest RIE_{OA_corr} value of 3.06 was observed with diluted deep fried experiments. This value is in agreement with Murphy [34] and Jimenez, et al. [35], who reported oleic acid to have an RIE of 2.8-4.0 and 3.2 respectively. After heating, oleic acid is the main component of rapeseed oil 63% - 70% [67, 68], and this hypothesis is further supported by the fact that high RIE_{OA_corr} values were present with deep fried experiments, where much of the particulate matter likely originates from the recondensation of semivolatiles from the oil or the mechanical ejection of oil by bubbles bursting during frying. The low RIE_{OA_corr} values for shallow fried indicate that the OA emissions from meat and vegetables have RIEs closer to the default of 1.4.

The increment on RIE_{OA}, combined with the assumed CE of 1, found in this study explains the good correlation but quantitative disagreement between PMF-AMS and CMB reported by Yin, et al. [32] and also agrees with Minguillón, et al. [33] who also found RIE_{OA} to be higher than 1.4. It is worth mentioning a possible limitation of SMPS mass concentrations obtained is that a density of 0.85 $g \cdot cm^{-3}$ is assumed, which may not be accurate. However, the deviations in RIE reported are deemed to be larger than the plausible uncertainty in density. The RIE result has significant implications for ambient measurements of COA. While COA concentrations have often been reported to be a significant contribution to primary OA aerosol concentrations, these could have been overestimated in previous studies. However, it is unlikely that the bulk OA concentrations have been systematically misreported overall, as these have frequently compared favorably with external comparisons.[35] If the COA specifically is being over-reported, then this should be accordingly corrected after it has been isolated using factorization.

4.2 Food cooking AMS mass spectra. Source apportionment tools, like the multilinear engine (ME-2), use inputs in the way of mass spectra or time series, to partially constrain solutions and better deconvolve OA sources.[28] Mass spectra of COA have certain characteristics that make them different to mass spectra from other sources, for example the signals at m/z 41, m/z 55 and m/z 57, with a higher signal at m/z 55 compared to m/z 57. [9, 12, 23] The generation of mass spectra, from different types of food cooking and a better understanding of their variations, will help to improve COA source apportionment. In this study, a comparison was performed within the mass spectra obtained from the experiments and with the mass spectra from other ambient and laboratory studies. Table S6 shows the uncentered Pearson's correlation coefficients ($_{u}r$, also known as the 'normalized dot product' or 'cosine angle') and Table S7 shows the list of external mass spectra used in the comparison.

The correlations performed within the experiments showed high $_{u}r$ values ranging from 0.876 when comparing two different cooking and meat types (diluted shallow fried chicken vs non-diluted deep fried burgers) to 0.999 when comparing deep fried burgers diluted vs non-diluted. Fish and chips and English breakfast also showed high $_{u}r$ values when comparing diluted and non-diluted experiments, suggesting diluting presents little effect on mass spectra.

A decrease on correlations were observed when comparing the mass spectra of this study with COA mass spectra from previous ambient studies, with $_{u}r$ values from 0.734 (non-diluted deep fried fish and chips vs COA from Lanz, et al. [8]) to 0.991 (diluted deep fried sausages vs COA from Reyes-Villegas, et al. [69]). The low correlations obtained when comparing mass spectra of this study with COA from Lanz, et al. [8] might be expected as the later was the first PMF-AMS study, focused more on the development of the methodology and was contained within a higher-order solution, where the authors expressed doubts as to its accuracy.

From these correlations, we can see that when cooking different types of meat/vegetables and using a variety of cooking styles (deep frying and shallow frying), mass spectra from fresh emissions do not vary significantly. However, the decrease in $_{u}r$ values when compared with mass spectra from past ambient studies from the literature, suggests aging of food cooking aerosols (through repartitioning or chemical reactions) in the atmosphere that are not capture here.

4.3 Effect of dilution on food cooking aerosols. From the desorption analysis, 69 compounds were identified in the particle phase (Table S3). From this list, Table 4 shows the 12 compounds that have been previously identified as cooking markers [4, 26, 70, 71] Levoglucosan ($C_6H_{10}O_5$), dicarboxylic acids: succinic ($C_4H_6O_4$), glutaric ($C_5H_8O_4$), pimelic ($C_7H_{12}O_4$), suberic ($C_8H_{14}O_4$), azelaic ($C_9H_{16}O_4$), sebacic ($C_{10}H_{18}O_4$), dodecanedioic ($C_{12}H_{22}O_4$), and carboxylic acids: palmitic ($C_{16}H_{32}O_2$), margaric ($C_{17}H_{34}O_2$), linoleic ($C_{18}H_{32}O_2$) and oleic ($C_{18}H_{34}O_2$). However, the majority of these markers have been identified from off-line measurements or from gas and particle measurements in separate studies. Here we show near real-time measurements of both gases and particles, gas-to-particle ratios (G/P) and the effect of dilution.

These 12 compounds are considered to be cooking markers in the particle phase as they were found mainly during the filter desorption. Even when they were identified as being present in the gas phase, the G/P ratio is still lower than unity. In contrast, for the gas phase cooking markers presented in Table 2, the G/P ratio was greater than unity. G/P ratios were calculated from average gas and particle counts·sec^{-1} (Table 3). It is worth mentioning that some of these compounds are also found to be in other sources; for example, levoglucosan has been used as a marker of biomass burning aerosols.[70] Succinic, glutaric, pimelic acids and levoglucosan were found mainly in the gas phase for the diluted deep frying experiments (F7 and F8). Denoting the high variability of gas-particle partitioning and the implication of different cooking conditions in the food cooking emissions.

Higher G/P ratios were observed with diluted experiments compared to non-diluted. Deep fried sausages (F9) present higher G/P ratios with Succinic, glutaric, pimelic, levoglucosan, suberic and azealic compared with diluted deep fried sausages (F8). A similar situation was present with diluted and non-diluted deep fried burgers (F7 and F6 respectively) and English breakfast (F11 and F10 respectively). This behavior is explained in that with diluting experiments, light molecular masses will tend to be more in the gas phase than species with high molecular mass, which will tend to stay in the particle phase. This suggests that the use of these as cooking markers for CMB analysis may be problematic, as their particle-phase concentrations may diminish with dilution, although whether this creates a positive or negative artifact will depend on whether their rate of evaporation is consistent with that of the overall mass of particulate used in the mass balance model.

ASSOCIATED CONTENT

Supporting Information

The supplement material includes a figure showing the instrument arrangement (Figure S1), a list of all cooking experiments (Table S1), a table with AMS and SMPS average concentrations (Table S2), a figure with mass and number size distributions (Figure S2), a list of all the compounds identified on gas and particle (Table S3), a table with O:C and H:C ratios from the literature (Table S4), a table with nitrogen-containing markers (Table S5), a table with uncentered Pearson values for mass spectra comparison (Table S6) and a list with the references of the external cooking mass spectra used on the comparison (Table S7).

AUTHOR INFORMATION

Corresponding author.

* e-mail: ernesto.reyesvillegas@manchester.ac.uk

∇ e-mail: james.allan@manchester.ac.uk

Notes

The authors declare no competing financial interest.

ACKNOWLEDGMENTS

Ernesto Reyes-Villegas is supported by a studentship by the National Council of Science and Technology-Mexico (CONACYT) under registry number 217687.

REFERENCES

(1) Pope III, C. A.; Dockery, D. W., Health effects of fine particulate air pollution: lines that connect. *J Air Waste Manage* **2006,** *56*, (6), 709-742.

(2) Fuzzi, S.; Baltensperger, U.; Carslaw, K.; Decesari, S.; Denier van der Gon, H.; Facchini, M. C.; Fowler, D.; Koren, I.; Langford, B.; Lohmann, U.; Nemitz, E.; Pandis, S.; Riipinen, I.; Rudich, Y.; Schaap, M.; Slowik, J. G.; Spracklen, D. V.; Vignati, E.; Wild, M.; Williams, M.; Gilardoni, S., Particulate matter, air quality and climate: lessons learned and future needs. *Atmos. Chem. Phys.* **2015,** *15*, (14), 8217-8299.

(3) Samoli, E.; Atkinson, R. W.; Analitis, A.; Fuller, G. W.; Beddows, D.; Green, D. C.; Mudway, I. S.; Harrison, R. M.; Anderson, H. R.; Kelly, F. J., Differential health effects of short-term exposure to source-specific particles in London, U.K. *Environ Int* **2016,** *97*, (Supplement C), 246-253.

(4) Abdullahi, K. L.; Delgado-Saborit, J. M.; Harrison, R. M., Emissions and indoor concentrations of particulate matter and its specific chemical components from cooking: A review. *Atmos Environ* **2013,** *71*, 260-294.

(5) Huang, X. F.; He, L. Y.; Hu, M.; Canagaratna, M. R.; Sun, Y.; Zhang, Q.; Zhu, T.; Xue, L.; Zeng, L. W.; Liu, X. G.; Zhang, Y. H.; Jayne, J. T.; Ng, N. L.; Worsnop, D. R., Highly time-resolved chemical characterization of atmospheric submicron particles during 2008 Beijing Olympic Games using an Aerodyne High-Resolution Aerosol Mass Spectrometer. *Atmos Chem Phys* **2010,** *10*, (18), 8933-8945.

(6) Sun, Y. L.; Zhang, Q.; Schwab, J. J.; Demerjian, K. L.; Chen, W. N.; Bae, M. S.; Hung, H. M.; Hogrefe, O.; Frank, B.; Rattigan, O. V.; Lin, Y. C., Characterization of the sources and processes of organic and inorganic aerosols in New York city with a high-resolution time-of-flight aerosol mass apectrometer. *Atmos Chem Phys* **2011,** *11*, (4), 1581-1602.

(7) Xu, J.; Zhang, Q.; Chen, M.; Ge, X.; Ren, J.; Qin, D., Chemical composition, sources, and processes of urban aerosols during summertime in northwest China: insights from high-resolution aerosol mass spectrometry. *Atmos. Chem. Phys.* **2014,** *14*, (23), 12593-12611.

(8) Lanz, V. A.; Alfarra, M. R.; Baltensperger, U.; Buchmann, B.; Hueglin, C.; Prevot, A. S. H., Source apportionment of submicron organic aerosols at an urban site by factor analytical modelling of aerosol mass spectra. *Atmos Chem Phys* **2007,** *7*, (6), 1503-1522.

(9) Allan, J. D.; Williams, P. I.; Morgan, W. T.; Martin, C. L.; Flynn, M. J.; Lee, J.; Nemitz, E.; Phillips, G. J.; Gallagher, M. W.; Coe, H., Contributions from transport, solid fuel burning and cooking to primary organic aerosols in two UK cities. *Atmos Chem Phys* **2010,** *10*, (2), 647-668.

(10) Young, D. E.; Allan, J. D.; Williams, P. I.; Green, D. C.; Flynn, M. J.; Harrison, R. M.; Yin, J.; Gallagher, M. W.; Coe, H., Investigating the annual behaviour of submicron secondary inorganic and organic aerosols in London. *Atmos. Chem. Phys.* **2015,** *15*, (11), 6351-6366.

(11) Reyes-Villegas, E.; Green, D. C.; Priestman, M.; Canonaco, F.; Coe, H.; Prévôt, A. S. H.; Allan, J. D., Organic aerosol source apportionment in London 2013 with ME-2: exploring the solution space with annual and seasonal analysis. *Atmos. Chem. Phys.* **2016,** *16*, (24), 15545-15559.

(12) Mohr, C.; DeCarlo, P. F.; Heringa, M. F.; Chirico, R.; Slowik, J. G.; Richter, R.; Reche, C.; Alastuey, A.; Querol, X.; Seco, R.; Penuelas, J.; Jimenez, J. L.; Crippa, M.; Zimmermann, R.; Baltensperger, U.; Prevot, A. S. H., Identification and quantification of organic aerosol from cooking and other sources in Barcelona using aerosol mass spectrometer data. *Atmos Chem Phys* **2012,** *12*, (4), 1649-1665.

(13) Crippa, M.; Canonaco, F.; Lanz, V. A.; Aijala, M.; Allan, J. D.; Carbone, S.; Capes, G.; Ceburnis, D.; Dall'Osto, M.; Day, D. A.; DeCarlo, P. F.; Ehn, M.; Eriksson, A.; Freney, E.; Ruiz, L. H.; Hillamo, R.; Jimenez, J. L.; Junninen, H.; Kiendler-Scharr, A.; Kortelainen, A. M.; Kulmala, M.; Laaksonen, A.; Mensah, A.; Mohr, C.; Nemitz, E.; O'Dowd, C.; Ovadnevaite, J.; Pandis, S. N.; Petaja, T.; Poulain, L.; Saarikoski, S.; Sellegri, K.; Swietlicki, E.; Tiitta, P.; Worsnop, D. R.; Baltensperger, U.; Prevot, A. S. H., Organic aerosol components derived from 25 AMS data sets across Europe using a consistent ME-2 based source apportionment approach. *Atmos Chem Phys* **2014,** *14*, (12), 6159-6176.

(14) Frohlich, R.; Crenn, V.; Setyan, A.; Belis, C. A.; Canonaco, F.; Favez, O.; Riffault, V.; Slowik, J. G.; Aas, W.; Aijala, M.; Alastuey, A.; Artinano, B.; Bonnaire, N.; Bozzetti, C.; Bressi, M.; Carbone, C.; Coz, E.; Croteau, P. L.; Cubison, M. J.; Esser-Gietl, J. K.; Green, D. C.; Gros, V.; Heikkinen, L.; Herrmann, H.; Jayne, J. T.; Lunder, C. R.; Minguillon, M. C.; Mocnik, G.; O'Dowd, C. D.; Ovadnevaite, J.; Petralia, E.; Poulain, L.; Priestman, M.; Ripoll, A.; Sarda-Esteve, R.; Wiedensohler, A.; Baltensperger, U.; Sciare, J.; Prevot, A. S. H., ACTRIS ACSM intercomparison - Part 2: Intercomparison of ME-2 organic source apportionment results from 15 individual, co-located aerosol mass spectrometers. *Atmos Meas Tech* **2015,** *8*, (6), 2555-2576.

(15) Bozzetti, C.; El Haddad, I.; Salameh, D.; Daellenbach, K. R.; Fermo, P.; Gonzalez, R.; Minguillon, M. C.; Iinuma, Y.; Poulain, L.; Elser, M.; Muller, E.; Slowik, J. G.; Jaffrezo, J. L.; Baltensperger, U.; Marchand, N.; Prevot, A. S. H., Organic aerosol source apportionment by offline-AMS over a full year in Marseille. *Atmos Chem Phys* **2017,** *17*, (13), 8247-8268.

(16) Alier, M.; van Drooge, B. L.; Dall'Osto, M.; Querol, X.; Grimalt, J. O.; Tauler, R., Source apportionment of submicron organic aerosol at an urban background and a road site in Barcelona (Spain) during SAPUSS. *Atmos. Chem. Phys.* **2013,** *13*, (20), 10353-10371.

(17) Dall'Osto, M.; Beddows, D. C. S.; McGillicuddy, E. J.; Esser-Gietl, J. K.; Harrison, R. M.; Wenger, J. C., On the simultaneous deployment of two single-particle mass spectrometers at an urban background and a roadside site during SAPUSS. *Atmos. Chem. Phys.* **2016,** *16*, (15), 9693-9710.

(18) Li, Y. J.; Sun, Y.; Zhang, Q.; Li, X.; Li, M.; Zhou, Z.; Chan, C. K., Real-time chemical characterization of atmospheric particulate matter in China: A review. *Atmos Environ* **2017,** *158*, 270-304.

(19) Zhang, X.; Zhang, Y.; Sun, J.; Yu, Y.; Canonaco, F.; Prévôt, A. S. H.; Li, G., Chemical characterization of submicron aerosol particles during wintertime in a northwest city of China using an Aerodyne aerosol mass spectrometry. *Environmental Pollution* **2017,** *222*, (Supplement C), 567-582.

(20) Xu, J. Z.; Shi, J. S.; Zhang, Q.; Ge, X. L.; Canonaco, F.; Prevot, A. S. H.; Vonwiller, M.; Szidat, S.; Ge, J. M.; Ma, J. M.; An, Y. Q.; Kang, S. C.; Qin, D. H., Wintertime organic and inorganic aerosols in Lanzhou, China: sources, processes, and comparison with the results during summer. *Atmos Chem Phys* **2016,** *16*, (23), 14937-14957.

(21) Bei, N.; Wu, J.; Elser, M.; Feng, T.; Cao, J.; El-Haddad, I.; Li, X.; Huang, R.; Li, Z.; Long, X.; Xing, L.; Zhao, S.; Tie, X.; Prévôt, A. S. H.; Li, G., Impacts of meteorological uncertainties on the haze formation in Beijing–Tianjin–Hebei (BTH) during wintertime: a case study. *Atmos. Chem. Phys.* **2017,** *17*, (23), 14579-14591.

(22) Wang, Y. C.; Huang, R. J.; Ni, H. Y.; Chen, Y.; Wang, Q. Y.; Li, G. H.; Tie, X. X.; Shen, Z. X.; Huang, Y.; Liu, S. X.; Dong, W. M.; Xue, P.; Fröhlich, R.; Canonaco, F.; Elser, M.; Daellenbach, K. R.; Bozzetti, C.; El Haddad, I.; Prévôt, A. S. H.; Canagaratna, M. R.; Worsnop, D. R.; Cao, J. J., Chemical composition, sources and secondary processes of aerosols in Baoji city of northwest China. *Atmos Environ* **2017,** *158*, 128-137.

(23) Dall'Osto, M.; Paglione, M.; Decesari, S.; Facchini, M. C.; O'Dowd, C.; Plass-Duellmer, C.; Harrison, R. M., On the Origin of AMS "Cooking Organic Aerosol" at a Rural Site. *Environmental Science & Technology* **2015,** *49*, (24), 13964-13972.

(24) Kaltsonoudis, C.; Kostenidou, E.; Louvaris, E.; Psichoudaki, M.; Tsiligiannis, E.; Florou, K.; Liangou, A.; Pandis, S. N., Characterization of fresh and aged organic aerosol emissions from meat charbroiling. *Atmos. Chem. Phys.* **2017,** *17*, (11), 7143-7155.

(25) Zhang, Q.; Jimenez, J. L.; Canagaratna, M. R.; Ulbrich, I. M.; Ng, N. L.; Worsnop, D. R.; Sun, Y., Understanding atmospheric organic aerosols via factor analysis of aerosol mass spectrometry: a review. *Analytical and bioanalytical chemistry* **2011,** *401*, (10), 3045-3067.

(26) Mancilla, Y.; Mendoza, A.; Fraser, M. P.; Herckes, P., Organic composition and source apportionment of fine aerosol at Monterrey, Mexico, based on organic markers. *Atmos. Chem. Phys.* **2016,** *16*, (2), 953-970.

(27) Hopke, P. K., Review of receptor modeling methods for source apportionment. *J Air Waste Manage* **2016,** *66*, (3), 237-259.

(28) Canonaco, F.; Crippa, M.; Slowik, J. G.; Baltensperger, U.; Prevot, A. S. H., SoFi, an IGOR-based interface for the efficient use of the generalized multilinear engine (ME-2) for the source apportionment: ME-2 application to aerosol mass spectrometer data. *Atmos Meas Tech* **2013,** *6*, (12), 3649-3661.

(29) Mugica, V.; Vega, E.; Chow, J.; Reyes, E.; Sánchez, G.; Arriaga, J.; Egami, R.; Watson, J., Speciated non-methane organic compounds emissions from food cooking in Mexico. *Atmos Environ* **2001,** *35*, (10), 1729-1734.

(30) Jayne, J. T.; Leard, D. C.; Zhang, X. F.; Davidovits, P.; Smith, K. A.; Kolb, C. E.; Worsnop, D. R., Development of an aerosol mass spectrometer for size and composition analysis of submicron particles. *Aerosol Science and Technology* **2000,** *33*, (1-2), 49-70.

(31) DeCarlo, P. F.; Kimmel, J. R.; Trimborn, A.; Northway, M. J.; Jayne, J. T.; Aiken, A. C.; Gonin, M.; Fuhrer, K.; Horvath, T.; Docherty, K. S.; Worsnop, D. R.; Jimenez, J. L., Field-deployable, high-resolution, time-of-flight aerosol mass spectrometer. *Anal Chem* **2006,** *78*, (24), 8281-8289.

(32) Yin, J.; Cumberland, S. A.; Harrison, R. M.; Allan, J.; Young, D. E.; Williams, P. I.; Coe, H., Receptor modelling of fine particles in southern England using CMB including comparison with AMS-PMF factors. *Atmos. Chem. Phys.* **2015,** *15*, (4), 2139-2158.

(33) Minguillón, M. C.; Ripoll, A.; Pérez, N.; Prévôt, A. S. H.; Canonaco, F.; Querol, X.; Alastuey, A., Chemical characterization of submicron regional background aerosols in the western Mediterranean using an Aerosol Chemical Speciation Monitor. *Atmos. Chem. Phys.* **2015,** *15*, (11), 6379-6391.

(34) Murphy, D. M., The effects of molecular weight and thermal decomposition on the sensitivity of a thermal desorption aerosol mass spectrometer. *Aerosol Science and Technology* **2016,** *50*, (2), 118-125.

(35) Jimenez, J. L.; Canagaratna, M. R.; Drewnick, F.; Allan, J. D.; Alfarra, M. R.; Middlebrook, A. M.; Slowik, J. G.; Zhang, Q.; Coe, H.; Jayne, J. T.; Worsnop, D. R., Comment on "The effects of molecular

weight and thermal decomposition on the sensitivity of a thermal desorption aerosol mass spectrometer”. *Aerosol Science and Technology* **2016,** *50*, (9), i-xv.
(36) Alfarra, M. R.; Coe, H.; Allan, J. D.; Bower, K. N.; Boudries, H.; Canagaratna, M. R.; Jimenez, J. L.; Jayne, J. T.; Garforth, A. A.; Li, S.-M.; Worsnop, D. R., Characterization of urban and rural organic particulate in the Lower Fraser Valley using two Aerodyne Aerosol Mass Spectrometers. *Atmos Environ* **2004,** *38*, (34), 5745-5758.
(37) Mohr, C.; Huffman, J. A.; Cubison, M. J.; Aiken, A. C.; Docherty, K. S.; Kimmel, J. R.; Ulbrich, I. M.; Hannigan, M.; Jimenez, J. L., Characterization of Primary Organic Aerosol Emissions from Meat Cooking, Trash Burning, and Motor Vehicles with High-Resolution Aerosol Mass Spectrometry and Comparison with Ambient and Chamber Observations. *Environmental Science & Technology* **2009,** *43*, (7), 2443-2449.
(38) Zhao, X. Y.; Hu, Q. H.; Wang, X. M.; Ding, X.; He, Q. F.; Zhang, Z.; Shen, R. Q.; Lu, S. J.; Liu, T. Y.; Fu, X. X.; Chen, L. G., Composition profiles of organic aerosols from Chinese residential cooking: case study in urban Guangzhou, south China. *J Atmos Chem* **2015,** *72*, (1), 1-18.
(39) Amouei Torkmahalleh, M.; Gorjinezhad, S.; Unluevcek, H. S.; Hopke, P. K., Review of factors impacting emission/concentration of cooking generated particulate matter. *Science of The Total Environment* **2017,** *586*, 1046-1056.
(40) Jimenez, J. L.; Jayne, J. T.; Shi, Q.; Kolb, C. E.; Worsnop, D. R.; Yourshaw, I.; Seinfeld, J. H.; Flagan, R. C.; Zhang, X.; Smith, K. A., Ambient aerosol sampling using the aerodyne aerosol mass spectrometer. *Journal of Geophysical Research: Atmospheres (1984–2012)* **2003,** *108*, (D7).
(41) Allan, J. D.; Delia, A. E.; Coe, H.; Bower, K. N.; Alfarra, M. R.; Jimenez, J. L.; Middlebrook, A. M.; Drewnick, F.; Onasch, T. B.; Canagaratna, M. R.; Jayne, J. T.; Worsnop, D. R., A generalised method for the extraction of chemically resolved mass spectra from aerodyne aerosol mass spectrometer data. *J Aerosol Sci* **2004,** *35*, (7), 909-922.
(42) Huffman, J. A.; Jayne, J. T.; Drewnick, F.; Aiken, A. C.; Onasch, T.; Worsnop, D. R.; Jimenez, J. L., Design, Modeling, Optimization, and Experimental Tests of a Particle Beam Width Probe for the Aerodyne Aerosol Mass Spectrometer. *Aerosol Science and Technology* **2005,** *39*, (12), 1143-1163.
(43) Middlebrook, A. M.; Bahreini, R.; Jimenez, J. L.; Canagaratna, M. R., Evaluation of Composition-Dependent Collection Efficiencies for the Aerodyne Aerosol Mass Spectrometer using Field Data. *Aerosol Science and Technology* **2012,** *46*, (3), 258-271.
(44) Matthew, B. M.; Middlebrook, A. M.; Onasch, T. B., Collection Efficiencies in an Aerodyne Aerosol Mass Spectrometer as a Function of Particle Phase for Laboratory Generated Aerosols. *Aerosol Science and Technology* **2008,** *42*, (11), 884-898.
(45) Hennigan, C. J.; Miracolo, M. A.; Engelhart, G. J.; May, A. A.; Presto, A. A.; Lee, T.; Sullivan, A. P.; McMeeking, G. R.; Coe, H.; Wold, C. E.; Hao, W. M.; Gilman, J. B.; Kuster, W. C.; de Gouw, J.; Schichtel, B. A.; Collett Jr, J. L.; Kreidenweis, S. M.; Robinson, A. L., Chemical and physical transformations of organic aerosol from the photo-oxidation of open biomass burning emissions in an environmental chamber. *Atmos. Chem. Phys.* **2011,** *11*, (15), 7669-7686.
(46) Aiken, A. C.; DeCarlo, P. F.; Jimenez, J. L., Elemental analysis of organic species with electron ionization high-resolution mass spectrometry. *Anal Chem* **2007,** *79*, (21), 8350-8358.
(47) Canagaratna, M. R.; Jimenez, J. L.; Kroll, J. H.; Chen, Q.; Kessler, S. H.; Massoli, P.; Hildebrandt Ruiz, L.; Fortner, E.; Williams, L. R.; Wilson, K. R.; Surratt, J. D.; Donahue, N. M.; Jayne, J. T.; Worsnop, D. R., Elemental ratio measurements of organic compounds using aerosol mass spectrometry: characterization, improved calibration, and implications. *Atmos Chem Phys* **2015,** *15*, (1), 253-272.
(48) Noureddini, H.; Teoh, B. C.; Davis Clements, L., Densities of vegetable oils and fatty acids. *Journal of the American Oil Chemists Society* **1992,** *69*, (12), 1184-1188.
(49) Lee, B. H.; Lopez-Hilfiker, F. D.; Mohr, C.; Kurtén, T.; Worsnop, D. R.; Thornton, J. A., An Iodide-Adduct High-Resolution Time-of-Flight Chemical-Ionization Mass Spectrometer: Application to Atmospheric Inorganic and Organic Compounds. *Environmental Science & Technology* **2014,** *48*, (11), 6309-6317.

(50) Lopez-Hilfiker, F. D.; Mohr, C.; Ehn, M.; Rubach, F.; Kleist, E.; Wildt, J.; Mentel, T. F.; Lutz, A.; Hallquist, M.; Worsnop, D.; Thornton, J. A., A novel method for online analysis of gas and particle composition: description and evaluation of a Filter Inlet for Gases and AEROsols (FIGAERO). *Atmos. Meas. Tech.* **2014,** *7*, (4), 983-1001.
(51) Gong, J. X., Clarifying the standard deviational ellipse. *Geogr. Anal.* **2002,** *34*, (2), 155-167.
(52) Kroll, J. H.; Donahue, N. M.; Jimenez, J. L.; Kessler, S. H.; Canagaratna, M. R.; Wilson, K. R.; Altieri, K. E.; Mazzoleni, L. R.; Wozniak, A. S.; Bluhm, H.; Mysak, E. R.; Smith, J. D.; Kolb, C. E.; Worsnop, D. R., Carbon oxidation state as a metric for describing the chemistry of atmospheric organic aerosol. *Nature Chemistry* **2011,** *3*, (2), 133-139.
(53) Ng, N.; Canagaratna, M.; Jimenez, J.; Chhabra, P.; Seinfeld, J.; Worsnop, D., Changes in organic aerosol composition with aging inferred from aerosol mass spectra. *Atmos Chem Phys* **2011,** *11*, (13), 6465-6474.
(54) Hayes, P. L.; Ortega, A. M.; Cubison, M. J.; Froyd, K. D.; Zhao, Y.; Cliff, S. S.; Hu, W. W.; Toohey, D. W.; Flynn, J. H.; Lefer, B. L.; Grossberg, N.; Alvarez, S.; Rappenglück, B.; Taylor, J. W.; Allan, J. D.; Holloway, J. S.; Gilman, J. B.; Kuster, W. C.; de Gouw, J. A.; Massoli, P.; Zhang, X.; Liu, J.; Weber, R. J.; Corrigan, A. L.; Russell, L. M.; Isaacman, G.; Worton, D. R.; Kreisberg, N. M.; Goldstein, A. H.; Thalman, R.; Waxman, E. M.; Volkamer, R.; Lin, Y. H.; Surratt, J. D.; Kleindienst, T. E.; Offenberg, J. H.; Dusanter, S.; Griffith, S.; Stevens, P. S.; Brioude, J.; Angevine, W. M.; Jimenez, J. L., Organic aerosol composition and sources in Pasadena, California, during the 2010 CalNex campaign. *Journal of Geophysical Research: Atmospheres* **2013,** *118*, (16), 9233-9257.
(55) Lee, A. K. Y.; Willis, M. D.; Healy, R. M.; Onasch, T. B.; Abbatt, J. P. D., Mixing state of carbonaceous aerosol in an urban environment: single particle characterization using the soot particle aerosol mass spectrometer (SP-AMS). *Atmos. Chem. Phys.* **2015,** *15*, (4), 1823-1841.
(56) Aiken, A. C.; Decarlo, P. F.; Kroll, J. H.; Worsnop, D. R.; Huffman, J. A.; Docherty, K. S.; Ulbrich, I. M.; Mohr, C.; Kimmel, J. R.; Sueper, D.; Sun, Y.; Zhang, Q.; Trimborn, A.; Northway, M.; Ziemann, P. J.; Canagaratna, M. R.; Onasch, T. B.; Alfarra, M. R.; Prevot, A. S. H.; Dommen, J.; Duplissy, J.; Metzger, A.; Baltensperger, U.; Jimenez, J. L., O/C and OM/OC ratios of primary, secondary, and ambient organic aerosols with high-resolution time-of-flight aerosol mass spectrometry. *Environmental Science & Technology* **2008,** *42*, (12), 4478-4485.
(57) Schmale, J.; Schneider, J.; Nemitz, E.; Tang, Y. S.; Dragosits, U.; Blackall, T. D.; Trathan, P. N.; Phillips, G. J.; Sutton, M.; Braban, C. F., Sub-Antarctic marine aerosol: dominant contributions from biogenic sources. *Atmos. Chem. Phys.* **2013,** *13*, (17), 8669-8694.
(58) Donahue, N. M.; Epstein, S. A.; Pandis, S. N.; Robinson, A. L., A two-dimensional volatility basis set: 1. organic-aerosol mixing thermodynamics. *Atmos Chem Phys* **2011,** *11*, (7), 3303-3318.
(59) Alfarra, M. R.; Prevot, A. S. H.; Szidat, S.; Sandradewi, J.; Weimer, S.; Lanz, V. A.; Schreiber, D.; Mohr, M.; Baltensperger, U., Identification of the mass spectral signature of organic aerosols from wood burning emissions. *Environmental Science & Technology* **2007,** *41*, (16), 5770-5777.
(60) Lopez-Hilfiker, F. D.; Mohr, C.; Ehn, M.; Rubach, F.; Kleist, E.; Wildt, J.; Mentel, T. F.; Carrasquillo, A. J.; Daumit, K. E.; Hunter, J. F.; Kroll, J. H.; Worsnop, D. R.; Thornton, J. A., Phase partitioning and volatility of secondary organic aerosol components formed from alpha-pinene ozonolysis and OH oxidation: the importance of accretion products and other low volatility compounds. *Atmos Chem Phys* **2015,** *15*, (14), 7765-7776.
(61) Yatavelli, R. L. N.; Mohr, C.; Stark, H.; Day, D. A.; Thompson, S. L.; Lopez-Hilfiker, F. D.; Campuzano-Jost, P.; Palm, B. B.; Vogel, A. L.; Hoffmann, T.; Heikkinen, L.; Aijala, M.; Ng, N. L.; Kimmel, J. R.; Canagaratna, M. R.; Ehn, M.; Junninen, H.; Cubison, M. J.; Petaja, T.; Kulmala, M.; Jayne, J. T.; Worsnop, D. R.; Jimenez, J. L., Estimating the contribution of organic acids to northern hemispheric continental organic aerosol. *Geophys Res Lett* **2015,** *42*, (14), 6084-6090.
(62) Stark, H.; Yatavelli, R. L. N.; Thompson, S. L.; Kang, H.; Krechmer, J. E.; Kimmel, J. R.; Palm, B. B.; Hu, W.; Hayes, P. L.; Day, D. A.; Campuzano-Jost, P.; Canagaratna, M. R.; Jayne, J. T.; Worsnop, D. R.; Jimenez, J. L., Impact of Thermal Decomposition on Thermal Desorption Instruments: Advantage of

Thermogram Analysis for Quantifying Volatility Distributions of Organic Species. *Environmental Science & Technology* **2017,** *51*, (15), 8491-8500.

(63) Coggon, M. M.; Veres, P. R.; Yuan, B.; Koss, A.; Warneke, C.; Gilman, J. B.; Lerner, B. M.; Peischl, J.; Aikin, K. C.; Stockwell, C. E.; Hatch, L. E.; Ryerson, T. B.; Roberts, J. M.; Yokelson, R. J.; de Gouw, J. A., Emissions of nitrogen-containing organic compounds from the burning of herbaceous and arboraceous biomass: Fuel composition dependence and the variability of commonly used nitrile tracers. *Geophys Res Lett* **2016,** *43*, (18), 9903-9912.

(64) Brady, J. M.; Crisp, T. A.; Collier, S.; Kuwayama, T.; Forestieri, S. D.; Perraud, V.; Zhang, Q.; Kleeman, M. J.; Cappa, C. D.; Bertram, T. H., Real-Time Emission Factor Measurements of Isocyanic Acid from Light Duty Gasoline Vehicles. *Environmental Science & Technology* **2014,** *48*, (19), 11405-11412.

(65) Roberts, J. M.; Veres, P. R.; Cochran, A. K.; Warneke, C.; Burling, I. R.; Yokelson, R. J.; Lerner, B.; Gilman, J. B.; Kuster, W. C.; Fall, R.; de Gouw, J., Isocyanic acid in the atmosphere and its possible link to smoke-related health effects (vol 108, pg 8966, 2011). *Proceedings of the National Academy of Sciences of the United States of America* **2011,** *108*, (41), 17234-17234.

(66) Huang, Q.; Wang, L.; Han, S., The genotoxicity of substituted nitrobenzenes and the quantitative structure-activity relationship studies. *Chemosphere* **1995,** *30*, (5), 915-923.

(67) Sakhno, L. O., Variability in the fatty acid composition of rapeseed oil: Classical breeding and biotechnology. *Cytology and Genetics* **2010,** *44*, (6), 389-397.

(68) Orsavova, J.; Misurcova, L.; Ambrozova, J.; Vicha, R.; Mlcek, J., Fatty Acids Composition of Vegetable Oils and Its Contribution to Dietary Energy Intake and Dependence of Cardiovascular Mortality on Dietary Intake of Fatty Acids. *International Journal of Molecular Sciences* **2015,** *16*, (6), 12871.

(69) Reyes-Villegas, E.; Priestley, M.; Ting, Y. C.; Haslett, S.; Bannan, T.; Le breton, M.; Williams, P. I.; Bacak, A.; Flynn, M. J.; Coe, H.; Percival, C.; Allan, J. D., Simultaneous Aerosol Mass Spectrometry and Chemical Ionisation Mass Spectrometry measurements during a biomass burning event in the UK: Insights into nitrate chemistry. *Atmos. Chem. Phys. Discuss.* **2017,** *2017*, 1-22.

(70) Chow, J. C.; Watson, J. G.; Lowenthal, D. H.; Chen, L. W. A.; Zielinska, B.; Mazzoleni, L. R.; Magliano, K. L., Evaluation of organic markers for chemical mass balance source apportionment at the Fresno Supersite. *Atmos. Chem. Phys.* **2007,** *7*, (7), 1741-1754.

(71) Pei, B.; Cui, H. Y.; Liu, H.; Yan, N. Q., Chemical characteristics of fine particulate matter emitted from commercial cooking. *Front Env Sci Eng* **2016,** *10*, (3), 559-568.

Table 1. List of all cooking experiments.

	Food	Exp. #	Diluted	OA [μg.m^{-3}]	SMPS [μg.m^{-3}]	Diameter (nm)	Peak dM/DlogDp	Filter #
Deep fried	Fish&chips	E1	N	23.8	16.1	346	37	F0
	Fish&chips	E2	N	54.7	21.9	429	18	F1
	Fish&chips	E3	Y	5.3	4.3	385	10	F2
	Fish&chips	E4	Y	5.8	4.3	334	11	
	Burgers	E5	Y	10.8	13.2	98	28	F3
	Burgers	E6	N	**	**	**	**	F4
	Burgers	E7	N	**	**	**	**	F5
	Burgers	E8	N	87.9	**	**	**	F6
	Burgers	E9	N	93.7	**	**	**	
	Burgers	E10	Y	7.6	11.1	136	17	F7
	Burgers	E11	Y	9.1	21.5	131	47	
	Sausages	E12	Y	9.7	12.3	105	18	F8
	Sausages	E13	N	183.0	223.5	151	452	F9
Shallow fried	Tomato	E14	N	240.1	226.5	346	286	F10
	Mushroom	E15	N	112.7	117.9	334	204	
	Eggs	E16	N	28.0	47.0	102	65	
	Bacon	E17	N	219.7	247.6	157	392	
	Black puddin	E18	N	19.0	9.6	146	12	
	Sausages	E19	N	424.1	395.0	260	540	
	Tomato	E20	Y	15.3	17.7	209	34	F11
	Mushroom	E21	Y	10.8	7.5	241	12	
	Eggs	E22	Y	1.8	**	**	**	
	Bacon	E23	Y	4.6	**	**	**	
	Sausages	E24	Y	16.8	**	**	**	
	Black puddin	E25	Y	4.0	3.5	109	5	
	Bacon	E26	Y	2.9	2.8	64	4	
	Salmon	E27	Y	20.8	18.2	131	30	F12
	Salmon_SF	E28	Y	16.9	16.1	131	32	
	Burgers	E29	Y	30.9	23.2	131	48	F13
	Vegetables_SF	E30	Y	61.1	**	**	**	F14
	Vegetables_SF	E31	Y	96.1	45.3	399	69	
	Pork	E32	Y	21.3	22.3	122	37	F15
	Lamb	E33	Y	49.0	51.8	175	98	F16
	Lamb_SF	E34	Y	8.3	8.3	269	13	
	Chicken	E35	Y	26.8	33.3	118	58	F17
	Chicken_SF	E36	Y	8.0	8.7	98	14	

E= Experiment, N=No Y=Yes, SF = steer-fried, ** samples were lost. , F=Filter.

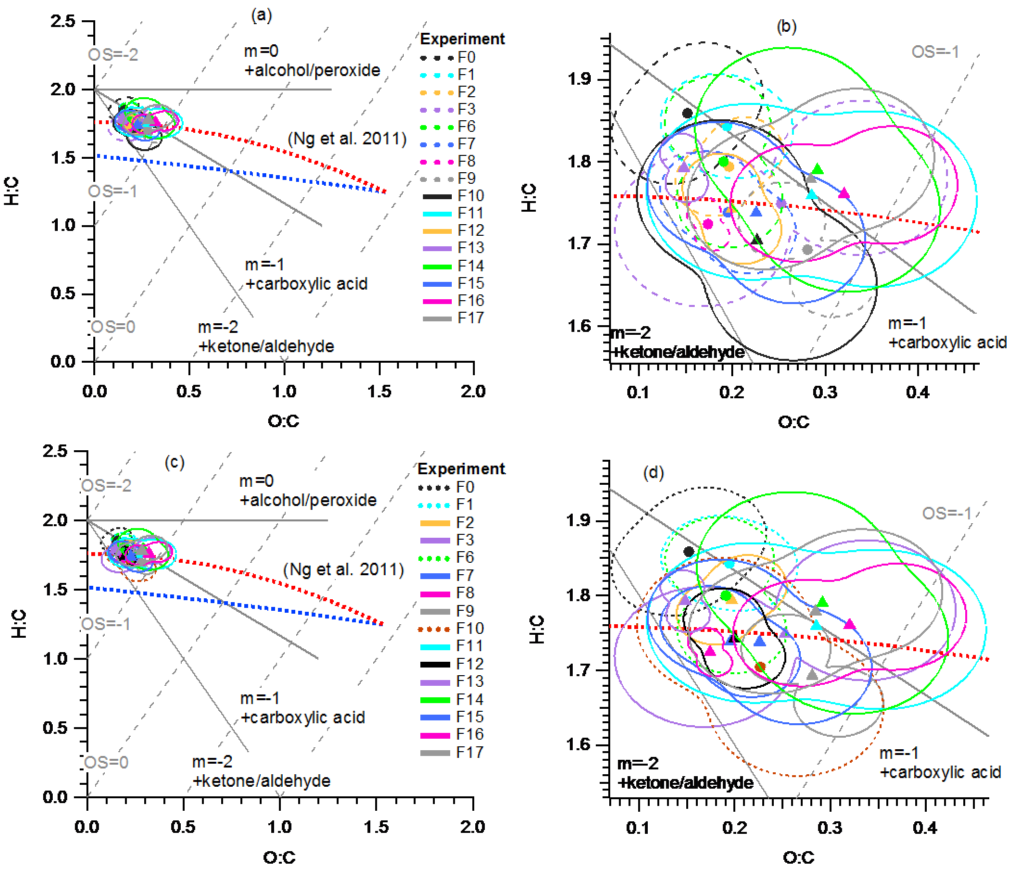

Figure 1. Van Krevelen diagram with mean (markers) and SDE (lines) of O:C and H:C.

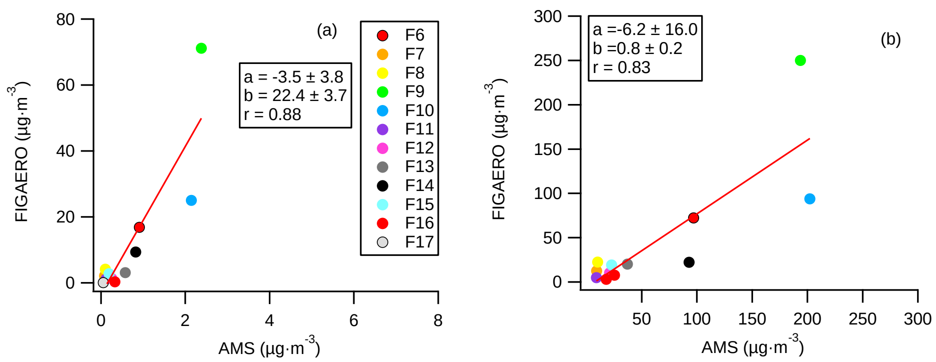

Figure 2. FIGAERO-AMS comparison for levoglucosan (a) and OA (b) concentrations. Red lines show linear regression. Description of filter numbers (F0-F17) is provided in Table 1.

Table 2. Cooking markers in the gas phase.

Formula	Name	*	F6	F7	F8	F9	F10	F11	F12	F13	F14	F15	F16	F17	Mass + I
CHNO	Isocyanic acid	G	7.84	17.01	13.11	3.94	9.16	1.56		3.34	2.14	1.32	2.68		169.91
		P													
		R													
CH_2O_2	Formic acid	G	16558.40	13439.20	8726.79	14167.10	5146.27		762.00						172.91
		P		1.12	2.40	2.18							0.11		
		R		65.38	40.60	83.42									
$C_3H_4O_2$	Acrylic acid	G	5167.44	1351.57	623.29	2737.11	55.43	8.42	12.65	25.36	19.44	1.97	3.99	13.57	198.93
		P	0.02	0.01	0.01	0.25									
		R	1404.82	766.57	467.14	143.03									
$C_3H_6O_2$	Propionic acid	G	17.58	9.24	4.57	8.63	6.02	3.66	1.54	5.62	6.17	0.89	1.94	1.42	200.95
		P	0.01			0.02									
		R	9.33			4.55									
$C_3H_6O_3$	Hydroxypropionic	G	109170.00	79445.60	78302.60	108587.00	3672.54		7397.47	5085.04		12600.70	11146.40	6038.39	216.94
		P	31.60	37.33	42.43	83.59	11.40	0.93	4.43	7.40	1.59	21.32	3.32	1.81	
		R	17.20	11.55	20.58	16.68	1.07		7.88	7.94		7.58	15.16	9.51	
$C_3H_4O_4$	Malonic Acid	G	215.06	184.02	149.88	198.71	5.73								230.92
		P	0.25	0.15	0.20	0.76	0.04								
		R	4.26	6.75	8.38	3.37	0.42								
$C_6H_{10}O_2$	Hexanoic acid	G	109.34	145.26	109.86	72.45	20.85	7.58	4.52	7.87	12.41				240.97
		P	0.11	0.04	0.07	0.46	0.19	0.01	0.03	0.01	0.004	0.06	0.06	0.03	
		R	4.83	19.22	17.52	2.01	0.36	1.16	0.70	8.89	16.08				
$C_6H_{10}O_4$	Adipic acid	G	99.32	105.15	95.84	144.49	15.05								272.96
		P	0.36			2.27	0.56								
		R	1.37			0.82	0.09								

* G= Gas [formic equiv. ppt], P = Particle [formic equiv. $\mu g \cdot m^{-3}$], R= G/P Ratio [calculated using raw signal]. Mass+I = Molecular mass of compound + I. Description of filters (f0-f17) is provided in Table 1.

Table 3. Cooking markers in the particle phase.

Formula	Name	*	F6	F7	F8	F9	F10	F11	F12	F13	F14	F15	F16	F17	Mass + I
$C_4H_6O_4$	Succinic acid	G	431.33	500.52	275.54	855.15	73.22	2.42							244.93
		P	14.05	0.93	2.00	53.14	6.61	0.08	0.15	0.38	0.97				
		R	0.15	2.92	1.54	0.21	0.04	0.04							
$C_5H_8O_4$	Glutaric acid	G	174.82	226.38	246.82	255.09	83.62	113.96	50.31	49.86	70.40	44.02			258.94
		P	4.12	0.51	1.13	28.63	10.83	0.33	0.45	1.01	2.37	0.80	0.11	0.04	
		R	0.21	2.43	2.44	0.11	0.03	0.43	0.53	0.57	0.16	0.70			
$C_7H_{12}O_4$	Pimelic acid	G	51.36	62.47	81.97	86.45	43.75	21.60		0.67	9.52				286.98
		P	0.99	0.20	0.38	4.70	1.37	0.05	0.07	0.15	0.36	0.02	0.05	0.04	
		R	0.26	1.73	2.44	0.24	0.11	0.55		0.05	0.14				
$C_6H_{10}O_5$	Levoglucosan	G	679.57	762.16	925.19	1351.71	427.93	261.77	76.61	117.53	521.84	165.73			288.96
		P	16.83	2.09	4.16	71.14	25.00	1.18	1.28	3.10	9.37	2.77	0.28	0.06	
		R	0.20	1.98	2.48	0.24	0.06	0.28	0.28	0.44	0.29	0.77			
$C_8H_{14}O_4$	Suberic acid	G	3.26	8.86	9.40	5.50	6.59	7.64							300.99
		P	0.29	0.06	0.12	1.06	0.95	0.05	0.10	0.16	0.20	0.06	0.07	0.05	
		R	0.06	0.83	0.85	0.07	0.02	0.20							
$C_9H_{16}O_4$	Azelaic acid	G		2.93	1.25			4.97					8.24	0.55	315.01
		P	0.37	0.07	0.16	1.24	0.70	0.04	0.10	0.20	0.12	0.07	0.11	0.06	
		R		0.22	0.09			0.14					0.34	0.02	
$C_{10}H_{18}O_4$	Sebacic acid	G						12.71	4.97	7.34	9.44	0.53	41.15	23.65	329.03
		P	0.08	0.04	0.09	0.32	0.34	0.02	0.06	0.14	0.06	0.03	0.18	0.09	
		R						0.67	0.37	0.62	0.78	0.25	1.02	0.78	
$C_{12}H_{22}O_4$	Dodecanedioic	G													357.06
		P	0.02			0.07	0.16	0.01	0.02	0.04	0.02		0.02	0.01	
		R													
$C_{16}H_{32}O_2$	Palmitic acid	G						36.36	19.19	23.19	19.12	12.96	0.06		383.14
		P	0.79	0.43	0.76	1.73	0.84	0.14	0.54	1.10	0.23	0.49	0.31	0.06	
		R						0.33	0.17	0.24	0.44	0.34	0.00		
$C_{17}H_{34}O_2$	Margaric acid	G						1.40	0.53	1.06	0.83	0.76			397.16
		P	0.06	0.03	0.07	0.13	0.09	0.02	0.04	0.12	0.04	0.05	0.06	0.01	
		R						0.12	0.06	0.10	0.12	0.20			
$C_{18}H_{32}O_2$	Linoleic acid	G		6.94	3.80			40.76	29.16	32.13	28.49	25.28	5.68	4.72	407.14
		P	1.44	0.59	0.91	2.82	1.96	0.28	0.66	1.27	0.50	0.92	0.18	0.12	
		R		0.06	0.05			0.18	0.21	0.29	0.30	0.35	0.15	0.11	
$C_{18}H_{34}O_2$	Oleic acid	G		9.90	2.47			77.77	56.31	65.38	61.71	55.90	9.54	9.88	409.16
		P	4.27	1.88	2.92	8.54	3.94	0.61	1.49	3.85	1.36	2.15	0.93	0.37	
		R		0.03	0.01			0.16	0.18	0.20	0.24	0.33	0.05	0.08	

* G= Gas [formic equiv. ppt], P = Particle [formic equiv. $\mu g \cdot m^{-3}$], R= G/P Ratio (of raw signals). Mass+I = Molecular mass of compound + I. Description of filters (f0-f17) is provided in Table 1.

TOC art

Supporting information for: **Online chemical characterization of food cooking organic aerosols: implications for source apportionment**

Ernesto Reyes-Villegas[1*], Thomas Bannan[1], Michael Le Breton[1, ϕ], Archit Mehra[1], Michael Priestley[1], Carl Percival[1, Δ], Hugh Coe[1], James D. Allan[1,2]

[1]School of Earth, Atmospheric and Environmental Sciences, The University of Manchester, Manchester, M13 9PL, UK

[2]National Centre for Atmospheric Science, The University of Manchester, Manchester, M13 9PL, UK

[ϕ]Now at University of Gothenburg, 40530 Gothenburg, Sweden

[Δ]Now at Jet Propulsion Laboratory, 4800 Oak Grove Drive, Pasadena, CA 91109, USA

*Corresponding author: ernesto.reyesvillegas@manchester.ac.uk

Pages: 10, Figures: 2, Tables: 7

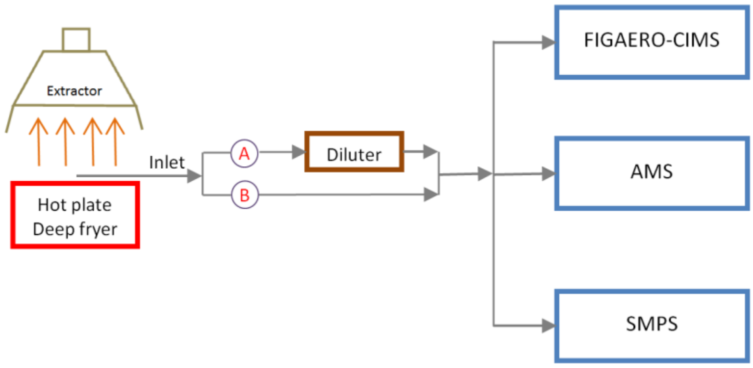

Figure S1. Instrument arrangement for diluted (A) and non-diluted (B) sampling. A bypass was used when doing non-diluted experiments.

S1. AMS RIE and aerosol concentrations

Table S1 shows the experiments performed with diluted/not diluted and different cooking methods. The OA concentrations measured with the AMS are high compared to SMPS concentrations. As mentioned in the manuscript, OA concentrations in Table S1 we firstly calculated with RIE_{OA} =1.4. A new RIE_{OA} is corrected (RIE_{OA_corr}), calculated, from average concentrations, by multiplying the OA/SMPS ratios by 1.4 (Table S2). Finally, OA concentrations are corrected and presented in table 1 in the manuscript.

Table S1. List of all cooking experiments.

	Food	Exp. #	Diluted	OA [μg.m^{-3}]	SMPS [μg.m^{-3}]	Diameter (nm)	Peak dM/DlogDp	OA/SMPS	Filter #
Deep fried	Fish&chips	E1	N	42.8	16.1	346	37	2.7	F0
	Fish&chips	E2	N	98.3	21.9	429	18	4.5	F1
	Fish&chips	E3	Y	11.6	4.3	385	10	2.7	F2
	Fish&chips	E4	Y	12.8	4.3	334	11	3.0	
	Burgers	E5	Y	23.6	13.2	98	28	1.8	F3
	Burgers	E6	N	**	**	**	**	**	F4
	Burgers	E7	N	**	**	**	**	**	F5
	Burgers	E8	N	157.9	**	**	**	**	F6
	Burgers	E9	N	168.2	**	**	**	**	
	Burgers	E10	Y	16.5	11.1	136	17	1.5	F7
	Burgers	E11	Y	19.9	21.5	131	47	0.9	
	Sausages	E12	Y	21.2	12.3	105	18	1.7	F8
	Sausages	E13	N	328.7	223.5	151	452	1.5	F9
Shallow fried	Tomato	E14	N	366.9	226.5	346	286	1.6	F10
	Mushroom	E15	N	172.2	117.9	334	204	1.5	
	Eggs	E16	N	42.8	47.0	102	65	0.9	
	Bacon	E17	N	335.7	247.6	157	392	1.4	
	Black puddin	E18	N	29.0	9.6	146	12	3.0	
	Sausages	E19	N	648.1	395.0	260	540	1.6	
	Tomato	E20	Y	25.8	17.7	209	34	1.5	F11
	Mushroom	E21	Y	18.2	7.5	241	12	2.4	
	Eggs	E22	Y	2.9	**	**	**	**	
	Bacon	E23	Y	7.8	**	**	**	**	
	Sausages	E24	Y	28.2	**	**	**	**	
	Black puddin	E25	Y	5.4	3.5	109	5	1.5	
	Bacon	E26	Y	3.8	2.8	64	4	1.3	
	Salmon	E27	Y	23.2	18.2	131	30	1.3	F12
	Salmon_SF	E28	Y	22.3	16.1	131	32	1.4	
	Burgers	E29	Y	34.5	23.2	131	48	1.5	F13
	Vegetables_SF	E30	Y	80.8	**	**	**	**	F14
	Vegetables_SF	E31	Y	127.0	45.3	399	69	2.8	
	Pork	E32	Y	23.8	22.3	122	37	1.1	F15
	Lamb	E33	Y	54.8	51.8	175	98	1.1	F16
	Lamb_SF	E34	Y	10.9	8.3	269	13	1.3	
	Chicken	E35	Y	29.9	33.3	118	58	0.9	F17
	Chicken_SF	E36	Y	10.6	8.7	98	14	1.2	

E= Experiment, N=No Y=Yes, SF = steer-fried, ** samples were lost. , F=Filter.

Table S2. AMS and SMPS average concentrations for different cooking methods.

Cooking methods		OA [μg·m^{-3}]		SMPS [μg·m^{-3}]		OA/SMPS	RIE_{OA_corr}	Diameter [nm]		Peak [dM/dlogDp]	
		Avg	Sdev	Avg	Sdev			Avg	Sdev	Avg	Sdev
Deep fried plus English Breakfast	Non-diluted	229.4	196.0	145.0	127.5	1.58	2.21	252.3	109.9	222.9	192.1
	Diluted	14.1	7.5	7.5	5.2	1.88	2.63	206.7	113.0	13.5	9.4
English Breakfast	Non-diluted	265.8	214.4	173.9	131.2	1.53	2.14	224.2	94.6	249.9	181.8
	Diluted	13.3	9.1	7.9	5.9	1.68	2.35	155.8	71.9	13.9	12.0
Deep fried	Non-diluted	156.6	123.8	87.2	96.4	1.79	2.51	308.7	116.5	168.9	200.5
	Diluted	15.2	4.3	7.0	3.8	2.17	3.06	274.7	121.8	12.9	3.5
Shallow Fried meat (Diluted)	Stir fried	14.6	5.5	11.1	3.6	1.31	1.85	224.3	74.1	19.8	8.8
	Chops	33.2	11.5	29.7	12.1	1.12	1.56	135.3	20.5	54.0	23.9

Figure S2. Mass (a,b and c) and number (d, e and f) distributions of the different experiments.

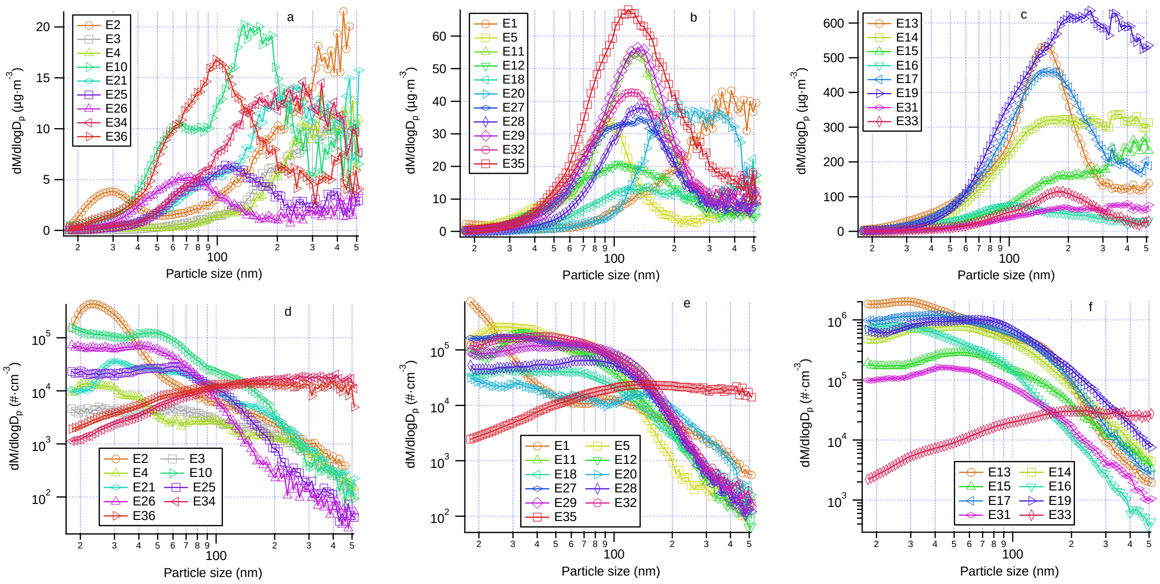

S2. FIGAERO-CIMS background correction and calibration.

Blank and Background subtractions

Prior to FIGAERO-CIMS analysis, data were corrected by filter blank subtractions to particle concentrations and background subtractions to gas concentrations. The filter was exposed to a second temperature ramping immediately after finishing one sample. The average aerosol concentrations measured during the second desorption were used to correct aerosol measurements. Background gas measurements were performed before starting cooking, average concentrations were used for background subtractions to gas concentrations.

Calibration.

A thermogram analysis was performed for the ions identified in gas phase to determine whether they were also identified in the particle phase. Ions with signal in the thermogram lower than background during desorption were discarded. During the cooking experiment, a formic acid sensitivity of 6 $cps \cdot ppt^{-1}$ was calculated. After the cooking experiment was finished, particle calibrations were carried out by depositing 10 µL of varied concentration solutions of levoglucosan in methanol, onto the filter. These were then thermally desorbed, and the peak area of the thermograms was used to determine a sensitivity of 1.01E+07 $counts \cdot \mu g^{-1}$ with a relative formic acid sensitivity of 2 $cps \cdot ppt^{-1}$. The levoglucosan sensitivity for the cooking experiment was scaled based on the formic acid sensitivity. Finally, particle concentrations were calculated using a levoglucosan sensitivity of 3.0e7 $counts \cdot \mu g^{-1}$ and gas concentrations were calculated using a formic acid sensitivity of 6 $counts \cdot ppt^{-1}$. We did not perform extensive calibrations as the aim of this study is to perform qualitative analysis. The use of the sensitivity of one compound to calculate concentrations of all the compounds measured with the CIMS have been successfully applied in previous studies. [1, 2].

Table S3. FIGAERO-CIMS list of compounds found on gas and particle+.

#	Formula	mass + I	Probable name	Part	#	Formula	mass + I	Probable name	Part	#	Formula	mass + I	Probable name	Part
1	H2O	144.9	Water Cluster		44	C5H6N2O3	268.9			87	C13H15NO2	344.0		+
2	HO2	159.9			45	C5H9N3O2	270.0			88	C12H10O4	345.0		+
3	H2O2	160.9	Hydrogen Peroxide		46	C10H8O	271.0	naphtol	+	89	C9H15O6	346.0		+
4	CHNO	169.9			47	C6H10O4	273.0	Adipic acid		90	C15H10O2	349.0		+
5	CH2O2	172.9	Formic acid		48	C9H8O2	275.0	Cinnamic acid	+	91	C15H12O2	351.0		+
6	C2H3NO	183.9	Methyl Isocyanate		49	C5H10O5	277.0			92	C18H10	353.0		+
7	CH4N2O	186.9	Urea	+	50	C5H12O5	279.0	Arabitol		93	C11H16O5	355.0		+
8	HNO3	189.9			51	C9H14O2	281.0			94	C12H22O4	357.1	Dodecanoic acid	+
9	C3H4O2	198.9	Acrylic acid		52	C8H12O3	283.0			95	C10H16O6	359.0		+
10	C2H2O3	200.9	Glyoxylic acid		53	C11H10O	285.0			96	C9H14O7	361.0		+
11	C3H6O2	200.9	Propionic acid		54	C7H12O4	287.0	Pimelic acid	+	97	C12H12O5	363.0		+
12	C2H4O3	202.9	Glycolic acid		55	C6H10O5	289.0	Levoglucosan	+	98	C12H14O5	365.0		+
13	C3H4O3	214.9	Pyruvic acid		56	C6H12O5	291.0	Fucose		99	C8H16O8	367.0		+
14	C4H9O2	216.0		+	57	C5H10O6	293.0		+	100	C8H18O8	369.0		+
15	C2H2O4	216.9	Oxalic acid		58	C9H11O3	294.0			101	C8H20O8	371.0		+
16	C3H6O3	216.9	Lactic acid		59	C10H16O2	295.0			102	C10H14O7	373.0		+
17	C3H8O3	219.0	Glycerol		60	C9H14O3	297.0	Pinalic-3-acid		103	C10H16O7	375.0		+
18	C4H2NO2	222.9			61	C9H16O3	299.0			104	C10H24O7	383.1		
19	C4H4O3	226.9			62	C8H14O4	301.0	Suberic acid		105	C16H32O2	383.1	palmitic acid	+
20	C5H9O2	228.0			63	C10H8O3	303.0	formylcinnamic acid		106	C16H18O3	385.0		+
21	C4H6O3	228.9			64	C10H10O3	305.0	Coniferyl aldehyde		107	C11H18O7	389.0		+
22	C3H4O4	230.9	Malonic Acid		65	C10H12O3	307.0	Coniferol		108	C18H16O2	391.0		+
23	C3H6O4	232.9	Glyceric acid		66	C10H14O3	309.0			109	C16H28O3	395.1		+
24	C5H6NO2	238.9		+	67	C10H16O3	311.0	Pinonic Acid	+	110	C17H20NO2	397.1		
25	C4H7N3O	240.0	Creatinine	+	68	C9H14O4	313.0	pinic acid	+	111	C17H34O2	397.2	margaric acid	+
26	C3H2N2O3	240.9	Parabanic acid		69	C9H16O4	315.0	Azelaic acid	+	112	C14H24O5	399.1		+
27	C6H10O2	241.0			70	C10H6O4	316.9		+	113	C13H22O6	401.0		+
28	C5H8O3	243.0	Levulinic acid		71	C8H14O5	317.0		+	114	C17H26O3	405.1		+
29	C4H6O4	244.9	Succinic acid	+	72	C7H12O6	319.0	Quinic acid	+	115	C18H32O2	407.1	Linoleic acid	+
30	C4H8O4	246.9	Methylglyceric Acid	+	73	C7H14O6	321.0		+	116	C18H34O2	409.2	Oleic acid	+
31	C6H6N2O	249.0	Nicotinamide	+	74	C11H16O3	323.0	Propylsyringol		117	C18H36O2	411.2	Stearic acid	+
32	C6H5NO2	249.9	Nitrobenzene	+	75	C13H25O	324.1			118	C21H26O	421.1		+
33	C6H7NO2	252.0		+	76	C10H14O4	325.0			119	C18H32O3	423.1	Vernolic acid	+
34	C6H6O3	252.9	Isomaltol	+	77	C11H20NO2	325.1			120	C17H30O4	425.1		+
35	C5H7N2O2	254.0			78	C10H16O4	327.0		+	121	C17H32O4	427.1	Heptadecanedioic acid	+
36	C6H8O3	255.0			79	C10H18O4	329.0	Sebacic acid	+	122	C17H20O5	431.0	Vanillyl syringyl	+
37	C5H7NO3	255.9	Pyroglutamic acid		80	C8H12O6	331.0		+	123	C20H32O2	431.1	Arachidonic acid	+
38	C5H8NO3	257.0			81	C11H12O4	335.0		+	124	C17H26O5	437.1		+
39	C6H13NO2	258.0			82	C14H10O2	337.0			125	C18H32O4	439.1	octadecenedioic acid	+
40	C5H8O4	258.9	Glutaric acid	+	83	C12H18O3	337.0			126	C16H26O6	441.1		+
41	C5H10O4	261.0			84	C11H15O4	338.0		+	127	C21H30O3	457.1		+
42	C8H8O2	263.0	Methyl benzoate		85	C10H13O5	340.0			128	C23H32O3	483.1		+
43	C6H5NO3	265.9	4-Nitrophenol	+	86	C10H15O5	342.0							

Mass+I = molecular mass of the compound + iodide (I).

Table S4 O:C and H:C ratios on the literature of cooking-related emissions. It is worth mentioning all these studies used a RIE of 1.4, either stated or by inference.

Type	H:C	O:C	Reference
Meat charbroiling		0.09-0.3	3
Ambient OA	1.4-1.9	0.2-0.8	4
regional OA		0.9	
HOA		0.06-0.1	
diesel-petrol		0.03-0.04	
BBOA		0.31	
OOA2		0.52-0.64	
OOA1 aged		0.83-1.02	
α-pinene - isoprene	1.40-1.86	0.4-0.72	5
Ambient OA	1.49	0.38	6
COA	1.6	0.21	7
HOA	1.6	0.14	
SVOOA	1.4	0.38	
LVOOA	1.2	0.8	
M-OOA	1.61	1.05	8
HOA		0.38	
BBOA	1.35	0.25 - 0.6	9
COA	1.69	0.1	10
HOA	1.58	0.17	11
COA	1.73	0.11	
SVOOA	1.33	0.47	
LVOOA	1.38	0.48	
COA	1.72	0.11	12
HOA	1.8	0.09	
BBOA	1.56	0.33	
OOA	1.43	0.42	
COA	1.74	0.13	6
OA	1.65	0.28	13
HOA	1.87	0.11	
COA	1.71	0.12	
OOA	1.48	0.48	
OOA - POA		1.2 - 0.7	14
HOA	1.96	0.13	15
BBOA	1.76	0.36	
COA	1.81	0.22	
OOA2	1.62	0.53	
OOA1	1.43	0.84	

Table S5 Average gas, particle and ratios (G/A) for nitrogen-containing markers.

Formula	Name	*	F6	F7	F8	F9	F10	F11	F12	F13	F14	F15	F16	F17	Mass + I
$C_4H_2NO_2$	C4H2NO2	G	21.034	16.947	10.834	16.580	3.756								222.914
		P	0.036	0.001		0.047	0.007								
		R	2.880	116.432		4.508	1.839								
$C_5H_6NO_2$	C5H6NO2	G	11.148	10.257	6.852	11.502	22.183	6.152	2.985	4.220	12.574	1.911		0.093	238.945
		P	0.152	0.037	0.067	0.849	0.390	0.025	0.078	0.102	0.048	0.091	0.027	0.080	
		R	0.365	1.493	1.138	0.174	0.190	0.302	0.181	0.477	1.386	0.269		0.003	
$C_4H_7N_3O$	Creatinine	G	5.508	4.013	3.525	4.338	1.214								239.964
		P	0.078	0.069	0.117	0.584	2.391	0.122	0.655	0.614	0.093	1.569	0.630	0.593	
		R	0.352	0.314	0.337	0.095	0.002								
$C_3H_2N_2O_3$	Parabanic acid	G	48.366	37.063	49.165	53.195	12.567								240.912
		P	0.071	0.018	0.040	0.209									
		R	3.392	11.196	13.702	3.273									
$C_6H_6N_2O$	Nicotinamide	G	34.177	39.594	31.376	38.793	22.532	48.323	38.443	31.704	17.169	28.973	18.523	27.951	248.953
		P	1.952	0.357	0.781	9.043	2.035	0.139	0.504	0.723	0.228	2.422	0.526	0.399	
		R	0.087	0.601	0.448	0.055	0.037	0.433	0.360	0.507	0.399	0.153	0.159	0.200	
$C_6H_5NO_2$	Nitrobenzene	G	35.712	33.886	3.708	36.815	93.088	11.354							249.937
		P	1.359	0.130	0.231	2.448	1.905	0.050	0.094	0.175	0.059	0.316	0.167	0.032	
		R	0.131	1.418	0.179	0.193	0.163	0.281							
$C_6H_7NO_2$	C6H7NO2	G	33.803	31.585	35.343	56.763	8.089	4.169							251.953
		P	0.432	0.137	0.264	3.409	0.789	0.046	0.078	0.173	0.092	0.194	0.046	0.015	
		R	0.390	1.251	1.494	0.214	0.034	0.112							
$C_5H_7N_2O_2$	C5H7N2O2	G	32.561	35.837	30.944	21.856	31.687	4.497							253.956
		P	0.309	0.123	0.158	0.665	0.295	0.014	0.033	0.043	0.018	0.028	0.025	0.014	
		R	0.524	1.584	2.179	0.422	0.358	0.406							
$C_5H_7NO_3$	Pyroglutamic acid	G	22.845	36.119	31.590	37.533	3.179	23.682	18.564	20.396	17.326	21.639	1.399	1.836	255.948
		P	6.413	1.371	1.841	11.781	5.865	0.340	0.581	1.773	1.040	0.917	0.677	0.534	
		R	0.018	0.143	0.191	0.041	0.002	0.087	0.151	0.133	0.088	0.303	0.009	0.010	
$C_5H_8NO_3$	C5H8NO3	G	363.571	358.711	500.564	241.724	65.121								256.955
		P	1.056	0.410	0.553	3.244	2.241	0.057	0.051	0.094	0.266	-0.157	0.045	0.020	
		R	1.714	4.750	10.092	0.957	0.097								
$C_6H_{13}NO_2$	C6H13NO2	G	30.515	33.003	35.099	29.944	4.602								258.000
		P	0.461	0.085	0.128	1.523	0.506	0.048	0.180	0.182	0.159	0.460	0.335	0.338	
		R	0.329	2.113	3.060	0.252	0.030								
$C_6H_5NO_3$	4-Nitrophenol	G	6.996	4.659	5.197	5.093							17.239	7.183	265.932
		P	0.039	0.005	0.002	0.161	0.109	0.002					0.084	0.032	
		R	0.897	4.952	25.148	0.405							0.928	0.638	
$C_5H_9N_3O_2$	C5H9N3O2	G	5.420	4.275	4.195	2.884	1.625	0.682							269.974
		P	0.146	0.027	0.040	0.384	0.295	0.013	0.024	0.044	0.040	0.041	0.013	0.007	
		R	0.185	0.870	1.173	0.096	0.018	0.065							
$C_{13}H_{15}NO_2$	C13H15NO2	G													344.015
		P	0.019	0.008	0.008	0.094	0.078	0.004	0.005	0.007	0.016		0.019	0.007	
		R													

* G= Gas [formic equiv. ppt ppt], P = Particle [formic equiv. ppt $\mu g.m^{-3}$], R= G/P Ratio. Mass+I = Molecular mass of compound + molecular mas of I. Description of filters (f0-f17) is provided in Table 1.

Table S6 Uncentered Pearson values for different mass spectra.

FC= fish and chips, BU=Burgers, SA = Sausages, EB= English breakfast, SAL = Salmon, VE = Vegetables, PO = Pork, LA = Lamb, CH = Chicken, Filter_av = Average of all experiments.
ND = Not diluted, DD = Diluted. DF = Deep fried, SF = Shallow fried.

Values higher than 0.95 are on blue and values lower than 0.90 are on red.

FC_ND_DF	FC_ND_DF	FC_DD_DF	BU_DD_DF	BU_ND_DF	BU_ND_DF	BU_ND_DF	BU_DD_DF	SA_DD_DF	SA_ND_DF	EB_ND_SF	EB_DD_SF	SAL_DD_SF	BU_DD_SF	VE_DD_SF	PO_DD_SF	LA_DD_SF	CH_DD_SF	Filter_av	Clear_cToF	ClearWin_HR	ClearSum_cToF	CrippaWin_HR	Mohr_HR	CrippaSum_HR	NK_Annual	NK_Spr	NK_Sum	NK_Aut	Bfire_nbf	Bfire_bfo	Bfire_nbfON	Bfire_bfoON	Lanz_WinQuad	M_CH_nsk_HR	M_FatBU_HR	M_LeanBU_HR	M_Salmon_HR	
1.000	0.994	0.989	0.985	0.989	0.937	0.976	0.973	0.972	0.966	0.968	0.955	0.963	0.958	0.951	0.944	0.927	0.922	0.976	0.860	0.938	0.934	0.918	0.895	0.922	0.880	0.920	0.885	0.763	0.930	0.924	0.966	0.933	0.709	0.889	0.877	0.880	0.908	FC_ND_DF
	1.000	0.997	0.983	0.990	0.951	0.979	0.977	0.977	0.976	0.983	0.957	0.962	0.974	0.963	0.937	0.915	0.903	0.983	0.889	0.960	0.958	0.938	0.900	0.950	0.894	0.946	0.899	0.773	0.947	0.946	0.977	0.946	0.734	0.919	0.912	0.913	0.941	FC_ND_DF
		1.000	0.984	0.990	0.952	0.977	0.981	0.981	0.974	0.982	0.956	0.962	0.976	0.962	0.936	0.909	0.899	0.982	0.904	0.960	0.957	0.948	0.901	0.953	0.908	0.955	0.910	0.796	0.957	0.954	0.980	0.953	0.747	0.914	0.905	0.907	0.939	FC_DD_DF
			1.000	0.999	0.945	0.994	0.997	0.996	0.986	0.983	0.984	0.992	0.981	0.973	0.977	0.963	0.956	0.992	0.907	0.957	0.955	0.956	0.946	0.944	0.931	0.950	0.930	0.821	0.959	0.957	0.985	0.968	0.791	0.910	0.879	0.891	0.914	BU_DD_DF
				1.000	0.948	0.994	0.996	0.995	0.988	0.987	0.982	0.988	0.984	0.976	0.971	0.955	0.946	0.994	0.910	0.962	0.960	0.957	0.941	0.951	0.928	0.954	0.929	0.815	0.962	0.959	0.988	0.967	0.783	0.917	0.891	0.900	0.924	BU_ND_DF
					1.000	0.946	0.944	0.945	0.947	0.961	0.932	0.938	0.956	0.940	0.919	0.897	0.876	0.954	0.860	0.965	0.962	0.933	0.903	0.928	0.878	0.936	0.884	0.722	0.910	0.938	0.952	0.936	0.792	0.949	0.948	0.950	0.957	BU_ND_DF
						1.000	0.995	0.995	0.997	0.992	0.994	0.992	0.989	0.989	0.979	0.971	0.956	0.999	0.906	0.972	0.970	0.960	0.964	0.954	0.932	0.952	0.933	0.815	0.959	0.955	0.985	0.962	0.823	0.935	0.904	0.917	0.932	BU_ND_DF
							1.000	1.000	0.991	0.988	0.989	0.993	0.989	0.981	0.979	0.963	0.954	0.995	0.928	0.966	0.965	0.970	0.956	0.957	0.948	0.963	0.946	0.843	0.972	0.968	0.990	0.974	0.821	0.923	0.889	0.902	0.923	BU_DD_DF
								1.000	0.992	0.990	0.989	0.992	0.991	0.983	0.976	0.960	0.949	0.995	0.932	0.970	0.969	0.972	0.957	0.961	0.948	0.967	0.947	0.841	0.974	0.971	0.991	0.975	0.822	0.928	0.895	0.908	0.929	SA_DD_DF
									1.000	0.997	0.993	0.985	0.993	0.994	0.970	0.961	0.940	0.999	0.915	0.983	0.981	0.966	0.965	0.967	0.933	0.961	0.935	0.807	0.963	0.959	0.986	0.961	0.832	0.953	0.925	0.937	0.949	SA_ND_DF
										1.000	0.983	0.978	0.996	0.990	0.958	0.942	0.919	0.997	0.922	0.990	0.989	0.969	0.950	0.977	0.930	0.971	0.933	0.797	0.964	0.968	0.989	0.965	0.817	0.962	0.943	0.952	0.967	EB_ND_SF
											1.000	0.990	0.980	0.992	0.983	0.980	0.966	0.992	0.899	0.968	0.962	0.958	0.979	0.944	0.941	0.943	0.941	0.825	0.954	0.943	0.975	0.950	0.855	0.931	0.890	0.908	0.915	EB_DD_SF
												1.000	0.981	0.972	0.994	0.983	0.974	0.989	0.905	0.955	0.956	0.956	0.964	0.940	0.937	0.944	0.934	0.828	0.951	0.950	0.978	0.965	0.827	0.917	0.876	0.893	0.908	SAL_DD_SF
													1.000	0.982	0.961	0.944	0.919	0.993	0.940	0.986	0.990	0.975	0.949	0.981	0.939	0.979	0.939	0.812	0.968	0.978	0.990	0.977	0.819	0.961	0.938	0.947	0.964	BU_DD_SF
														1.000	0.957	0.950	0.930	0.991	0.911	0.983	0.975	0.965	0.965	0.963	0.939	0.959	0.943	0.821	0.963	0.952	0.977	0.945	0.857	0.950	0.921	0.934	0.942	VE_DD_SF
															1.000	0.993	0.988	0.973	0.874	0.931	0.931	0.933	0.965	0.911	0.922	0.913	0.917	0.816	0.926	0.921	0.956	0.941	0.832	0.895	0.845	0.868	0.874	PO_DD_SF
																1.000	0.993	0.961	0.849	0.917	0.916	0.913	0.967	0.891	0.908	0.889	0.906	0.798	0.905	0.898	0.939	0.921	0.829	0.884	0.828	0.854	0.852	LA_DD_SF
																	1.000	0.944	0.831	0.887	0.882	0.896	0.950	0.862	0.902	0.867	0.897	0.812	0.895	0.878	0.923	0.903	0.816	0.841	0.779	0.807	0.809	CH_DD_SF
																		1.000	0.915	0.981	0.979	0.966	0.959	0.965	0.934	0.962	0.936	0.811	0.964	0.962	0.989	0.965	0.820	0.946	0.920	0.931	0.946	Filter_av
																			1.000	0.918	0.927	0.960	0.875	0.963	0.950	0.971	0.944	0.874	0.968	0.973	0.949	0.954	0.776	0.887	0.852	0.860	0.885	Clear_cToF
																				1.000	0.996	0.969	0.943	0.980	0.926	0.976	0.933	0.783	0.955	0.964	0.976	0.950	0.834	0.980	0.967	0.973	0.979	ClearWin_HR
																					1.000	0.969	0.938	0.985	0.922	0.977	0.927	0.772	0.953	0.969	0.978	0.959	0.817	0.985	0.971	0.977	0.983	ClearSum_cToF
																						1.000	0.942	0.970	0.983	0.983	0.982	0.876	0.986	0.983	0.981	0.968	0.846	0.951	0.911	0.926	0.940	CrippaWin_HR
																							1.000	0.912	0.927	0.909	0.920	0.800	0.924	0.912	0.943	0.926	0.903	0.914	0.860	0.885	0.882	Mohr_HR
																								1.000	0.936	0.987	0.940	0.813	0.969	0.977	0.977	0.957	0.791	0.960	0.944	0.949	0.963	CrippaSum_HR
																									1.000	0.956	0.997	0.934	0.975	0.955	0.951	0.936	0.852	0.899	0.839	0.862	0.874	NK_Annual
																										1.000	0.960	0.848	0.980	0.990	0.977	0.968	0.807	0.950	0.928	0.935	0.954	NK_Spr
																											1.000	0.923	0.973	0.956	0.951	0.933	0.838	0.910	0.853	0.875	0.885	NK_Sum
																												1.000	0.892	0.845	0.832	0.821	0.794	0.731	0.658	0.685	0.712	NK_Aut
																													1.000	0.978	0.984	0.957	0.818	0.917	0.881	0.892	0.914	Bfire_nbf
																														1.000	0.983	0.986	0.798	0.941	0.915	0.923	0.944	Bfire_bfo
																															1.000	0.980	0.798	0.945	0.919	0.928	0.945	Bfire_nbfON
																																1.000	0.784	0.924	0.894	0.903	0.926	Bfire_bfoON
																																	1.000	0.809	0.749	0.780	0.770	Lanz_WinQuad
																																		1.000	0.987	0.995	0.987	M_CH_nsk_HR
																																			1.000	0.997	0.992	M_FatBU_HR
																																				1.000	0.991	M_LeanBU_HR
																																					1.000	M_Salmon_HR

Table S7 Reference of the external cooking mass spectra used on the comparison.

ID	Reference	ID	Reference
Clear_cToF	16	Bfire_nbf	17
ClearWin_HR	18	Bfire_bfo	
ClearSum_cToF	16	Bfire_nbfON	
CrippaWin_HR	19	Bfire_bfoON	
Mohr_HR	20	Lanz_WinQuad	21
CrippaSum_HR	6	M_CH_nsk_HR	22
NK_Annual	23	M_FatBU_HR	
NK_Spr		M_LeanBU_HR	
NK_Sum		M_Salmon_HR	
NK_Aut			

References.

(1) Lopez-Hilfiker, F. D.; Iyer, S.; Mohr, C.; Lee, B. H.; D'Ambro, E. L.; Kurtén, T.; Thornton, J. A., Constraining the sensitivity of iodide adduct chemical ionization mass spectrometry to multifunctional organic molecules using the collision limit and thermodynamic stability of iodide ion adducts. *Atmos. Meas. Tech.* **2016,** *9*, (4), 1505-1512.

(2) Mohr, C.; Lopez-Hilfiker, F. D.; Yli-Juuti, T.; Heitto, A.; Lutz, A.; Hallquist, M.; D'Ambro, E. L.; Rissanen, M. P.; Hao, L.; Schobesberger, S.; Kulmala, M.; Mauldin, R. L., III; Makkonen, U.; Sipilä, M.; Petäjä, T.; Thornton, J. A., Ambient observations of dimers from terpene oxidation in the gas phase: Implications for new particle formation and growth. *Geophys Res Lett* **2017,** *44*, (6), 2958-2966.

(3) Kaltsonoudis, C.; Kostenidou, E.; Louvaris, E.; Psichoudaki, M.; Tsiligiannis, E.; Florou, K.; Liangou, A.; Pandis, S. N., Characterization of fresh and aged organic aerosol emissions from meat charbroiling. *Atmos. Chem. Phys.* **2017,** *17*, (11), 7143-7155.

(4) Aiken, A. C.; Decarlo, P. F.; Kroll, J. H.; Worsnop, D. R.; Huffman, J. A.; Docherty, K. S.; Ulbrich, I. M.; Mohr, C.; Kimmel, J. R.; Sueper, D.; Sun, Y.; Zhang, Q.; Trimborn, A.; Northway, M.; Ziemann, P. J.; Canagaratna, M. R.; Onasch, T. B.; Alfarra, M. R.; Prevot, A. S. H.; Dommen, J.; Duplissy, J.; Metzger, A.; Baltensperger, U.; Jimenez, J. L., O/C and OM/OC ratios of primary, secondary, and ambient organic aerosols with high-resolution time-of-flight aerosol mass spectrometry. *Environmental Science & Technology* **2008,** *42*, (12), 4478-4485.

(5) Kuwata, M.; Zorn, S. R.; Martin, S. T., Using Elemental Ratios to Predict the Density of Organic Material Composed of Carbon, Hydrogen, and Oxygen. *Environmental Science & Technology* **2012,** *46*, (2), 787-794.

(6) Crippa, M.; El Haddad, I.; Slowik, J. G.; DeCarlo, P. F.; Mohr, C.; Heringa, M. F.; Chirico, R.; Marchand, N.; Sciare, J.; Baltensperger, U.; Prevot, A. S. H., Identification of marine and continental aerosol sources in Paris using high resolution aerosol mass spectrometry. *J Geophys Res-Atmos* **2013,** *118*, (4), 1950-1963.

(7) Hayes, P. L.; Ortega, A. M.; Cubison, M. J.; Froyd, K. D.; Zhao, Y.; Cliff, S. S.; Hu, W. W.; Toohey, D. W.; Flynn, J. H.; Lefer, B. L.; Grossberg, N.; Alvarez, S.; Rappenglück, B.; Taylor, J. W.; Allan, J. D.; Holloway, J. S.; Gilman, J. B.; Kuster, W. C.; de Gouw, J. A.; Massoli, P.; Zhang, X.; Liu, J.; Weber, R. J.; Corrigan, A. L.; Russell, L. M.; Isaacman, G.; Worton, D. R.; Kreisberg, N. M.; Goldstein, A. H.; Thalman, R.; Waxman, E. M.; Volkamer, R.; Lin, Y. H.; Surratt, J. D.; Kleindienst, T. E.; Offenberg, J. H.; Dusanter, S.; Griffith, S.; Stevens, P. S.; Brioude, J.; Angevine, W. M.; Jimenez, J. L., Organic aerosol composition and sources in Pasadena, California, during the 2010 CalNex campaign. *Journal of Geophysical Research: Atmospheres* **2013,** *118*, (16), 9233-9257.

(8) Schmale, J.; Schneider, J.; Nemitz, E.; Tang, Y. S.; Dragosits, U.; Blackall, T. D.; Trathan, P. N.; Phillips, G. J.; Sutton, M.; Braban, C. F., Sub-Antarctic marine aerosol: dominant contributions from biogenic sources. *Atmos. Chem. Phys.* **2013,** *13*, (17), 8669-8694.

(9) Brito, J.; Rizzo, L. V.; Morgan, W. T.; Coe, H.; Johnson, B.; Haywood, J.; Longo, K.; Freitas, S.; Andreae, M. O.; Artaxo, P., Ground-based aerosol characterization during the South American Biomass Burning Analysis (SAMBBA) field experiment. *Atmos. Chem. Phys.* **2014,** *14*, (22), 12069-12083.

(10) Xu, J.; Zhang, Q.; Chen, M.; Ge, X.; Ren, J.; Qin, D., Chemical composition, sources, and processes of urban aerosols during summertime in northwest China: insights from high-resolution aerosol mass spectrometry. *Atmos. Chem. Phys.* **2014,** *14*, (23), 12593-12611.

(11) Huang, X. F.; He, L. Y.; Hu, M.; Canagaratna, M. R.; Sun, Y.; Zhang, Q.; Zhu, T.; Xue, L.; Zeng, L. W.; Liu, X. G.; Zhang, Y. H.; Jayne, J. T.; Ng, N. L.; Worsnop, D. R., Highly time-resolved chemical characterization of atmospheric submicron particles during 2008 Beijing Olympic Games using an Aerodyne High-Resolution Aerosol Mass Spectrometer. *Atmos Chem Phys* **2010,** *10*, (18), 8933-8945.

(12) Ge, X. L.; Setyan, A.; Sun, Y. L.; Zhang, Q., Primary and secondary organic aerosols in Fresno, California during wintertime: Results from high resolution aerosol mass spectrometry. *J Geophys Res-Atmos* **2012,** *117*.

(13) Lee, A. K. Y.; Willis, M. D.; Healy, R. M.; Onasch, T. B.; Abbatt, J. P. D., Mixing state of carbonaceous aerosol in an urban environment: single particle characterization using the soot particle aerosol mass spectrometer (SP-AMS). *Atmos. Chem. Phys.* **2015,** *15*, (4), 1823-1841.

(14) Corbin, J. C.; Keller, A.; Lohmann, U.; Burtscher, H.; Sierau, B.; Mensah, A. A., Organic Emissions from a Wood Stove and a Pellet Stove before and after Simulated Atmospheric Aging. *Aerosol Science and Technology* **2015,** *49*, (11), 1037-1050.

(15) Canagaratna, M. R.; Jimenez, J. L.; Kroll, J. H.; Chen, Q.; Kessler, S. H.; Massoli, P.; Hildebrandt Ruiz, L.; Fortner, E.; Williams, L. R.; Wilson, K. R.; Surratt, J. D.; Donahue, N. M.; Jayne, J. T.; Worsnop, D. R., Elemental ratio measurements of organic compounds using aerosol mass spectrometry: characterization, improved calibration, and implications. *Atmos Chem Phys* **2015,** *15*, (1), 253-272.

(16) Young, D. E.; Allan, J. D.; Williams, P. I.; Green, D. C.; Flynn, M. J.; Harrison, R. M.; Yin, J.; Gallagher, M. W.; Coe, H., Investigating the annual behaviour of submicron secondary inorganic and organic aerosols in London. *Atmos. Chem. Phys.* **2015,** *15*, (11), 6351-6366.

(17) Reyes-Villegas, E.; Priestley, M.; Ting, Y. C.; Haslett, S.; Bannan, T.; Le breton, M.; Williams, P. I.; Bacak, A.; Flynn, M. J.; Coe, H.; Percival, C.; Allan, J. D., Simultaneous Aerosol Mass Spectrometry and Chemical Ionisation Mass Spectrometry measurements during a biomass burning event in the UK: Insights into nitrate chemistry. *Atmos. Chem. Phys. Discuss.* **2017,** *2017*, 1-22.

(18) Young, D. E.; Allan, J. D.; Williams, P. I.; Green, D. C.; Harrison, R. M.; Yin, J.; Flynn, M. J.; Gallagher, M. W.; Coe, H., Investigating a two-component model of solid fuel organic aerosol in London: Processes, PM1 contributions, and seasonality. *Atmos Chem Phys* **2015,** *15*, (5), 2429-2443.

(19) Crippa, M.; DeCarlo, P. F.; Slowik, J. G.; Mohr, C.; Heringa, M. F.; Chirico, R.; Poulain, L.; Freutel, F.; Sciare, J.; Cozic, J.; Di Marco, C. F.; Elsasser, M.; Nicolas, J. B.; Marchand, N.; Abidi, E.; Wiedensohler, A.; Drewnick, F.; Schneider, J.; Borrmann, S.; Nemitz, E.; Zimmermann, R.; Jaffrezo, J. L.; Prevot, A. S. H.; Baltensperger, U., Wintertime aerosol chemical composition and source apportionment of the organic fraction in the metropolitan area of Paris. *Atmos Chem Phys* **2013,** *13*, (2), 961-981.

(20) Mohr, C.; DeCarlo, P. F.; Heringa, M. F.; Chirico, R.; Slowik, J. G.; Richter, R.; Reche, C.; Alastuey, A.; Querol, X.; Seco, R.; Penuelas, J.; Jimenez, J. L.; Crippa, M.; Zimmermann, R.; Baltensperger, U.; Prevot, A. S. H., Identification and quantification of organic aerosol from cooking and other sources in Barcelona using aerosol mass spectrometer data. *Atmos Chem Phys* **2012,** *12*, (4), 1649-1665.

(21) Lanz, V. A.; Alfarra, M. R.; Baltensperger, U.; Buchmann, B.; Hueglin, C.; Prevot, A. S. H., Source apportionment of submicron organic aerosols at an urban site by factor analytical modelling of aerosol mass spectra. *Atmos Chem Phys* **2007,** *7*, (6), 1503-1522.

(22) Mohr, C.; Huffman, J. A.; Cubison, M. J.; Aiken, A. C.; Docherty, K. S.; Kimmel, J. R.; Ulbrich, I. M.; Hannigan, M.; Jimenez, J. L., Characterization of Primary Organic Aerosol Emissions from Meat Cooking, Trash Burning, and Motor Vehicles with High-Resolution Aerosol Mass Spectrometry and

Comparison with Ambient and Chamber Observations. *Environmental Science & Technology* **2009,** *43*, (7), 2443-2449.

(23) Reyes-Villegas, E.; Green, D. C.; Priestman, M.; Canonaco, F.; Coe, H.; Prévôt, A. S. H.; Allan, J. D., Organic aerosol source apportionment in London 2013 with ME-2: exploring the solution space with annual and seasonal analysis. *Atmos. Chem. Phys.* **2016,** *16*, (24), 15545-15559.

Chapter 7

Conclusions

The work presented in this thesis shows the importance of investigating OA, the different types of instruments and models available to the study of their chemical composition and sources. In this work, a range of different mass spectrometers (AMS, ACSM, CIMS) was used to measure near real-time particle and gas concentrations in urban locations (London and Manchester, UK) and in a laboratory-based experiment to measure cooking emissions.

Source apportionment tools were used to identify OA sources in urban environments under two types of ambient conditions; long-term measurements (March-December 2013) at the urban background site, North Kensington, in London, looking at OA sources and their seasonal behaviour (Section 6.1). Short-term measurements were performed during a special event with high biomass burning emissions in 2014, named Bonfire Night (Section 6.2).

Cooking OA (COA) have been considered as one of the main POA in urban environments (Mohr et al. 2012;Yin et al. 2015), yet not completely studied and characterised. While other OA sources may have seasonal behaviour, for instance, BBOA with high concentrations during winter (Vicente and Alves 2018) and SOA with high concentrations during summer (Canonaco et al. 2015), COA concentrations are present over the year as a result of inhabitants' activities, highlighting the importance of achieving a better understanding of COA composition. In order to study the chemical composition of COA emissions, a laboratory-based study was designed to perform on-line measurements of the particle and the gas phases (Section 6.3).

Source apportionment tools

PMF and ME-2 source apportionment tools were used, through the SoFi interphase (Canonaco et al. 2013), to deconvolve OA sources. When performing source apportionment to long datasets, it resulted better to run ME-2 for short periods of time, performing seasonal analysis. Other possible approaches to analyse the data involve dividing the dataset based on different pollutant events or meteorological conditions (Wang et al. 2017b;Reyes-Villegas et al. 2017). It is worth to highlight the importance of using different target profiles and *a* values to analyse a number of possible solutions. The strategy proposed here, which was used in Section 6.1 and Section 6.2, proved to be an effective way to objectively explore the solution space. The trilinear analysis was used to compare different solutions provided additional information such as diesel/petrol contribution to HOA concentrations in the North Kensington site, London.

Both models presented a good performance for long-term and seasonal analysis, with ME-2 showing a better performance than PMF. However, both models struggled to deconvolve OA sources when analysing a special event with high biomass burning emissions. In this special event, the best way to perform OA source apportionment was to run PMF/ME-2 to the period before and after Bonfire Night and using BBOA, HOA and COA mass spectra from this period to constrain solutions when analysing the Bonfire Night event. However, it was not able to completely separate OA sources, showing COA, HOA and SVOOA mixed with BBOA. While ME-2 was not been able to completely deconvolve BBOA concentrations, it was capable of identifying BBOA trend over the Bonfire Night event, which is corroborated by the good correlation with the absorption coefficient for wood burning ($babs_{\_470wb}$ r^2 = 0.88).

Mass spectrometers and their performance to study OA sources

Different types of mass spectrometers were deployed in this work. An ACSM during the long-term measurements in North Kensington, London; the cToF-AMS and HR-ToF-CIMS during Bonfire Night 2014 in Manchester, UK; the HR-ToF-AMS and the

FIGAERO-HR-ToF-CIMS in a laboratory-based study to characterise COA and their relationship with gases.

Ambient measurements provided high time-resolution of OA sources, which provided the opportunity to study their seasonal behaviour. The ACSM presented a good performance, providing 30 minute concentrations of submicron non-refractory aerosols over the 10 months of the sampling campaign. Primary OA presented high concentrations in autumn and secondary OA high concentrations in summer. A cToF-AMS and a HR-ToF-CIMS were deployed during the Bonfire Night measurement campaign, which presented high biomass burning emissions, being possible to study night-time OA sources and processes. An emphasis on nitrogen chemistry was placed and it was possible to identify primary and secondary contributions of particulate organic oxides of nitrogen (PON). While the method of Farmer et al. (2010) to identify PON was proposed to be used with HR-ToF-AMS measurements, here it was demonstrated that this method could be applied to cToF-AMS data measured in this study, after proving low CH_2O^+ and mineral nitrate interferences.

The HR-ToF-CIMS provided additional information to the AMS analysis, by determining biomass burning tracers. High correlations (r^2) were observed with BBOA and Hydrogen cyanide (0.76), propionic acid (0.85), nitrous acid (0.86), Acrylic acid (0.90) and methacrylic acid (0.92), which have been previously determined as biomass burning tracers (Veres et al. 2010;Le Breton et al. 2013). The HR-ToF-CIMS resulted to be a fundamental tool to identify the nature of PON obtained from the AMS-PMF analysis. During the Bonfire Night event, primary PON showed high r^2 values with Dimethylformamide (0.63), Methylformamide (0.65) and hydrogen cyanide (0.77), gases that have been related to combustion processes (Borduas et al. 2015) while secondary PON showed low correlations with $ClNO_2$ (0.52). $ClNO_2$ is known to be produced from secondary reactions (Bannan et al. 2015). During the episode with low aerosol concentrations, high correlations were observed between $ClNO_2$ and LVOOA (0.67) and sPON (0.74) proving their secondary origin.

The laboratory-based measurements, using the FIGAERO-HR-ToF-CIMS provided a chemical characterisation of particles and gases from different types of food.

This instrument presents a soft ionisation; hence, it was possible to obtain molecular information of both particles and gases, which provides additional information to AMS-PMF analysis in order to further investigate OA sources. The calibration using levoglucosan, for particle phase calibration, and formic acid, for gas phase calibration, provided qualitative analysis, with it possible to compare with AMS total OA concentrations. The fact FIGAERO identified ~80% of OA measured by the AMS agrees with previous studies. For instance, Lopez-Hilfiker et al. (2015) determined FIGAERO aersol concentrations accounted for 25%-50% of OA measure by the AMS. Stark et al. (2017) concluded the total acid aerosol concentration measured with a FIGAERO represented about 50% of AMS D'Ambro et al. (2017) identified compounds with six or more carbons contributed 25% to the total OA-AMS.

OA sources and new findings

Different primary and secondary organic aerosol sources were identified. Primary sources are biomass burning OA (BBOA), hydrocarbon-like OA (HOA) and cooking OA (COA), primary particulate organic oxides of nitrogen (pPON). Secondary OA sources include semi-volatile OA (SVOOA), low volatility OA (LVOOA) and secondary particulate organic oxides of nitrogen (sPON). It was possible to observe daily trends in OA sources such as HOA, with the possibility of identifying heavy-duty and light-duty diesel contributions to HOA (HDD and LDD, respectively). The highest contributor to HOA concentrations was found to be LDD. Hence, LDD should be targeted in order to reduce HOA concentrations during weekdays.

When comparing PON concentrations with $babs_{470wb}$, BBOA and LVOOA, results suggest that pPON absorbed at wavelength 470 nm during Bonfire Night and LVOOA absorbed at wavelength 470 nm during the period identified with high SOA. sPON did not absorb at wavelength 470 nm. It has been previously identified brown carbon to be absorbing light near the UV region (Bones et al. 2010;Saleh et al. 2014) and PON has been identified to be a potential contributor to brown carbon (Mohr et al. 2013). These findings with pPON and LVOOA absorbing light at 470 nm will impact on Aethalometer model studies, and the $babs_{\_470wb}$ should be corrected from SOA interferences.

A better understanding of COA was accomplished by cooking different types of food in a laboratory-based experiment measuring particles and gases in near-real time. Dilution showed to have an important effect on food cooking experiments, varying G/P ratios and increasing the O:C ratios. Hence, future studies on identifying food cooking markers should be performed with diluting samples to better simulate ambient conditions. Future studies should also include chamber experiments in dark and light conditions to get a better understanding of food cooking emissions and their processing in the atmosphere.

Moreover, it was possible to determine an overestimation of OA-AMS concentrations compared to SMPS measurements. It was determined that this overestimation was explained by a higher relative ionisation of OA (RIE_{OA}) produced from the rapeseed oil emissions, with a RIE_{OA} value of around 3 rather than the typical value of 1.4 (Alfarra et al. 2004). This overestimation would have implications on the analysis performed in Papers 1 (Section 6.1) and 2 (Section 6.2). For instance, in the trilinear regression analysis of NO_x and POA (Section 6.1-Figure 3a), the COA slope is slightly higher than unity, when COA is not necessarily related to NO_x emissions. This is more noticeable during the summer period with even the COA slope higher than the BBOA slope. If COA concentrations were corrected with the RIE_{COA} = 3, COA slopes would decrease tending towards zero. Moreover, the COA contribution to PM_1 composition for the long-term measurements was found to be 8%, this value will decrease when using the correct RIE_{COA} value and the COA concentrations will decrease by around 50% of the calculated concentrations.

Target profiles and food cooking markers

The importance of using adequate mass spectra as target profiles when performing source apportionment with ME-2 has been already stated (Canonaco et al. 2013;Crippa et al. 2014). In this work, mass spectra of OA sources were generated in three different environments to be used in future OA source apportionment. An urban-background site in North Kensington, London, where a seasonal analysis (spring, summer and autumn) produced mass spectra for BBOA, HOA, COA, SVOOA, LVOOA (Section 6.1). However, it has been previously mentioned that is not a good practice to constrain SOA as they evolve in completely different ways from one site to another one. Hence, SVOOA and LVOOA must never be constrained when performing OA source apportionment.

One more ambient study was performed during a special nocturnal event with high biomass burning emissions in Manchester, 2014, named Bonfire Night (Section 6.2). Here, different sets of target profiles were generated. One set of target profiles (BBOA, HOA and COA) from the period before and after Bonfire Night and another set of target profiles (BBOA, HOA, COA, sPON and pPON) generated during the Bonfire Night event. The first set of target profiles represents typical mass spectra of Manchester during Autumn-Winter period. The second set of target profiles should be used with caution if it is going to be used in future source apportionments. It was possible to observe that, due to the high aerosols emitted from burning biomass, BBOA concentrations were mixed with HOA and COA. This mixing of OA concentrations was observed by the high concentrations of these sources HOA and COA during the Bonfire Night event, even when their mass spectra did not show apparent mixing, for instance, each mass spectrum presented their characteristic peaks and peaks from one mass spectrum were not present on another one. A wider range of *a* values should be used when using mass spectra generated during the Bonfire Night as target profiles.

A large set of target profiles from food cooking organic aerosols (COA) was generated in a laboratory-based study. This study included different types of cooking methods such as deep-frying and shallow frying and a range of foods including English breakfast, fish and chips and a variety of meat and vegetables, both with diluted and non-diluted experiments. In general, a significant variation was not observed between the different types of food with uncentered Pearson values (r_u) between 0.876-0.999. The mass spectra from this laboratory study correlated well with COA mass spectra obtained from the studies performed in London (Section 6.1) and Manchester (Section 6.2), with r_u values of 0.934 for the 10 month analysis in London and 0.989 for the analysis performed before and after Bonfire Night in Manchester. However, slightly lower r_u values were observed both when doing the seasonal analysis (0.811-0.962) and when analysing the Bonfire Night event (0.962), which highlights two important observations when doing source apportionment, first the importance of performing seasonal source apportionment and second to be cautious when analysing short periods with high aerosol concentrations.

However, these high uncentered Pearson values, obtained when comparing with mass spectra from previous studies, suggest COA mass spectra represent a stable mass spectrum despite corresponding concentrations mixing with other sources, still generating a clear COA mass spectrum.

It is here where the use of the FIGAERO-HR-ToF-CIMS measurements provided additional information to be used to better deconvolve COA concentrations (Paper 3). The FIGAERO-HR-ToF-CIMS identified several cooking markers both on gas (Organic acis: isocyanic, formic, acrylic, propionic, hydroxypropionic, malonic, hexanoic and adipic) and particle phases (dicarboxylic acids: succinic, glutaric, pimelic, suberic, azelaic, sebacic, dodecanedioic and carboxylic acids: palmitic, margaric, linoleic and oleic). While these species have been previously identified as cooking markers, mainly in the particle phase, a wide variability has been observed on the gas-particle ratios (G/P), with different G/P ratios over different types of food and cooking methods. Moreover, an effect of dilution on semi-volatility was observed, with diluted samples showing a higher G/P ratio, probably resulting from dilution facilitating low volatility gases to remain in gas phase. Hence, these markers should be used carefully as their contribution to gas and particle concentrations may vary.

7.1 Closing remarks and future work

This work presents an extensive analysis of OA sources and composition in different urban environment conditions and a laboratory-based experiment. Ambient studies proved POA to represent a high contribution to total OA concentrations, principally during the special event Bonfire Night, where BBOA dominated OA concentrations. Different POA and SOA sources were identified from ambient data using ME-2 factorisation tool from OA-AMS measurements. Long-term measurements in London allowed the analysis of OA seasonality and Bonfire Night in Manchester allowed the study of OA sources in a nocturnal environment with high biomass burning concentrations. It was possible to determine particulate oxygenated organic nitrogen concentrations, their nature and their absorbing properties in the UV region. A series of mass spectra were generated to be used in future studies as target profiles.

ME-2 factorisation tool was found to perform better than PMF; however, both PMF and ME-2 struggled to completely separate OA sources during Bonfire Night with BBOA mixed with the other OA sources. From the source apportionment performed on the ambient datasets, London and Manchester, it was possible to develop a strategy to more objectively determine the optimal solution that deconvolves OA sources. While this study involved looking at the seasonal behaviour of the long-term measurements, further work will involve testing the ME-2 response analysing the datasets sorted according to other parameters, for instance, different temperatures, wind parameters, and events with high/low aerosol concentrations.

London is a megacity where spatial variation of OA sources is expected. The results presented in this work were collected at North Kensington, an urban-background site, using an ACSM. To my knowledge, this instrument has been operating at this site since it was first deployed in 2013 (with a few interruptions during maintenance or when was used in other sites for short periods). Another ACSM has been deployed periodically at the kerbside site in Marylebone. Further simultaneous analysis at different sites in London, for long periods will give a better characterisation of OA sources.

The laboratory-based study allowed a more complete characterisation of COA. When comparing the AMS mass spectra obtained in the laboratory-based experiment with the mass spectra from the studies at London (Section 6.1) and Manchester (Section 6.2), high correlations were observed. This suggests that no significant changes in COA quantification would be observed if the mass spectra generated in this laboratory-based study were used as target profiles in the London dataset. However, the $RIE_{COA} \approx 3$ obtained from the laboratory-based study of COA, which was found to overestimate COA concentrations typically calculated using an $RIE_{OA} = 1.7$, will decrease the COA concentrations determined in London by approximately 50% (in summary, OA quantification involves, among other parameters, dividing the AMS raw signal by the RIE_{OA}, which means the higher the RIE_{OA} the lower the OA concentration).

The COA overestimation will affect the COA concentrations and contribution to total OA concentrations. For instance, Figure 6 in section 6.1 shows COA contributed 8% to OA concentrations, which corresponded to 0.42 $\mu g \cdot m^{-3}$, after scaling the COA concentrations by 50%, taking into consideration the RIE_{COA} of 3 rather than the typical RIE_{OA} of 1.7, an average COA concentration of 0.21 $\mu g \cdot m^{-3}$ that corresponds to a 4.1% of total OA concentrations is estimated. While in this case, there is not a major impact on the COA contribution to OA concentrations, it is suggested that further ambient studies of COA concentrations take into account the variability of RIE_{COA} and scale the concentrations accordingly.

A wide range of OA-AMS mass spectra has been generated in previous studies with data sets stored in a website created by the University of Colorado (http://cires1.colorado.edu/jimenez-group/AMSsd/, accessed: 12/12/2017). However, an increased number of studies have been performed identifying new sources. Hence, more efforts should be aimed to collect and categorise all this new information. Moreover, further studies should be aimed at generating mass spectra representative of different environmental conditions and monitoring sites, working together with scientific communities from other countries to share their experience in order to gain a broader perspective of OA source apportionment. This can be achieved with projects such as the e-COST action: Chemical On-Line cOmpoSition and Source Apportionment of fine aerosol (COLOSSAL) action (http://www.cost.eu/COST_Actions/ca/CA16109, accessed: 12/12/2017), of which I am an active member and aims to harmonise aerosol source apportionment approaches and methodologies around Europe.

The CIMS proved to be a useful instrument that provides additional information to improve OA source apportionment. However, further efforts should be aimed to perform source apportionment to CIMS data using ME-2. This will certainly increase our understanding of sources of gases and their relationship with OA sources, in particular, with the secondary organic aerosols. The FIGAERO-CIMS instrumentation provides fundamental information, being possible to identify markers in the gas and particle phases. While it was possible to identify approximately 80% of the AMS mass concentration, the FIGAERO-CIMS analysis performed in the laboratory-based experiment with food cooking emissions is considered to be qualitative, as the calibration was performed using only Levoglucosan. Further studies should perform extensive calibrations of the FIGAERO-CIMS in order to obtain a quantitative analysis.

The long-term OA source apportionment, together with aerosol concentrations and chemical composition during Bonfire Night provide invaluable information to understand better aerosol processes and sources in urban environments. The particle and gas markers obtained from the laboratory-based food cooking experiment can be used to improve models and would be key information to support the future addition of PM_1 to inventories. These findings can be used to carry out health studies and for decision makers to create policies aiming to improve the air quality in urban environments.

References

Alfarra, M. R., Coe, H., Allan, J. D., Bower, K. N., Boudries, H., Canagaratna, M. R., Jimenez, J. L., Jayne, J. T., Garforth, A. A., Li, S.-M. & Worsnop, D. R. (2004). Characterization of urban and rural organic particulate in the Lower Fraser Valley using two Aerodyne Aerosol Mass Spectrometers. *Atmospheric Environment,* 38(34), 5745-5758.

Alfarra, M. R., Prevot, A. S. H., Szidat, S., Sandradewi, J., Weimer, S., Lanz, V. A., Schreiber, D., Mohr, M. & Baltensperger, U. (2007). Identification of the mass spectral signature of organic aerosols from wood burning emissions. *Environmental Science & Technology,* 41(16), 5770-5777.

Allan, J. D., Delia, A. E., Coe, H., Bower, K. N., Alfarra, M. R., Jimenez, J. L., Middlebrook, A. M., Drewnick, F., Onasch, T. B., Canagaratna, M. R., Jayne, J. T. & Worsnop, D. R. (2004). A generalised method for the extraction of chemically resolved mass spectra from aerodyne aerosol mass spectrometer data. *Journal of Aerosol Science,* 35(7), 909-922.

Allan, J. D., Williams, P. I., Morgan, W. T., Martin, C. L., Flynn, M. J., Lee, J., Nemitz, E., Phillips, G. J., Gallagher, M. W. & Coe, H. (2010). Contributions from transport, solid fuel burning and cooking to primary organic aerosols in two UK cities. *Atmospheric Chemistry and Physics,* 10(2), 647-668.

Allen, G., Sioutas, C., Koutrakis, P., Reiss, R., Lurmann, F. W. & Roberts, P. T. (1997). Evaluation of the TEOM(R) method for measurement of ambient particulate mass in urban areas. *Journal of the Air & Waste Management Association,* 47(6), 682-689.

Allen, G. A., Lawrence, J. & Koutrakis, P. (1999). Field validation of a semi-continuous method for aerosol black carbon (aethalometer) and temporal patterns of summertime hourly black carbon measurements in southwestern PA. *Atmospheric Environment,* 33(5), 817-823.

Bannan, T. J., Booth, A. M., Bacak, A., Muller, J. B. A., Leather, K. E., Le Breton, M., Jones, B., Young, D., Coe, H., Allan, J., Visser, S., Slowik, J. G., Furger, M., Prevot, A. S. H., Lee, J., Dunmore, R. E., Hopkins, J. R., Hamilton, J. F., Lewis, A. C., Whalley, L. K., Sharp, T., Stone, D., Heard, D. E., Fleming, Z. L., Leigh, R., Shallcross, D. E. & Percival, C. J. (2015). The first UK measurements of nitryl chloride using a chemical ionization mass spectrometer in central London in the summer of 2012, and an investigation of the role of Cl atom oxidation. *Journal of Geophysical Research-Atmospheres,* 120(11), 5638-5657.

Barceló, D. (1992). Mass spectrometry in environmental organic analysis. *Analytica Chimica Acta,* 263(1), 1-19.

Baron, P. A. (1986). Calibration and Use of the Aerodynamic Particle Sizer (APS 3300). *Aerosol Science and Technology,* 5(1), 55-67.

Baron, P. A. & Willeke, K. (2001). *Aerosol measurement: principles, techniques, and applications* (Second edition ed.). Canada: John Wiley and Sons, Inc.

Bauer, J. J., Yu, X.-Y., Cary, R., Laulainen, N. & Berkowitz, C. (2009). Characterization of the Sunset Semi-Continuous Carbon Aerosol Analyzer. *Journal of the Air & Waste Management Association,* 59(7), 826-833.

Beevers, S. D., Kitwiroon, N., Williams, M. L., Kelly, F. J., Anderson, H. R. & Carslaw, D. C. (2013). Air pollution dispersion models for human exposure predictions in

London. *Journal of Exposure Science and Environmental Epidemiology,* 23(6), 647-653.
Begum, B., Biswas, S. K. & Hopke, P. K. (2007). Source Apportionment of Air Particulate Matter by Chemical Mass Balance (CMB) and Comparison with Positive Matrix Factorization (PMF) Model. *Aerosol and Air Quality Research,* 7(4), 446-468.
Bertram, T. H., Kimmel, J. R., Crisp, T. A., Ryder, O. S., Yatavelli, R. L. N., Thornton, J. A., Cubison, M. J., Gonin, M. & Worsnop, D. R. (2011). A field-deployable, chemical ionization time-of-flight mass spectrometer. *Atmospheric Measurement Techniques,* 4(7), 1471-1479.
Bones, D. L., Henricksen, D. K., Mang, S. A., Gonsior, M., Bateman, A. P., Nguyen, T. B., Cooper, W. J. & Nizkorodov, S. A. (2010). Appearance of strong absorbers and fluorophores in limonene-O3 secondary organic aerosol due to NH4+-mediated chemical aging over long time scales. *Journal of Geophysical Research: Atmospheres,* 115(D5), n/a-n/a.
Borduas, N., da Silva, G., Murphy, J. G. & Abbatt, J. P. D. (2015). Experimental and Theoretical Understanding of the Gas Phase Oxidation of Atmospheric Amides with OH Radicals: Kinetics, Products, and Mechanisms. *The Journal of Physical Chemistry A,* 119(19), 4298-4308.
Bozzetti, C., El Haddad, I., Salameh, D., Daellenbach, K. R., Fermo, P., Gonzalez, R., Minguillon, M. C., Iinuma, Y., Poulain, L., Elser, M., Muller, E., Slowik, J. G., Jaffrezo, J. L., Baltensperger, U., Marchand, N. & Prevot, A. S. H. (2017a). Organic aerosol source apportionment by offline-AMS over a full year in Marseille. *Atmospheric Chemistry and Physics,* 17(13), 8247-8268.
Bozzetti, C., Sosedova, Y., Xiao, M., Daellenbach, K. R., Ulevicius, V., Dudoitis, V., Mordas, G., Bycenkiene, S., Bycenkiene, S., Plauskaite, K., Vlachou, A., Golly, B., Chazeau, B., Besombes, J. L., Baltensperger, U., Jaffrezo, J. L., Slowik, J. G., El Haddad, I. & Prevot, A. S. H. (2017b). Argon offline-AMS source apportionment of organic aerosol over yearly cycles for an urban, rural, and marine site in northern Europe. *Atmospheric Chemistry and Physics,* 17(1), 117-141.
Brophy, P. & Farmer, D. K. (2015). A switchable reagent ion high resolution time-of-flight chemical ionization mass spectrometer for real-time measurement of gas phase oxidized species: characterization from the 2013 southern oxidant and aerosol study. *Atmos. Meas. Tech.,* 8(7), 2945-2959.
Brunekreef, B. & Holgate, S. T. (2002). Air pollution and health. *The lancet,* 360(9341), 1233-1242.
Butterfield, D., Beccaceci, S., Quincey, P., SWEENEY, B., Sweeney, A., Bradshaw, C., Fuller, G., Green, D. & Font, A. (2016). 2015 ANNUAL REPORT FOR THE UK BLACK CARBON NETWORK. National Physical Laboratory.
Byun, D. W. & Ching, J. K. S. (1999). Science algorithms of the EPA Models-3 Community Multiscale Air Quality (CMAQ) modeling system. *In:* Agency, U. S. E. P. (ed.). Byun, D. W., and J. K. S. Ching: Off. of Res. and Dev.
Cai, Y., Montague, D. C., Mooiweer-Bryan, W. & Deshler, T. (2008). Performance characteristics of the ultra high sensitivity aerosol spectrometer for particles between 55 and 800 nm: Laboratory and field studies. *Journal of Aerosol Science,* 39(9), 759-769.

Cai, Y., Snider, J. R. & Wechsler, P. (2013). Calibration of the passive cavity aerosol spectrometer probe for airborne determination of the size distribution. *Atmospheric Measurement Techniques,* 6(9), 2349-2358.
Calvo, A. I., Alves, C., Castro, A., Pont, V., Vicente, A. M. & Fraile, R. (2013). Research on aerosol sources and chemical composition: Past, current and emerging issues. *Atmospheric Research,* 120(Supplement C), 1-28.
Canagaratna, M. R., Jayne, J. T., Jimenez, J. L., Allan, J. D., Alfarra, M. R., Zhang, Q., Onasch, T. B., Drewnick, F., Coe, H., Middlebrook, A., Delia, A., Williams, L. R., Trimborn, A. M., Northway, M. J., DeCarlo, P. F., Kolb, C. E., Davidovits, P. & Worsnop, D. R. (2007). Chemical and microphysical characterization of ambient aerosols with the aerodyne aerosol mass spectrometer. *Mass Spectrometry Reviews,* 26(2), 185-222.
Canonaco, F., Crippa, M., Slowik, J. G., Baltensperger, U. & Prevot, A. S. H. (2013). SoFi, an IGOR-based interface for the efficient use of the generalized multilinear engine (ME-2) for the source apportionment: ME-2 application to aerosol mass spectrometer data. *Atmospheric Measurement Techniques,* 6(12), 3649-3661.
Canonaco, F., Slowik, J. G., Baltensperger, U. & Prévôt, A. S. H. (2015). Seasonal differences in oxygenated organic aerosol composition: Implications for emissions sources and factor analysis. *Atmospheric Chemistry and Physics,* 15(12), 6993-7002.
Chakraborty, A., Rajeev, P., Rajput, P. & Gupta, T. (2017). Water soluble organic aerosols in indo gangetic plain (IGP): Insights from aerosol mass spectrometry. *Science of The Total Environment,* 599-600(Supplement C), 1573-1582.
Chen, W.-H., Chen, Z.-B., Yuan, C.-S., Hung, C.-H. & Ning, S.-K. (2016). Investigating the differences between receptor and dispersion modeling for concentration prediction and health risk assessment of volatile organic compounds from petrochemical industrial complexes. *Journal of Environmental Management,* 166, 440-449.
Claeys, M., Roberts, G., Mallet, M., Arndt, J., Sellegri, K., Sciare, J., Wenger, J. & Sauvage, B. (2017). Optical, physical and chemical properties of aerosols transported to a coastal site in the western Mediterranean: A focus on primary marine aerosols. *Atmospheric Chemistry and Physics,* 17(12), 7891-7915.
Crippa, M., Canonaco, F., Lanz, V. A., Aijala, M., Allan, J. D., Carbone, S., Capes, G., Ceburnis, D., Dall'Osto, M., Day, D. A., DeCarlo, P. F., Ehn, M., Eriksson, A., Freney, E., Ruiz, L. H., Hillamo, R., Jimenez, J. L., Junninen, H., Kiendler-Scharr, A., Kortelainen, A. M., Kulmala, M., Laaksonen, A., Mensah, A., Mohr, C., Nemitz, E., O'Dowd, C., Ovadnevaite, J., Pandis, S. N., Petaja, T., Poulain, L., Saarikoski, S., Sellegri, K., Swietlicki, E., Tiitta, P., Worsnop, D. R., Baltensperger, U. & Prevot, A. S. H. (2014). Organic aerosol components derived from 25 AMS data sets across Europe using a consistent ME-2 based source apportionment approach. *Atmospheric Chemistry and Physics,* 14(12), 6159-6176.
Crippa, M., DeCarlo, P. F., Slowik, J. G., Mohr, C., Heringa, M. F., Chirico, R., Poulain, L., Freutel, F., Sciare, J., Cozic, J., Di Marco, C. F., Elsasser, M., Nicolas, J. B., Marchand, N., Abidi, E., Wiedensohler, A., Drewnick, F., Schneider, J., Borrmann, S., Nemitz, E., Zimmermann, R., Jaffrezo, J. L., Prevot, A. S. H. & Baltensperger, U. (2013). Wintertime aerosol chemical composition and

source apportionment of the organic fraction in the metropolitan area of Paris. *Atmospheric Chemistry and Physics,* 13(2)**,** 961-981.
Cubison, M. J., Ortega, A. M., Hayes, P. L., Farmer, D. K., Day, D., Lechner, M. J., Brune, W. H., Apel, E., Diskin, G. S., Fisher, J. A., Fuelberg, H. E., Hecobian, A., Knapp, D. J., Mikoviny, T., Riemer, D., Sachse, G. W., Sessions, W., Weber, R. J., Weinheimer, A. J., Wisthaler, A. & Jimenez, J. L. (2011). Effects of aging on organic aerosol from open biomass burning smoke in aircraft and laboratory studies. *Atmospheric Chemistry and Physics,* 11(23)**,** 12049-12064.
D'Ambro, E. L., Lee, B. H., Liu, J., Shilling, J. E., Gaston, C. J., Lopez-Hilfiker, F. D., Schobesberger, S., Zaveri, R. A., Mohr, C., Lutz, A., Zhang, Z., Gold, A., Surratt, J. D., Rivera-Rios, J. C., Keutsch, F. N. & Thornton, J. A. (2017). Molecular composition and volatility of isoprene photochemical oxidation secondary organic aerosol under low- and high-NOx conditions. *Atmospheric Chemistry and Physics,* 17(1)**,** 159-174.
Daellenbach, K. R., Stefenelli, G., Bozzetti, C., Vlachou, A., Fermo, P., Gonzalez, R., Piazzalunga, A., Colombi, C., Canonaco, F., Hueglin, C., Kasper-Giebl, A., Jaffrezo, J. L., Bianchi, F., Slowik, J. G., Baltensperger, U., El-Haddad, I. & Prévôt, A. S. H. (2017). Long-term chemical analysis and organic aerosol source apportionment at nine sites in central Europe: source identification and uncertainty assessment. *Atmos. Chem. Phys.,* 17(21)**,** 13265-13282.
Dall'Osto, M., Healy, R. M., Wenger, J. C., O'Dowd, C., Ovadnevaite, J., Ceburnis, D., Harrison, R. M. & Beddows, D. C. S. (2017). Distinct high molecular weight organic compound (HMW-OC) types in aerosol particles collected at a coastal urban site. *Atmospheric Environment,* 171(Supplement C)**,** 118-125.
Dall'Osto, M., Paglione, M., Decesari, S., Facchini, M. C., O'Dowd, C., Plass-Duellmer, C. & Harrison, R. M. (2015). On the Origin of AMS "Cooking Organic Aerosol" at a Rural Site. *Environmental Science & Technology,* 49(24)**,** 13964-13972.
De Hoffmann, E. & Stroobant, V. (2007). *Mass Spectrometry. Principles and applications* (Third edition ed.): John Wiley & Sons, Ltd.
De Visscher, A. (2014). *Air dispersion modeling : foundations and applications*. Hoboken, New Jersey: John Wiley & Sons, Inc.
DeCarlo, P. F., Kimmel, J. R., Trimborn, A., Northway, M. J., Jayne, J. T., Aiken, A. C., Gonin, M., Fuhrer, K., Horvath, T., Docherty, K. S., Worsnop, D. R. & Jimenez, J. L. (2006). Field-deployable, high-resolution, time-of-flight aerosol mass spectrometer. *Analytical Chemistry,* 78(24)**,** 8281-8289.
DEFRA (2007). The Air Quality Strategy for England, Scotland, Wales and Northern Ireland (Volume 1). The United Kingdom.
DEFRA (2010). Air Pollution: Action in a Changing Climate. *In:* Department for Environment, F. a. R. A. (ed.). London: Department for Environment, Food and Rural Affairs.
DEFRA. (2016). *National atmospheric emissions inventory* [Online]. Available: http://naei.defra.gov.uk/data/ [Accessed 15/08/2016 2016].
DEFRA. (2017). *Automatic Urban and Rural Network (AURN)* [Online]. Available: http://uk-air.defra.gov.uk/networks/network-info?view=aurn [Accessed September 28, 2017 2014].
Deguen, S., Segala, C., Pedrono, G. & Mesbah, M. (2012). A New Air Quality Perception Scale for Global Assessment of Air Pollution Health Effects. *Risk Analysis,* 32(12)**,** 2043-2054.
Demographia. (2017). Demographia world urban areas.

Douglas, I., Hodgson, R. & Lawson, N. (2002). Industry, environment and health through 200 years in Manchester. *Ecological Economics,* 41(2), 235-255.
Drewnick, F., Hings, S. S., DeCarlo, P., Jayne, J. T., Gonin, M., Fuhrer, K., Weimer, S., Jimenez, J. L., Demerjian, K. L., Borrmann, S. & Worsnop, D. R. (2005). A new time-of-flight aerosol mass spectrometer (TOF-AMS) - Instrument description and first field deployment. *Aerosol Science and Technology,* 39(7), 637-658.
Drinovec, L., Gregoric, A., Zotter, P., Wolf, R., Anne Bruns, E., Bruns, E. A., Prevot, A. S. H., Favez, O., Sciare, J., Arnold, I. J., Chakrabarty, R. K., Moosmüller, H., Filep, A. & Mocnik, G. (2017). The filter-loading effect by ambient aerosols in filter absorption photometers depends on the coating of the sampled particles. *Atmospheric Measurement Techniques,* 10(3), 1043-1059.
Du, H., Kong, L., Cheng, T., Chen, J., Du, J., Li, L., Xia, X., Leng, C. & Huang, G. (2011). Insights into summertime haze pollution events over Shanghai based on online water-soluble ionic composition of aerosols. *Atmospheric Environment,* 45(29), 5131-5137.
EEA (2017). Air quality in Europe — 2017 report. *In:* Agency, E. E. (ed.). Luxembourg:: Publications Office of the European Union.
Elmes, M. & Gasparon, M. (2017). Sampling and single particle analysis for the chemical characterisation of fine atmospheric particulates: A review. *Journal of Environmental Management,* 202(Part 1), 137-150.
EPA (2006). National Ambient Air Quality Standards for Particulate Matter; Final Rule. *In:* regulations, R. a. (ed.). The United States of America.
Farmer, D. K., Matsunaga, A., Docherty, K. S., Surratt, J. D., Seinfeld, J. H., Ziemann, P. J. & Jimenez, J. L. (2010). Response of an aerosol mass spectrometer to organonitrates and organosulfates and implications for atmospheric chemistry. *Proceedings of the National Academy of Sciences of the United States of America,* 107(15), 6670-6675.
Fernandez, P., Grifoll, M., Solanas, A. M., Bayona, J. M. & Albaiges, J. (1992). Bioassay-directed chemical analysis of genotoxic components in coastal sediments. *Environmental Science & Technology,* 26(4), 817-829.
Florou, K., Papanastasiou, D. K., Pikridas, M., Kaltsonoudis, C., Louvaris, E., Gkatzelis, G. I., Patoulias, D., Mihalopoulos, N. & Pandis, S. N. (2017). The contribution of wood burning and other pollution sources to wintertime organic aerosol levels in two Greek cities. *Atmos. Chem. Phys.,* 17(4), 3145-3163.
Frohlich, R., Cubison, M. J., Slowik, J. G., Bukowiecki, N., Prevot, A. S. H., Baltensperger, U., Schneider, J., Kimmel, J. R., Gonin, M., Rohner, U., Worsnop, D. R. & Jayne, J. T. (2013). The ToF-ACSM: a portable aerosol chemical speciation monitor with TOFMS detection. *Atmospheric Measurement Techniques,* 6(11), 3225-3241.
Fuzzi, S., Baltensperger, U., Carslaw, K., Decesari, S., Denier van der Gon, H., Facchini, M. C., Fowler, D., Koren, I., Langford, B., Lohmann, U., Nemitz, E., Pandis, S., Riipinen, I., Rudich, Y., Schaap, M., Slowik, J. G., Spracklen, D. V., Vignati, E., Wild, M., Williams, M. & Gilardoni, S. (2015). Particulate matter, air quality and climate: lessons learned and future needs. *Atmos. Chem. Phys.,* 15(14), 8217-8299.
Gaston, C. J., Lopez-Hilfiker, F. D., Whybrew, L. E., Hadley, O., McNair, F., Gao, H. L., Jaffe, D. A. & Thornton, J. A. (2016). Online molecular characterization of fine

particulate matter in Port Angeles, WA: Evidence for a major impact from residential wood smoke. *Atmospheric Environment,* 138**,** 99-107.
Ge, X., He, Y., Sun, Y., Xu, J., Wang, J., Shen, Y. & Chen, M. (2017). Characteristics and formation mechanisms of fine particulate nitrate in typical Urban Areas in China. *Atmosphere,* 8(3).
GLA. (2013). *London Atmospheric Emissions Inventory 2013* [Online]. Available: http://data.london.gov.uk/dataset/london-atmospheric-emissions-inventory-2013 [Accessed 18/08/2017 2017].
GMCA (2016). Greater Manchester air quality action plan 2016–2021. *In:* Manchester, T. f. G. (ed.). Manchester.
Greenburg, L., Jacobs, M. B., Drolette, B. M., Field, F. & Braverman, M. M. (1962). Report of an Air-Pollution Incident in New-York-City, November 1953. *Public Health Reports,* 77(1)**,** 7-16.
Gross, J. (2004). *Mass spectrometry. A text book*. Germany: Springer.
Hallquist, M., Wenger, J. C., Baltensperger, U., Rudich, Y., Simpson, D., Claeys, M., Dommen, J., Donahue, N. M., George, C., Goldstein, A. H., Hamilton, J. F., Herrmann, H., Hoffmann, T., Iinuma, Y., Jang, M., Jenkin, M. E., Jimenez, J. L., Kiendler-Scharr, A., Maenhaut, W., McFiggans, G., Mentel, T. F., Monod, A., Prévôt, A. S. H., Seinfeld, J. H., Surratt, J. D., Szmigielski, R. & Wildt, J. (2009). The formation, properties and impact of secondary organic aerosol: current and emerging issues. *Atmos. Chem. Phys.,* 9(14)**,** 5155-5236.
Hao, L. Q., Kortelainen, A., Romakkaniemi, S., Portin, H., Jaatinen, A., Leskinen, A., Komppula, M., Miettinen, P., Sueper, D., Pajunoja, A., Smith, J. N., Lehtinen, K. E. J., Worsnop, D. R., Laaksonen, A. & Virtanen, A. (2014). Atmospheric submicron aerosol composition and particulate organic nitrate formation in a boreal forestland-urban mixed region. *Atmospheric Chemistry and Physics,* 14(24)**,** 13483-13495.
Harrison, R. M., Laxen, D., Moorcroft, S. & Laxen, K. (2012). Processes affecting concentrations of fine particulate matter (PM2.5) in the UK atmosphere. *Atmospheric Environment,* 46**,** 115-124.
Heald, C. L., Coe, H., Jimenez, J. L., Weber, R. J., Bahreini, R., Middlebrook, A. M., Russell, L. M., Jolleys, M., Fu, T. M., Allan, J. D., Bower, K. N., Capes, G., Crosier, J., Morgan, W. T., Robinson, N. H., Williams, P. I., Cubison, M. J., DeCarlo, P. F. & Dunlea, E. J. (2011). Exploring the vertical profile of atmospheric organic aerosol: comparing 17 aircraft field campaigns with a global model. *Atmos. Chem. Phys.,* 11(24)**,** 12673-12696.
Heintzenberg, J. & Charlson, R. J. (1996). Design and Applications of the Integrating Nephelometer: A Review. *Journal of Atmospheric and Oceanic Technology,* 13(5)**,** 987-1000.
Henry, R. C. (2002). Multivariate receptor models - current practice and future trends. *Chemometrics and Intelligent Laboratory Systems,* 60(1-2)**,** 43-48.
Henry, R. C., Chang, Y.-S. & Spiegelman, C. H. (2002). Locating nearby sources of air pollution by nonparametric regression of atmospheric concentrations on wind direction. *Atmospheric Environment,* 36(13)**,** 2237-2244.
Herrera, A., Navas, N. & Cardell, C. (2016). An evaluation of the impact of urban air pollution on paint dosimeters by tracking changes in the lipid MALDI-TOF mass spectra profile. *Talanta,* 155**,** 53-61.
Holmes, H., Aubry, C. & Mayer, P. (2007). *Assigning structures to ions in mass spectrometry*: Taylor and Francis Group.

Hopke, P. K. (1991). An Introduction to Receptor Modeling. *Chemometrics and Intelligent Laboratory Systems,* 10(1-2), 21-43.
Huang, X. F., He, L. Y., Hu, M., Canagaratna, M. R., Sun, Y., Zhang, Q., Zhu, T., Xue, L., Zeng, L. W., Liu, X. G., Zhang, Y. H., Jayne, J. T., Ng, N. L. & Worsnop, D. R. (2010). Highly time-resolved chemical characterization of atmospheric submicron particles during 2008 Beijing Olympic Games using an Aerodyne High-Resolution Aerosol Mass Spectrometer. *Atmospheric Chemistry and Physics,* 10(18), 8933-8945.
IPCC. (2013). *Climate Change 2013: The Physical Science Basis* [Online]. Cambridge, UK: Cambridge Univ. Press. [Accessed.
Jayne, J. T., Leard, D. C., Zhang, X. F., Davidovits, P., Smith, K. A., Kolb, C. E. & Worsnop, D. R. (2000). Development of an aerosol mass spectrometer for size and composition analysis of submicron particles. *Aerosol Science and Technology,* 33(1-2), 49-70.
Jimenez, J., Canagaratna, M., Donahue, N., Prevot, A., Zhang, Q., Kroll, J., DeCarlo, P., Allan, J., Coe, H. & Ng, N. (2009). Evolution of organic aerosols in the atmosphere. *Science,* 326(5959), 1525-1529.
Jimenez, J. L., Jayne, J. T., Shi, Q., Kolb, C. E., Worsnop, D. R., Yourshaw, I., Seinfeld, J. H., Flagan, R. C., Zhang, X. & Smith, K. A. (2003). Ambient aerosol sampling using the aerodyne aerosol mass spectrometer. *Journal of Geophysical Research: Atmospheres (1984–2012),* 108(D7).
Kaltsonoudis, C., Kostenidou, E., Louvaris, E., Psichoudaki, M., Tsiligiannis, E., Florou, K., Liangou, A. & Pandis, S. N. (2017). Characterization of fresh and aged organic aerosol emissions from meat charbroiling. *Atmos. Chem. Phys.,* 17(11), 7143-7155.
Kiendler-Scharr, A., Mensah, A. A., Friese, E., Topping, D., Nemitz, E., Prevot, A. S. H., Äijälä, M., Allan, J., Canonaco, F., Canagaratna, M., Carbone, S., Crippa, M., Dall Osto, M., Day, D. A., De Carlo, P., Di Marco, C. F., Elbern, H., Eriksson, A., Freney, E., Hao, L., Herrmann, H., Hildebrandt, L., Hillamo, R., Jimenez, J. L., Laaksonen, A., McFiggans, G., Mohr, C., O'Dowd, C., Otjes, R., Ovadnevaite, J., Pandis, S. N., Poulain, L., Schlag, P., Sellegri, K., Swietlicki, E., Tiitta, P., Vermeulen, A., Wahner, A., Worsnop, D. & Wu, H. C. (2016). Ubiquity of organic nitrates from nighttime chemistry in the European submicron aerosol. *Geophysical Research Letters,* 43(14), 7735-7744.
Kolb, C. E. & Worsnop, D. R. (2012). Chemistry and Composition of Atmospheric Aerosol Particles. *Annual Review of Physical Chemistry,* 63(1), 471-491.
Kulmala, M., Asmi, A., Lappalainen, H. K., Baltensperger, U., Brenguier, J. L., Facchini, M. C., Hansson, H. C., Hov, O., O'Dowd, C. D., Poschl, U., Wiedensohler, A., Boers, R., Boucher, O., de Leeuw, G., van der Gon, H. A. C. D., Feichter, J., Krejci, R., Laj, P., Lihavainen, H., Lohmann, U., McFiggans, G., Mentel, T., Pilinis, C., Riipinen, I., Schulz, M., Stohl, A., Swietlicki, E., Vignati, E., Alves, C., Amann, M., Ammann, M., Arabas, S., Artaxo, P., Baars, H., Beddows, D. C. S., Bergstrom, R., Beukes, J. P., Bilde, M., Burkhart, J. F., Canonaco, F., Clegg, S. L., Coe, H., Crumeyrolle, S., D'Anna, B., Decesari, S., Gilardoni, S., Fischer, M., Fjaeraa, A. M., Fountoukis, C., George, C., Gomes, L., Halloran, P., Hamburger, T., Harrison, R. M., Herrmann, H., Hoffmann, T., Hoose, C., Hu, M., Hyvarinen, A., Horrak, U., Iinuma, Y., Iversen, T., Josipovic, M., Kanakidou, M., Kiendler-Scharr, A., Kirkevag, A., Kiss, G., Klimont, Z., Kolmonen, P., Komppula, M., Kristjansson, J. E., Laakso, L., Laaksonen, A., Labonnote, L., Lanz, V. A., Lehtinen, K. E. J., Rizzo,

L. V., Makkonen, R., Manninen, H. E., McMeeking, G., Merikanto, J., Minikin, A., Mirme, S., Morgan, W. T., Nemitz, E., O'Donnell, D., Panwar, T. S., Pawlowska, H., Petzold, A., Pienaar, J. J., Pio, C., Plass-Duelmer, C., Prevot, A. S. H., Pryor, S., Reddington, C. L., Roberts, G., Rosenfeld, D., Schwarz, J., Seland, O., Sellegri, K., et al. (2011). General overview: European Integrated project on Aerosol Cloud Climate and Air Quality interactions (EUCAARI) - integrating aerosol research from nano to global scales. *Atmospheric Chemistry and Physics,* 11(24)**,** 13061-13143.

Kupiainen, K. & Klimont, Z. (2007). Primary emissions of fine carbonaceous particles in Europe. *Atmospheric Environment,* 41(10)**,** 2156-2170.

Kurtén, T., Petäjä, T., Smith, J., Ortega, I. K., Sipilä, M., Junninen, H., Ehn, M., Vehkamäki, H., Mauldin, L., Worsnop, D. R. & Kulmala, M. (2011). The effect of H₂SO₄ – amine clustering on chemical ionization mass spectrometry (CIMS) measurements of gas-phase sulfuric acid. *Atmos. Chem. Phys.,* 11(6)**,** 3007-3019.

Lagzi, I., Mészáros, R., G, G. & Leelőssy, A. (2013). *Atmospheric Chemistry*: Eötvös Loránd University.

Lanz, V. A., Alfarra, M. R., Baltensperger, U., Buchmann, B., Hueglin, C. & Prevot, A. S. H. (2007). Source apportionment of submicron organic aerosols at an urban site by factor analytical modelling of aerosol mass spectra. *Atmospheric Chemistry and Physics,* 7(6)**,** 1503-1522.

Lanz, V. A., Alfarra, M. R., Baltensperger, U., Buchmann, B., Hueglin, C., Szidat, S., Wehrli, M. N., Wacker, L., Weimer, S., Caseiro, A., Puxbaum, H. & Prevot, A. S. H. (2008). Source attribution of submicron organic aerosols during wintertime inversions by advanced factor analysis of aerosol mass spectra. *Environmental Science & Technology,* 42(1)**,** 214-220.

Lanz, V. A., Prevot, A. S. H., Alfarra, M. R., Weimer, S., Mohr, C., DeCarlo, P. F., Gianini, M. F. D., Hueglin, C., Schneider, J., Favez, O., D'Anna, B., George, C. & Baltensperger, U. (2010). Characterization of aerosol chemical composition with aerosol mass spectrometry in Central Europe: an overview. *Atmospheric Chemistry and Physics,* 10(21)**,** 10453-10471.

Lawrence, M., Butler, T., Steinkamp, J., Gurjar, B. & Lelieveld, J. (2007). Regional pollution potentials of megacities and other major population centers. *Atmospheric Chemistry and Physics,* 7(14)**,** 3969-3987.

Le Breton, M., Bacak, A., Muller, J. B. A., Bannan, T. J., Kennedy, O., Ouyang, B., Xiao, P., Bauguitte, S. J. B., Shallcross, D. E., Jones, R. L., Daniels, M. J. S., Ball, S. M. & Percival, C. J. (2014). The first airborne comparison of N2O5 measurements over the UK using a CIMS and BBCEAS during the RONOCO campaign. *Analytical Methods,* 6(24)**,** 9731-9743.

Le Breton, M., Bacak, A., Muller, J. B. A., O'Shea, S. J., Xiao, P., Ashfold, M. N. R., Cooke, M. C., Batt, R., Shallcross, D. E., Oram, D. E., Forster, G., Bauguitte, S. J. B., Palmer, P. I., Parrington, M., Lewis, A. C., Lee, J. D. & Percival, C. J. (2013). Airborne hydrogen cyanide measurements using a chemical ionisation mass spectrometer for the plume identification of biomass burning forest fires. *Atmos. Chem. Phys.,* 13(18)**,** 9217-9232.

Lee, B. H., Lopez-Hilfiker, F. D., Mohr, C., Kurtén, T., Worsnop, D. R. & Thornton, J. A. (2014). An Iodide-Adduct High-Resolution Time-of-Flight Chemical-Ionization Mass Spectrometer: Application to Atmospheric Inorganic and

Organic Compounds. *Environmental Science & Technology,* 48(11), 6309-6317.
Lee, B. H., Mohr, C., Lopez-Hilfiker, F. D., Lutz, A., Hallquist, M., Lee, L., Romer, P., Cohen, R. C., Iyer, S., Kurtén, T., Hu, W., Day, D. A., Campuzano-Jost, P., Jimenez, J. L., Xu, L., Ng, N. L., Guo, H., Weber, R. J., Wild, R. J., Brown, S. S., Koss, A., De Gouw, J., Olson, K., Goldstein, A. H., Seco, R., Kim, S., McAvey, K., Shepson, P. B., Starn, T., Baumann, K., Edgerton, E. S., Liu, J., Shilling, J. E., Miller, D. O., Brune, W., Schobesberger, S., D'Ambro, E. L. & Thornton, J. A. (2016). Highly functionalized organic nitrates in the southeast United States: Contribution to secondary organic aerosol and reactive nitrogen budgets. *Proceedings of the National Academy of Sciences of the United States of America,* 113(6), 1516-1521.
Lee, K., Park, J., Kang, M., Kim, D., Batmunkh, T., Bae, M. S. & Park, K. (2017). Chemical Characteristics of Aerosols in Coastal and Urban Ambient Atmospheres. *Aerosol and Air Quality Research,* 17(4), 908-919.
Leelossy, A., Molnar, F., Izsak, F., Havasi, A., Lagzi, I. & Meszaros, R. (2014). Dispersion modeling of air pollutants in the atmosphere: a review. *Central European Journal of Geosciences,* 6(3), 257-278.
Li, H., Zhang, Q., Zhang, Q., Chen, C., Wang, L., Wei, Z., Zhou, S., Parworth, C., Zheng, B., Canonaco, F., Prévôt, A. S. H., Chen, P., Zhang, H., Wallington, T. J. & He, K. (2017a). Wintertime aerosol chemistry and haze evolution in an extremely polluted city of the North China Plain: Significant contribution from coal and biomass combustion. *Atmospheric Chemistry and Physics,* 17(7), 4751-4768.
Li, H. Y., Zhang, Q., Zhang, Q., Chen, C. R., Wang, L. T., Wei, Z., Zhou, S., Parworth, C., Zheng, B., Canonaco, F., Prevot, A. S. H., Chen, P., Zhang, H. L., Wallington, T. J. & He, K. B. (2017b). Wintertime aerosol chemistry and haze evolution in an extremely polluted city of the North China Plain: significant contribution from coal and biomass combustion. *Atmospheric Chemistry and Physics,* 17(7), 4751-4768.
Li, W., Li, H., Li, J., Cheng, X., Zhang, Z., Chai, F., Zhang, H., Yang, T., Duan, P., Lu, D. & Chen, Y. (2017c). TOF–SIMS surface analysis of chemical components of size–fractioned urban aerosols in a typical heavy air pollution event in Beijing. *Journal of Environmental Sciences*.
Li, Y., Zhang, F., Li, Z., Sun, L., Wang, Z., Li, P., Sun, Y., Ren, J., Wang, Y., Cribb, M. & Yuan, C. (2017d). Influences of aerosol physiochemical properties and new particle formation on CCN activity from observation at a suburban site of China. *Atmospheric Research,* 188, 80-89.
Li, Y. J., Sun, Y., Zhang, Q., Li, X., Li, M., Zhou, Z. & Chan, C. K. (2017e). Real-time chemical characterization of atmospheric particulate matter in China: A review. *Atmospheric Environment,* 158, 270-304.
Lim, S. S., Vos, T., Flaxman, A. D., Danaei, G., Shibuya, K., Adair-Rohani, H., AlMazroa, M. A., Amann, M., Anderson, H. R., Andrews, K. G., Aryee, M., Atkinson, C., Bacchus, L. J., Bahalim, A. N., Balakrishnan, K., Balmes, J., Barker-Collo, S., Baxter, A., Bell, M. L., Blore, J. D., Blyth, F., Bonner, C., Borges, G., Bourne, R., Boussinesq, M., Brauer, M., Brooks, P., Bruce, N. G., Brunekreef, B., Bryan-Hancock, C., Bucello, C., Buchbinder, R., Bull, F., Burnett, R. T., Byers, T. E., Calabria, B., Carapetis, J., Carnahan, E., Chafe, Z., Charlson, F., Chen, H., Chen, J. S., Cheng, A. T.-A., Child, J. C., Cohen, A., Colson, K. E., Cowie, B. C., Darby, S., Darling, S., Davis, A., Degenhardt, L., Dentener, F., Des Jarlais, D. C., Devries, K.,

Dherani, M., Ding, E. L., Dorsey, E. R., Driscoll, T., Edmond, K., Ali, S. E., Engell, R. E., Erwin, P. J., Fahimi, S., Falder, G., Farzadfar, F., Ferrari, A., Finucane, M. M., Flaxman, S., Fowkes, F. G. R., Freedman, G., Freeman, M. K., Gakidou, E., Ghosh, S., Giovannucci, E., Gmel, G., Graham, K., Grainger, R., Grant, B., Gunnell, D., Gutierrez, H. R., Hall, W., Hoek, H. W., Hogan, A., Hosgood Iii, H. D., Hoy, D., Hu, H., Hubbell, B. J., Hutchings, S. J., Ibeanusi, S. E., Jacklyn, G. L., Jasrasaria, R., Jonas, J. B., Kan, H., Kanis, J. A., Kassebaum, N., Kawakami, N., Khang, Y.-H., Khatibzadeh, S., Khoo, J.-P., Kok, C., et al. (2012). A comparative risk assessment of burden of disease and injury attributable to 67 risk factors and risk factor clusters in 21 regions, 1990–2010: a systematic analysis for the Global Burden of Disease Study 2010. *The lancet,* 380(9859)**,** 2224-2260.

Liu, D., Allan, J., Corris, B., Flynn, M., Andrews, E., Ogren, J., Beswick, K., Bower, K., Burgess, R., Choularton, T., Dorsey, J., Morgan, W., Williams, P. I. & Coe, H. (2011). Carbonaceous aerosols contributed by traffic and solid fuel burning at a polluted rural site in Northwestern England. *Atmospheric Chemistry and Physics,* 11(4)**,** 1603-1619.

Liu, J., D'Ambro, E. L., Lee, B. H., Lopez-Hilfiker, F. D., Zaveri, R. A., Rivera-Rios, J. C., Keutsch, F. N., Iyer, S., Kurten, T., Zhang, Z., Gold, A., Surratt, J. D., Shilling, J. E. & Thornton, J. A. (2016). Efficient Isoprene Secondary Organic Aerosol Formation from a Non-IEPOX Pathway. *Environmental Science and Technology,* 50(18)**,** 9872-9880.

Liu, Q., Sun, Y., Hu, B., Liu, Z. R., Akio, S. & Wang, Y. S. (2012). In situ measurement of PM1 organic aerosol in Beijing winter using a high-resolution aerosol mass spectrometer. *Chinese Science Bulletin,* 57(7)**,** 819-826.

Loader, A. (2006). UK Smoke and Sulphur Dioxide Network 2004 United Kingdom: AEAT.

Lopez-Hilfiker, F. D., Mohr, C., Ehn, M., Rubach, F., Kleist, E., Wildt, J., Mentel, T. F., Carrasquillo, A. J., Daumit, K. E., Hunter, J. F., Kroll, J. H., Worsnop, D. R. & Thornton, J. A. (2015). Phase partitioning and volatility of secondary organic aerosol components formed from alpha-pinene ozonolysis and OH oxidation: the importance of accretion products and other low volatility compounds. *Atmospheric Chemistry and Physics,* 15(14)**,** 7765-7776.

Lopez-Hilfiker, F. D., Mohr, C., Ehn, M., Rubach, F., Kleist, E., Wildt, J., Mentel, T. F., Lutz, A., Hallquist, M., Worsnop, D. & Thornton, J. A. (2014). A novel method for online analysis of gas and particle composition: description and evaluation of a Filter Inlet for Gases and AEROsols (FIGAERO). *Atmos. Meas. Tech.,* 7(4)**,** 983-1001.

Louvaris, E. E., Karnezi, E., Kostenidou, E., Kaltsonoudis, C. & Pandis, S. N. (2017). Estimation of the volatility distribution of organic aerosol combining thermodenuder and isothermal dilution measurements. *Atmos. Meas. Tech.,* 10(10)**,** 3909-3918.

McCarroll, J. (1967). Measurements of morbidity and mortality related to air pollution. *J Air Pollut Control Assoc,* 17(4)**,** 203-9.

McCarthy, M. C., O'Brien, T. E., Charrier, J. G. & Hather, H. R. (2009). Characterization of the Chronic Risk and Hazard of Hazardous Air Pollutants in the United States Using Ambient Monitoring Data. *Environmental Health Perspectives,* 117(5)**,** 790-796.

McCulloch, R., Alvaro, A., Astudillo, A. M., del Castillo, J. C., Gómez, M., Martín, J. M. & Amo-González, M. (2017). A novel atmospheric pressure photoionization –

Mass spectrometry (APPI-MS) method for the detection of polychlorinated dibenzo P- dioxins and dibenzofuran homologues in real environmental samples collected within the vicinity of industrial incinerators. *International Journal of Mass Spectrometry,* 421(Supplement C), 135-143.

Michoud, V., Sciare, J., Sauvage, S., Dusanter, S., Leonardis, T., Gros, V., Kalogridis, C., Zannoni, N., Feron, A., Petit, J. E., Crenn, V., Baisnee, D., Sarda-Esteve, R., Bonnaire, N., Marchand, N., DeWitt, H. L., Pey, J., Colomb, A., Gheusi, F., Szidat, S., Stavroulas, I., Borbon, A. & Locoge, N. (2017a). Organic carbon at a remote site of the western Mediterranean Basin: sources and chemistry during the ChArMEx SOP2 field experiment. *Atmospheric Chemistry and Physics,* 17(14), 8837-8865.

Michoud, V., Sciare, J., Sauvage, S., Dusanter, S., Léonardis, T., Gros, V., Kalogridis, C., Zannoni, N., Féron, A., Petit, J. E., Crenn, V., Baisnée, D., Sarda-Estève, R., Bonnaire, N., Marchand, N., Dewitt, H. L., Pey, J., Colomb, A., Gheusi, F., Szidat, S., Stavroulas, I., Borbon, A. & Locoge, N. (2017b). Organic carbon at a remote site of the western Mediterranean Basin: Sources and chemistry during the ChArMEx SOP2 field experiment. *Atmospheric Chemistry and Physics,* 17(14), 8837-8865.

Minguillón, M. C., Ripoll, A., Pérez, N., Prévôt, A. S. H., Canonaco, F., Querol, X. & Alastuey, A. (2015). Chemical characterization of submicron regional background aerosols in the western Mediterranean using an Aerosol Chemical Speciation Monitor. *Atmos. Chem. Phys.,* 15(11), 6379-6391.

Mittal, L. & Fuller, G. (2017). London Air Quality Network Summary Report 2016. London: King’s College London.

Mohr, C., DeCarlo, P. F., Heringa, M. F., Chirico, R., Slowik, J. G., Richter, R., Reche, C., Alastuey, A., Querol, X., Seco, R., Penuelas, J., Jimenez, J. L., Crippa, M., Zimmermann, R., Baltensperger, U. & Prevot, A. S. H. (2012). Identification and quantification of organic aerosol from cooking and other sources in Barcelona using aerosol mass spectrometer data. *Atmospheric Chemistry and Physics,* 12(4), 1649-1665.

Mohr, C., Huffman, J. A., Cubison, M. J., Aiken, A. C., Docherty, K. S., Kimmel, J. R., Ulbrich, I. M., Hannigan, M. & Jimenez, J. L. (2009). Characterization of Primary Organic Aerosol Emissions from Meat Cooking, Trash Burning, and Motor Vehicles with High-Resolution Aerosol Mass Spectrometry and Comparison with Ambient and Chamber Observations. *Environmental Science & Technology,* 43(7), 2443-2449.

Mohr, C., Lopez-Hilfiker, F. D., Zotter, P., Prevot, A. S. H., Xu, L., Ng, N. L., Herndon, S. C., Williams, L. R., Franklin, J. P., Zahniser, M. S., Worsnop, D. R., Knighton, W. B., Aiken, A. C., Gorkowski, K. J., Dubey, M. K., Allan, J. D. & Thornton, J. A. (2013). Contribution of Nitrated Phenols to Wood Burning Brown Carbon Light Absorption in Detling, United Kingdom during Winter Time. *Environmental Science & Technology,* 47(12), 6316-6324.

Molina, M. J. & Molina, L. T. (2004). Megacities and atmospheric pollution. *Journal of the Air & Waste Management Association,* 54(6), 644-680.

Morgan, W. T., Allan, J. D., Bower, K. N., Highwood, E. J., Liu, D., McMeeking, G. R., Northway, M. J., Williams, P. I., Krejci, R. & Coe, H. (2010). Airborne measurements of the spatial distribution of aerosol chemical composition across Europe and evolution of the organic fraction. *Atmospheric Chemistry and Physics,* 10(8), 4065-4083.

Muthuramu, K., Shepson, P. B. & Obrien, J. M. (1993). Preparation, Analysis, and Atmospheric Production of Multifunctional Organic Nitrates. *Environmental Science & Technology,* 27(6)**,** 1117-1124.

Ng, N. L., Canagaratna, M. R., Zhang, Q., Jimenez, J. L., Tian, J., Ulbrich, I. M., Kroll, J. H., Docherty, K. S., Chhabra, P. S., Bahreini, R., Murphy, S. M., Seinfeld, J. H., Hildebrandt, L., Donahue, N. M., DeCarlo, P. F., Lanz, V. A., Prevot, A. S. H., Dinar, E., Rudich, Y. & Worsnop, D. R. (2010). Organic aerosol components observed in Northern Hemispheric datasets from Aerosol Mass Spectrometry. *Atmospheric Chemistry and Physics,* 10(10)**,** 4625-4641.

Ng, N. L., Herndon, S. C., Trimborn, A., Canagaratna, M. R., Croteau, P., Onasch, T. B., Sueper, D., Worsnop, D. R., Zhang, Q. & Sun, Y. (2011). An Aerosol Chemical Speciation Monitor (ACSM) for routine monitoring of the composition and mass concentrations of ambient aerosol. *Aerosol Science and Technology,* 45(7)**,** 780-794.

NRC, N. R. C. (1998). *Research Priorities for Airborne Particulate Matter: I. Immediate Priorities and a Long-Range Research Portfolio*. Washington, DC: The National Academies Press.

O'Connor, S., O'Connor, P. F., Feng, H. A. & Ashley, K. (2014). Gravimetric Analysis of Particulate Matter using Air Samplers Housing Internal Filtration Capsules. *Gefahrstoffe, Reinhaltung der Luft = Air quality control / Herausgeber, BIA und KRdL im VDI und DIN,* 74(10)**,** 403-410.

Oberdorster, G., Oberdorster, E. & Oberdorster, J. (2005). Nanotoxicology: An emerging discipline evolving from studies of ultrafine particles. *Environmental Health Perspectives,* 113(7)**,** 823-839.

Paatero, P. (1999). The Multilinear Engine: A Table-Driven, Least Squares Program for Solving Multilinear Problems, including the n-Way Parallel Factor Analysis Model. *Journal of Computational and Graphical Statistics,* 8(4)**,** 854-888.

Paatero, P. & Hopke, P. K. (2009). Rotational tools for factor analytic models. *Journal of Chemometrics,* 23(2)**,** 91-100.

Paatero, P., Hopke, P. K., Song, X. H. & Ramadan, Z. (2002). Understanding and controlling rotations in factor analytic models. *Chemometrics and Intelligent Laboratory Systems,* 60(1-2)**,** 253-264.

Paatero, P. & Tapper, U. (1994). Positive matrix factorization: A non-negative factor model with optimal utilization of error estimates of data values. *Environmetrics,* 5(2)**,** 111-126.

Parliament, E. (2008). Directive 2008/50/EC of the European Parliament and of the Council of 21 May 2008 on ambient air quality and cleaner air for Europe.

Parworth, C. L., Young, D. E., Kim, H., Zhang, X., Cappa, C. D., Collier, S. & Zhang, Q. (2017). Wintertime water-soluble aerosol composition and particle water content in Fresno, California. *Journal of Geophysical Research: Atmospheres,* 122(5)**,** 3155-3170.

Peng, R. D., Dominici, F., Pastor-Barriuso, R., Zeger, S. L. & Samet, J. M. (2005). Seasonal analyses of air pollution and mortality in 100 US cities. *American journal of epidemiology,* 161(6)**,** 585-594.

Pirjola, L., Niemi, J. V., Saarikoski, S., Aurela, M., Enroth, J., Carbone, S., Saarnio, K., Kuuluvainen, H., Kousa, A., Ronkko, T. & Hillamo, R. (2017). Physical and chemical characterization of urban winter-time aerosols by mobile measurements in Helsinki, Finland. *Atmospheric Environment,* 158**,** 60-75.

Pope, I. C., Burnett, R. T., Thun, M. J. & et al. (2002). Lung cancer, cardiopulmonary mortality, and long-term exposure to fine particulate air pollution. *JAMA,* 287(9), 1132-1141.
Pope III, C. A. & Dockery, D. W. (2006). Health effects of fine particulate air pollution: lines that connect. *Journal of the Air & Waste Management Association,* 56(6), 709-742.
Pöschl, U. (2005). Atmospheric Aerosols: Composition, Transformation, Climate and Health Effects. *Angewandte Chemie International Edition,* 44(46), 7520-7540.
Qin, Y. M., Tan, H. B., Li, Y. J., Schurman, M. I., Li, F., Canonaco, F., Prévôt, A. S. H. & Chan, C. K. (2017). Impacts of traffic emissions on atmospheric particulate nitrate and organics at a downwind site on the periphery of Guangzhou, China. *Atmos. Chem. Phys.,* 17(17), 10245-10258.
Quincey, P. (2007). A relationship between Black Smoke Index and Black Carbon concentration. *Atmospheric Environment,* 41(36), 7964-7968.
Ramgolam, K., Favez, O., Cachier, H., Gaudichet, A., Marano, F., Martinon, L. & Baeza-Squiban, A. (2009). Size-partitioning of an urban aerosol to identify particle determinants involved in the proinflammatory response induced in airway epithelial cells. *Part Fibre Toxicol,* 6(10), 6-9.
Rattanavaraha, W., Canagaratna, M. R., Budisulistiorini, S. H., Croteau, P. L., Baumann, K., Canonaco, F., Prevot, A. S. H., Edgerton, E. S., Zhang, Z., Jayne, J. T., Worsnop, D. R., Gold, A., Shaw, S. L. & Surratt, J. D. (2017). Source apportionment of submicron organic aerosol collected from Atlanta, Georgia, during 2014–2015 using the aerosol chemical speciation monitor (ACSM). *Atmospheric Environment,* 167(Supplement C), 389-402.
Reinhold, V. N. (1987). [5] Direct chemical ionization mass spectrometry of carbohydrates. *Methods in Enzymology.* Academic Press.
Reyes-Villegas, E., Priestley, M., Ting, Y. C., Haslett, S., Bannan, T., Le breton, M., Williams, P. I., Bacak, A., Flynn, M. J., Coe, H., Percival, C. & Allan, J. D. (2017). Simultaneous Aerosol Mass Spectrometry and Chemical Ionisation Mass Spectrometry measurements during a biomass burning event in the UK: Insights into nitrate chemistry. *Atmos. Chem. Phys. Discuss.,* 2017, 1-22.
Rigby, M. & Toumi, R. (2008). London air pollution climatology: Indirect evidence for urban boundary layer height and wind speed enhancement. *Atmospheric Environment,* 42(20), 4932-4947.
Ripoll, A., Minguillón, M. C., Pey, J., Jimenez, J. L., Day, D. A., Sosedova, Y., Canonaco, F., Prévôt, A. S. H., Querol, X. & Alastuey, A. (2015). Long-term real-time chemical characterization of submicron aerosols at Montsec (southern Pyrenees, 1570 m a.s.l.). *Atmospheric Chemistry and Physics,* 15(6), 2935-2951.
Rivellini, L. H., Chiapello, I., Tison, E., Fourmentin, M., Feron, A., Diallo, A., N'Diaye, T., Goloub, P., Canonaco, F., Prevot, A. S. H. & Riffault, V. (2017). Chemical characterization and source apportionment of submicron aerosols measured in Senegal during the 2015 SHADOW campaign. *Atmospheric Chemistry and Physics,* 17(17), 10291-10314.
Saleh, R., Robinson, E. S., Tkacik, D. S., Ahern, A. T., Liu, S., Aiken, A. C., Sullivan, R. C., Presto, A. A., Dubey, M. K., Yokelson, R. J., Donahue, N. M. & Robinson, A. L. (2014). Brownness of organics in aerosols from biomass burning linked to their black carbon content. *Nature Geoscience,* 7(9), 647-650.

Samet, J. & Krewski, D. (2007). Health effects associated with exposure to ambient air pollution. *Journal of Toxicology and Environmental Health-Part a-Current Issues,* 70(3-4), 227-242.
Satheesh, S. K. & Krishna Moorthy, K. (2005). Radiative effects of natural aerosols: A review. *Atmospheric Environment,* 39(11), 2089-2110.
Schauer, J. J., Rogge, W. F., Hildemann, L. M., Mazurek, M. A., Cass, G. R. & Simoneit, B. R. T. (1996). Source apportionment of airborne particulate matter using organic compounds as tracers. *Atmospheric Environment,* 30(22), 3837-3855.
Schlag, P., Rubach, F., Mentel, T. F., Reimer, D., Canonaco, F., Henzing, J. S., Moerman, M., Otjes, R., Prevot, A. S. H., Rohrer, F., Rosati, B., Tillmann, R., Weingartner, E. & Kiendler-Scharr, A. (2017). Ambient and laboratory observations of organic ammonium salts in PM1. *Faraday Discussions,* 200, 331-351.
Schneider, J., Weimer, S., Drewnick, F., Borrmann, S., Helas, G., Gwaze, P., Schmid, O., Andreae, M. O. & Kirchner, U. (2006). Mass spectrometric analysis and aerodynamic properties of various types of combustion-related aerosol particles. *International Journal of Mass Spectrometry,* 258(1-3), 37-49.
Schobesberger, S., Lopez-Hilfiker, F. D., Taipale, D., Millet, D. B., D'Ambro, E. L., Rantala, P., Mammarella, I., Zhou, P., Wolfe, G. M., Lee, B. H., Boy, M. & Thornton, J. A. (2016). High upward fluxes of formic acid from a boreal forest canopy. *Geophysical Research Letters,* 43(17), 9342-9351.
Seinfeld, J. H. & Pandis, S. N. (2016). *Atmospheric chemistry and physics: from air pollution to climate change* (Third edition ed.). Hoboken,NewJersey: John Wiley & Sons.
Sexton, K. & Linder, S. H. (2015). Houston's Novel Strategy to Control Hazardous Air Pollutants: A Case Study in Policy Innovation and Political Stalemate. *Environ Health Insights,* 9(Suppl 1), 1-12.
Stark, H., Yatavelli, R. L. N., Thompson, S. L., Kang, H., Krechmer, J. E., Kimmel, J. R., Palm, B. B., Hu, W., Hayes, P. L., Day, D. A., Campuzano-Jost, P., Canagaratna, M. R., Jayne, J. T., Worsnop, D. R. & Jimenez, J. L. (2017). Impact of Thermal Decomposition on Thermal Desorption Instruments: Advantage of Thermogram Analysis for Quantifying Volatility Distributions of Organic Species. *Environmental Science & Technology,* 51(15), 8491-8500.
Struckmeier, C., Drewnick, F., Fachinger, F., Gobbi, G. P. & Borrmann, S. (2016). Atmospheric aerosols in Rome, Italy: sources, dynamics and spatial variations during two seasons. *Atmospheric Chemistry and Physics,* 16(23), 15277-15299.
Sun, Y. L., Wang, Z. F., Fu, P. Q., Yang, T., Jiang, Q., Dong, H. B., Li, J. & Jia, J. J. (2013). Aerosol composition, sources and processes during wintertime in Beijing, China. *Atmospheric Chemistry and Physics,* 13(9), 4577-4592.
Takahama, S., Johnson, A., Guzman Morales, J., Russell, L. M., Duran, R., Rodriguez, G., Zheng, J., Zhang, R., Toom-Sauntry, D. & Leaitch, W. R. (2013). Submicron organic aerosol in Tijuana, Mexico, from local and Southern California sources during the CalMex campaign. *Atmospheric Environment,* 70(0), 500-512.
Takegawa, N., Miyakawa, T., Watanabe, M., Kondo, Y., Miyazaki, Y., Han, S., Zhao, Y., van Pinxteren, D., Bruggemann, E., Gnauk, T., Herrmann, H., Xiao, R., Deng, Z., Hu, M., Zhu, T. & Zhang, Y. (2009). Performance of an Aerodyne Aerosol Mass Spectrometer (AMS) during Intensive Campaigns in China in the Summer of 2006. *Aerosol Science and Technology,* 43(3), 189-204.

Thompson, S. L., Yatavelli, R. L. N., Stark, H., Kimmel, J. R., Krechmer, J. E., Day, D. A., Hu, W. W., Isaacman-VanWertz, G., Yee, L., Goldstein, A. H., Khan, M. A. H., Holzinger, R., Kreisberg, N., Lopez-Hilfiker, F. D., Mohr, C., Thornton, J. A., Jayne, J. T., Canagaratna, M., Worsnop, D. R. & Jimenez, J. L. (2017). Field intercomparison of the gas/particle partitioning of oxygenated organics during the Southern Oxidant and Aerosol Study (SOAS) in 2013. *Aerosol Science and Technology,* 51(1), 30-56.

Ulbrich, I. M., Canagaratna, M. R., Zhang, Q., Worsnop, D. R. & Jimenez, J. L. (2009). Interpretation of organic components from Positive Matrix Factorization of aerosol mass spectrometric data. *Atmospheric Chemistry and Physics,* 9(9), 2891-2918.

United Nations, D. o. E. a. S. A. (2012). World Urbanization Prospects: The 2011 Revision. CD-ROM Edition - Data in digital form. Available: http://esa.un.org/unup/pdf/WUP2011_Highlights.pdf [Accessed 13/05/2014].

Valavanidis, A., Fiotakis, K. & Vlachogianni, T. (2008). Airborne Particulate Matter and Human Health: Toxicological Assessment and Importance of Size and Composition of Particles for Oxidative Damage and Carcinogenic Mechanisms. *Journal of Environmental Science and Health, Part C,* 26(4), 339-362.

Veres, P., Roberts, J. M., Burling, I. R., Warneke, C., de Gouw, J. & Yokelson, R. J. (2010). Measurements of gas-phase inorganic and organic acids from biomass fires by negative-ion proton-transfer chemical-ionization mass spectrometry. *Journal of Geophysical Research: Atmospheres,* 115(D23), n/a-n/a.

Veres, P., Roberts, J. M., Warneke, C., Welsh-Bon, D., Zahniser, M., Herndon, S., Fall, R. & de Gouw, J. (2008). Development of negative-ion proton-transfer chemical-ionization mass spectrometry (NI-PT-CIMS) for the measurement of gas-phase organic acids in the atmosphere. *International Journal of Mass Spectrometry,* 274(1), 48-55.

Viana, M., Kuhlbusch, T. A. J., Querol, X., Alastuey, A., Harrison, R. M., Hopke, P. K., Winiwarter, W., Vallius, A., Szidat, S., Prevot, A. S. H., Hueglin, C., Bloemen, H., Wahlin, P., Vecchi, R., Miranda, A. I., Kasper-Giebl, A., Maenhaut, W. & Hitzenberger, R. (2008). Source apportionment of particulate matter in Europe: A review of methods and results. *Journal of Aerosol Science,* 39(10), 827-849.

Vicente, E. D. & Alves, C. A. (2018). An overview of particulate emissions from residential biomass combustion. *Atmospheric Research,* 199(Supplement C), 159-185.

Visser, S., Slowik, J. G., Furger, M., Zotter, P., Bukowiecki, N., Canonaco, F., Flechsig, U., Appel, K., Green, D. C., Tremper, A. H., Young, D. E., Williams, P. I., Allan, J. D., Coe, H., Williams, L. R., Mohr, C., Xu, L., Ng, N. L., Nemitz, E., Barlow, J. F., Halios, C. H., Fleming, Z. L., Baltensperger, U. & Prévôt, A. S. H. (2015). Advanced source apportionment of size-resolved trace elements at multiple sites in London during winter. *Atmos. Chem. Phys.,* 15(19), 11291-11309.

Wallace, J. M. & Hobbs, P. V. (2006). *Atmospheric science: an introductory survey* (Second edition ed. Vol. 92). San Diego, California: Elsevier Inc.

Wang, C., Huang, X. F., Zhu, Q., Cao, L. M., Zhang, B. & He, L. Y. (2017a). Differentiating local and regional sources of Chinese urban air pollution based on the effect of the Spring Festival. *Atmospheric Chemistry and Physics,* 17(14)**,** 9103-9114.

Wang, S. C. & Flagan, R. C. (1990). Scanning Electrical Mobility Spectrometer. *Aerosol Science and Technology,* 13(2)**,** 230-240.

Wang, Y. C., Huang, R. J., Ni, H. Y., Chen, Y., Wang, Q. Y., Li, G. H., Tie, X. X., Shen, Z. X., Huang, Y., Liu, S. X., Dong, W. M., Xue, P., Fröhlich, R., Canonaco, F., Elser, M., Daellenbach, K. R., Bozzetti, C., El Haddad, I., Prévôt, A. S. H., Canagaratna, M. R., Worsnop, D. R. & Cao, J. J. (2017b). Chemical composition, sources and secondary processes of aerosols in Baoji city of northwest China. *Atmospheric Environment,* 158**,** 128-137.

Watson, J. G. (2002). Visibility: Science and Regulation. *Journal of the Air & Waste Management Association,* 52(6)**,** 628-713.

WHO (2006). WHO Air quality guidelines for particulate matter, ozone, nitrogen dioxide and sulfur dioxide: global update 2005: summary of risk assessment.

WHO (2016). Ambient air pollution:a global assessment of exposure and burden of desease. *In:* Organization, W. H. (ed.). Switzerland: WHO Press.

Wolf, R., El-Haddad, I., Slowik, J. G., Dallenbach, K., Bruns, E., Vasilescu, J., Baltensperger, U. & Prevot, A. S. H. (2017). Contribution of bacteria-like particles to PM2.5 aerosol in urban and rural environments. *Atmospheric Environment,* 160**,** 97-106.

Wolf, R., Slowik, J. G., Schaupp, C., Amato, P., Saathoff, H., Mohler, O., Prevot, A. S. H. & Baltensperger, U. (2015). Characterization of ice-nucleating bacteria using on-line electron impact ionization aerosol mass spectrometry. *Journal of Mass Spectrometry,* 50(4)**,** 662-671.

Wu, W. S. & Wang, T. (2007). On the performance of a semi-continuous PM2.5 sulphate and nitrate instrument under high loadings of particulate and sulphur dioxide. *Atmospheric Environment,* 41(26)**,** 5442-5451.

Xu, L., Suresh, S., Guo, H., Weber, R. J. & Ng, N. L. (2015). Aerosol characterization over the southeastern United States using high-resolution aerosol mass spectrometry: spatial and seasonal variation of aerosol composition and sources with a focus on organic nitrates. *Atmos. Chem. Phys.,* 15(13)**,** 7307-7336.

Yang, T., Sun, Y., Zhang, W., Wang, Z., Liu, X., Fu, P. & Wang, X. (2017). Evolutionary processes and sources of high-nitrate haze episodes over Beijing, Spring. *Journal of Environmental Sciences (China),* 54**,** 142-151.

Yin, J., Cumberland, S. A., Harrison, R. M., Allan, J., Young, D. E., Williams, P. I. & Coe, H. (2015). Receptor modelling of fine particles in southern England using CMB including comparison with AMS-PMF factors. *Atmos. Chem. Phys.,* 15(4)**,** 2139-2158.

Yin, J. X., Harrison, R. M., Chen, Q., Rutter, A. & Schauer, J. J. (2010). Source apportionment of fine particles at urban background and rural sites in the UK atmosphere. *Atmospheric Environment,* 44(6)**,** 841-851.

Young, D. E., Allan, J. D., Williams, P. I., Green, D. C., Flynn, M. J., Harrison, R. M., Yin, J., Gallagher, M. W. & Coe, H. (2015). Investigating the annual behaviour of submicron secondary inorganic and organic aerosols in London. *Atmos. Chem. Phys.,* 15(11)**,** 6351-6366.

Zhang, Q., Jimenez, J. L., Canagaratna, M. R., Allan, J. D., Coe, H., Ulbrich, I., Alfarra, M. R., Takami, A., Middlebrook, A. M., Sun, Y. L., Dzepina, K., Dunlea, E., Docherty, K., DeCarlo, P. F., Salcedo, D., Onasch, T., Jayne, J. T., Miyoshi, T., Shimono, A., Hatakeyama, S., Takegawa, N., Kondo, Y., Schneider, J., Drewnick, F., Borrmann, S., Weimer, S., Demerjian, K., Williams, P., Bower, K., Bahreini, R., Cottrell, L., Griffin, R. J., Rautiainen, J., Sun, J. Y., Zhang, Y. M. & Worsnop, D. R. (2007). Ubiquity and dominance of oxygenated species in organic aerosols in anthropogenically-influenced Northern Hemisphere midlatitudes. *Geophysical Research Letters,* 34(13).

Zhang, X., Zhang, Y., Sun, J., Yu, Y., Canonaco, F., Prévôt, A. S. H. & Li, G. (2017a). Chemical characterization of submicron aerosol particles during wintertime in a northwest city of China using an Aerodyne aerosol mass spectrometry. *Environmental Pollution,* 222(Supplement C), 567-582.

Zhang, Y., Tang, L., Sun, Y., Favez, O., Canonaco, F., Albinet, A., Couvidat, F., Liu, D., Jayne, J. T., Wang, Z., Croteau, P. L., Canagaratna, M. R., Zhou, H.-c., Prévôt, A. S. H. & Worsnop, D. R. (2017b). Limited formation of isoprene epoxydiols-derived secondary organic aerosol under NOx-rich environments in Eastern China. *Geophysical Research Letters,* 44(4), 2035-2043.

Zhang, Y. L., Huang, R. J., El Haddad, I., Ho, K. F., Cao, J. J., Han, Y., Zotter, P., Bozzetti, C., Daellenbach, K. R., Canonaco, F., Slowik, J. G., Salazar, G., Schwikowski, M., Schnelle-Kreis, J., Abbaszade, G., Zimmermann, R., Baltensperger, U., Prévôt, A. S. H. & Szidat, S. (2015). Fossil vs. non-fossil sources of fine carbonaceous aerosols in four Chinese cities during the extreme winter haze episode of 2013. *Atmos. Chem. Phys.,* 15(3), 1299-1312.

Zhao, J., Du, W., Zhang, Y., Wang, Q., Chen, C., Xu, W., Han, T., Wang, Y., Fu, P., Wang, Z., Li, Z. & Sun, Y. (2017a). Insights into aerosol chemistry during the 2015 China Victory Day parade: Results from simultaneous measurements at ground level and 260ĝ€m in Beijing. *Atmospheric Chemistry and Physics,* 17(4), 3215-3232.

Zhao, Y., Chan, J. K., Lopez-Hilfiker, F. D., McKeown, M. A., D'Ambro, E. L., Slowik, J. G., Riffel, J. A. & Thornton, J. A. (2017b). An electrospray chemical ionization source for real-time measurement of atmospheric organic and inorganic vapors. *Atmospheric Measurement Techniques,* 10(10), 3609-3625.

Appendix A. Co-authorship in peer reviewed publications

Black-carbon absorption enhancement in the atmosphere determined by particle mixing state

Dantong Liu, James Whitehead, M. Rami Alfarra, **Ernesto Reyes-Villegas**, Dominick V. Spracklen, Carly L. Reddington, Shaofei Kong, Paul I.Williams, Yu-Chieh Ting, Sophie Haslett, JonathanW. Taylor, Michael J. Flynn,William T. Morgan, Gordon McFiggans, Hugh Coe and James D. Allan

doi.org/10.1038/ngeo2901

I participated in the measurements and writing of the manuscript. I performed the OA source apportionment.

Observations of isocyanate, amide, nitrate and nitro compounds from an anthropogenic biomass burning event using a TOF-CIMS

Michael Priestley, Michael Le Breton, Thomas J. Bannan, Kimberly E. Leather, Asan Bacak, **Ernesto Reyes-Villegas**, Frank De Vocht, Beth M. A. Shallcross, Toby Brazier, M. Anwar Khan, James Allan, Dudley E. Shallcross, Hugh Coe, Carl J. Percival

DOI: 10.1002/2017JD027316

I participated in the measurements and discussed the results with Michael Priestley.

Observations of organic and inorganic chlorinated compounds and their contribution to chlorine radical concentrations in an urban environment in Northern Europe during the wintertime

Michael Priestley, Michael Le Breton, Thomas J. Bannan, Stephen Worrall, Asan Bacak, Andrew R. D. Smedley, **Ernesto Reyes-Villegas**, Archit Mehra, James Allan, Ann R. Webb, Dudley E. Shallcross, Hugh Coe, Carl J. Percival.

doi.org/10.5194/acp-2018-236

I participated in the measurements and discussed the results with Michael Priestley.